DE GRUYTER

Alina Mariana Balu,
Araceli Garcia (Eds.)

BIOMASS AND BIOWASTE

NEW CHEMICAL PRODUCTS FROM OLD

Biomass and Biowaste

Also of interest

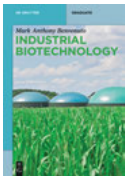

Industrial Biotechnology
Benvenuto, Mark Anthony, 2019
ISBN 978-3-11-053639-3, e-ISBN 978-3-11-053662-1,
e-ISBN (EPUB) 978-3-11-053676-8

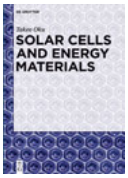

Solar Cells and Energy Materials
Oku, Takeo, 2016
ISBN 978-3-11-029848-2, e-ISBN 978-3-11-029850-5,
e-ISBN (EPUB) 978-3-11-038106-1

Drinking Water Treatment
An Introduction
Worch, Eckhard, 2019
ISBN 978-3-11-055154-9, e-ISBN 978-3-11-055155-6,
e-ISBN (EPUB) 978-3-11-055166-2

Green Pulp and Paper Industry
Biotechnology for Ecofriendly Processing
Hrsg. v. Kumar, Amit / Pathak, Puneet / Dutt, Dharm, 2019
ISBN 978-3-11-059184-2, e-ISBN 978-3-11-059241-2,
e-ISBN (EPUB) 978-3-11-059187-3

Biomass and Biowaste

New Chemical Products from Old

Edited by
Alina M. Balu and Araceli García Nuñez

DE GRUYTER

Editors
Dr. Alina Mariana Balu
University of Cordoba
Department of Organic Chemistry
Campus de Rabanales
Edificio Marie Curie (C-3)
Crta. Nacional IV-A, km. 396
14014 Cordoba
Spain
qo2balua@uco.es

Dr. Araceli García Nuñez
University of Cordoba
Department of Organic Chemistry
Campus de Rabanales
Edificio Marie Curie (C-3)
Crta. Nacional IV-A, km. 396
14014 Cordoba
Spain
qo2ganua@uco.es

ISBN 978-3-11-053778-9
e-ISBN (PDF) 978-3-11-053815-1
e-ISBN (EPUB) 978-3-11-053782-6

Library of Congress Control Number: 2020933290

Bibliographic information published by the Deutsche Nationalbibliothek
The Deutsche Nationalbibliothek lists this publication in the Deutsche Nationalbibliografie; detailed bibliographic data are available on the Internet at http://dnb.dnb.de.

Cover image: arturbo/E+/getty images
Typesetting: Integra Software Services Pvt. Ltd.
Printing and binding: CPI books GmbH, Leck

www.degruyter.com

Preface

Valorization of biomass focuses on the transformation of biomass molecules into substitutes for petroleum-based chemicals that can be reused. The monograph ***Biomass and Biowaste: New chemical products from Old*** discusses the chemistry and composition of alternative biowaste as renewable resources for advanced applications toward biodegradable materials. At present, the use of biomass as a renewable and inexhaustible source of products has become a research hotspot. Scientific community is carrying out great efforts for the development of bioproducts that could replace those produced from petroleum. Considering the biorefinery concept, the development of processes and products is more effective when it emerges in a circular economy, reusing and valuing wastes of activities that nowadays are considered unprofitable by the society, such as agriculture or fishing, or from the human consumption (urban and industrial wastes).

The first chapter of this book, authored by Funez et al. in a joint work from the Universities of Malaga and Cordoba in Spain, provides a detailed overview of the lignocellulosic biomass, its composition and renewable character as source of bio-based chemicals and products from a biorefinery point of view. Here a comprehensive use of carbohydrates is proposed, focusing on the application of furfural derivatives and their catalytic obtaining by different thermochemical, biochemical, chemical and mechanical processes.

- *Furfural Derivatives from Agricultural and Agri-Food Wastes by Heterogeneous Catalysis*. **I. Funez, C. García, P.J. Maireles, L. Serrano**.

In Chapter 2, Juodeikiene et al., from Kaunas University of Technology and the University of Health Sciences in Lithuania, present the comprehensive use of agro-industrial wastes via biotechnological and chemical methodologies toward the production of lactic acid, giving a complete overview on green metrics (process efficiency, land use and costs).

- *Biorefinery Approach for the Utilization of Dairy By-products and Lignocellulosic Biomass to Lactic Acid*. **G. Juodeikiene, E. Bartkiene, D. Zadeike, D. Klupsaite**.

Chapter 3, stated by Briones et al. from the Advanced Polymer Research Center (CIPA) of Chile, deals with the use of macroalgae biomass and its transformation into alginate-based biopolymers by means of $CaCl_2$/acid methodologies. In addition, the authors report a complete review of algae sourced biomaterials and their potential advanced applications from recent literature.

- *Biomass and Biowastes: Renewable Resources for Biodegradable Materials in Advanced Applications*. **R. Briones, K. Varaprasad**.

https://doi.org/10.1515/9783110538151-202

Later chapters introduce novel nanomaterials and discuss green methods of process intensification and heterogeneous catalysis in order to increase conversion of biomass/biowastes.

Chapter 4, by Coman et al., from the University of Bucharest (Romania), is dedicated to the evolution of the supported metal catalysts (bi- and multimettalic particles based on noble metals supported over oxides such as silica, TiO_2 and Al_2O_3) for biomass upgrading, following the principles of green chemistry through heterogeneously catalyzed processes and looking at the efficient conversion of biomass to value-added fine chemicals and fuels.

- *Supported Metals Catalysts for the Sustainable Upgrading of Renewable Biomass to Value-Added Fine Chemicals and Fuels*. **S.M. Coman, V.I. Parvulescu**.

In continuation with the topic on heterogeneous catalysis, Chapter 5 from Triantafyllidis et al., from the University of Aristoteles in Greece, is looking at the state of the art in biomass fast pyrolysis using acidic catalysts, and Chapter 6, by Ivars-Barceló et al. from Madrid (Spain) in collaboration with the group of Rodríguez-Castellón from the University of Malaga (Spain), is focusing on the recent advances made in the development of transition metal catalysts for hydrodeoxygenation reactions of bio-oil from biomass pyrolysis.

- *State of the Art in Biomass Fast Pyrolysis Using Acidic Catalysts: Direct Comparison between Microporous Zeolites, Mesoporous Aluminosilicates and Hierarchical Zeolites*. **K.S. Triantafyllidis, S.D. Stefanidis, S.A. Karakoulia, A. Pineda, A. Margellou, K.G. Kalogiannis, E.F. Iliopoulou, A.A. Lappas**.
- *Advances in the Application of Transition Metal Phosphide Catalysts for Hydrodeoxygenation Reactions of Bio-oil from Biomass Pyrolysis*. **F. Ivars-Barceló, E. Asedegbega-Nieto, E. Rodríguez-Aguado, J.A. Cecilia, A. Infantes-Molina, E. Rodríguez-Castellón**.

Finally, Chapter 7 of this book proposes the industrial use of biomass and biowastes in the co-processing with fossil resources. The work, stated by Hidalgo et al. from the Unipetrol Centre for Research and Education (UNICRE) in Czech Rebublic, first details different types of biowastes, non-edible lipids, Fisher Tropsch paraffins and low value biomass, which can be considered in the co-processing with oil fractions in refineries. Later, a complete description of catalytic co-hydroprocessing pathway is provided, emphasizing the reduction of the net final CO_2 production (carbon footprint of the fossil/biomass produced fuels) and the enhancement of fuel renewability in the near future.

- *Biowaste and Petroleum Fractions Co-processing to Fuels*. **J.M. Hidalgo, H.P. Carmona, J. Fratczak**.

Acknowledgments

Alina M. Balu acknowledges the COST Actions FP1306 (LIGNOVAL) and CA17128 (LIGNOCOST) for the networking, and Araceli García would like to thank the Spanish Ministry of Economy, Industry and Competitiveness (postdoctoral contract Juan de la Cierva Incorporación IJCI-2015-23168) for the financial support during this work.

https://doi.org/10.1515/9783110538151-203

Contents

List of contributing authors

Elena Rodríguez Aguado
Departamento de Química Inorgánica
Cristalografía y Mineralogía
(Unidad Asociada al ICP-CSIC)
Facultad de Ciencias
Universidad de Málaga
Campus de Teatinos
29071 Málaga
Spain

Esther Asedegbega-Nieto
Departamento de Química Inorgánica y
Química Técnica
Facultad de Ciencias
UNED
Paseo Senda del Rey, nº 9
28040 Madrid
Spain

Rodrigo Briones
Centro de investigación de polímeros
avanzados (CIPA)
Edificio de Laboratorio CIPA
Avenida Collao
1202 Concepción, Bío-Bío
Chile

Juan Antonio Cecilia
Departamento de Química Inorgánica
Cristalografía y Mineralogía (Unidad
Asociada al ICP-CSIC)
Facultad de Ciencias
Universidad de Málaga
Campus de Teatinos
29071 Málaga
Spain

Simona M. Coman
University of Bucharest
Faculty of Chemistry
Department of Organic Chemistry
Biochemistry and Catalysis
Bdul Regina Elisabeta 4–12
030016 Bucharest
Romania

Hector de Paz Carmona
Unipetrol Centre for Research and Education
(UNICRE)
Areal Chempark
436 70 Záluží 1
Czech Republic

Jakub Fratczak
Unipetrol Centre for Research and Education
(UNICRE)
Areal Chempark
436 70 Záluží 1
Czech Republic

Inmaculada Funez
Inorganic Chemistry
Crystallography and Mineralogy
University of Malaga
29071 Malaga
Spain

Cristina García
Inorganic Chemistry
Crystallography and Mineralogy
University of Malaga
29071 Malaga
Spain

José Miguel Hidalgo
Unipetrol Centre for Research and Education
(UNICRE)
Areal Chempark
436 70 Záluží 1
Czech Republic
jose.hidalgo@unicre.cz

Antonia Infantes Molina
Departamento de Química Inorgánica
Cristalografía y Mineralogía (Unidad
Asociada al ICP-CSIC)
Facultad de Ciencias
Universidad de Málaga
Campus de Teatinos
29071 Málaga
Spain

https://doi.org/10.1515/9783110538151-205

E.F. Iliopoulou
Chemical Process and Energy Resources Institute
CERTH
Thermi
570 01 Thessaloniki
Greece

Francisco Ivars-Barceló
Departamento de Química Inorgánica y Química Técnica
Facultad de Ciencias
UNED
Paseo Senda del Rey, nº 9
28040 Madrid
Spain

S.A. Karakoulia
Chemical Process and Energy Resources Institute
CERTH
Thermi
570 01 Thessaloniki
Greece

A.A. Lappas
Chemical Process and Energy Resources Institute
CERTH
Thermi
570 01 Thessaloniki
Greece

Pedro Jesus Maireles
Inorganic Chemistry
Crystallography and Mineralogy
University of Malaga
29071 Malaga
Spain

A. Margellou
Chemical Process and Energy Resources Institute
CERTH
Thermi
570 01 Thessaloniki
Greece

Vasile I. Parvulescu
University of Bucharest
Faculty of Chemistry
Department of Organic Chemistry
Biochemistry and Catalysis
Bdul Regina Elisabeta 4–12
030016 Bucharest
Romania
vasile.parvulescu@chimie.unibuc.ro

A. Pineda
Chemical Process and Energy Resources Institute
CERTH
Thermi
570 01 Thessaloniki
Greece

and

Departamento de Química Orgánica
Universidad de Córdoba
Campus de Rabanales
Edificio Marie Curie (C-3)
Ctra Nnal IV, km. 396
E-14014 Cordoba
Spain

Enrique Rodríguez-Castellón
Departamento de Química Inorgánica Cristalografía y Mineralogía (Unidad Asociada al ICP-CSIC)
Facultad de Ciencias
Universidad de Málaga
Campus de Teatinos
29071 Málaga
Spain
castellon@uma.es

Luis Serrano
Inorganic Chemistry and Chemical Engineering Department
University of Cordoba
14014 Cordoba
Spain

S.D. Stefanidis
Chemical Process and Energy Resources Institute
CERTH
Thermi
570 01 Thessaloniki
Greece

K.S. Triantafyllidis
Department of Chemistry
Aristotle University of Thessaloniki
541 24 Thessaloniki
Greece

and

Chemical Process and Energy Resources Institute
CERTH
Thermi
570 01 Thessaloniki
Greece

Kokkarachedu Varaprasad
Centro de investigación de polímeros avanzados (CIPA)
Edificio de Laboratorio CIPA
Avenida Collao
1202 Concepción, Bío-Bío
Chile

Inmaculada Funez, Cristina García, Pedro Jesus Maireles, Luis Serrano

1 Furfural derivatives from agricultural and agri-food wastes by heterogeneous catalysis

1.1 Introduction

Currently, the depletion of fossil fuel reserves, which account for 75% of the world's primary energy consumption [1], together with the persistent price of crude oil and environmental concerns such as the increase of greenhouse gases or acid rain due global warming and pollution are driving the development of alternative and clean synthetic routes to produce chemicals and fuels from nonfossil carbon sources, such as renewable energies. There are interesting alternatives to reduce our dependence on oil as the main energy resource, such as electric vehicles, the use of solar energy, hydrogen batteries or biofuels [2].

For the most developed nations, which for the most part lack energy resources, guarantee the security of energy supply, it is vital to maintain their industry, their economy and their social welfare model. To this end, a series of measures are being adopted, such as those included in the Kyoto Protocol (1997) [3] to reduce greenhouse gas (GHG) emissions or the "20/20/20 package" (2008) of the European Union [4], which aims to reduce these emissions at European level, so that by 2020, 20% of the energy consumed comes from renewable sources, and that the consumption of biofuels reaches 10%. Other countries such as the US, China and so on are also developing policies in this same direction.

On the other hand, fossil fuels are used as raw material in a multitude of processes, such as the synthesis of a wide variety of chemical products. Unlike other renewable energy sources, biomass can be used both for the production of energy and for obtaining fuels and chemical products. In this context, the industrialized countries have begun to reconsider biomass as a raw material of enormous potential, given its renewable nature, its wide geographical distribution and its high carbon content, which would allow the development of a whole chemical industry similar to that of the one that derives from fossil fuels, mainly petroleum (petrochemical industry), in the current refineries. In this way, the production of future transportation fuels and chemical products requires the deployment of new catalytic processes that transform biomass into products with high added value under competitive conditions [5].

Recently, *the use of lignocellulosic biomass*, composed mostly of carbohydrates, has been used to produce the so-called second-generation biofuels and chemical products derived from biomass. In addition, it is considered more beneficial from the geopolitical and environmental point of view. Therefore, in this context, the use

https://doi.org/10.1515/9783110538151-001

of lignocellulosic biomass seems to be one of the most attractive and promising options to achieve a more sustainable production of fuels and chemical products [5].

1.2 Lignocellulosic biomass

Biomass refers to the set of organic matter of biological origin and that originated through processes of transformation of it, either produced naturally or artificially, but always in a recent time on a human temporal scale. This definition excludes organic matter of fossil origin that, although it is organic biological material, has its origin millions of years ago.

Thus, AENOR uses the definition of the European Technical Specification CEN/TS 14588 to catalog biomass as "all material of biological origin excluding those that have been included in geological formations undergoing a process of mineralization," among which would be oil, coal and natural gas [6].

Therefore, any organic matter of a renewable nature can be considered biomass, being the case of wood and waste generated in its manufacture, agricultural crops and their residues, energy crops, urban waste, animal waste, waste from the processing of food and plants aquatic (Figure 1.1). Currently, most of the energy coming from biomass is produced from wood and its residues (64%) [7].

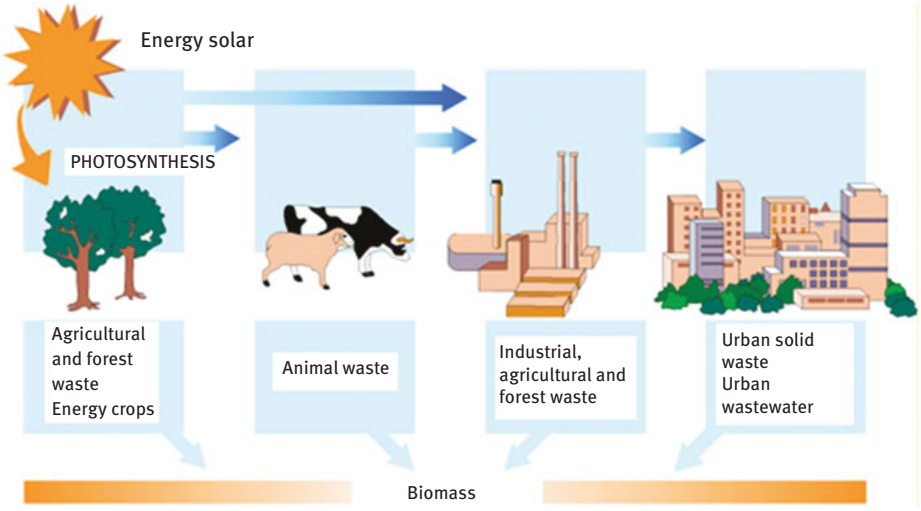

Figure 1.1: Different sources of biomass production.

In recent times, oil, natural gas and, to a lesser extent, coal have been the main sources of organic raw material to obtain a large part of chemical products. Biomass is

the only renewable source of carbon-based energy that allows the production of chemicals, materials and fuels. Among the renewable resources, lignocellulosic biomass is considered of great interest due to its abundance, its low cost as a raw material for the production of chemical products, fuels and energy to replace fossil resources and, in addition, it is not too competitive with the food industry, so it is considered potentially more sustainable [8, 9].

1.2.1 Chemical composition

Lignocellulose is a material whose main constituents are cellulose (40–50% by weight), hemicellulose (25–35%) and lignin (15–20%), which are linked together to provide structural strength and flexibility to the plants (Figure 1.2). In addition, lignocellulosic biomass also contains minor amounts of water and extracts and inorganic compounds ("ashes").

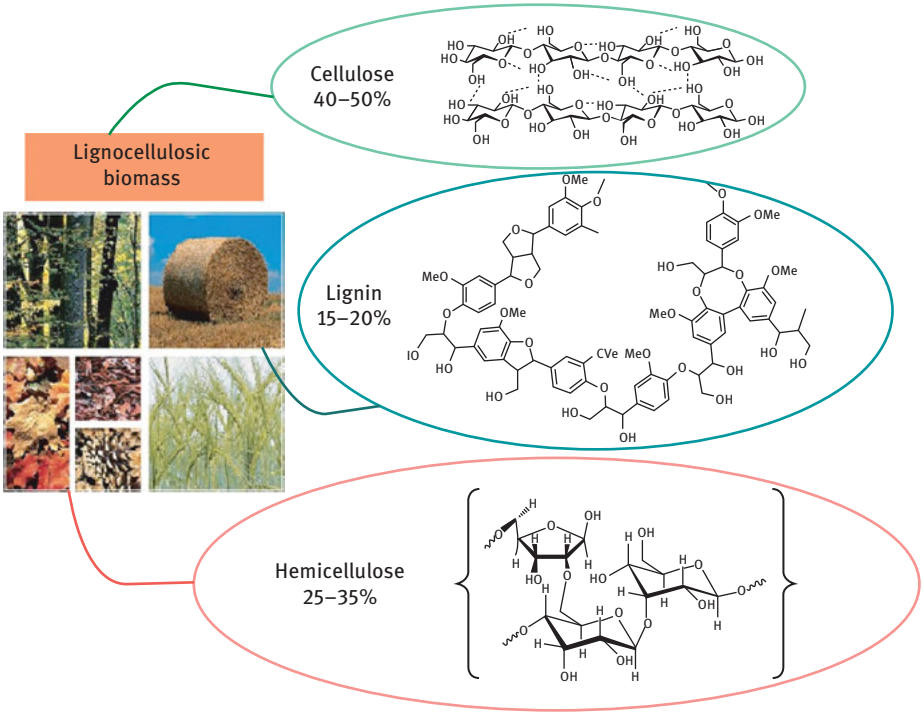

Figure 1.2: Schematic structure of Lignocellulose components.

Due to distinct differences of structure and reactivity of cellulose, hemicelluloses and lignin, they have to be processed under different reaction conditions [10].

The quantity and type of these compounds can greatly influence industrial processes. Next, each of the lignocellulosic material compounds is described.

1.2.1.1 Cellulose

Cellulose is the most abundant homopolysaccharide in nature presenting about 1.5 × 1,012 tons of the annual biomass production. The cellulose macromolecule is composed of D-glucose monomer units connected to each other via β-1,4-glycosidic bonds (Figure 1.2, green circle). The degree of polymerization (DP) of cellulose is dependent on the cellulose source. Cellulose chains in primary plant cell walls have a DP ranging from 5,000 to 7,500 glucose units, and in wood and cotton-based materials between 10,000 and 15,000 units [11].

Each repeating unit of cellulose contains three hydroxyl groups, which are involved in networking of the units with hydrogen bonds. The intrachain hydrogen bonding between hydroxyl groups and oxygen of the adjacent ring molecules makes the linkage stable and results in the linear configuration of the cellulose chains [12].

The cellulose structure consists of crystalline and amorphous domains. The hydroxyl groups in cellulose chains form intra- and intermolecular hydrogen bonds constituting the crystalline structure. The crystalline structure of cellulose can be classified into seven allomorphic forms denoted as cellulose I_α, I_β, II, III_I, III_{II}, IV_I and IV_{II}. Celluloses I_α and I_β are the major crystal forms in nature and are also known as *native cellulose*. Among all forms, cellulose II is the most thermodynamically stable. It can be formed from celluloses I_α and I_β by treatment with aqueous sodium hydroxide or through dissolution of cellulose and subsequent regeneration [12]. The arrangement of cellulose molecules with respect to each other and to the fiber axis determines the physical and chemical properties of cellulose. The fiber structure of cellulose provides its high chemical stability. Crystalline domains of cellulose are less accessible to chemical reactants. On the other hand, amorphous regions are easily penetrated by reactants during chemical reactions [12]. The reactivity of cellulose can be determined by several factors such as hydrogen bonding, the length of chains, the distribution of chain length, the crystallinity and the distribution of functional groups within the repeating units and along the polymer chains [11].

For the transformation of cellulose into alkanes, it must be broken down into their corresponding monomers, glucose, and then followed with the total hydrodeoxygenation. By pretreatment and acid-catalyzed hydrolysis, cellulose can be decomposed to hexose via water-soluble oligosaccharides, and then liquid fuels and other value-added chemicals can be produced through dehydration, hydrogenation and hydrogenolysis over different catalysts [13–16]. There are several routes for cellulose conversion to alkanes through deconstruction and hydrodeoxygenation.

1.2.1.2 Lignin

Lignin is an amorphous, thermoplastic polymer, with three-dimensional structure based on subunits of phenylpropane (aromatic monomers) that provide stiffness to plants (Figure 1.2, blue circle). Lignin is associated with cellulose and hemicellulose to form lignocellulose, and is found coating the whole, being very chemically inert and providing the material with a high resistance to chemical and/or biological attacks.

Lignin is the only large-volume renewable aromatic feedstock, which is found in most terrestrial plants typically in a range of 15–30% by dry weight and 40% by energy [17, 18]. The monomers from the depolymerization of lignin are a complex mixture of different phenolic compounds including phenol, syringol, guaiacol and other derivatives, which is impeditive to be directly used as fine chemicals or fuels [19]. Most of lignin obtained from the pulp and paper factory is directly burned. Therefore, the conversion of lignin with its unique structure has enormous potential as an important source for the sustainable production of liquid alkanes, aromatics and value-added chemicals [20–23].

1.2.1.3 Carbohydrates

It should be noted that most of the lignocellulosic biomass is composed of carbohydrates (65–85%), from which a large variety of chemical products can be obtained economically and on a large scale.

The hemicellulose is a complex structure of carbohydrates and is the second most abundant polysaccharide after cellulose in plant cell walls, accounting for 15–30% of lignocellulosic biomass by weight [24]. Among the three main components in biomass, hemicellulose is a promising material to produce value-added chemicals. Unlike cellulose, hemicellulose consists of short, highly branched polymer of five- and six-carbon polysaccharide units, such as xylan, mannan, β-glucans and xyloglucans [25–27], formed mainly by five types of monomeric sugars: D-xylose, L-arabinose, D-galactose, D-glucose and D-mannose, with xylose being the most abundant (Figure 1.2, pink circle).

The highly branched and amorphous nature of hemicellulose enables it to be easily converted. Noteworthy is that hemicellulose has a much lower DP (100–200 U) compared with that of cellulose and lignin. Hemicellulose is more unstable than cellulose and therefore, degrades more easily when subjected to heat treatment [28].

So, the development of effective methods toward the selective conversion of hemicellulose in products with high yield and selectivity is crucial in facilitating the effective utilization of the same, avoiding significant decomposition of cellulose and lignin.

Hemicellulose shows many excellent properties, including biodegradability, biocompatibility, bioactivity and so on, which enable it be applied in a variety of areas such as food, medicine, energy, chemical industry and polymeric materials

[29–34]. At present, there are many researches about the conversion of cellulose and lignin; however, the reports about hemicellulose conversion are limited.

The C5 sugars mainly xylose obtained from hemicellulose have a great potential in the preparation of several platform chemicals like levulinic acid for current chemical industry [35]. In addition, the pretreatment methods of hemicellulose to monomers are similar with that of cellulose, mainly including physical, chemical and physicochemical processes under relatively mild pretreatment conditions [36, 37]. Recently, there are numerous researches concentrated on the catalytic transformation of hemicellulose, starting from the hydrolysis to pentose, then further dehydration to furfural [31, 38, 39] or hydrogenation to xylitol [40–42].

On the other hand, the conversion of biomass involves multiscale complexity from molecular to macro raw biomass level, which limits the conversion of biomass into valuable products [43–45].

Thus, there are two main strategies for the processing of lignocellulosic biomass [46]:

- *Thermochemical routes* that allows lignocellulose to be processed directly at high temperatures and/or pressures without the need for any prior treatment (pyrolysis, gasification, combustion or liquefaction).
- *Fractionation and hydrolysis* by means of which the sugars and the lignin are separated and processed selectively, either by chemical route or by biological route.

In general, the hydrolysis of the biomass is more complex and more expensive than the thermochemical conversion.

All treatment must meet a series of requirements [47, 48]:

1. Improve the formation of sugars or the ability to form them later in hydrolysis.
2. Avoid the degradation or loss of carbohydrates.
3. Avoid the formation of by-products that they can inhibit later stages as in the processes of hydrolysis and fermentation.
4. Must be profitable.

Therefore, the lignocellulosic biomass can be the source to obtain different high added value products, among which are the furfural and 5-hydroxymethylfurfural (HMF). Among the three main biomass components, hemicellulose is a promising resource to produce furfural.

Furfural (furan-2-carboxaldehyde) is a viscous, colorless liquid, with a boiling point of about 160 °C. It has a pleasant aromatic odor and turns dark, brown or black when exposed to air. It is identified by the US Department of Energy (DOE) as one of the top 12 value-added products and is a valuable product with a word market of around 300,000 tons per year [49, 50].

Furfural is a key platform chemical produced in lignocellulosic biorefineries could further be transformed to fuels and useful chemicals, which is widely used in oil refining, plastics, and pharmaceutical and agrochemical industries [5]. For

example, the papers in books contain hemicelluloses that are the sources of furfural. Furfural is one of the many chemicals that contribute to the aroma of books. On the other hand, furfural is used in agriculture/horticulture as a weed killer [51]. Furfural is the active ingredient in several nematicides such as crop guard and protected, which are currently used in parts of Africa [52].

Furfural is generally recognized as safe and easy to apply. It is a natural degradation product of vitamin C (ascorbic acid) and it is a significant component of wines and fruit juices. Despite the fact that furfural has an LD50 of 2,330 $mg \cdot kg^{-1}$ for dogs, its toxicity to humans is relatively low [53]. Cocoa and coffee have the highest concentrations of furfural (55–255 ppm). Its concentration in alcoholic beverages is 1–33 ppm and 0.8–26 ppm in brown bread [54]. A few bioplastics companies make use of furfural as a building block in their bioplastics chemistry or have expressed an interest in using furfural provided that there are supply and price security [55].

Today, the major part of furfural production (90%) is carried out in three countries, with China leading the market followed by South Africa and the Dominican Republic [56]. China is the major producer as well as major consumer of furfural in the world. Low production cost of furfural in China is expected to remain a key driving factor for the domestic market. However, the furfural industry in China has been facing an issue of availability of corn cob [38].

The first commercial process for the production of furfural was developed by the company QuakerOats in 1921 and was carried out in a batch reactor, using oats shells as raw material and sulfuric acid as a catalyst, both for hydrolysis and for dehydration. Nowadays, most of the furfural is obtained in continuous processes, such as the modified Huaxia technology used in China, or the Supra Yield process used in Australia.

Today, furfural is produced industrially by the use of batch or continuous reactors, by a one-step or a two-step process (Figure 1.3). In the one-step process, pentosans are hydrolyzed into xylose and then dehydrated into furfural simultaneously.

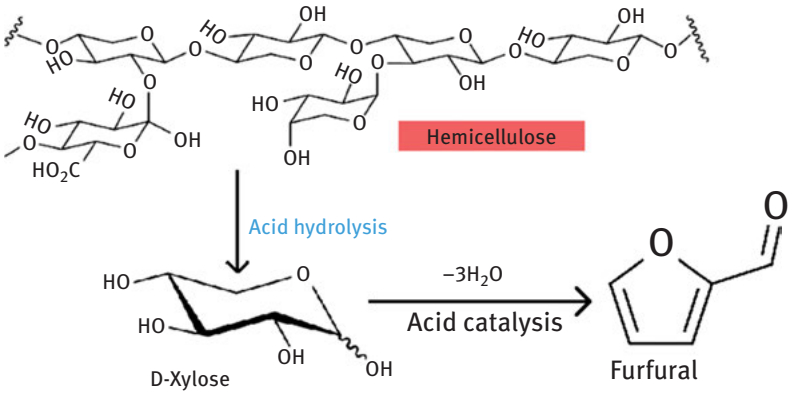

Figure 1.3: Conversion of hemicellulose to furfural by acid catalysis.

However, in the two-step process, hydrolysis of pentosans occurs under mild conditions followed by the dehydration of xylose into furfural [57, 58].

The advantage of the two-step process is that a higher quantity of furfural is produced when compared to the one-step process. Again, solid residues are less degraded and can be converted to other chemicals such as ethanol, phenol, glucose and others in the subsequent step by fermentation.

1.3 Application of furfural derivatives

The furfural turns out to be a very versatile precursor for the synthesis of a great variety of chemical products, which we will talk about later, such as furfuryl alcohol (FOL), furoic acid, furan, tetrahydrofurfuryl alcohol (THFA), tetrahydrofuran (THF), 2-methylfuran (2-MF) or 2-methyltetrahydrofuran (2-MTHF) [53, 59] (Figure 1.4). Many of them are very interesting from an industrial point of view, since they are either commercial or are currently obtained from fossil fuels. An investigation, supported by US DOE to identify the most promising platform chemicals, revealed that furfural and two of its derivatives, furan dicarboxylic acid and levulinic acid were ranked among the list of 30 chemicals.

1.3.1 Furfuryl alcohol (FOL)

It should be noted that between 60–65% of the furfural synthesized in the industry is used for the production of FOL (Figure 1.4, pink circle), which is the most important derivative of furfural, and can be used individually or in combination with phenol, acetone or urea to make resins in the production and manufacture of casting molds, automotive brake linings, abrasive wheels and refectory products of the steel industry, fiberglass and some aircraft components. When phenols are reacted with the corresponding furfural derivatives, FOL, used in the production of thermosetting furan resin and furan cement is formed [60, 61]. On the other hand, furfural stops tropical deforestation, which is responsible for GHG emissions. FOL is the main ingredient in wood-modification processes that convert softwoods to products that look like and have properties that are similar to tropical hardwoods. Furfurylation of wood produces nontoxic woods, suitable for internal and external applications that demand high performance and good aesthetic appearance such as playgrounds, floors, cladding and so on.

FOL has also been used in reinforced carbon–carbon composite materials, developed to protect the shuttle around its nose and wing leading edge from extremely high and cold temperatures (–121–1,649 °C) encountered during the reentry of shuttles into space. NASA created the US space shuttle orbiter thermal protection system [62]. In

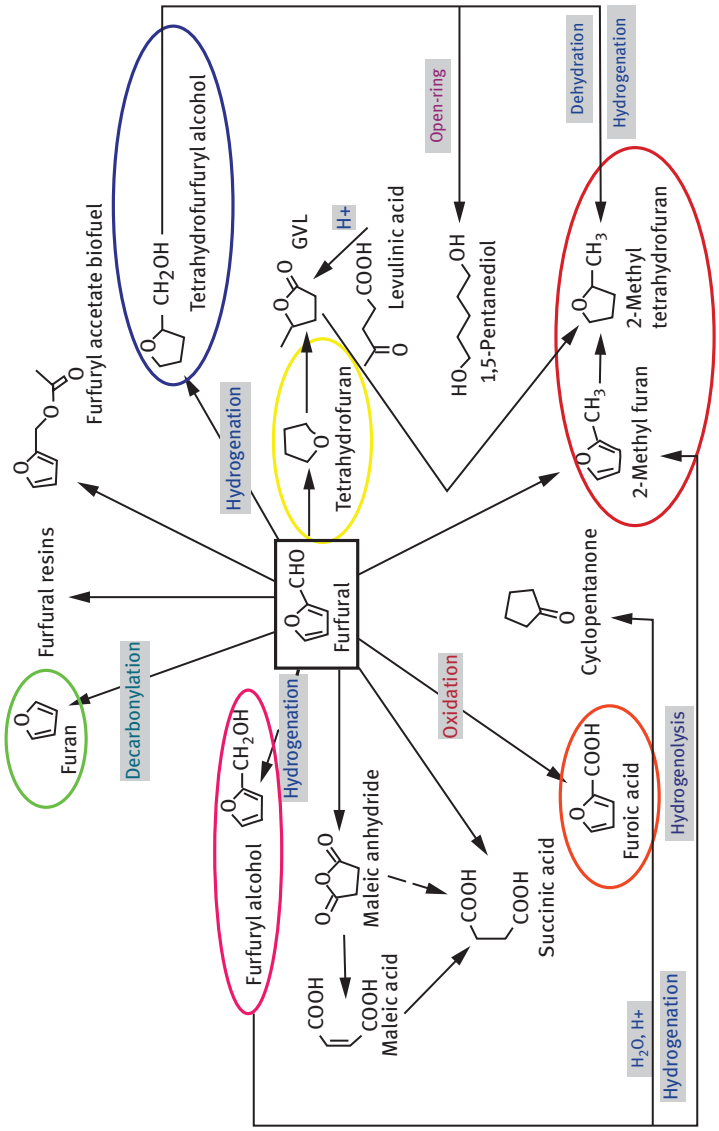

Figure 1.4: Conversion of furfural to value-added chemicals. Adapted from [5].

this system, after pyrolysis and rough trimming of graphite fabric, the polymer resin is converted into carbon, which is then impregnated with FOL. With further pyrolysis, the density of this material is increased leading to improved mechanical properties.

1.3.2 Furoic acid

Furoic acid is the first down-line oxidation derivative of furfural (Figure 1.4, orange circle). It is a versatile starting material for the synthesis of pharmaceutical, agricultural and industrial chemicals. Furoic acid is extensively converted to furoyl chloride, used in the production of drugs and insecticides. The furan ring is an important pharmacophore in modern drug discovery.

Furan-2,5-dicarboxylic acid, an important renewable building block that can substitute for terephthalic acid in the production of polyesters, is produced from furoic acid.

1.3.3 Furan

Furan is also deployed as a chemical intermediate and solvent is a family of organic compounds of the heterocyclic aromatic series, characterized by a five-membered aromatic ring, consisting of four CH_2 groups and one oxygen atom (Figure 1.4, green circle). Furan resins, having excellent chemical and heat transfer resistances, have a wide range of applications as foundry sand binders, chemically resistant cements and as laminates in chemical plants [63]. Furthermore, user-friendly furan resin systems have been developed for a variety of composite applications in the automotive and building industries as the interior of aircraft cabins, internal fittings for buildings and rail carriages [63, 64].

1.3.4 Tetrahydrofurfuryl alcohol (THFA)

THFA is a widely used precursor in the production of specialty chemicals (Figure 1.4, blue circle). It is also employed as a catalyst binder for new pebblebed reactors [65]. In this case, 5-chloromethyl furfural can be synthesized to prothrin, a synthetic pyrethroid insecticide.

1.3.5 Tetrahydrofuran (THF)

When furfural is hydrogenated, THF is formed (Figure 1.4, yellow circle). This derivative of furfural is a very important commercial solvent used as the starting material

in the production of nylon and polytetramethylene ether glycols (spandex) by polymerizing THF. Polyester is a synthetic polymer made of purified terephthalic acid.

Polytetramethylene ether glycol or poly-THF is a polymer, used in the manufacture of spandex fiber (e.g., Invista-Lycra®) and polyurethanes. Currently, they are produced from crude-oil-derived chemicals. However, the synthesis of its green equivalent can be achieved via furfural, furan, THF or polytetramethylene ether glycols.

1.3.6 Methyltetrahydrofuran (2-MTHF) and 2-methylfuran (MF)

The aldol condensation of furfural and acetone followed by hydrogenation leads to the production of high yields of liquid alkanes, which are used as transportation fuels [66]. Furfural can be converted by hydrogenation to 2-MF and 2-MTHF, which are used as gasoline additives (Figure 1.4, red circle).

2-MTHF has the potential application for green fuel production in the so-called P-series, developed in USA [67], which are blends of ethanol, butanol and 2-MTHF with higher alkanes, and are used to solve the cold start issues of pure ethanol fuels. Pertaining to second-generation biofuel [59, 68, 69], 2-MTHF has several advantages, such as high energy density compared to those of ethanol and gasoline, a lower heating value, which resembles that of gasoline and is higher than that of ethanol [70], so it is also considered as a platform chemical for the near future. On the other hand, MF is also often used as solvent and as feedstock for the production of antimalarial drugs (chloroquine), methylfurfural and nitrogen and sulfur heterocycles.

1.4 Substitution of oil refineries products: Biorefinery concept

As we have seen throughout the chapter, biomass has a quite complex composition, and so previous separation treatments are necessary in the main groups of components. The subsequent treatment and processing of these substances gives rise to a whole range of products. Therefore, the need arises for an installation in which this type of operations can be carried out, where biomass is used as a renewable source of energy, chemical products and biofuels, thus giving rise to the concept of biorefinery.

The definition of biorefinery is becoming increasingly important in the area of new sustainable technologies. There are several definitions of biorefinery, being relevant the one formulated by the International Energy Agency (IEA) Bioenergy, associated with the sustainable treatment of biomass for the production of bioproducts and bioenergy: a biorefinery is based on a set of processes that use biological sources or raw materials renewable to produce a product or final products, so that the

amount of waste is minimal, and through which each component of the process is converted or used in a way that increases its value, thus improving the sustainability of the plant [71].

So, IEA Bioenergy has developed the following definition for biorefinery: "Biorefinery is the sustainable processing of biomass into a spectrum of marketable products and energy."

IEA Bioenergy is an organization setup in 1978 by the IEA, with the aim of improving cooperation and information exchange between countries that have national programs in bioenergy research, development and deployment. IEA Bioenergy's vision is to achieve a substantial bioenergy contribution to future global energy demands by accelerating the production and use of environmentally sound, socially accepted and cost-competitive bioenergy on a sustainable basis, thus providing increased security of supply while reducing GHG emissions from energy use. The major objective is to assess the worldwide position and potential of the biorefinery concept, and to gather new insights that will indicate the possibilities for new competitive, sustainable, safe and eco-efficient processing routes for the simultaneous manufacture of transportation biofuels, added value chemicals, power and heat and materials from biomass. Therefore, the definition of biorefinery is analogous to that of a conventional oil refinery, with the difference that biomass is used as a raw material instead of oil, in such a way that GHG emissions are reduced (Figure 1.5) [72].

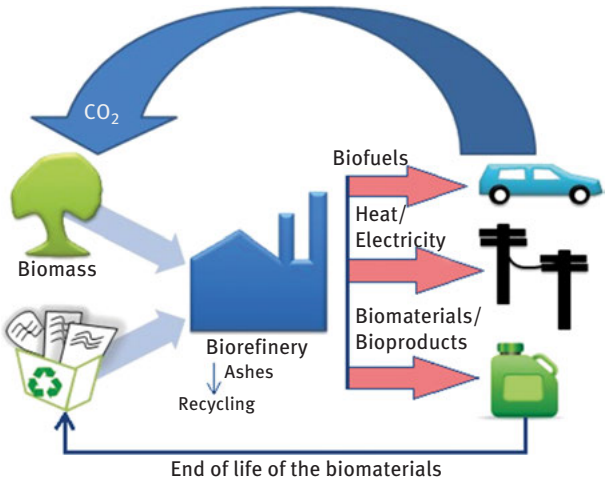

Figure 1.5: Sustainable technology of an integrated biorefinery.

Apart from this, another objective of such a bio-economy based on a significantly increased use of biomass for energy and materials is to replace conventional crude

oil-based processes or products, respectively, by ones based on renewable biogenic resources characterized by a significantly lower effect on global climate.

Taking into account all the above, we must consider some important aspects when talking about biorefineries:

- A main driver for the establishment of biorefineries is the sustainability aspect. All biorefineries should be assessed for the entire value chain on their environmental, economic and social sustainability covering the whole life cycle (construction–operation–dismantling).
- A biorefinery is the integral upstream, midstream and downstream processing of biomass into a range of products.
- A biorefinery can use all kinds of biomass from forestry, agriculture, aquaculture and residues from industry and households including wood, agricultural crops, organic residues (both plant and animal derived), forest residues and aquatic biomass (algae and seaweeds).
- A biorefinery should produce a spectrum of marketable products and energy. The products can be both intermediates and final products, and include food, feed, materials and chemicals, whereas energy includes fuels, power and/or heat. The volume and prices of present and forecasted products should be *market competitive*.

1.4.1 Classification of biorefineries

The concept of biorefinery has evolved over time, since initially these were facilities that processed a single type of raw material, which was subjected to a process and a single product was obtained (first generation biorefineries). Subsequently, they began to develop biorefineries similar to the previous ones, but which allowed obtaining different products depending on different external factors, such as demand or price (second-generation biorefineries). Currently, although they are in research and development, the trend is toward the implementation of biorefineries that process different types of raw materials, which undergo different transformation processes and generate a wide variety of products (third-generation biorefineries), so that they can become comparable to conventional refineries [73]. In this way, future applications of biomass will be based on a single facility, called *integrated biorefinery*, where all the fractions and byproducts of biomass will be used to produce energy (electricity, heat), biofuels, chemical bioproducts and biomaterials. This will increase the profitability of the use of biomass as a raw material and will achieve greater flexibility in the face of possible market fluctuations.

The number of different types of biorefineries is currently in continuous growth, so giving a general classification is complicated. Recently, the IEA has developed a fairly complete classification, so that each biorefinery can be classified according to

four main variables: platforms, products (energy and bio-based materials and chemicals), raw materials and processes [74].

The platforms (e.g., sugars C5/C6, synthesis gas, biogas) are intermediates that can connect different biorefinery systems and their processes, although they can also be a final product itself. The number of platforms involved is an indication of the complexity of the system. The two groups of biorefinery products are energy (e.g., bioethanol, biodiesel, synthetic biofuels) and products (e.g., chemicals, materials, food and feed). The two main groups of raw materials are "energy crops" from agriculture (e.g., starch crops, short-rotation forestry) and "biomass residues" from agriculture, forestry, trade and industry (e.g., straw, bark), wood chips from forest residues, used cooking oils and waste streams from biomass processing. In the classification system, a differentiation was made between four main conversion processes, which include biochemical, thermochemical, chemical and mechanical processes [75].

Within the thermochemical process, there are two main ways to convert biomass into energy and chemical products. The first is gasification, which consists of maintaining the biomass at high temperature (> 700 °C) with low oxygen levels to produce syngas, which can be used directly as a stationary biofuel or can be a chemical intermediate (platform) for the production of fuels (FT fuels, dimethyl ether, ethanol, isobutene) or chemicals (alcohols, organic acids, ammonia, methanol and so on). The second thermochemical way to convert biomass is pyrolysis, which uses intermediate temperatures (300–600 °C) in the absence of oxygen to convert the raw material into liquid pyrolytic oil (or bio-oil), solid carbon and gas-like light gases of synthesis [76, 77].

On the other hand, biochemical processes occur at lower temperatures and have lower reaction rates. The most common types of biochemical processes are fermentation and anaerobic digestion. The fermentation uses micro-organisms and/or enzymes to convert a fermentable substrate into recoverable products (usually alcohols or organic acids). The main final product of these processes is biogas, which can be used as a substitute for natural gas [78].

Mechanical processes are processes that do not change the state or composition of the biomass, but only make a reduction in size or a separation of the components of the raw material. In a biorefinery route, they are usually applied first. The separation processes involve the separation of the substrate into its components, while extraction methods extract and concentrate valuable compounds from a voluminous and nonhomogeneous substrate [79]. Lignocellulosic pretreatment methods (e.g., the division of lignocellulosic biomass into cellulose, hemicellulose and lignin) fall into this category, even if part of the hemicellulose is also hydrolyzed to individual sugars [80].

As for the chemical processes, they are those that carry a change in the chemical structure of the molecule when reacting with other substances. Hydrolysis and transesterification are the most common in biomass conversion, but this group also includes the broad class of chemical reactions in which a change in the molecular

formula occurs. Hydrolysis uses acids, alkalis or enzymes to depolymerize polysaccharides and proteins into their component sugars or chemical derivatives [80], while transesterification is a chemical process by which vegetable oils can be converted into methyl or ethyl esters of fatty acids, being currently the most common method to produce biodiesel.

By combining the four main variables in which we can classify a biorefinery, the different configurations of existing biorefineries can be described in a consistent manner (Figure 1.6).

Because some processes are suitable for more than one platform, some are interconnected, thus combining two or more types of biorefineries, so allowing fossil resources to be replaced more efficiently, to obtain energy, materials and chemical products.

Thus, of all the variables existing within a biorefinery, the most important classification is the one that is made according to the different platforms, which are considered the basic pillars for the classification of biorefineries, as listed in Table 1.1.

The biomass demand for food, feed, materials and energy will significantly increase in the future due to growing world population. As a sustainable expansion of cultivation areas is only possible to a very limited extent, it is necessary to optimize the entire biomass utilization. Biorefinery concepts in which a wide variety of biomasses are completely converted to different marketable products with minimal energy input without generating waste offer appropriate solutions. In developing such concepts, however, the already existing structures and existing biomass conversion facilities should be taken into account and included.

1.5 The use of agricultural wastes to high added value products

Agriculture wastes are very challenging nowadays and there are many available in our environment every day. Green chemicals and bio-based products should derive from a wide range of agro-bioenergy coproducts and agricultural residues; therefore, the main challenge for big players and stakeholders is to transform complex, heterogeneous and disposable biomasses into really valuable and marketable high value-added products in place of fossil sources alone. These organic residuals include mainly raw feedstocks that are finely converted into many high value-added products.

The largest portion of plant-based waste is from the nongrain part of crops, such as wheat straw, rice straw and corn stover. The high availability and relatively stable composition of these agricultural byproducts make them promising feedstocks in large-scale industrial biorefineries [81]. The second largest food waste is from the beverage

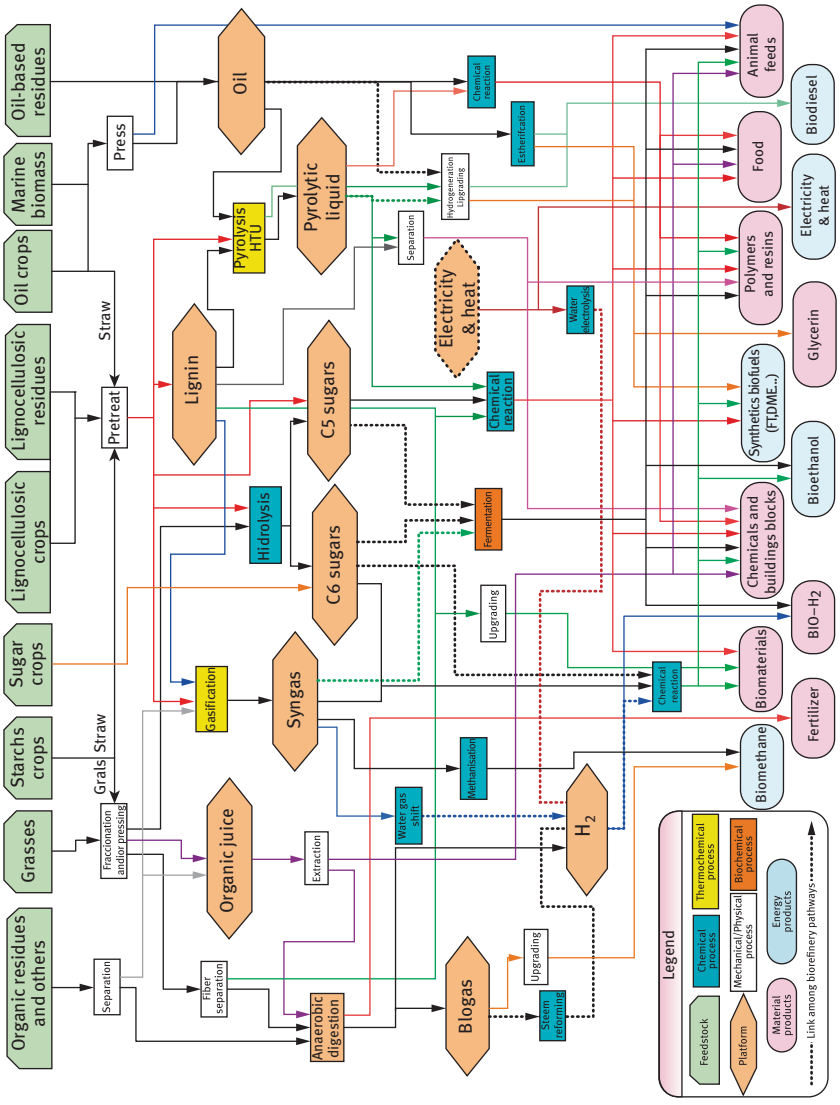

Figure 1.6: Connection between individual biorefineries according to the classification of IEA. Reproduced with permission from [74].

Table 1.1: Classification of the main platforms within an integrated biorefinery.

Platform biorefinery	Raw material	Obtention process	Products
Biogas	Mixes CH_4 and CO_2	Anaerobic digestion	Volatile carboxylic acids, fertilizers, hydrogen
Syngas	Mixture of CO and H_2	Gasification	Biofuels and/or chemicals: FT diesel, dimethylether, bioethanol, ethylene, propylene, butadiene, acetic acid, CO_2, gases C1–C5, hydrogen
Oleochemical	Vegetable oil, acids and fatty esters and glycerol	Grinding, pressing, filtering, extraction, refining	Biodiesel, acids and fatty esters, fatty alcohols, diols, epichlorohydrin, glycerol
Lignocellulosic	Lignocellulosic crops, agricultural, harvesting and forest residues, industrial and urban waste	Fractionation, grinding, delignification, hydrolysis, gasification	2,5-Furandicarboxylic acid (FDA), acetic acid, formic acid, levulinic acid, C5 and C6 sugars, diols, furfural, hydroxymethylfurfural (HMF), synthesis gas, γ-valerolactone
Sugars	Algae, alcoholic crops, industrial and urban waste, lignocellulosic crops	Extraction, grinding, pressing, drying/ dehydration, liquefaction, pyrolysis, hydrolysis, refining, fermentation and enzymatic hydrolysis	FDA, citric acid, furoic acid, Lactic acid, fevulinic acid, malic acid, pyruvic acid, propanol, furfuryl alcohol, 2,3-butanediol, isopropanol, aspartic acid, glutamic acid, fermentable sugars, CO2, acetone, xanthan, vitamins, unicellular protein, furan, HMF, MTHF, THF, enzymes, 1,3-butadiene, Isoprene, xylene, γ-valerolactone, polyethylenefuranoate, sorbitol, xylitol, mannitol, bioethanol, biokerosene

industry, which generates a large amount of pomace, such as grape pomace and apple pomace. Besides plant fibers, the pomace contains considerable quantities of high-value functional compounds, such as polyphenols, essential oils and vitamins [82, 83].

As we have seen throughout the chapter, cellulose can be used to produce biofuels, organic acids and nanocellulose materials; hemicellulose can be degraded to xylose, and then xylite and furfural, which are valuable chemical products and lignin is used as natural binder and adhesives. Besides structural compounds, other reserves rich in plant-derived waste including sugars, proteins and oils and phytochemicals also show potential for various applications.

Fruit and vegetable wastes are generated by agriculture, postharvest grading and mass discarded by consumers in industrialized regions such as North America, Europe and parts of Asia. Currently, most of them are used as low-value animal feed and only a small portion of the wastes is used as feedstock for the extraction of phytochemicals, soluble and insoluble dietary fibers [84]. Proteins in plant-derived waste with well-balanced essential amino acids can be introduced to food to enhance sensory and functional properties. For example, soy protein has been used in imitation cheese, soy milk and whipped toppings [85]. Phytochemicals, such as polyphenols and carotenoids, have been related to health promoting effects including lowering cholesterol and lipid oxidation [86]. Besides health promoting effects, the addition of these antioxidant compounds into food matrices can extend their shelf life and delay the formation of off-flavors of food products and rancidity [85]. Vegetable oils in plant-derived waste can be used to derive sugar-based surfactants (e.g., alkyl polyglucosides) with low toxicity and good detergent properties compared to traditional surfactants derived from fossil oil [87].

On the other hand, citrus fruits are among the most abundant crops worldwide, with about 121 million tons produced annually [88]. The industrial utilization of these citrus fruits for juice production results in large quantities of waste. Citrus wastes include peels, pulps and seeds, which represent about 50% of the fruit weight [89]. Citrus wastes are good sources for sugars, oils, polyphenols, enzymes, vitamins and minerals. Therefore, there is huge potential of the integrated utilization of citrus wastes to produce multiple high value products. For example, Pourbafrani et al. developed an integrated process using citrus waste to obtain multiple value-added products: D-limonene, ethanol, pectin and biogas [90].

Grape is the world's second largest fruit crop with an annual production of more than 60 million tons. About 80% of grapes are used to produce wine, which is one of the most important alcoholic beverages in the world, with an increasing demand to 25 billion liters [85]. Winery wastes can be divided into four categories: grape stalks, grape pomace (marc), wine lees and waste water. Many components such as dietary fibers, polyphenols, grape seed oil and tartrates can be separated from winery waste [85].

- Grape stalks as the wastes of vineyards are composed of high concentrations of lignin, cellulose and hemicellulose, which, if fractionated, can be an excellent renewable carbon source. In this sense, Amendola et al. applied autohydrolysis pretreatment on grape stalks followed by a noncatalyzed ethanol organosolv extraction of the solid residue [91]. Ethanol was used to precipitate hemicellulose

in the autohydrolysis liquor, while acid was used to precipitate lignin from both autohydrolysis liquor and organosolv liquid.

- Grape pomace, the main solid waste generated during wine making consists about 50% skin, 25% seed and 25% stem [82]. Grape pomace contains large amounts of polyphenols, lipid, proteins, fiber and minerals [92].
- The biorefinery concept was also applied on wine lees, which are the residues obtained at the bottom of tanks after wine fermentation, during storage, or after centrifuge or filtration of wine [93]. In the study of Dimou et al. wine lees were centrifuged, and the liquid part was distilled to get ethanol. For the solid part, organosolv extraction was applied to recover antioxidants, and the residual solid was treated with HCl to solubilize tartaric acid. Finally, the solid residue after tartaric acid extraction and the ethanol free liquid part were combined as the feedstock for enzymatic lysis of yeast cells to generate nutrients for further poly(3-hydroxybutyrate) production by aerobic fermentation [94].

Likewise, since apple pomace contains valuable compounds such as carbohydrates, pectin and polyphenols, there is an increasing global trend toward the efficient utilization of apple pomace. Approximately 25–30% of the apples are used to produce juice, and the leftover of juice extraction (apple pomace) is normally used as animal feed or compost [83, 95]. Recently, Yates et al. used apple pomace to produce various value-added compounds including sugars, polyphenols, pectin and biomaterials, which can be used as biocompatible scaffolds in tissue engineering [8].

The tomato is another agricultural waste used to obtain high added value products. Millions tons of tomato are processed every year to produce tomato juice, paste and concentrate [96]. During processing, about 4% of the total processed tomatoes are produced as byproducts, including tomato peels and seeds, which are rich in sugars, polyphenols, proteins, oils and organic acids [97]. Kehili et al. used supercritical CO_2 technology to extract carotenoids inside the oil fraction of tomato peels and seeds. The residue obtained was used to extract protein by alkali solubilization and acid precipitation. After that, the protein-free residue was treated by hot water to hydrolyze cellulose and hemicellulose to monomer and oligomer sugars [96].

Cereal grains, the most important sources of calories for the majority of the world's population, have been the primary food source for human since thousands of years ago [98]. Among different cereals, wheat is the major crop in Europe, North America and Oceania and Industrialized Asia. However, in low-income regions such as densely populated region of South and Southeast Asia, rice is the major crop [99].

About 21% of the global food supply depends on wheat, and the production is still increasing to meet the growing demand [100]. During harvesting, wastes such as wheat straw are left on the field. Other byproducts such as wheat bran, germ and

parts of the endosperm are generated during wheat milling [101]. Wheat straw mainly consists of cellulose, hemicellulose and lignin. Kaparaju et al. used wheat straw to produce bioethanol, biohydrogen and methane based on the biorefinery concept [102].

On the other hand, rice is an important staple crop for more than half of the world's population. The global production of rice is about 671 million tons per year [103]. Wastes such as rice straw and rice husk are generated during rice harvesting and processing, and both of them contain a large amount of cellulose, hemicellulose and lignin, which can be good resources for the production of value-added chemicals and biofuels.

In 2015, the world production of corn was estimated at 1,026 million tons, with the US, China and Brazil the leading countries in production [104]. The main components in corn are starch, protein, fiber and oil; therefore, corn is traditionally used as human food or animal feed. During the last 10 years, corn has been increasingly used as feedstock to produce a renewable biofuel, ethanol. Dry grind fermentation is the most popular process used for converting corn to ethanol. The unfermentable residues, including protein, fiber, and oil are collected and dried as distiller's dried grains with solubles (DDGS) [105]. DDGS has been long-time used as a source of carbohydrates, protein and oil for animal feed. However, the increase in DDGS production is expected to drive its value down; thus, there is a great interest to use DDGS as a starting raw material for the production of commodities, platform molecules or specialty chemicals. One approach is to convert fibers, mainly cellulose and hemicellulose, to sugars for ethanol production. Bals et al. applied ammonia fiber expansion process to pretreat DDGS, followed by enzymatic hydrolysis to produce sugars, such as glucose, for ethanol fermentation [106].

As to the oil crop wastes, about 6–20% of the wastes are generated during agricultural production, followed by postharvest and processing processes [99]. For example, after oil extraction, a large amount of oil pressed cakes remains, which contain substantial quantities of protein, minerals, residual oil and other nutrients. These compounds can be recovered and reused in the food industry [107].

The production of olive oil generates approximately four times more wastes than the commercial oil, which is a heavy burden for the industry as well as the environment. Among the wastes generated during olive oil production, olive mill waste is the one that has drawn attention to many researchers. Schievano et al. have proposed an integrated biorefinery concept for the utilization of olive mill waste to produce polyphenols, mono/polyunsaturated fatty acids and biofuels [108].

Particularly, the rapeseed plant is normally used for the production of vegetable oil for human consumption, animal feed and biodiesel synthesis [109]. After oil extraction and biodiesel production, other byproducts such as rapeseed cake and glycerol waste are generated. For example, Luo et al. used rapeseed straw along with cake and glycerol obtained after biodiesel production to produce several biofuels [110].

By last, as to the roots and tubers, potatoes are the major crops in Europe, North America, Oceania and Industrialized Asia [99]. The dominating wastes (20% of the total waste) in these areas are produced during agricultural period. Processing of potatoes is conducted mainly for chips, which generates solid wastes including peels or cull potatoes. These solid wastes are usually composed of starch, fiber, polyphenols and minerals [107]. The nutrients rich in potato wastes can be valorized in an integrated process. For example, Chintagunta et al. incubated potato peels and mash with Aspergillus niger and Saccharomyces cerevisiae to obtain ethanol [111].

Therefore, the recovery of valuable compounds from agricultural wastes is an important challenge for the field-related scientists. Conversely, its commercial implementation is a complex approach depending on several parameters to be considered.

1.6 Catalytic transformation of biomass into furfural derivatives

The catalytic conversion of lignocellulosic biomass into biochemicals and fuels is of great significance. Therefore, the separate and efficient conversion of cellulose, hemicellulose and lignin is of great interest.

As we have seen in Section 1.3, in a biorefinery we distinguish between four main groups of raw material conversion processes: thermochemical, biochemical, chemical and mechanical processes. From some of these processes can be obtained some derivatives of furfural, such as FOL, furan and MF of which we have spoken previously (Figure 1.4).

Furfural can be produced by acid-catalyzed dehydration of xylose obtained from hemicelluloses. However, furfural presents an obstacle for catalytic upgrading processes: first of all, the number of carbons in a furfural molecule after deoxygenation is too low to be added with gasoline; and secondly, furfural is thermally unstable and rapidly polymerizes forming humins. Furfural is highly reactive under typical biomass processing conditions and even at room temperature. This rapid polymerization complicates the condensation approach since the furfural will have already polymerized.

1.6.1 Furfural hydrogenation to furfuryl alcohol (FOL)

Furfural holds two useful functional groups, a carbonyl and a conjugated furan ring, making its role as a versatile building block for various applications. The carbonyl (C=O) group of the furfural ring can be reduced leading to FOL (Figure 1.4, pink circle),

which is the main hydrogenation product obtained from furfural [112]. The industrial production of FOL is performed by selective hydrogenation of furfural in the gas or liquid phase using Cu–Cr catalysts. Chromium causes serious environmental problems due to its high toxicity. As a consequence of the high toxicity of chromium, experimental and theoretical methods have been studied for the selective hydrogenation of furfural over a variety of environmentally acceptable metal catalysts (Cu, Pd, Pt, Co and Zn) leading to different reaction pathways [113–115]. Among those reaction mechanisms proposed, Cu-based catalysts and group VIII metal catalysts are the most widely accepted. In addition, the hydrogenation of C=C bonds in the furan ring of furfural can produce tetrahydrofurfural (THF) and THFA. Since the furan ring is stable, metals with strong affinities for C=C bonds allow furfural to adsorb parallel to the metal surface, facilitating the saturation of the ring [116].

In another report, vapor phase furfural hydrogenation studies were performed on a series of silica-supported monodisperse Pt nanoparticle catalysts where the extent of decarbonylation and hydrogenation of carbonyl group was highly dependent on the size and shape of Pt NPs [117]. Small particles were found to predominantly give furan as major product (via decarbonylation) while larger sized particles yielded both furan and FOL (carbonyl hydrogenation product). Octahedral particles were found to be highly selective toward FOL, while cube-shaped particles produced an equal amount of furan and FOL.

1.6.2 Furfural decarbonylation to furan

Experimental and theoretical studies have shown when the reaction temperature increases, the preferred binding mode of furfural changes from the η-aldehyde configuration to the η-acyl configuration, leading to the formation of furan via decarbonylation (Figure 1.4, green circle) [116]. Different catalysts have been investigated for this reaction, including supported noble metal catalysts and mixed metal oxides based on nonnoble metals such as Zn–Fe, Zn–Fe–Mn, Zn–Cr and so on. Pd has been identified as the more selective catalyst for furfural decarbonylation, at high temperature and H_2 pressure, while catalysts with oxophilic sites have been shown to stabilize the metal oxygen bond more strongly and hinder the formation of surface acyl species, leading to decreased selectivity of decarbonylation products [118, 119]. Although Pd catalysts are more active than other catalysts, the yield of furan decreases sharply with time on stream. Among the various possible reasons for the observed deactivation, the most commonly proposed is carbon deposition, which could be due to side reactions, such as condensation and/or decomposition of furfural. The change of oxidation state and the sintering of the particles can also promote deactivation. The further hydrogenation of C=C bonds in the furan ring can produce THF, which has been widely used as a solvent and intermediate for chemical production [116].

1.6.3 Furfural conversion to methylfuran (MF)

From the point of view of fuel production, either hydrogenation or decarbonylation is desirable. While the hydrogenation does not remove O, decarbonylation loses C in the process. More interestingly, 2-MF (Figure 1.4, red circle) is desirable since it not only has intrinsically good fuel properties (high octane number, RON = 131, low water solubility, 7 g/L) but also can be considered an archetypical product of the desired reaction paths in bio-oil upgrading [120]. 2-MF is produced from the hydrogenolysis of the C–O bond of FOL. Sitthisa et al. have shown that the combination of metals with oxophilic sites can facilitate the selective cleavage of this bond, for example, through the use of SiO_2-supported Ni–Fe alloys [116, 121]. Results proved that the addition of Fe suppressed the decarbonylation activity of Ni while promoting C=O hydrogenation (at low temperatures) and C–O hydrogenolysis (at high temperatures). Furfural could then be readily hydrogenated to FOL and subsequently hydrogenolyzed to 2-MF. The strong interaction between O (from the carbonyl group) and the oxyphilic Fe atoms supports a preferential hydrogenolysis reaction on the bimetallic alloy. In another study, 2-MF was obtained in the vapor phase hydrodeoxygenation (HDO) of furfural using Mo_2C catalysts at low temperature (150 °C) and ambient pressure [122].

1.6.4 Other furfural conversions

Two effective methods to extend the carbon chain length for furfural upgrading to fuels are the aldol condensations and hydroxyalkylation–alkylation (HAA) reactions. Furfural can undergo aldol condensation with external carbonyl containing molecules having an α-hydrogen (e.g., ketones) in the presence of a base or an acid catalyst. Further hydrogenation of aldol products can produce high-quality longer-chain alkanes. Barrett et al. developed a sequential aldol condensation and hydrogenation strategy for furfural upgrading in the aqueous phase using a bifunctional $Pd/MgO–ZrO_2$ catalyst [123]. The cross aldol condensation of furfural with acetone results in water-insoluble monomer and dimer products, which are subsequently hydrogenated to give products with high overall carbon yields (>80%). On the other hand, HAA combined with HDO is a comparatively promising route for the synthesis of renewable high-quality diesel or jet fuel. Taking advantage of this combined process, 2-MF can be used in the Sylvan diesel process where it serves as starting material [124, 125], which consists of two consecutive steps, HAA and HDO. Further implementation of HAA-HDO was reported by Zhang et al. where different types of resins (such as, Nafion, Amberlyst, etc.) were utilized to couple 2-MF and furfural [126, 127], where the Nafion-212 resin demonstrated the highest activity and stability.

Acknowledgments: The authors thank the Spanish Ministry of Economy, Industry and Competitiveness (CTQ2015-64226-C03-3-R project and Ramon y Cajal contract ref. RYC-2015-17109), Junta de Andalucia (RNM-1565), FEDER (European Union) and Malaga University for the financial support during this work.

References

[1] Stöcker M. Biofuels and biomass-to-liquid fuels in the biorefinery: catalytic conversion of lignocellulosic biomass using porous materials. Angew Chem Int Ed Engl 2008, 47, 9200–9211.
[2] Hierro Ausin I, Pérez Arriaga JI. Informe anual del Observatorio de Energía y Desarrollo Sostenible en España 2004. Cátedra BP de Desarrollo Sostenible. Universidad Pontífica de Comillas de Madrid, Madrid, 2005.
[3] Kyoto protocol to the United Nations framework convention on climate change. Kyoto, Japan: United Nations, 1997. (Accessed September 20, 2018, at https://unfccc.int/resource/docs/convkp/kpeng.pdf).
[4] COM 772. Communication from the Commission – Energy efficiency: delivering the 20% target. Brussels: Commission of the European Communities, 2008. (Accessed September 20, 2018, at http://ec.europa.eu/transparency/regdoc/rep/1/2008/EN/1-2008-772-EN-F1-1.Pdf).
[5] Mariscal R, Maireles-Torres P, Ojeda M, Sádaba I, López-Granados M. Furfural: A renewable and versatile platform molecule for the synthesis of chemicals and fuels. Energy Environ Sci 2016, 9, 1144–1189.
[6] Energía de la biomasa. Madrid: Instituto para la Diversificación y Ahorro de la Energía (IDAE), 2007. (Accessed September 24, 2018, at http://www.idae.es/uploads/documentos/documentos_10374_Energia_de_la_biomasa_07_28e17c9c.pdf).
[7] Demirbas A. Biomass resource facilities and biomass conversion processing for fuels and chemicals. Energ Convers Manage 2001, 42, 1357–1378.
[8] De Wild P, Van der Laan R, Kloekhorst A, Heeres E. Lignin valorization for chemicals and (transportation) fuels via (catalytic) pyrolysis and hydrodeoxygenetaion. Environ Prog Sustain Energy 2009, 28, 461.
[9] De Wild P, Den Uil H, Reith H, Lunshof A, Hendriks C, Van Eck E, Heeres HJ. Bioenergy II: Biomass valorisation by a hybrid thermochemical fractionation approach. Int J Chem React Eng 2009, 7, Article A51, 1.
[10] Carrasco F, Roy C. Kinetic study of dilute-acid prehydrolysis of xylan-containing biomass. Wood Sci Technol 1992, 26, 189–208.
[11] Dumitriu S. Polysaccharides: Structural diversity and functional versatility, 2nd. Marcel Dekker, NY, USA, 2005.
[12] Klemm D, Heublein B, Fink HP, Bohn A. Cellulose: fascinating biopolymer and sustainable raw material. Angew Chem Int Ed 2005, 44, 3358–3393.
[13] Roman-Leshkov Y, Chheda JN, Dumesic JA. Phase modifiers promote efficient production of Hydroxymethylfurfural from fructose. Science 2006, 312, 1933–1937.
[14] Gallezot P, Cerino PJ, Blanc B, Flèche G, Fuertes P. Glucose hydrogenation on promoted Raney-Nickel catalysts. J Catal 1994, 146, 93–102.
[15] Huber GW, Cortright RD, Dumesic JA. Renewable alkenes by aqueous-phase reforming of biomass-derived oxygenates. Angew Chem Int Ed 2004, 43, 1549–1551.
[16] Nakagawa Y, Shinmi Y, Koso S, Tomishige K. Direct hydrogenolysis of glycerol in-to 1,3-propanediol over rhenium –modified iridium catalyst. J Catal 2010, 272, 191–194.

[17] Gillet S, Aguedo M, Petitjean L, Morais ARC, Da Costa Lopes AM, Łukasik RM, Anastas PT. Lignin transformations for high value applications: Towards targeted modifications using green chemistry. Green Chem 2017, 19, 4200–4233.
[18] Lupoi JS, Singh S, Parthasarathi R, Simmons BA, Henry RJ. Recents innovations in analytical methods for the qualitative and quantitative assessment of lignin. Renew Sust Energ Rev 2015, 49, 871–906.
[19] Zakzeski J, Bruijnincx PCA, Jongerius AL, Weckhuysen BM. The catalytic valorization of lignin for the production of renewable chemicals. Chem Rev 2010, 110, 3552–3599.
[20] Adler E. Lignin chemistry - past, present and future. Wood Sci Technol 1977, 11, 169–218.
[21] Gosselink RJA, De Jong E, Guran B, Abächerli A. Co-ordination network for lignin-standardisation, production and applications adapted to market requirements (EUROLIGNIN). Ind Crops Prod 2004, 20, 121–129.
[22] Li N, Huber GW. Aqueous-phase hydrodeoxygenation of sorbitol with Pt/SiO_2-Al_2O_3. Identification of reaction intermediates. J Catal 2010, 270, 48–59.
[23] Xing R, Subrahmanyam AV, Olcay H, Qi W, Walsum GPV, Pendse H, Huber GW. Production of jet and diesel fuel range alkanes from waste hemicellulose-derived aqueous solutions. Green Chem 2010, 12, 1933–1946.
[24] Sella Kapu N, Trajano HL. Review of hemicellulose hydrolysis in softwoods and bamboo. Biofuels Bioprod Biorefin 2014, 8, 857–870.
[25] Peng P, She D. Isolation, structural characterization, and potential applications of hemicelluloses from bamboo: A review. Carbohydr Polym 2014, 112, 701–720.
[26] Scheller HV, Ulvskov P. Hemicelluloses. Annu Rev Plant Biol 2010, 61, 263–289.
[27] Negahdar L, Delidovich I, Palkovits R. Aqueous-phase hydrolysis of cellulose and hemicelluloses over molecular acidic catalysts: Insights into the kinetics and reaction mechanism. Appl Catal B 2016, 184, 285–298.
[28] Tekin K, Karagöz S, Bektas S. A review of hydrothermal biomass processing. Renew Sustain Energ Rev 2014, 40, 673–687.
[29] Otieno DO, Ahring BK. The potencial for oligosaccharide production from the hemicelluloses fraction of biomasses through pretreatment processes: xylooligosaccharides (XOS), arabinooligosaccharides (AOS), and mannooligosaccharides (MOS). Carbohydr Res 2012, 360, 84–92.
[30] Sahu R, Dhepe PL. A one-pot method for the selective conversion of hemicellulose from crop waste into C_5 sugars and furfural by using solid acid catalysts. ChemSusChem 2012, 5, 751–761.
[31] Yi GS, Zhang YG. One-Pot selective conversion of hemicellulose (xylan) to Xylitol under mild conditions. ChemSusChem 2012, 5, 1383–1387.
[32] Bian J, Peng F, Peng XP, Peng P, Xu F, Sun RC. Structural features and antioxidant activity of xylooligosaccharides enzimatically produced from sugarcane bagasse. Bioresour Technol 2013, 127, 236–241.
[33] Weeks BS, Perez PP. The hemicellulose preparation, Natramune (PDS-2865), increases macrophage phagocytosis and nitric oxide production and increases circulating human lymphocytes levels. Med Sci Monit 2009, 15, 43–46.
[34] Hansen NM, Plackett D. Sustainable films and coatings from hemicelluloses: A review. Biomacromolecules 2008, 9, 1493–1505.
[35] Bozell JJ, Moens L, Elliott DC, Wang Y, Neuenscwander GG, Fitzpatrick SW, Bilski RJ, Jarnefeld JL. Production of levulinic acid and use as a platform chemical for derived products. Resour Conserv Recycl 2000, 28, 227–239.
[36] Ropars M, Marchal R, Pourquié J, Vandecasteele JP. Large scale enzymatic hydrolysis of agricultural lignocellulose biomass, Part I: Pretreatment Procedures. Bioresour Technol 1992, 42, 197–204.

[37] Öhgren K, Bura R, Saddler J, Zacchi G. Effect of hemicellulose and lignin removal on enzymatic hydrolysis of steam pretreated corn stover. Bioresour Technol 2007, 98, 2503–2510.
[38] Mamman AS, Lee J, Kim Y, Hwang IT, Park N, Hwang Y, Chang J, Hwang J. Furfural: Hemicellulose/Xylose-Derived Biochemical. Biofuels Bioprod Biorefin 2008, 2, 438–454.
[39] Gürbüz EI, Gallo JM, Alonso DM, Wettstein SG, Lim WY, Dumesic JA. Conversion of hemicellulose into furfural using solid acid catalysts in γ-valerolactone. Angew Chem Int Ed Engl 2013, 52, 1270–1274.
[40] Hilpmann G, Becher N, Pahner FA, Kusema B, Mäki-Arvela P, Lange R, Murzin DY, Salmi T. Acid hydrolysis of xylan. Catal Today 2016, 259, 376–380.
[41] Salmi T, Murzin DY, Mäki-Arvela P, Kusema B, Holmbom B, Willför S, Wärnå J. Kinetic modeling of hemicellulose hydrolysis in the presence of homogeneous and heterogeneous catalysts. AIChE J 2014, 60, 1066–1077.
[42] Matsagar BM, Dhepe PL. Brönsted acidic ionic liquid-catalyzed conversion of hemicellulose into sugars. Catal Sci Technol 2015, 5, 531–539.
[43] Mccann MC, Carpita NC. Biomass recalcitrance: A multi-scale, multi-factor, and conversion-specific property. J Exp Bot 2015, 66, 4109–4118.
[44] Himmel ME, Ding SY, Johnson DK, Adney WS, Nimlos MR, Brady JW, Foust TD. Biomass recalcitrance: Engineering plants and enzymes for biofuels production. Science 2007, 315, 804–807.
[45] Mettler MS, Vlachos DG, Dauenhauer PJ. Top ten fundamental challenges of biomass pyrolysis for biofuels. Energy Environ Sci 2012, 5, 7797–7809.
[46] Alonso D, Bond J, Dumesic J. Catalytic conversion of biomass to biofuels. Green Chem 2010, 12, 1493–1513.
[47] Kumar P, Barrett DM, Delwiche MJ, Stroeve P. Methods for pretreatment of lignocellulosic biomass for efficient hydrolysis and biofuel production. Ind Eng Chem Res 2009, 48(8), 3713–3729.
[48] Mosier N, Wyman C, Dale B, Elander R, Lee YY, Holtzapple M, Ladisch M. Features of promising technologies for pretreatment of lignocellulosic biomass. Bioresour Technol 2005, 96(6), 673–686.
[49] Werpy TA, Petersen G, Ridge O. Top Value Added Chemicals from Biomass: Volume I – Results of screening for potential candidates from sugars and synthesis gas. US Department of Energy. Oak Ridge, USA, 2004.
[50] Montané D, Salvadó J, Torras C, Farriol X. High-temperature dilute-acid hydrolysis of olive stones for furfural production. Biomass Bioenergy 2012, 22, 295–304.
[51] Zeitsch KJ. Furfural production needs chemical innovation. Chem Innov 2000, 30(4), 29–32.
[52] Hensley J, Burger G. Nematicidal properties of furfural and the development for nematode contol in various crops for the United States markets. J Nematol 2006, 38(2), 274.
[53] Zeitsch KJ. The chemistry and technology of furfural and its many by-products. In: Sugar Series 13, Amsterdam, The Netherlands, Elsevier Science, 2000.
[54] Safety evaluation of certain food additives. Furfural. WHO food additives series: 42. Geneva: World Health Organization, 1999. First draft prepared by R. Kroes. Research Institute of Toxicology, Utrecht University, Utrecht, Netherlands (Accessed October 10, 2018, at http://www.inchem.org/documents/jecfa/jecmono/v042je03.htm).
[55] Tachibana Y, Kimura S, Kasuya K. Synthesis and verification of biobased terephthalic acid from furfural. Sci Rep 2015, 5, 8249–8253.
[56] Dashtban M, Gilbert A, Fatehi P. Production of furfural: Overview and challenges. J Sci Technol For Prod Process 2012, 2, 4.

[57] Perego C, Bianchi D. Biomass upgrading through acid–base catalysis. Chem Eng J 2010, 161, 314–322.
[58] Serrano L, Egües I, Alriols MG, Llano-Ponte R, Labidi J. Miscanthus sinensis fractionation by different reagents. Chem Eng J 2010, 156, 49–55.
[59] Lange JP, Van Der Heide E, Van Buijtenen J, Price R. Furfural–a promising platform for lignocellulosic biofuels. ChemSusChem 2012, 5, 150–166.
[60] Brydson JA. Furan resins. Plastics Materials (Seventh Edition). Butterworth-Heinemann. Oxford, Engl. 1999, 28, 810–813.
[61] Ibeh CC. Amino and furan resins. In: Handbook of Thermoset Plastics2nd ed. Raytheon Systems Company, El Segundo, California, William Andrew Ed, 1999, 72–96.
[62] Pirolini AP. Materials used in space shuttle thermal protection systems, 2015. (Accessed October 15, 2018, at https://www.azom.com/article.aspx?ArticleID=11443).
[63] Kumar R, Anandjiwala RD. Compression-molded flax fabric-reinforced polyfurfuryl alcohol bio-composites. J Therm Anal Calorim 2013, 112, 755–760.
[64] Hoydonckx HE, Van Rhijn WM. Application of novel furan resins in composites, JEC Magazine 2008, 45, 34–35.
[65] Eastman J, Crandell G. Putting GMBOND to the test, 2003 (Accessed October 15, 2018, at http://foundrymag.com).
[66] Huber GW, Cheda JN, Barrett CJ, Dumesic JA. Production of liquid alkanes by aqueous-phase processing of biomass-derived carbohydrates. Science 2005, 308, 1446–1450.
[67] Kar Y, Deveci H. Importance of P-series fuels for flexible-fuel vehicles (FFVs) and alternative fuels. Energ Source 2006, Part A 28, 909–921.
[68] Yang W, Sen A. One-step catalytic transformation of carbohydrates and cellulosic biomass to 2,5-dimethyltetrahydrofuran for liquid fuels. ChemSusChem 2010, 3(5), 597–603.
[69] Huber GW, Iborra S, Corma A. Synthesis of transportation fuels from biomass: Chemistry, catalysts, and engineering. Chem Rev 2006, 106 (9), 4044–4098.
[70] Tran LS, Sirjean B, Glaude PA, R. Fournet, Battin-Leclerc F. Progress in detailed kinetic modeling of the combustion of oxygenated components of biofuels. Energy 2012, 43(1), 4–18.
[71] De Jong E, Langeveld H, Van Ree R. IEA Bioenergy Task 42 biorefinery. 2009. (Accessed October 21, 2018, at http://www.iea-bioenergy.task42-biorefineries.com).
[72] Bernardes MADS. Biofuel's Engineering Process Technology. CRP Henri Tudor. Luxembourg, Intech, 2011.
[73] Fernando S, Adhikari S, Chandrapal C, Murali N. Biorefineries: Current status, challenges, and future direction. Energy Fuels 2006, 20, 1727–1737.
[74] Cherubini F, Jungmeier G, Wellisch M, Willke T, Skiadas I, Van Ree R, De Jong E. Toward a common classification approach for biorefinery systems. Biofuel Bioprod Bior 2009, 3, 534–546.
[75] De Jong Ed, Jungmeier G. Biorefinery concepts in comparison to petrochemical refineries. Industrial Biorefineries & White Biotechnology, 1st edn. New York, USA, Elsevier, 2015, 3–33.
[76] Bridgwater AV, Peacocke GVC. Fast pyrolysis processes for biomass. Renew Energy Rev 2000, 4, 1–73.
[77] Guo Y, Wang Y, Wei F, Yong J. Research progress in biomass flash pyrolysis technology for liquids production. Chem Ind Eng Progr 2001, 8, 13–17.
[78] Romano RT, Zhang R. Co-digestion of onion juice and wastewater sludge using an anaerobic mixed biofilm reactor. Bioresour Technol 2008, 99(3), 631–637.
[79] Huang HJ, Ramaswamy S, Tschirner UW, Ramarao BV. A review of separation technologies in current and future biorefineries. Sep Purif Technol 2008, 62, 1–21.

[80] Sun Y, J Cheng. Hydrolysis of lignocellulosic materials for ethanol production: A review. Bioresour Technol 2002, 83(1), 1–11.
[81] Kamm B, Kamm M. Principles of biorefineries. Appl Microbiol Biot 2004, 64, 137–145.
[82] Martinez GA, Rebecchi S, Decorti D, Domingos JM, Natolino A, Del Rio D, Bertín L, Da Porto C, Fava F. Towards multi-purpose biorefinery platforms for the valorisation of red grape pomace: production of polyphenols, volatile fatty acids, polyhydroxyalkanoates and biogas. Green Chem 2016, 18, 261–270.
[83] Yates M, Gomez MR, Martin-Luengo MA, Ibañez VZ, Serrano AMM. Multivalorization of apple pomace of towards materials and chemicals. Waste to wealth. J Clean Prod 2017, 143, 847–853.
[84] Galanakis CM. Recovery of high added-value components from food wastes: Conventional, emerging technologies and commercialized applications. Trends Food Sci Tech 2012, 26, 68–87.
[85] Oreopoulou V, Tzia C. Utilization of plant by-products for the recovery of proteins, dietary fibers, antioxidants, and colorants. In: Utilization of By-products and Treatment of Waste in the Food Industry. New York, USA, Springer Science + Business Media, 2007, 209–232.
[86] O'Shea N, Arendt EK, Gallagher E. Dietary fibre and phytochemical characteristics of fruit and vegetable by-products and their recent applications as novel ingredients in food products. Innov Food Sci Emerg 2012, 16, 1–10.
[87] Foley PM, Beach ES, Zimmerman JB. Algae as a source of renewable chemicals: Opportunities and challenges. Green Chem 2011, 13, 1399–1405.
[88] Citrus fruit statistics. Rome: Food and agriculture organization of the United Nations, FAO, 2015. (Accessed October 22, 2018, at http://www.fao.org/3/a-i5558e.pdf).
[89] Bampidis V, Robinson P. Citrus by-products as ruminant feeds: A review. Anim Feed Sci Tech 2006, 128, 175–217.
[90] Pourbafrani M, Forgács G, Horváth IS, Niklasson C, Taherzadeh MJ. Production of biofuels, limonene and pectin from citrus wastes. Bioresour Technol 2010, 101, 4246–4250.
[91] Amendola D, De Faveri DM, Egües I, Serrano L, Labidi J, Spigno G. Autohydrolysis and organosolv process for recovery of hemicelluloses, phenolic compounds and lignin from grape stalks. Bioresour Technol 2012, 107, 267–274.
[92] Zheng Y, Lee C, Yu C, Cheng YS, Simmons CW, Zhang R, Jenkins BM, VanderGheynst JS. Ensilage and bioconversion of grape pomace into fuel ethanol. J Agric Food Chem 2012, 60, 11128–11134.
[93] Pérez-Serradilla J, De Castro ML. Microwave-assisted extration of phenolic compounds from wine lees and spray-drying of the extract. Food Chem 2011, 124, 1652–1659.
[94] Dimou C, Kopsahelis N, Papadaki A, Papanikolaou S, Kookos IK, Mandala I, Koutinas AA. Wine lees valorization: Biorefinery development including production of a generic fermentation feedstock employed for poly(3-hydroxybutyrate) synthesis. Food Res Int 2015, 73, 81–87.
[95] Dhillon GS, Kaur S, Brar SK. Perspective of apple processing wastes as low-cost substrates for bioproduction of high value products: A review. Renew Sust Energ Rev 2013, 27, 789–805.
[96] Kehili M, Schmidt LM, Reynolds W, Zammel A, Zetzl C, Smirnova I, Allouche N, Sayadi S. Biorefinery cascade processing for creating added value on tomato industrial by-products from Tunisia. Biotechnol Biofuels 2016, 9, 261.
[97] Del Valle M, Cámara M, Torija ME. Chemical characterization of tomato pomace. J Sci Food Agr 2006, 86, 1232–1236.
[98] ElMekawy A, Diels L, De Wever H, Pant D. Valorization of cereal based biorefinery byproducts: Reality and expectations. Environ Sci Technol 2013, 47, 9014–9027.

[99] Global food losses and food waste-extent, causes and prevention. Rome: Food and agriculture organization of the United Nations, FAO, 2011. (Accessed October 22, 2018, at http://www.fao.org/3/a-i2697e.pdf).
[100] Ortiz R, Sayre KD, Govaerts B, Gupta R, Subbarao G, Ban T, Hodson D, Dixon JM, Ortiz-Monasterio JI, Reynolds M. Climate change: Can wheat beat the heat?. Agr Ecosyst Environ 2008, 126, 46–58.
[101] Dorado MP, Lin SKC, Koutinas A, Du C, Wang R, Webb C. Cereal-based biorefinery development: Utilisation of wheat milling by-products for the production of succinic acid. J Biotechnol 2009, 143, 51–59.
[102] Kaparaju P, Serrano M, Thomsen AB, Kongjan P, Angelidaki I. Bioethanol, biohydrogen and biogas production from wheat straw in a biorefinery concept. Bioresour Technol 2009, 100, 2562–2568.
[103] Barana D, Salanti A, Orlandi M, Ali DS, Zoia L. Biorefinery process for the simultaneous recovery of lignin, hemicelluloses, cellulose nanocrystals and silica from rice husk and Arundo donax. Ind Crop Prod 2016, 86, 31–39.
[104] Food outlook. Biannual report on global food markets. Rome: Food and agriculture organization of the United Nations, FAO, 2016. (Accessed October 22, 2018, at http://www.fao.org/3/a-I5703E.pdf).
[105] Huang H, W Liu, Singh V, Danao MGC, Eckhoff SR. Effect of harvest moisture content on selected yellow dent corn: Dry-grind fermentation characteristics and DDGS composition. Cereal Chem 2012, 89, 217–221.
[106] Bals B, Dale B, Balan V. Enzymatic hydrolysis of distiller's grain and solubles (DDGS) using ammonia fiber expansion pretreatment. Energy Fuels 2006, 20, 2732–2736.
[107] Tamer CE, Çopur ÖU. Development of value-added products from food wastes. In: Food Processing: Strategies for Quality Assessment. New York, USA, Springer Science Business Media, 2014, 453–475.
[108] Schievano A, Adani F, Buessing L, Botto A, Casoliba EN, Rossoni M, Goldfarbe JL. An integrated biorefinery concept for olive mill waste management: Supercritical CO_2 extraction and energy recovery. Green Chem 2015, 17, 2874–2887.
[109] López-Linares JC, Romero I, Cara C, Ruiz E, Moya M, Castro E. Bioethanol production from rapeseed straw at high solids loading with different process configurations. Fuel 2014, 122, 112–118.
[110] Luo G, Talebnia F, Karakashev D, Xie L, Zhou Q, Angelidaki I. Enhanced bioenergy recovery from rapeseed plant in a biorefinery concept. Bioresour Technol 2011, 102, 1433–1439.
[111] Chintagunta AD, Jacob S, Banerjee R. Integrated bioethanol and biomanure production from potato waste. Waste Manage 2016, 49, 320–325.
[112] Hoydonckx H, Van Rhijn W, De Vos D, Jacobs P. Furfural and derivatives. In: Ullmann's encyclopedia of industrial chemistry. Weinheim, Germany, Wiley-VCH, 2007, 285–313.
[113] Nagaraja BM, Kumar SV, Shasikala V, Padmasri AH, Sreedhar B, Raju BD, Rao KSR. A highly efficient Cu/MgO catalyst for vapour phase hydrogenation of furfural to furfuryl alcohol. Catal Commun 2003, 4, 287–293.
[114] Jiménez-Gómez CP, Cecilia JA, Martín D, Moreno-Tost R, Santamaría-González J, Mérida-Robles J, Mariscal R, Maireles-Torres P. Gas-phase hydrogenation of furfural to furfuryl alcohol over Cu/ZnO catalysts. J Catal 2016, 336, 107–115.
[115] Bhogeswararao S, Srinivas D. Catalytic conversion of furfural to industrial chemicals over supported Pt and Pd catalysts. J Catal 2015, 327, 65–77.
[116] Sitthisa S, Resasco DE. Hydrodeoxygenation of furfural over supported metal catalysts: A comparative study of Cu, Pd and Ni. Catal Lett 2011, 141, 784–791.

[117] Pushkarev VV, Musselwhite N, An K, Alayoglu S, Somorjai GA. High structure sensitivity of vapor-phase furfural decarbonylation/hydrogenation reaction network as a function of size and shape of Pt nanoparticles. Nano Lett 2012, 12, 5196–5201.
[118] Sitthisa S, Pham T, Prasomsri T, Sooknoi T, Mallinson RG, Resasco DE. Conversion of furfural and 2-methylpentanal on Pd/SiO_2 and $Pd–Cu/SiO_2$ catalysts. J Catal 2011, 280, 17–27.
[119] Wang S, Vorotnikov V, Vlachos DG. A DFT study of furan hydrogenation and ring opening on Pd(111). Green Chem 2014, 16, 736–747.
[120] Li X, Jia P, Wang T. Furfural: A promising platform compound for sustainable production of C_4 and C_5 chemicals. ACS Catal 2016, 6, 7621–7640.
[121] Sitthisa S, An W, Resasco DE. Selective conversion of furfural to methylfuran over silica-supported Ni-Fe bimetallic catalysts. J Catal 2011, 284, 90–101.
[122] Lee WS, Wang Z, Zheng W, Vlachos DG, Bhan A. Vapor phase hydrodeoxygenation of furfural to 2-methylfuran on molybdenum carbide catalysts. Catal Sci Technol 2014, 4, 2340–2352.
[123] Barrett CJ, Chheda JN, Huber GW, Dumesic JA. Single-reactor process for sequential aldol-condensation and hydrogenation of biomass-derived compounds in water. Appl Catal B: Environ 2006, 66, 111–118.
[124] Corma A, De la Torre O, Renz M, Villandier N. Production of high-quality diesel from biomass waste products. Angew Chem Int Ed 2011, 50, 2375–2378.
[125] Corma A, De la Torre O, Renz M. Production of high quality diesel from cellulose and hemicellulose by the Sylvan process: Catalysts and process variables. Energy Environ Sci 2012, 5, 6328–6344.
[126] Li G, Li N, Wang Z, Li C, Wang A, Wang X, Cong Y, Zhang T. Synthesis of high-quality diesel with furfural and 2-methylfuran from hemicellulose. ChemSusChem 2012, 5, 1958–1966.
[127] Li G, Li N, Yang J, Wang A, Wang X, Cong Y, Zhang T. Synthesis of renewable diesel with the 2-methylfuran, butanal and acetone derived from lignocellulose. Bioresour Technol 2013, 134, 66–72.

Grazina Juodeikiene, Elena Bartkiene, Daiva Zadeike,
Dovile Klupsaite

2 Biorefinery approach for the utilization of dairy by-products and lignocellulosic biomass to lactic acid

Bioproduction of optically pure lactic acid (LA) has roused interest in the recent years due to its potential application in a wide range of fields, and there is a significant interest to further development of sustainable and cost-effective process. However, the efficient utilization of agro-industrial wastes for LA production still causes considerable challenges. The biotechnological LA production within the targeted cost still required the development of high-performance LA-producing microorganisms and the lowering of the costs of raw materials and fermentation process. Cheap biomass, such as starchy and cellulosic agricultural residues or by-products from the food industry, has a potential for the cost-effective production of LA, but raw materials also should have a high production rate and yield without by-product formation and the ability to be fermented with low pretreatment [1]. However, the LA made by fermentation route refers optically active, consequently a suitable microorganism could selectively produce dextro (levo)-rotation enantiomers, and the greatest demand is for the L-LA isomer [2]. Targeted conversion of starchy substrates to LA can be performed using the amylolytic microorganisms [3]. Fungi species from *Rhizopus*, such as *Rhizopus oryzae* and *Rhizopus arrhizus*, excrete amylolytic activity that enables to convert starch directly into L-LA in the presence of oxygen [4]. However, LA-producing microorganisms, including the fungus *R. oryzae*, have low productivity depending on the low reaction rate caused by mass transfer limitation [5]. Most of the world's commercial L (+)-LA is produced by the fermentation of carbohydrates using homolactic microbes such as a variety of modified or developed strains of the genus *Lactobacilli* [6, 7]. This can be considered to be an advantage, since the productivity of the industrial process may become independent of oxygen supply.

Nowadays, the development of sustainable processes requires the efficient exploitation of food-processing residues and maximization of the value derived from such waste source. In this field, the dairy industry by-products (e.g., whey, whey permeate) received considerable attention as a suitable carbon source, since they are substrates that do not require extensive purification, and can be the most appropriate option for the production of biodegradable polymers as well as for many other applications. While the efficient lactose consumption depends on the different factors affecting the LAB growth in the fermentation medium, the selection of LAB strain without complex nutritional requirements and pH regulation is one of the most important factors influencing LA production rate [8]. Our recent studies,

https://doi.org/10.1515/9783110538151-002

related to the development of a cost-effective and sustainable process, focus on an application of novel acid tolerant microorganisms evolving different enzyme activities on the efficient LA stereoisomers production from different cereal-based food residues and dairy by-products, including enzymatic hydrolysis and acid neutralization [9, 10].

2.1 Introduction

Lactic acid (LA) or 2-hydroxypropionic acid or $CH_3CH(OH)COOH$, is the simplest hydroxylcarboxylic acid with an asymmetrical carbon atom. LA exists in two optically active isomeric forms: L(+)-LA and D(−)-LA [11]. LA is classified as GRAS (generally recognized as safe) for use as a food additive by the US Food and Drug Administration, but D(−)-LA is at times harmful to human metabolism and can result in acidosis and decalcification. LA, as a platform chemical, and its salts have a long history of commercial uses and applications [12]. It is used in the food and beverage sector as a preservative and pH-adjusting agent, and in the chemical industry as a starting material in the production of polylactic acid (PLA) polymer and new "green" solvents, for example, ethyl lactate. LA has many pharmaceutical and cosmetic applications and formulations in topical ointments, lotions, antiacne solutions, humectants, parenteral solutions and dialysis applications, such as anticarries agent. Calcium lactate can be used for calcium-deficiency therapy and as anticarries agent. PLA is a biodegradable polymer that has medical applications such as sutures, orthopedic implants, controlled drug release and so on. PLA thermoplastic properties approach those of petroleum-derived plastics. PLA with a low degree of polymerization can help in controlled release or degradable mulch films for large-scale agricultural applications. LA can also be used for the production of propylene oxide (via the formation of propylene glycol), which has an important role in the production of polyurethanes. Another high-volume derivative from LA is acrylic acid. This is the primary building block for the formation of acrylate polymers, which have numerous applications, for example, in surface coatings and adhesives. The LA market is currently at a watershed with the commercial reality of PLA polymers and lactate esters. LA global demand was expected to grow at a compound annual growth rate of 22% through 2005–2015. Growth in PLA bioplastics market is the driving demand for LA in industrial applications [13]. The application spectrum of PLAs is expanding due to their opportunities to replace various fossil-based polymers. The life-cycle assessment (LCA) studies show that PLA biopolymers result in significantly lower emissions of greenhouse gasses, and less use of material resources and nonrenewable energy, compared to fossil-based polymers [14, 15]. Major LA producers are Corbion Purac (The Netherlands), Galactic (Belgium), Nature Works LLC (USA) and several

Chinese companies [16]. LA and its products, for example, lactide, could be produced through fermentation processes as well as through synthetic routes. In recent years, the amount of LA obtained by chemical route decreased due to several reasons. One of them is that synthetic LA made from petrochemical feedstocks is optically inactive, that is, a racemic mixture. Another problem is environmental pollution and the limited supply of petrochemical resources [17]. Contrary, LA made biochemically by fermentation is optically active and suitable organisms can selectively produce levo- or dextro-rotation antiomers. In addition, LA can esterify itself providing a mixture of esters in equilibrium with acid and oligomers are present. Therefore, there is a significant interest to further enhance and develop such complexes to produce chemical intermediates and polymers through sustainable manufacturing to compete cost effectively with those derived from petrochemical sources [18].

2.2 Production of lactic acid

For the production of LA, there are two manufacturing methods with industrial importance: (a) chemical synthesis and (b) microbial fermentation. Figure 2.1 shows main production steps as well as the advantages and disadvantages of these technologies.

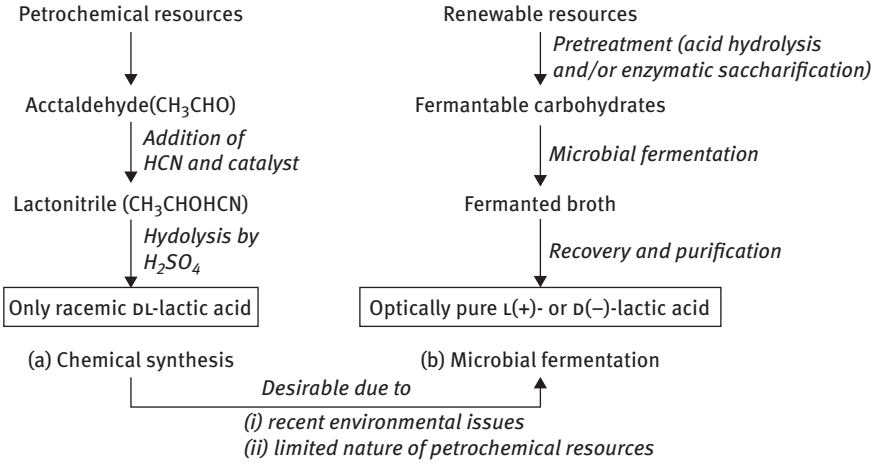

Figure 2.1: Overview of the two manufacturing methods of lactic acid: (a) chemical synthesis and (b) microbial fermentation [12].

According to the Wee et al. [12], microbial fermentation has the biggest advantage because an optically pure LA can be obtained by choosing a suitable strain

of microorganism, whereas chemical synthesis always results in a mixture of different LA isomers.

2.2.1 Biotechnological approach of LA production from agro-industrial and dairy by-products

Bioproduction of optically pure LA has roused interest in the recent years due to its potential application in a wide range of fields, and there is a significant interest to further development of sustainable and cost-effective process. However, the efficient utilization of agro-industrial wastes for LA production still causes considerable challenges. The biotechnological LA production within the targeted cost still required the development of high-performance LA-producing microorganisms and the lowering of the costs of raw materials and fermentation process.

LA can be produced from cheap biomass, such starchy and lignocellulosic agriculture residues or by-products from the food industry, obtained after simultaneous gelatinization and liquefaction or gelatinization, liquefaction and saccharification steps or by direct conversion by amylolytic LA-producing microorganisms or by the simultaneous hydrolysis and fermentation by adding enzymes and inoculum together (Figure 2.2).

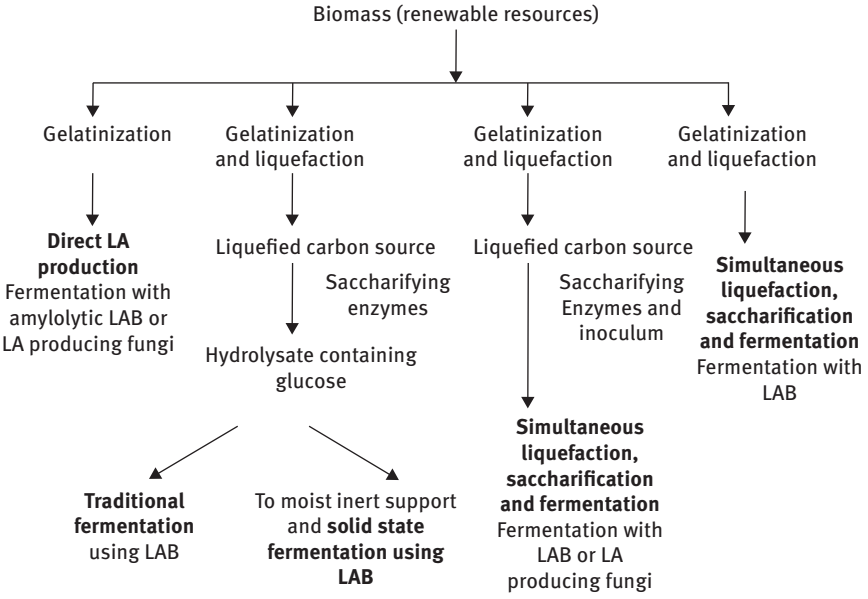

Figure 2.2: Different processes for lactic acid fermentation using renewable starchy or lignocellulosic resources [19].

Although the LA made by fermentation route refers optically active, consequently a suitable microorganism could selectively produce dextro (levo)-rotation enantiomers, and the greatest demand is for the L-LA isomer [2]. Targeted conversion of starchy substrates to LA can be performed using the amylolytic microorganisms [3]. Fungi species from *Rhizopus*, such as *Rhizopus oryzae* and *Rhizopus arrhizus*, excrete amylolytic activity that enables to convert starch directly into l-LA in the presence of oxygen [4]. However, LA-producing microorganisms, including the fungus *R. oryzae*, have low productivity depending on the low reaction rate caused by mass transfer limitation [5]. Most of the world's commercial l-LA is produced by the fermentation of carbohydrates using homolactic microbes such as a variety of modified or developed strains of the genus *Lactobacilli* [6, 7]. This can be considered to be an advantage, since the productivity of the industrial process may become independent of oxygen supply. Nowadays, the development of sustainable processes requires the efficient exploitation of food-processing residues and maximization of the value derived from such waste source. In this field, the dairy industry by-products (e.g., whey, whey permeate (WP)) received considerable attention as a suitable carbon source, since they are substrates that do not require extensive purification, and can be the most appropriate option for the production of biodegradable polymers as well as for many other applications.

2.2.2 Chemical synthesis

The chemical synthesis of LA can be divided into two stages: first stage is a catalytic reaction of acetaldehyde with hydrogencyanide in the liquid phase under atmospheric conditions to produce lactonitrile (acetaldehyde cyanohydrin), which acts as an intermediate. The lactonitrile intermediate is then isolated and purified by distillation. The next stage is a hydrolysis step catalyzed by sulfuric and/or hydrochloric acid at 100 °C, producing a crude LA and ammonium salt (sulfate or chloride) as a by-product. In order to produce pure LA (purification stage), the crude LA is esterified with methanol in the presence of an acid or basic catalysis and then purified by distillation. The methyl lactate ester (a valuable product in its own right) is hydrolyzed under acidic conditions to LA and methanol (which is recycled). Obtained LA is purified by distillation (steaming) to yield high-purity LA. First stage of the LA synthesis is an efficient step with an atom utilization of 100%, while the second stage has a lower atom utilization of around 60%. Esterification and hydrolysis are both efficient processes. The chemically synthesized LA gives the racemic mixture (50% D(−) and 50% L(+)), which does not guarantee the best crystalline melting point (T_m) for PLA production. The most widely used method for improving PLA processability is based on melting point depression by the random incorporation of small amounts of lactide enantiomers of opposite configuration into the polymer (i.e., mixtures of poly-D(−) and poly-L(+) give the best T_m).The commercial

process for LA chemical synthesis uses by-products like acetaldehyde from other industries. Hydrogencyanide is added to acetaldehyde in liquid phase in the presence of a base catalyst under high pressure when lactonitrile is produced [20, 21]. Two companies Musashino Chemical Laboratory Ltd. (Japan) and Sterling Chemicals Inc. (USA) are using this technology. The process is often dependent on other by-product industries and considered expensive where petroleum-based raw material is the major cost-contributor [20].

2.2.3 Green metrics for sustainability of biobased lactic acid production versus chemical synthesis

2.2.3.1 Green metrics of sustainability

For the metrics of sustainability of high optical purity LA, different production routes (biotechnological and chemical) have been taken into consideration for material efficiency evaluation and economic value-added analysis. The biotechnological production of 70% purity LA from wheat biomass was investigated by using a process that consists of the following steps. The wheat starch is enzymatically hydrolyzed to glucose in two steps: liquefaction and saccharification. The fermentable sugars are converted to LA in the fermentation step, using components from the wheat biomass as nutrients. The wheat residues and LA bacteria (*L. plantarum* L10) are removed by centrifugation and the proteins as well as the enzymes are removed by ultrafiltration after fermentation. The fermentation step is performed at a controlled pH, producing mainly lactate. Using water-splitting electrodialysis, the lactate is converted to LA, and sodium hydroxide is produced as a by-product. LA is concentrated by evaporation of water below atmospheric pressure [22]. The selected chemical synthesis method is the reaction of acetaldehyde with hydrogen cyanide, followed by the hydrolysis of the resulting lactonitrile. Crude lactonitrile is then purified by distillation and subsequently hydrolyzed to LA by hydrochloric acid or sulfuric acid [20].

2.2.3.2 Material efficiency and *E*-factor

The results of material efficiency for the biobased LA production have been selected from different publications (Table 2.1).

It can be described by following steps:

$$C_6H_{12}O_6 + 2NaOH \rightarrow 2(CH_3CHOHCOO^-)Na^+ + 2H_2O \quad (2.1)$$

$$(CH_3CHOHCOO^-)Na^+ + H_2O \rightarrow CH_3CHOHCOOH + NaOH \quad (2.2)$$

Table 2.1: The material efficiency of biotechnological lactic acid production.

Raw material	Initial Fermentable Sugar (g/L)	Process	Product, G/L/ LA purity, W/W	Yield (g/g)	Ref.
Whole-wheat flour	87.0±1.1	Fermentation by Lactococcus lactis subslactis, electrodialysis Batch fermentation by *Enterococcus faecalis* RKY1	73.1/>70%	0.64	[24]
Lime-treated wheat straw	50.2	Fermentation by *Bacillus coagulans*	40.7/>70%	0.81	[25]
Oat flour	116.5 (glucose)	Fermentation by *Rhizopus oryzae*	51.7/>70%	0.68	[26]
Barley flour	130 (glucose)	Batch fermentation by *Enterococcus faecalis* RKY1	36/85%	0.94	[27]
Glucose	150	Fermentation by *Lactobacillus casei*	12.5/>70%	0.75	[28]

$$CH_3CHOHCOOH + CH_3OH \rightarrow CH_3CHOHCOOCH_3 + H_2O \quad (2.3)$$

$$CH_3CHOHCOOCH_3 + H_2O \rightarrow CH_3CHOHCOOH + CH_3OH \quad (2.4)$$

Assuming that LA is the only product (and the other products are waste), an *E*-factor of 3.26 can be calculated that leads to a material efficiency of 48%. By an esterification step different potentially useful chemicals such as lactate ester can be produced from LA. If more products from the fermentation broth can be used, the material efficiency increases (68%). The process for chemical synthesis is based on lactonitrile. Hydrogen cyanide is added to acetaldehyde in the presence of a base to produce lactonitrile (1). This reaction occurs in liquid phase at high atmospheric pressures. The crude lactonitrile is recovered and purified by distillation. It is then hydrolyzed to LA, either by concentrated HCl or by H_2SO_4 to produce the corresponding ammonium salt and LA (2). LA is then esterified with methanol to produce methyl lactate (3), which is removed and purified by distillation and hydrolyzed by water under acid catalyst to produce LA and the methanol (4), which is recycled. The chemical synthesis method produces a racemic mixture of LA. This process is represented by the following reactions:

$$CH_3CHO + HCN \rightarrow CH_3CHOHCN \quad (2.5)$$

$$CH_3CHOHCN + 2H_2O + 1/2H_2SO_4 \rightarrow CH_3CHOHCOOH + 1/2(NH_4)_2SO_4 \quad (2.6)$$

$$CH_3CHOHCOOH + CH_3OH \rightarrow CH_3CHOHCOOCH_3 + H_2O \quad (2.7)$$

$$CH_3CHOHCOOCH_3 + H_2O \rightarrow CH_3CHOHCOOH + CH_3OH \quad (2.8)$$

With a 95% yield of LA, 0.515 kg acetaldehyde, 0.300 kg hydrogen cyanide and 0.573 kg sulfuric acid are used for the production of 1 kg LA. An *E*-factor of 1.29 and a material efficiency of 75% can be calculated. This is in accordance with Sheldon [23], who reported an *E*-factor of 1–5 for bulk chemicals. Process like hydrolysis is 81% atom efficient [24].

2.2.3.3 Energy efficiency and total energy input

For the calculation of the total energy input, the data of the BREW project [25] on a cradle-to-factory-gate basis were used. For the calculation of the energy efficiency, the calorific value (higher heating value) of LA (16.56 GJ/ton) was used. For the biotechnological process, the sum of energy input to convert wheat starch into dextrose (D-glucose) is 9.4 GJ/ton of LA and energy input required for LA production is 26.3 GJ/ton [26]. However, the information of energy use due to dextrose processing indifferent bioproduction steps of LA has not been published. Thus, the LA production from one existing plant was applied by distributing the energy efficiency in the process operation as follows:12 GJ/ton of LA for the hydrolysis and fermentation, 2 GJ/ton of LA for the separation and 6 GJ/ton of LA for the recovery. The total energy input for the bio-based process is 35.7 GJ/ton and the energy efficiency is 47%. This is within 17% of the 30.4 GJ/ton estimated by Bohlmann in LCA of PLA production [27]. In the latest cradle-to-polymer-factory-gate life-cycle inventory data for Ingeo PLA (Nature Works LLC product started in 2009) total nonrenewable energy used for LA production system is calculated to be 20.57 GJ/ton In geo [28].

For the chemical synthesis, 9 GJ/ton of LA for the hydrolysis, 14 GJ/ton of LA for the esterification, 6 GJ/ton of LA for the distillation and 7 GJ/ton of LA for the recovery have been taken [29]. The total energy input for the chemical process is 52 GJ/ton and the energy efficiency is 32%.

2.2.3.4 Land use

For wheat-derived starch we base our model calculation on BREW Project report [25]. Wheat crop yield 5.1 ton/ha was taken from FAOSTAT (2013) [30]. LA yield 0.64 ton/ton wheat was calculated from the literature [22]. Therefore, 1.56 ton of wheat are needed as the input for the 1 ton of LA. To receive such amount of wheat requires 0.31 ha of land. The extraction of starch from wheat results in by-products from milling, gluten and pulp. If wholesome wheat is used, these by-products can be sold at current market prices and to substitute reference feed products. After accounting for these by-products, the net input of wheat is 1.06 ton. To receive such amount of wheat, 0.21 ha of land is required. For comparison, in the BREW Project [25] a land use

for different LA biotechnological processes from maize starch was reported between 0.15 and 0.22 ha/ton of LA. For the chemical process, the land use is set at 0 ha/ton.

2.2.3.5 Total costs

The total costs of the fermentative 70% LA production from wheat biomass were calculated according to the methodology used by Akerberg and Zacchi [22]. They reported a total capital investment of 3.8 × 106 USD for an LA plant of 4 × 103 ton/year, that is, 950 USD/ton. The capital costs for the biotechnological process are calculated as 20% of the total capital investment and are 190 USD/ton. It should be mentioned that the capital costs will get reduced at higher production capacity. Operational costs are 830 USD/ton and include costs of labor, process water, power, steam, wheat biomass, enzymes, sodium hydroxide, ultrafiltration and electrodialysis membranes. The total costs for the fermentative LA production from wheat biomass are then 1020 USD/ton (1.020 USD/kg). Economical evaluation of LA production costs showed that the operational costs contribute about 77% of the total costs. Costs of raw materials (26%), fermentation (34%), electrodialysis (27%) and hydrolysis (12%) are the major operational costs. The cost of enzyme mixture dominates the operational costs in the hydrolysis step and the cost of sodium hydroxide in the fermentation step. The recovery step (electrodialysis and evaporator), representing about 40% of the investment costs, followed by fermentation step (28%), is the main contributors to the capital costs. The capital costs do not influence the total costs to any large degree and the variation in these costs will not affect the total production costs as much as the wheat price and other operational costs. As to compare with the integrated process for production and purification of 50% food grade LA from whey, which was economically evaluated by Gonzalez et al. [3], the annual costs of 1.25 USD/kg for 50% LA were calculated. It was observed that the highest contribution of the investment costs correspond to the concentration step, representing 40% of the total capital costs, whereas the fermentation step requires the highest operating costs (47% of the total operating cost). The total costs for the petrochemical process of LA production are the sum of the raw material costs and the capital costs. Based on an acetaldehyde, hydrogen cyanide and sulfuric acid price of 1,001 USD/ton, 1,320 USD/ton and 90 USD/ton (www.ICIS.com), respectively, and a material efficiency of 95%, the raw material costs for the petrochemical process of LA production are 942 USD/ton. The capital costs are estimated as 30% of the raw material costs or 283 USD/ton. The total costs for the petrochemical process are 1,225 USD/ton (1.225 USD/kg).

Currently, the commercial prices of food grade LA range between 1.38 USD/kg (for 50% purity) and 1.54–1.76 USD/kg (for 88% purity). Technical grade LA with 88% purity has been priced as much as 1.58–1.87 USD/kg (www.ICIS.com). According to the Wee et al. [1], on an industrial scale, the production costs of LA will be targeted to

less than 0.8 USD/kg, because the selling price of PLA should decrease roughly by half from its present price of 2.2 USD/kg. An overview of the sustainability metrics for LA is shown in Table 2.2 for the fermentative and chemical processes.

Table 2.2: The comparison of the sustainability metrics for the biotechnological and chemical processes of lactic acid.

Process	Mass efficiency (%)	*E*-factor	Energy efficiency (%)	Land use (ha/ton)	Total costs (USD/ton)
Biotechnological	48	3.26	47	0.21[a]–0.31[b]	1020
Chemical	75	1.29	32	0	1225

[a]By-products are used for gluten and feed production.
[b]By-products cannot be used for feed production; wheat grains are damaged by fungi.

The obtained metrics demonstrated that the biotechnological process for wheat biomass conversion into LA gave an energy efficiency higher by 47% than that by the chemical route and lower total costs for the production by approximately 17%. Although the mass efficiency of the biotechnological production of LA was found to be 36% lower than the chemical process, the *E*-factor of biobased LA demonstrates the low quantity of waste that is produced. Thus, the majority of the big LA manufacturing industries like Musashino Chemical Laboratory, Ltd. (Japan), Corbion Purac (The Netherlands), Nature Works LLC (USA), Galactic (Belgium) and so on have switched over to a fermentation-based technology. Musashino Chemical (China) Co., Ltd. is engaged in the exploitation and innovation of LA industry by combining the latest biofermentation technique and advanced refinement technique. Corbion Purac, the world's largest supplier of LA, has built a plant in Thailand to produce LA from cane sugar or tapioca starch. Fermentation-derived LA mixtures typically consist of 99.5% of the L-isomer and 0.5% of the D-isomer giving the best crystalline melting point (T_m), which is a very important criterion for improving PLA processability by in bioplastics production. Chemical synthesis from petrochemical resources always results in a racemic mixture (50/50) of L(+)- and D(−)-LA, which is a major disadvantage of this approach. Conversely, LA fermentation offers an advantage in terms of the utilization of renewable carbohydrate biomass, low production temperature, low energy consumption and the production of optically highly pure LA by selecting an appropriate strains of microorganisms. The biotechnological production of LA has received a significant amount of interest recently, since it offers an alternative to environmental pollution caused by the petrochemical industry and the limited supply of petrochemical resources. Significant advantage over chemical synthesis is that biotechnological production can use cheap raw materials, such

as renewable carbohydrate biomass. However, there are still several issues that need to be addressed to produce LA biotechnologically within the targeted cost, such as the development of high-performance LA-producing microorganisms and the lowering of the costs of raw materials and fermentation processes.

2.3 Intensification of a fermentation process for the production of lactic acid

Nutrient concentration in the medium is one of the important factors affecting the growth of microorganisms. LAB usually requires complex nutrients (peptones, yeast extracts, vitamins). To achieve maximum LA yields and productivity, all sugars from lignocellulose materials must be utilized. Therefore, the evaluation of the effect of LAB enzymatic activities and their effect on the saccharification process is an essential subject for the intensification of the bio-processes. The endoxylanase and α-amylase activities in wheat bran (WB) media excreted by selected LAB (*L. sakei, P. pentosaceus* and *P. acidilactici*) during 48 h of fermentation have been analyzed (Figure 2.3).

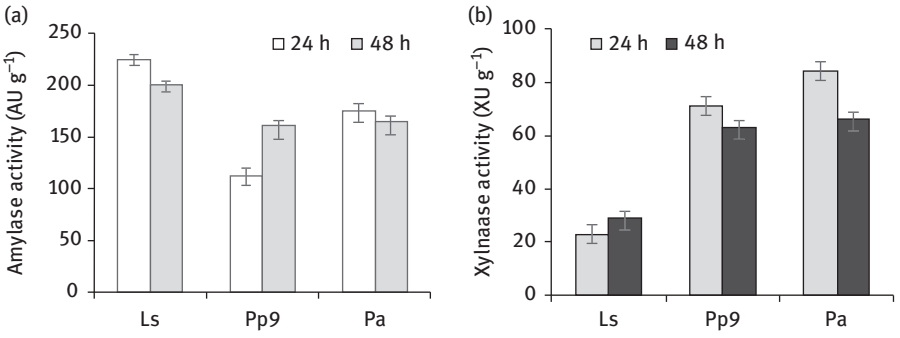

Figure 2.3: Amylase (a) and xylanase (b) activities of *L. sakei* (Ls), *P. pentosaceus* (Pp9) and *P. acidilactici* (Pa) strains in the wheat bran medium after 24 and 48 h fermentation.

Lactobacillus sakei excreted the highest amylase activity (up to 255.6 and 198 AU g^{-1}) after 24 and 48 h of fermentation, respectively, whereas the amylase activity of *P. pentosaceus* and *P. acidilactici* was lower by 50.2% and 22.2%, and by 19.5% and 18%, respectively, after 24 and 48 h of fermentation. The highest endoxylanase activities were excreted by *P. acidilactici* (84.1 and 66 XUg^{-1}) after 24 h and 48 h of fermentation, respectively, followed by *P. pentosaceus* KTU05-9 (71 and 63 XU g^{-1}).

The lowest endoxylanase activity in the WB medium was excreted by *L. sakei* (23 and 29 XUg^{-1}). Saccharide analysis showed a significant ($P < 0.05$) increase in carbohydrates level probably due to the increase in microbial amylase activity. After 24 h fermentation of WB with *L. sakei*, *P. pentosaceus* and *P. acidilactici*, the maltose concentration in the fermentation medium was increased by 85%, 55% and 78%, respectively (Figure 2.4a) compared to the initial value (0.99 mg g^{-1}).

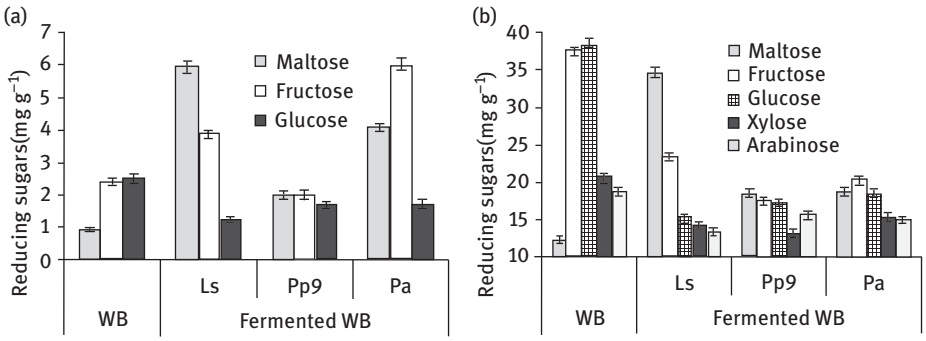

Figure 2.4: Reducing sugars in nonhydrolyzed (a) and enzymatically hydrolyzed (b) wheat bran (WB) before and after 24 h fermentation. LAB: *L. sakei* (Ls), *P. pentosaceus* (Pp9) and *P. acidilactici* (Pa).

According to the HPLC analysis, fructose was not consumed initially by LAB. The concentration of fructose was measured by 38.5% and 60% higher in samples fermented with *L. sakei* and *P. acidilactici*, respectively, compared to the initial value (2.4 mg g^{-1}). Glucose concentrations measured in the fermented WB samples were lower from 32% to 50% compared to initial value (2.5 mg g^{-1}). The sharp decrease in glucose content at the end of fermentation could be due to utilization of glucose by the microorganisms. Similar to glucose, fructose content significantly ($P < 0.05$) decreased at the end of fermentation. Similar results were reported by Khetarpaul and Chauhan [31], indicating that the increase or the decrease in reducing sugars during LA fermentation of pearl millet could be attributed to the action of microflora. Maltose content decreased very rapidly during fermentation, indicating that maltose is preferentially metabolized by the microorganisms. Similar findings were reported during the traditional process of converting pearl millet into fermented gruel [32]. *Lactobacillus sakei* KTU05-6, *P. pentosaceus* KTU05-9 and *P. acidilactici* KTU05-7 should be taken into consideration as starter cultures. Efficient amylolysis could be taken as a main criterion of strain selection, whereas partial starch hydrolysis can be performed by endogenous microflora provided a pregelatinization step [33].

The evaluation of the effect of enzyme treatment on the saccharification process is an essential subject for the intensification of the fermentation process, and for this purpose WB biomass as model system has been taken in consideration. An extensive

monosaccharides target analysis by HPLS-MS after degradation using commercial enzymes such as broad spectrum carbohydrase preparation Depol 692L selected from previous studies was performed in the study. The following tendency in the perspective of the selected enzyme for WB treatment was noticed. Application of Depol 692L for polysaccharide hydrolysis allowed the 13.6-fold and on average 15.4-fold increase of the maltose, fructose and glucose concentrations compared to the raw material (Table 2.3), thus increasing the consumption of glucose and fructose during fermentation with LAB up to 52–60% and 37–53%, respectively. Consumption of other simple saccharides such as xylose and arabinose during lactic fermentation was from 25.8% to 37.9% and from 16.4% to 28.7%, respectively (Figure 2.4b).

Table 2.3: Chemical composition (g 100 g^{-1} d.w.) of agroinustrial by-products.

Materials	Dry matter	Protein	Starch	Total carbohydrates	Total sugars
Wheat bran	87.0 ± 1.1	17.3 ± 3.1	23.2 ± 2.8	64.2 ± 4.2	7.1 ± 1.3
DGS	90.6 ± 1.3	37.3 ± 1.7	4.2 ± 1.5	34.0 ± 1.8	2.9 ± 1.0
BSG	78.1 ± 1.1	24.2 ± 3.1	7.8 ± 4.5	56.3 ± 5.7	–
Lupin	88.5 ± 1.8	36.7 ± 1.2	0.98 ± 0.04	52.1 ± 2.2	6.5 ± 1.1

DGS – spent distiller's grain with solids, BSG – Brewer's spent grain, d.w. – dry weight.

The application of commercial enzymes and LAB evolving required enzyme activities indicates the following tendency in the perspective of the biomass enzymatic pretreatment and fermentative LA production [9, 10]. As was confirmed by an extensive monosaccharide target analysis, the 15-fold increase in maltose, fructose and glucose concentrations can be fixed after the WB polysaccharide enzymatic pretreatment by commercial hemicellulose. Thus, the increase up to 60, 38 and 29% in consumption of glucose, xylose and arabinose (Figure 2.4a), respectively, could be reached during fermentation by LAB [9, 10]. Consumption of other simple saccharides such as xylose and arabinose during lactic fermentation was from 25.8% to 37.9% and from 16.4% to 28.7%, respectively (Figure 2.4b).

The maximum L-LA concentration and yield of 86 g kg^{-1} and 1.45 g^{-1}, respectively, could be achieved after the bioconversion of WB using enzymatic hydrolysis in combination with 48 h fermentation by *P. pentosaceus* KTU05-9 strain [9]. It is a challenge to confirm that other carbon sources (e.g., enzymatically pretreated lignocellulosic brans, DGS and molasse) are suitable media for LAB cultivation [34].

The whey pretreatment with commercial β-galactosidase could increase the lactose hydrolysis up to 36%, thereby resulting the L-LA production up to 28 g L^{-1} using *Pediococcus acidilactici* KTU05-7 strain for the 48 h fermentation [10]. Furthermore, the performed study revealed the tested LAB to display β-galactosidase activity significantly ($P < 0.05$) dependent on the fermentation time (Figure 2.5).

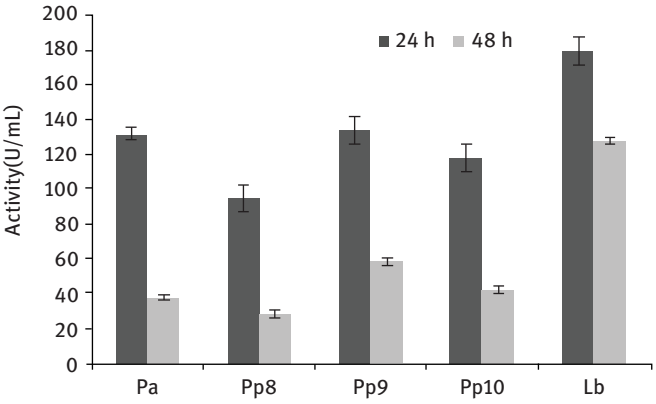

Figure 2.5: β-Galactosidase activity of LAB after 24 and 48 h of cultivation in whey medium. LAB: Pa – *P. acidilactici*; Pp8, Pp9, Pp10 – *P. pentosaceus* strains; *L. bulgaricus*.

The highest β-galactosidase activity of *L. bulgaricus* (180 U/mL), followed by the Pp9 and *P. acidilactici* (on average 133 U/mL) and Pp10 (118 U/mL) was measured after 24 h cultivation in the whey medium. The maximum β-galactosidase activity excreted the Pp9 (57 U/mL) after 48 h of growth; however, the β-galactosidase activities of tested LAB were found lower on average by 65% than that of *L. bulgaricus*, which could be defined as a starter culture able to produce the highest yield of β-galactosidase (128 U/mL) in dairy medium. The longer incubation decreased the β-galactosidase activity of tested strains approximately by 66.2% (Figure 2.2).

Efficient lactose consumption could be taken as the main criterion of strain selection, because in a lactose-rich waste matrix it is expected to increase the availability of energy sources to contribute to a rapid pH decrease [35]. Therefore, the *P. pentosaceus* KTU05-9 and *P. acidilactici* KTU05-7 should be taken into account as the cultures that can be applied for the whey lactose fermentation.

With reference to the results, lactose consumption could reach the same level approximately at 15th- and 16th h in hydrolyzed whey as compared to nontreated samples; therefore, lactose hydrolysis prior to the lacto-fermentation could reduce the fermentation time. In the literature, WB pretreatment using acid hydrolysis (80 °C; 20 h) showed a better performance than that without treatment, especially for L-LA yield (0.99 g g^{-1}) [36]. Maximum L-LA concentration (33 g L^{-1}) was reached employing barley bran hydrolyzates after dilute acid hydrolysis [37]. Also, the L-LA content of 9 g L^{-1} was obtained from soybean straw enzymatic hydrolyzate at 30 °C when using *Lactobacillus casei* for the 54 h fermentation [38]. The tested antimicrobial LAB strains could be selected by excreted specific enzymatic activity dependent on the composition of fermentation medium and fermentation time.

The fermentation of whey with the selected LAB might affect the saccharification process close to the one displayed within the applied commercial β-glucosidase [10].

Moreover, according to the Matijević et al. [39], hydrolysis of whey lactose allows to reduce the fermentation time and increase the viable cell count of bacteria. The higher level of lactose hydrolysis initiates the higher LA productivity; however, the faster pH-value change in the hydrolyzed whey could cause the lower LAB β-galactosidase activity [40]. While the LAB producing bacteriocins are not sensitive for enzymatic treatment used for saccharification of substrate [41], it confirms the outlook of the LAB application for different bioprocesses including the saccharification of fermentation medium.

2.4 Advantage of the use of lactic acid tolerant lab strains for the increasing the efficiency of LA production

A constant important objective during industrial production of LA is the cost reduction not only searching for cheap raw materials but also using of low-cost fermentation processes. Typical LAB fermentation processes are carried out at a minimum pH of 5–5.5, which is much higher than pK_a-value of LA (i.e., 3.78), considering that the LA production requires of neutralizing process. Acid neutralization with traditional reagent $CaCO_3$ at amounts between 10 and 25% (w/v) usually is applied in industry, mainly to make the processing easier and cheaper [42, 43]. On the other hand, the LA extraction process is complicated because of the resulting high salt content; thus, low pH significantly reduces the consumption of neutralizing agent in the fermentation stage and subsequent formation of gypsum in the product recovery stage. Microorganisms that have the capability to ferment raw materials rapidly and provide a high yield of required stereospecific LA under low-pH and high-temperature conditions are industrially desirable. Currently, research on LA production from cheese whey is being conducted on the reduction of hazardous waste, because for microbial fermentation, less sensitive and low pH LAB strains could be applied. LAB strains used in this work have been isolated from rye flour sourdoughs, where the pH could range from 3.2 to 4.2. The object of this experiment was to analyze the effect of neutralization using $CaCO_3$ on LA yields during cheese whey fermentation by the tested LAB. Figure 2.6 presents the pH values in fermented by different LAB hydrolyzed whey with the addition of $CaCO_3$ (2, 4 and 6%, w/v). The maximum decrease in the pH has been detected in whey samples without $CaCO_3$ (Figure 2.6).

Neutralization in all cases lowered the decrease in the pH to a different degree depending on the LAB used could be seen from Table 2.4, the D/L ratio depended on LAB strain used; however, the significant effect ($P < 0.05$) of lactose enzymatic hydrolysis on the reduction of the D(–)-LA content was found. The use of hydrolyzed whey as a fermentation medium reduced the D/L ratio from 0.38 to 0.42 (Pp10 and

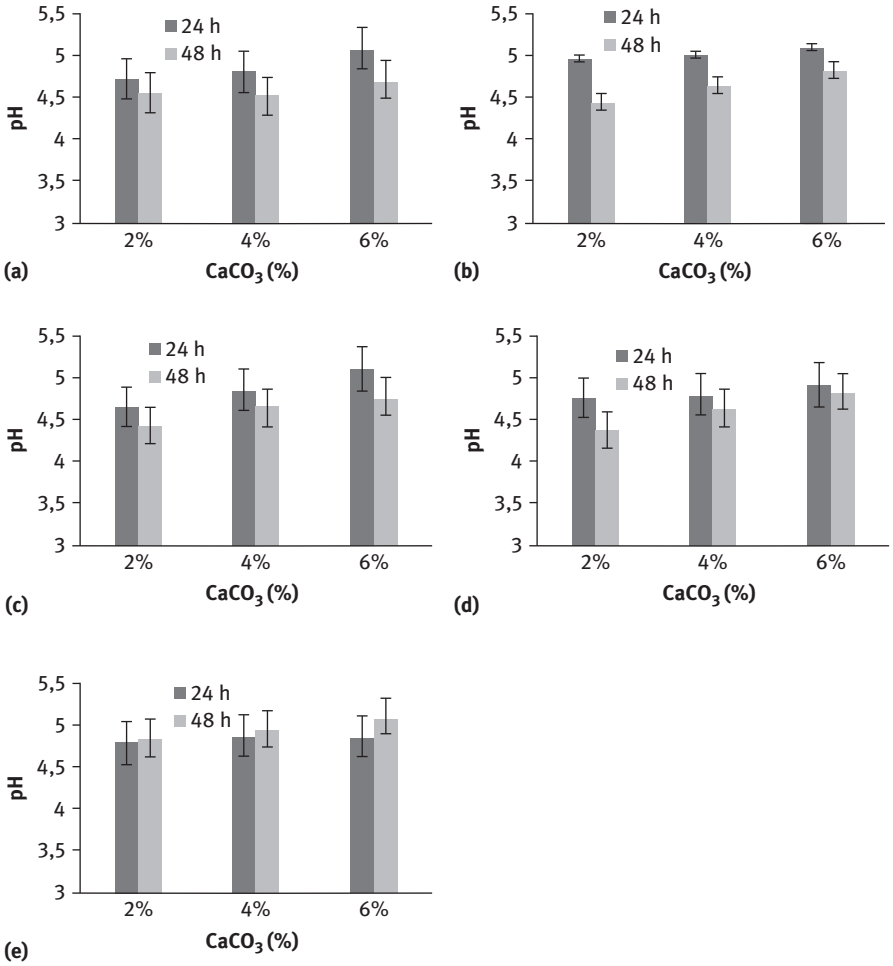

Figure 2.6: The pH profile of whey fermentation by *P. pentosaceus* KTU05-8 (a), *P. pentosaceus* KTU05-9 (b), *P. pentosaceus* KTU05-10 (c), *P. acidilactici* KTU05-7 (d), *L. bulgaricus* (e) with different amounts of $CaCO_3$ (2, 4, 6%, w/v).

Pp9, respectively) (Table 2.4). Lactose hydrolysis prior to the fermentation did not influenced the ability of the *P. acidilactici* and *L. bulgaricus* to produce pure product.

These results are in an agreement with the literature data presented: that by choosing LAB strain an optically pure product can be obtained [44]. Panesar et al. [45] reported the L-LA production from whey using *Lactobacillus casei*. Krischke, Schroder, and Trosch [46] also used Lactobacillus casei for whey fermentation. In all cases the pH was maintained between 4.7 and 5.2 during 24 h of fermentation, and between 4.4 and 5.1 during the next 24 h (Figure 2.5).

Table 2.4: The total lactic acid (LA), L(+) and D(–) isomer contents (g/L) produced by different LAB from nonhydrolyzed and hydrolyzed cheese whey after 24 and 48 h of fermentation.

LAB	Total LA	L(+)	D(–)	Total LA	L(+)	D(–)	Yield*	Qv
	24 h			48 h				
Cheese whey								
Lb	19.05 ± 0.16	n.d.	19.05 ± 0.16	26.56 ± 0.27	n.d.	26.56 ± 0.27	0.540	0.553
Pa	18.36 ± 0.32	18.36 ± 0.34	n.d.	24.54 ± 0.48	24.54 ± 0.48	n.d.	0.499	0.511
Pp10	12.72 ± 0.15	9.53 ± 0.14	3.19 ± 0.01	19.46 ± 0.41	13.91 ± 0.11	5.55 ± 0.18	0.396	0.405
Pp9	17.34 ± 0.13	13.23 ± 0.11	4.11 ± 0.12	25.49 ± 0.62	16.30 ± 0.42	9.19 ± 0.21	0.519	0.531
Pp8	12.24 ± 0.12	7.10 ± 0.09	5.14 ± 0.13	21.45 ± 0.24	12.07 ± 0.22	9.38 ± 0.25	0.436	0.447
Hydrolyzed cheese whey								
Lb	26.02 ± 0.21	n.d.	26.02 ± 0.27	31.70 ± 0.34	n.d.	31.70 ± 0.32	0.645	0.660
Pa	25.13 ± 0.12	25.13 ± 0.12	n.d.	27.86 ± 0.23	27.86 ± 0.23	n.d.	0.567	0.580
Pp10	18.82 ± 0.32	14.77 ± 0.31	4.05 ± 0.34	22.82 ± 0.26	17.54 ± 0.37	5.28 ± 0.24	0.464	0.475
Pp9	25.51 ± 0.23	20.19 ± 0.24	5.32 ± 0.28	28.06 ± 0.54	20.73 ± 0.52	7.33 ± 0.35	0.571	0.584
Pp8	16.40 ± 0.18	10.37 ± 0.44	6.23 ± 0.26	25.21 ± 0.32	14.68 ± 0.31	10.53 ± 0.13	0.513	0.525

Data values are expressed as means with the standard deviations ($n = 3$).
LA – lactic acid; LAB – lactic acid bacteria; Pa – *P. acidilactici*; Pp8, Pp9, Pp10 – *P. pentosaceus* strains; Lb – *L. bulgaricus*; *calculated as g LA/g lactose; Qv=productivity, g LA/(L·h).

The results confirmed that lactose was more utilized for LA fermentation in the samples with $CaCO_3$ (data not shown). This occurrence could be explained by the fact that $CaCO_3$ transformed LA into Ca-lactate during the fermentation. Ca-lactate reduces the inhibition of LA fermentation, which appears by produced LA [47]. In this way, only a part of LA stayed dissolved in whey and only that part was measured [48]. In the presence of $CaCO_3$ lower acidity of medium was achieved from the 24th hour to the end of fermentation.

The addition of $CaCO_3$ in all cases was effective ($P < 0.05$) on the LA yields during fermentation of cheese whey, increasing the total LA as well as L(+)-LA contents (Table 2.5).

The yield of LA obtained during utilization of enzyme hydrolyzed cheese whey at acid neutralization conditions by *L. bulgaricus* was 1.16 g LA/g lactose with productivity of 1.19 g/(L·h), while in the case of tested Pediococci the LA yield and productivity were between 0.69 and 1.15 g LA/g lactose and between 0.71 and 1.17 g LA/(L·h), respectively.

Amounts of $CaCO_3$ required for acid neutralization to optimize LA productivity depended on LAB strain used for whey fermentation (Table 2.5). The most tolerant to acidic medium were Pp9 and *P. acidilactici* strains; the addition of even 2% (w/v) $CaCO_3$ was sufficient to achieve the higher LA yields and productivity from the 24th hour to the end of fermentation, while larger quantities of neutralizing reagent (6%, w/v) influenced more efficient LA production by the Pp8 and Pp10 (Table 2.5).

It was found that production of the more appreciated LA isomer was influenced by the fermentation time and the pH of medium. The effect of neutralization on the D(−)-LA formation in whey medium was ambiguous: the increase in $CaCO_3$ concentration influenced the increase in the D/L ratio in with Pp8 and *P. acidilactici* fermented whey samples, and the decrease in D/L ratio in with Pp10 and Pp9 fermented samples. However, the significant ($P < 0.05$) increase in the D/L ratio during longer fermentation (48 h) was obtained (Table 2.5). According to the results, the maximum L(+)-LA contents were produced by *P. acidilactici* and Pp9 at pH 4.4, by Pp8 and Pp10 at pH 4.7–4.8, while the pH 5.1 was optimal for D(−)-LA production by *L. bulgaricus* (Figure 2.6). In the literature, the optimal pH for LA production varies between 5.0 and 7.0. A pH below 5.7 was only optimal for Lactobacillus strains, which are known to tolerate lower pH than Lactococci [49, 4].

A constant important objective during industrial production of LA is to reduce costs not only searching for cheap raw materials but also using of low-cost fermentation processes. Neutralization of LA fermentation with traditional agent $CaCO_3$ at amounts of 10–25% (w/v) usually is applied in industry, mainly to make the processing easier and cheaper [42, 43]. The low concentration of neutralizing agent, herewith the low content of calcium lactate, did not reduce the growth of fermentation microorganisms [43], and also allows to obtain the higher LA concentration and the maximum productivity [48].

Table 2.5: The total lactic acid (LA), L(+) and D(–) isomer contents (g/L) produced by different LAB from hydrolyzed cheese whey with addition of $CaCO_3$ after 24 and 48 h of fermentation.

$CaCO_3$ (w/v)	Total LA	L(+)	D(–)	Total LA	L(+)	D(–)	Yield*	Qv
	24 h			48 h				
L. bulgaricus								
2	25.43 ± 0.12	n.d.	25.43 ± 0.25	40.19 ± 0.16	n.d.	40.19 ± 0.26	0.816	0.837
4	26.66 ± 0.29	n.d.	26.66 ± 0.17	50.74 ± 0.12	n.d.	50.74 ± 0.32	1.033	1.057
6	28.09 ± 0.23	n.d.	28.09 ± 0.25	56.92 ± 0.25	n.d.	56.92 ± 0.17	0.159	1.186
P. acidilactici								
2	28.76 ± 0.30	28.76 ± 0.21	n.d.	56.22 ± 0.53	56.22 ± 0.53	n.d.	1.145	1.171
4	36.33 ± 0.32	36.33 ± 0.15	n.d.	52.51 ± 0.37	52.51 ± 0.37	n.d.	1.069	1.094
6	35.88 ± 0.19	35.88 ± 0.25	n.d.	47.49 ± 0.27	47.49 ± 0.27	n.d.	0.967	0.989
Pp10								
2	20.12 ± 0.09	14.67 ± 0.12	6.45±0.3	37.68 ± 0.35	31.95 ± 0.29	0.73 ± 0.23	0.783	0.785
4	33.59 ± 0.21	25.51 ± 0.11	8.08±0.30	46.53 ± 0.25	46.65 ± 0.27	8.68 ± 0.21	0.948	0.969
6	28.98 ± 0.30	28.98 ± 0.32	n.d.	52.97 ± 0.45	43.31 ± 0.33	9.66 ± 0.30	1.079	1.104
Pp9								
2	26.39 ± 0.11	22.37 ± 0.30	4.12±0.30	55.65 ± 0.57	47.00 ± 0.45	8.65 ± 0.25	1.133	1.159
4	27.31 ± 0.41	27.31 ± 0.25	n.d.	41.09 ± 0.25	35.36 ± 0.26	5.73 ± 0.37	0.837	0.856
6	29.05 ± 0.32	29.05 ± 0.25	n.d.	42.46 ± 0.25	36.33 ± 0.34	6.13 ± 0.23	0.865	1.104
Pp8								
2	15.99 ± 0.09	15.99 ± 0.26	n.d.	34.22 ± 0.27	27.33 ± 0.26	6.89 ± 0.21	0.697	0.713
4	21.82 ± 0.42	21.82 ± 0.46	n.d.	40.08 ± 0.42	33.18 ± 0.34	6.90 ± 0.20	0.816	0.835
6	23.27 ± 0.28	23.27 ± 0.37	n.d.	46.77 ± 0.55	39.50 ± 0.28	7.27 ± 0.18	0.952	0.974

Data values are expressed as means with the standard deviations ($n = 3$).
LA – lactic acid; LAB – Lactic acid bacteria; Pa – *P. acidilactici*; Pp8, Pp9, Pp10 – *P. pentosaceus* strains; Lb – L. bulgaricus; *calculated as g LA/g lactose; Qv=productivity, g LA/(L·h).

The obtained results confirm the peculiarity of different LAB strains to tolerate acid medium and promising development of new microorganisms for LA production [50]. The high LA yields (1.13–1.14 g/g lactose) and tolerance of low pH conditions indicate a great potential for the use of *P. acidilactici* KTU05-7 and *P. pentosaceus* KTU05-9 strains for industrial applications. The major advantage within the present investigations is the possibility to increase the effectiveness of fermentative LA production from whey reducing the costs of enzyme in the hydrolysis step, and neutralizing reagent in the fermentation step using acid tolerant LA bacteria strains with high β-galactosidase activity in all cases.

2.5 L(+)-lactic acid and D(–)-lactic acid separation and purification from lacto fermented dairy wastes

LA purification is one of the most costly steps of the production process [51, 52]. A combined process of nanofiltration (NF) and reverse osmosis (RO) was applied to separate and concentrate LA after fermentation. The concentrations of LA isomers obtained in the final products (permeate after NF and retentate after RO) are listed in Table 2.6.

The higher lactose retention (89 ± 1%) was obtained by the NF of the broth fermented with Pa compared to Lb (lactose retention was 85 ± 1%). The LA content in the permeate after the NF reached 55.5 g/L for *P. acidilactici* (Pa) with total volume of 94 L and 54.9 g/L for *L. bulgaricus* (Lb) with a total volume of 105 L. A fourfold (Pa) and threefold (Lb) increase in LA concentration was obtained in the retentate after the concentration by the RO. After the membrane filtration, the same tendency of LA isomers distribution was observed as it was after 48 h of LAB fermentation: a higher content of LLA was obtained in WP fermented by *P. acidilactici* (D/L ratio 0.3). In the case of *L. bulgaricus* fermented WP, a greater content of DLA was determined in NF permeate and RO retentate with D/L ratios 5.8 and 5.6, respectively. The complexity of the medium, affecting the NF separation conditions, has been observed by comparing visually the fermentation broth, obtained after fermentations using different LAB strains. Protein aggregates were formed in broth fermented with Lb, while protein aggregation did not occur in broth fermented with Pa. Therefore, due to the biomass and other nondissolved compounds in the fermented broth, a covering layer was formed on the membrane surface, or even in some cases inside the membrane pores. This causes an attenuation of the membrane flux shortly after the filtration starts and needed to be filtered before being transferred to the NF.

A study on the proteolytic action of LAB allowed to provide useful information on the relationship between the flocculation process in the fermented broth and

Table 2.6: The influence of nanofiltration and reverse osmosis on the lactic acid isomers and lactose content (g/L) in permeate and retentate.

Process	*P. acidilactici KTU05-7*	*L. bulgaricus*
Nanofiltration		
Quantity of retentate, L	56	45
LLA, g/L	9.7 ± 0.68^{b}	1.7 ± 0.54^{a}
DLA, g/L	3.2 ± 0.34^{a}	10.1 ± 0.24^{b}
Lactose, g/L	28.9 ± 0.25^{a}	30.7 ± 0.18^{a}
Quantity of permeate, L	94	105
LLA, g/L	42.3 ± 0.27^{b}	8.1 ± 0.54^{a}
DLA, g/L	13.2 ± 0.18^{a}	46.8 ± 0.76^{b}
Lactose, g/L	1.4 ± 0.2^{a}	1.6 ± 0.2^{a}
Reverse osmosis		
Quantity of retentate, L	18.4	30
LLA, g/L	176.0 ± 0.97^{b}	23.9 ± 0.99^{a}
DLA, g/L	56.7 ± 0.98^{a}	135.1 ± 0.97^{b}
Quantity of permeate, L	70.6	70
LLA, g/L	7.4 ± 0.18^{b}	1.9 ± 0.48^{a}
DLA, g/L	2.4 ± 0.24^{a}	9.0 ± 0.43^{b}

All data are means followed by standard deviations ($n = 3$); means within a row with different superscript letters are significantly different ($P < 0.05$); NF – nanofiltration, RO – reverse osmosis, LLA – L(+)- lactic acid isomer, DLA – D(–)-lactic acid isomer.

enzymatic activity of LAB strains. Proteins can be broken down by enzyme hydrolysis into small peptide molecules and amino acids. This positive effect of Pa, possessing the proteolytic activity (0.3 PU/mL), might be due to the solubilization of the precipitated proteins during the long fermentation leading to the antifouling effect in fermented broth, while Lb did not show these activities. The undenaturated protein content could decrease with the increase in acidity of medium (pH 4.6–4.8), indicating the effect of *P. acidilactici* strain in a more intensive denaturation of whey proteins during fermentation.

Current research was focused on the evaluation of performance criteria of membrane filtration (permeate flux, transmembrane pressure (TMP) and volumetric concentration factor) using different LAB strains for L(+)-LA acid and D(–)-LA production (Table 2.7).

After the separation and concentration operations had begun, the flux strongly decreases within 60–70 min (NF) and 15–20 min (RO). The following changes have been noted within the application of the different LAB strains for WP fermentation: the lower decrease (by 66.7%) in the permeate flux during the NF was reached in the Pa sample; during concentration stage (RO), the decrease in permeate flux was lower (by 41.4%) in the Lb sample. Permeate flux can decrease with time due to

Table 2.7: The influence of fermented with different LAB strain whey permeate on membrane filtration parameters.

Samples	Time (h:min)	Qp	TMP	VCF	*J*
Nanofiltration					
P. acidilactici KTU05-9	0:00	0.15	12.75	1.00	20.00
	0:20	0.12	14.25	1.00	16.00
	1:10	0.05	19.25	2.68	6.67
L. bulgaricus	0:00	0.28	12.75	1.00	37.33
	0:20	0.20	12.75	1.00	26.67
	1:10	0.04	20.25	3.33	5.33
Reverse osmosis					
P. acidilactici KTU05-9	0:00	0.29	14.25	1.00	38.67
	0:20	0.12	16.25	4.84	16.00
L. bulgaricus	0:00	0.14	9.25	1.00	38.67
	0:10	0.21	13.25	1.00	28.00
	0:15	0.17	14.25	16.67	22.67

Qp – permeate flow (m^3h^{-1}); TMP – transmembrane pressure (bar); VCF – volumetric concentration factor; J – permeate flux ($Lm^{-2}h^{-1}$).

membrane fouling and concentration polarization [53, 54]. Membrane surface and pore clogging by small molecules is one of the reasons for fouling [55]. Cake layer formation by sludge particle deposition is the most common reason for the flux decline. When the equilibrium between the formation and the washing away of the covering layer was established, the permeability settled at a steady state. TMP varied during NF within the range of 12.75–20.25 bar and during RO from 9.25 to 16.25 bar. When filtration and concentration of with Pa and Lb fermented WP is carried out at the same TMP [12.75 bar (NF); 14.25 (RO)], a permeate flux of 37.33 Lm^{-2} h (NF, Lb); 38.67 Lm^{-2} h (RO, Pa) was obtained with a higher permeate flow 0.28 m^3 h^{-1} (NF, Lb); 0.29 m^3 h^{-1} (RO, Pa), because the covering layer is reduced by a better flush effect and is not as thick as by a lower flow velocity. The development of an effective method of LA separation and purification from a fermentation broth is essential for economic viability. Membrane-based processes have a broad application in dairy industry and are used for dairy wastewater treatment and production of high-purity LA [56 –59]. Several membrane separation steps are combined together to design specific schemes of LA production for industrial use. Furthermore, membrane-based processes allow to eliminate many stages and chemicals used in traditional LA production [60].

The findings of the research suggest that a combined process of NF and RO is an efficient method for LA recovery form fermentation broth, while *P. acidilactici* KTU05-7 strain has a potential to improve the biotechnological production and recovery of LA.

2.6 Conclusions

Microorganisms, isolated from acidic spontaneous fermented cereal media, should be taken into consideration as starter cultures for agroindustrial by-products as well as dairy waste bioconversion to the LA. They demonstrate a longer microbial viability during the fermentation and also allow obtaining the higher concentrations of LA and the maximum productivity. Regular important objective of industrial LA production is the reduction of the cost of neutralizing reagent and avoid environmental problems encountered as a result of the gypsum formation. However, there is still a big need to produce the LA biotechnologically at the lowest costs not only by using cheap raw materials but also by improving the biomass pretreatment process to increase the availability of sugars by microorganisms. To accomplish this task, very promising achievements could be reached by evaluating the enzymatic activities excreting by particular LAB strain in the fermentation medium and based on the obtained results adjust the deficient activities of commercial enzymes. Economical evaluation of costs of the fermentative LA production showed that the operational costs that consist of raw materials, fermentation, electrodialysis and hydrolysis costs contribute about 77% of the total costs [61]. Thus, the combination of enzymatic pretreatment with selected acid tolerant antimicrobial organisms evolving enzyme systems appears to be promising for increasing the economic efficiency of fermentative LA production.

References

[1] Wee Y-J, Kim J-N, Ryu H-W. Biotechnological production of lactic acid and its recent applications. Food Technol Biotechnol 2006, 44, 163–172.
[2] Sheldon RA. Utilisation of biomass for sustainable fuels and chemicals: molecules, methods and metrics. Catal Today 2011, 167, 3–13.
[3] Gonzalez MI, Alvarez S, Riera F, Alvatez RJ. Economic evaluation of an integrated process for lactic acid production from ultrafiltered whey. J Food Eng 2007, 80, 553–561.
[4] Hofvendahl K, Hahn-Hägerdal B. Factors affecting the fermentative lactic acid production from renewable resources. Enzyme Microbiol Technol 2000, 26, 87–107.
[5] Okano K, Tanaka T, Ogino C, Fukuda H, Kondo A. Biotechnological production of enantiomeric pure lactic acid from renewable resources: recent achievements, perspectives, and limits. Appl Microbiol Biotechnol 2010, 85, 413–423.
[6] Naveena BJ, Altaf M, Bhadrayya K, Madhavendra SS, Reddy G. Direct fermentation of starch to L(+) lactic acid in SSF by *Lactobacillus amylophilus* GV6 using wheat bran as support and substrate: medium optimization using RSM. Process Biochem 2005, 40, 681–690.
[7] Ohkouchi Y, Inoue Y. Direct production of L(+)-lactic acid from starch and food wastes using *Lactobacillus manihotivorans* LMG18011. Bioresour Technol 2006, 97, 1554–1562.
[8] Guha A, Banerjee S, Bera D. Production of lactic acid from sweet meat industry waste by Lactobacillus delbruckii. Int J Res Eng Technol 2013, 2, 630–634.
[9] Juodeikiene G, Klupsaite D, Zadeike D, Cizeikiene D, Vidziunaite I, Bartkiene E, et al. Bioconversion of agro-industrial by-products to lactic acid using *Lactobacillus sakei* and two *Pediococcus* spp. strains. Int J Food Sci Technol 2016, 51, 2682–2691.

[10] Juodeikiene G, Zadeike D, Bartkiene E, Klupsaite D. Application of acid tolerant *Pedioccocus* strains for increasing the sustainability of lactic acid production from cheese whey. LWT Food Sci Technol 2016, 72, 399–406.
[11] Bizzari SN, Kishi A. Lactic Acid, its Salts and Esters. Chemical Economics Handbook. Menlo Park, Calif., SRI Int, 2003.
[12] Wee YJ, Kim JN, Ryu HW. Biotechnological production of lactic acid and its recent applications. Food Technol Biotech 2006, 44(2), 163–172.
[13] Södergård A, Stolt M. Properties of lactic acid based polymers and their correlation with composition. Prog polym sci 2002, 27(6), 1123–1163.
[14] Groot WJ, Borén T. Life cycle assessment of the manufacture of lactide and PLA biopolymers from sugarcane in Thailand. Int J Life Cycle Assess 2010, 15(9), 970–984.
[15] Madival S, Auras R, Singh SP, Narayan R. Assessment of the environmental profile of PLA, PET and PS clamshell containers using LCA methodology. J Clean Prod 2009, 17(13), 1183–1194.
[16] Gonzalez MI, Alvarez S, Riera F, Alvarez R. Economic evaluation of an integrated process for lactic acid production from ultrafiltered whey. J Food Eng 2007, 80(2), 553–561.
[17] Sheldon RA. Utilisation of biomass for sustainable fuels and chemicals: Molecules, methods and metrics. Catal Today 2011, 167(1), 3–13.
[18] Rosen MA, Kishawy HA. Sustainable manufacturing and design: Concepts, practices and needs. Sustainability 2012, 4(2), 154–174.
[19] John RP, Nampoothiri KM, Pandey A. Fermentative production of lactic acid from biomass: an overview on process developments and future perspectives. Appl Microbiol Biotechnol 2007, 74(3), 524–534.
[20] Zhao W, Sun X, Wang Q, Ma H, Teng Y. Lactic acid recovery from fermentation broth of kitchen garbage by esterification and hydrolysis method. Biomass Bioenergy, 2009, 33(1), 21–25.
[21] Pal P, Sikder J, Roy S, Giorno L. Process intensification in lactic acid production: a review of membrane based processes. Chem Eng Process 2009, 48(11–12), 1549–1559.
[22] Åkerberg C, Zacchi G An economic evaluation of the fermentative production of lactic acid from wheat flour. Bioresource Technol 2000, *75*(2), 119–126.
[23] Oh H, Wee YJ, Yun JS, Han, SH, Jung S, Ryu HW. Lactic acid production from agricultural resources as cheap raw materials. Bioresource Technol 2005, 96(13), 1492–1498.
[24] Patel M, Ou M, Ingram LO, Shanmugam KT. Fermentation of sugar cane bagasse hemicellulose hydrolysate to L (+)-lactic acid by a thermotolerant acidophilic Bacillus sp. Biotechnol Lett 2004, *26*(11), 865–868.
[25] Patel M, Crank M, Dornberg V, Hermann B, Roes L, Huesing B, . . . Recchia E. Medium and long-term opportunities and risk of the biotechnological production of bulk chemicals from renewable resources-The potential of white biotechnology. Utrecht University, Department of Science, Technology and Society (STS)/Copernicus Institute, 2006.
[26] Vink ET, Rabago KR, Glassner DA, Gruber PR. Applications of life cycle assessment to NatureWorks™ polylactide (PLA) production. Polym Degrad Stab 2003, 80(3), 403–419.
[27] Bohlmann GM. Biodegradable packaging life-cycle assessment. Environ Prog 2004, 23(4), 342–346.
[28] Vink ET, Davies S, Kolstad JJ. The eco-profile for current Ingeo® polylactide production. Ind Biotechnol, 2010, 6(4), 212–224.
[29] Sheldon RA. E factors, green chemistry and catalysis: an odyssey. Chem Commun, 2008, 29, 3352–3365.
[30] FAOSTAT, 2013, http://faostat.fao.org/site/291/default.aspx (last accessed 03. 03.14).
[31] Khetarpaul N, Chauhan BM. Effect of germination and fermentation on available carhohydrate content of pearl millet. Food Chem 1990, *38*(1), 21–26.

[32] Tou EH, Mouquet-Rivier C, Picq C, Traoré AS, Trèche S, Guyot JP. Improving the nutritional quality of ben-saalga, a traditional fermented millet-based gruel, by co-fermenting millet with groundnut and modifying the processing method. LWT-Food Sci and Technol 2007, 40(9), 1561–1569.
[33] Charalampopoulos D, Pandiella SS, Webb C. Growth studies of potentially probiotic lactic acid bacteria in cereal-based substrates. J App Microbiol 2002, 92(5), 851–859.
[34] Kosseva MR, Panesar PS, Kaur G, Kennedy JF. Use of immobilised biocatalysts in the processing of cheese whey. Int J Biol Macromol 2009, 45, 437–447.
[35] Guha A, Banerjee S, Bera D. Production of lactic acid from sweet meat industry waste by Lactobacillus delbrucki. Int J Res Eng Tech, 2013, 2(4), 630–634.
[36] Li Z, Han L, Ji Y, Wang X, Tan T. Fermentative production of L-lactic acid from hydrolysate of wheat bran by *Lactobacillus rhamnosus*. Biochem Eng J 2010, 49, 138–142.
[37] Moldes AB, Torrado A, Converti A, Domínguez JM. Complete bioconversion of hemicellulosic sugars from agricultural residues into lactic acid by *Lactobacillus pentosus*. Appl Biochem Biotechnol 2006, 135, 219–227.
[38] Wang J, Wang Q, Xu Z, Zhang W, Xiang J. Effect of fermentation conditions on L-lactic acid production from soybean straw hydrolysate. J. Microbiol. Biotechnol 2015, 25, 26–32.
[39] Matijević B, Lisak K, Božanić R, Tratni L. Impact of enzymatic hydrolyzed lactose on fermentation and growth of probiotic bacteria in whey. Mljekarstvo, 2011, 61, 154–160.
[40] Wang, D., and Sakakibara, M. Lactose hydrolysis and β-galactosidase activity in sonicated fermentation with *Lactobacillus* strains. Ultrason Sonochem 1997, 4, 255–261.
[41] Narbutaite V, Fernandez A, Horn N, Juodeikiene G, Narbad A Influence of baking enzymes on antimicrobial activity of five bacteriocin-like inhibitory substances produced by lactic acid bacteria isolated from Lithuanian sourdoughs. Lett Appl Microbiol 2008, 47, 555–560.
[42] Huang LP, Jin B, Lant P. Direct fermentation of potato starch wastewater to lactic acid by *Rhizopus oryzae* and *Rhizopus arrhizus*. Bioprocess Biosyst Eng 2005, 27, 229–238.
[43] Nakano S, Ugwu CU, Tokiwa Y. Efficient production of D-lactic acid from broken rice by *Lactobacillus delbrueckii* using $Ca(OH)_2$ as a neutralizing agent. Bioresour Technol 2012, 104, 791–794.
[44] Gonzalez-Vara A, Pinelli D, Rossi M, Fajner D, Magelli F, Matteuzzi D. Production of L(+) and D(-) lactic acid isomers by Lactobacillus casei subsp casei DSM 20011 and Lactobacillus coryniformis subsp. torquens DSM 20004 in continuous fermentation. J Ferm and Bioeng 1996, 81, 548–552.
[45] Panesar PS, Kennedy JF, Knill CJ, Kosseva M. Production of L (+) lactic acid using Lactobacillus casei from whey. Brazilian archives of Biology and Technology 2010, 53(1), 219–226.
[46] Krischke W, Schroder M, Trosch W. Continuous production of L-lactic acid from whey permeate by immobilized Lactobacillus casei subsp. casei. App Microbiol Biotechnol 1991, 34, 573–578.
[47] de Lima CJB, Coelho LF, Blanco KC, Contiero J. Response surface optimization of D-lactic acid production by Lactobacillus SMI8 using corn steep liquor and yeast autolysate as an alternative nitrogen source. Afr J Biotechnol 2009, 8, 5842–5846.
[48] Yen HW, Chen TJ, Pan WC, Wu HJ Effects of neutralizing agents on lactic acid production by Rhizopus oryzae using sweet potato starch. World J Microbiol Biotechnol 2010, 26, 437–441.
[49] Ghaly AE, Tango MSA, Mahmood NS, Avery AC. Batch propagation of Lactobacillus helveticus for production of lactic acid from lactose concentrated cheese whey with microaeration and nutrient supplementation. World J Microbiol Biotechnol 2004, 20, 65–75.
[50] Singh SK, Ahmed SU, Pandey A. Metabolic engineering approaches for lactic acid production. Process Biochem 2006, 41, 991–1000.

[51] Abdel-Rahman MA, Tashiro Y, Sonomoto K. Lactic acid production from lignocellulose-derived sugars using lactic acid bacteria: overview and limits. J Biotechnol 2011, 156(4),286–301.
[52] Datta R, Henry M. Lactic acid: recent advances in products, processes and technologies – a review. J. Chem Technol Biotechnol 2006, 81(7), 1119–1129.
[53] Wojtyniak B, Szaniawska D. Separation of lactic acid solutions from whey fermentation broth using zirconium (IV) hydrous oxide dynamically formed membranes. Pol J Environ Stud 2015, 24(3), 1387–1393.
[54] Silalahi SH, Leiknes T. High frequency back-pulsing for fouling development control in ceramic microfiltration for treatment of produced water. Desalin Water Treat 2011, 28(1–3), 137–152.
[55] Sondhi R, Bhave, R. Role of backpulsing in fouling minimization in crossflow filtration with ceramic membranes. J Membr Sci 2001, 186(1), 41–52.
[56] Yorgun M, Balcioglu IA, Saygin O. Performance comparison of ultrafiltration, nanofiltration and reverse osmosis on whey treatment. Desalination 2008, 229(1–3), 204–216.
[57] Vourch M, Balannec B, Chaufer B, Dorange G Nanofiltration and reverse osmosis of model process waters from the dairy industry to produce water for reuse. Desalination 2005, 172(3), 245–256.
[58] Giorno L, Chojnacka K, Donato L, Drioli E. Study of a cell recycle membrane fermentor for the production of lactic acid by Lactobacillus bulgaricus. Ind Eng Chem Res 2002, 41(3), 433–440.
[59] Gonzalez MI, Alvarez S, Riera FA, Alvarez R. Lactic acid recovery from whey ultrafiltrate fermentation broths and artificial solutions by nanofiltration. Desalination 2008, 228(1–3), 84–96.
[60] Pal P, Sikder J, Roy S, Giorno L Process intensification in lactic acid production: a review of membrane based processes. Chem Eng Process 2009, 48(11), 1549–1559.
[61] Juodeikiene G, Vidmantiene D, Basinskiene L, Cernauskas D, Bartkiene E, Cizeikiene D. Green metrics for sustainability of biobased lactic acid from starchy biomass vs chemical synthesis. Catal Today 2015, 239, 11–16.

Rodrigo Briones, Kokkarachedu Varaprasad

3 Biomass and biowastes: renewable resources for biodegradable materials in advanced applications

3.1 Introduction

Marine algae are photosynthetic organisms that are low-cost and safe renewable resources for several applications. Marine algae are classified into two forms such as microalgae (small-sized algae) and macroalgae (seaweeds) [1]. Macroalgaes (seaweeds) are one of the critical biomass that is available in many coastal areas of different countries worldwide [2, 3]. The cell wall of macroalgae generally has alginic acid, cellulose and polysaccharides [4]. The cellulose in the macroalgae can be hydrolyzed to produce sugars and ethanol. However, they are a source of many polysaccharides as agar, fucoidan, agarose, carrageenan as well as alginate [5]. According to their color, they are classified into brown, green and red algae. Among them, brown algae are an excellent source of extraction of alginate (alginic acid) polymers with better physicochemical properties.

Alginate or algin is a linear anionic polysaccharide polymer of β-(1–4)-D-mannuronic (M) and α-L-gluronic acid (G) and is naturally available in the cell wall of seaweed. These uronic acids can be arranged in heteropolymeric (MG) blocks that have a nearly equal proportion of the monomers and homopolymeric (MM and GG) blocks [6, 7]. The M/G fraction ratio and their structure have a substantial effect on the properties of alginate [8]. The quality of alginate mainly depends on the source of algal species. However, alginate and their derivate polymers can be able to create gelling and increase the swelling properties of the biomaterials and as an emulsifier (stabilizer). These characteristics made them accessible in several kinds of industrial applications such as food, textile, pharmaceutical, cosmetics, paper coatings, adhesives, dyes, gels, explosives, biomedical and environmental technological applications [6, 8, 9].

This chapter describes the alginate extraction from macroalgae and the recent development of biodegradable alginate films, gels and hydrogels for advanced applications.

3.2 Extraction of alginate from brown macroalgae (seaweeds)

Alginates are present in the cell wall of the brown macroalgae, which are insoluble salts of alginic acid. To enhancing the alginate applicability, it was extracted from

https://doi.org/10.1515/9783110538151-003

the macroalgae in the form of water-soluble sodium alginate [10]. Generally, alginate is extracted from the macroalgae via acid method, calcium method and $CaCl_2$–HCl method (Figure 3.1). In this process, a biomass obtained from the seacoast of the marine. The collected biomass was washed with water to remove impurities. Then, the macroalgae samples are dried and cut into small pieces. The resulting pieces were used for extraction of alginic acid.

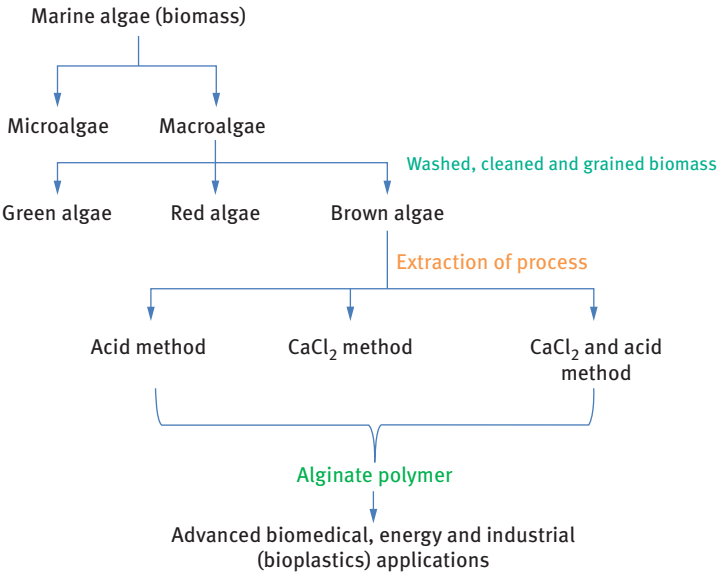

Figure 3.1: Schematic diagram of alginate extraction from marine algae.

3.2.1 Acid method [11–14]

The known amount of dried small macroalgae pieces were soaked for 12 or 24 h in the known percentage of formaldehyde solution to remove the color of macroalgae, then washed with distilled water and added to a known amount of diluted acid (HCl or H_2SO_4) to remove soluble phenolic compounds and impurities. Acid-treated seaweed gives colorless and increases viscosity product, due to a reduced level of phenolic compounds [15]. The obtained product was rewashed with distilled water to eliminate acid excess, after that the solution was filtered, and the known amount of sodium carbonate solution was added up to pH 11. The resulting product was dissolved in the sodium carbonate (Na_2CO_3) solution at room temperature. In this solution, solvent or solvent mixture (Isopropanol, ethanol, water) was added to get

precipitation of alginic acid (collide). The obtained precipitation material was rewashed with solvents (Isopropanol, ethanol) to get pure alginate. Then, it was filtered and dried to use further.

3.2.2 $CaCl_2$ method [11, 15]

In this process, the known amount of seaweed was suspended in the known amount of calcium dichloride ($CaCl_2$) to remove phenolic compounds for 7–24 h. After that, it was treated with the known amount of formaldehyde for 1–12 h to cross-link phenolic compounds. Furthermore, the resulting samples were washed with distilled water and known amount of sodium carbonate (Na_2CO_3) solution is added for 5–48 h. The solution was filtered and precipitated in solvents and dried for the further use.

3.2.3 $CaCl_2$ and acid method

Chee et al. [9] used the cold method and hot method for the extraction of alginic acid. In the cold process, the known amount of seaweed was soaked in known amount of aqueous $CaCl_2$ at room temperature. Furthermore, it was washed with distilled water and stored in HCl for 1 h and again washed with distilled water.
To this, the known amount of Na_2CO_3 was added and kept for 24 h and then 250 mL of water was added. This viscous mixture was obtained via centrifugation. Na-alginate extracted was precipitated by adding an ethanol/water mixture. Finally, the resulting alginate was rewashed with ethanol and dried in a vacuum oven. Similar processes were used in the hot method, except that the storing time was 3 h at 50 °C.

3.3 Characterizations of alginate

Functional groups of alginate were identified from the Fourier transform infrared spectroscopy [13, 16]. Nuclear magnetic resonance spectroscopy is used to know the (uronic acid block) structure in the alginates, which gives M/G ratio for the alginate extracted from the seaweeds [13]. The purification degree of alginate polymer was characterized via fluorescence spectroscopy [13, 17]. Intrinsic viscosity (hydrodynamic volume) of the alginate polymer was measured by employing viscometer [7, 9, 17]. Intrinsic viscosity is mainly dependent on the molar mass, composition and sequence of M and G residues and ionic strength [18]. Rheological behavior is an essential parameter for the food and medical industries. These properties were calculated using rheometer [7, 18].

3.4 Applications

Pure alginates of biomass were used for industrial uses due to their ability to form several biomaterials such as films, gels and hydrogels.

3.4.1 Biodegradable films

During the last few decades, smart films were developed from the macroalgae-based natural polymers for several applications due to their renewable and abundant sources [19]. These materials are alternatives for the nonbiodegradable plastic packing materials. The use of natural polymers in packaging applications can reduce waste disposal since they are biodegradable, renewable and biocompatible. But synthetic plastics cannot decompose naturally and they create environmental problems [20]. Therefore, natural polymer-based films have been used as packaging materials because of their eco-friendly nature. Alginate is one of the biodegradable polymers obtained from the macroalgae and it has been used in the preparation of biodegradable films [21]. According to the literature, alginate films are used to extend the shelf life of foods by preventing moisture loss, oxidative rancidity and microbial spoilage [22]. Kim et al. have reported the alginate extraction from *Sargassum fulvellum* [20]. The obtained alginate was used in the preparation of biodegradable films. Similarly, Kok and Wong extracted alginate from Malaysian *Sargassum polycystum* C. Agardh (marine seaweeds), and they used that alginate for the development of flexible film [23]. Li et al. developed chitosan-alginate films through layer-by-layer assembly and ferulic acid as an effective cross-linker. This film exhibited good mechanical and hydrophobic properties [24]. Yang et al. prepared alginate composite films with high strength and they are used for food packaging application [25]. In this study, ammonium persulfate was used as an initiator to form a grafting between alginate and methacrylate polymer to enhance the mechanical property of films. Lately, antimicrobial alginate films were developed from using antimicrobial enzymes via sonication process. In this process, they achieved better films [26]. Abou Okeil et al. have prepared new topical bioactive alginate films for the wound dressing applications [27]. In this film, they added sulfadiazine alone and silver nanoparticles to enhance the antibacterial activity. However, alginate and alginate derivative biomaterials and nanocomposites exhibited strong antibacterial activity against several bacterias [28]. Table 3.1 explains the new alginate polymer-based films and their applications in advanced fields.

Table 3.1: Alginate polymer-based biodegradable films and applications.

Materials for films	Applications	References
Alginate, glycerol, glucurono-xylooligosaccharides and antioxidant extracts	Bioactive packaging	[29]
Cellulose, alginate	Packaging	[30]
Alginate and collagen	Bone	[31]
Bioactive glass and alginate	Bone regeneration	[32]
Alginate, chitosan, silver nanoparticles	Antibacterial	[33]
Alginate and carboxymethyl cellulose	Wound dressing	[34]
Porous Co–Ni and alginate	Drug delivery	[35]
Calcium and alginate	Harvest water wave energy	[36]
Alginate, calcium chloride and graphene oxide	Industrial applications: heterogeneous catalysis, tissue engineering odontology and biodegradable packaging	[37]
Alginate and glycerin	Water resistant	[38]

3.4.2 Alginate gels and hydrogels

Alginate is a water-soluble polymer and it can increase the viscosity of water due to its functional (GG block) groups. This hydrophilic viscous liquid phase is called as a gel. In addition, alginate polymer in an acidic medium gives a strong H-bond network. This phenomenon makes them more popular in several applications, especially in foods (jams and jellies). In addition, alginate polymers are used as additives and as a stabilizing agent in pharmaceutical industries. However, in biomedical field, it is used for controlled drug release, cell encapsulation, scaffold ligament and tendon tissue engineering.

Hydrogels are a three-dimensional (3D) network of hydrophilic polymer materials that are composed of natural and synthetic materials [8, 39]. Hydrogels can hold a large amount of water or biological fluids [40]. Water or biological fluid holding capacity is based on the functional properties of raw materials for hydrogels. Alginate polymer (macroalgae-based polymer) has been used for the preparation of hydrophilic hydrogels to achieve a cell adhesion, biocompatible, biodegradable and tissue-like properties for advanced applications [41]. In addition, hydrogel swelling and pore property can be regulated by using alginate polymer. Emami et al. reported the formation of hydrogels network is controlled by the aldehyde groups of alginate or low-molecular-weight ratio of oxidized alginate [42]. However, based on hydrogel

properties they can be used in their respective applications. Lately, Park et al. explain that alginate hydrogels are promising materials for the removal of heavy metal ions due to their effective functionals (carboxylic acid of alginate) [43]. Magnetic hydrogel beads were developed from using alginate and nanocellulose to the controlled delivery of drugs. According to the literature, most of the alginate hydrogels were stable at acidic condition due to their functional (carboxylic) groups [44]. Due to this phenomenon, hydrogels are used in limited fields. To enhance the alginate hydrogel applicability in various fields, they have been prepared with other suitable polymers for respective applications. All these studies explained the use of alginate polymer and its main role with other materials to form a hydrogel in biomedical application. Table 3.2 shows the alginate polymer-based materials and their applications.

Table 3.2: Alginate polymer-based hydrogels and their applications.

Materials for hydrogel	Applications	References
Alginate, collagen and hydroxyapatite	Bone tissue engineering	[44]
Alginate and poly(vinyl alcohol)	Agriculture	[45]
Alginate and nanocellulose	3D printing	[46]
Alginate and cellulose nanofibers	Energy storage	[47]
Alginate, gelatin and cellulose nanocyrstals	Cartilage	[48]
Alginate, poly (*N*-isopropylacrylamide) and clay	Wastewater treatment	[49]
Alginate and poly (*N*-isopropylacrylamide)	Drug delivery	[50]
Alginate and gum arabic	Wound healing	[51]
Methacrylated alginate and dialdehyde	Lung disease/cancer	[52]

3.4.3 Recent applications

Alginate is a biocompatible, biodegradable, nanotoxic and gelling biopolymer that can be used in cosmetic, therapeutic, medical, agricultural and environmental technology and in several industrial applications [53]. However, alginate has been used for the development of innovative biomaterials. Alginate can provide an excellent network with inorganic hybrid materials via a covalent coupling [54]. Due to its coupling, hybrid materials gain excellent mechanical strength, which is used in the bone and cartilage regeneration applications. It can be used as a polyelectrolyte additive, especially increasing the physical and chemical strength of paper in paper industries [55]. Alginate in the form of aerogels with nonwoven PET can resist a significant amount of heat, and has higher mechanical strength. Hence, this makes

them popular in thermal clothing applications [56]. Alginate aerogels can be used not only to increase the mechanical strength of materials and stabilization of nanomaterials, and it can also be used to remove toxic materials from waste systems [57]. It can create an excellent polyelectrolyte complexation (charge) with chitosan, which can inhibit the growth of bacteria effectively [58]. Alginate-based polymeric materials significantly interacted with organic and inorganic materials [59–61]. This phenomenon can offer preparation for novel biomedical materials to control medical applications. However, alginate in its salt form has good medical value and economic concerns. Therefore, it has been used for controlled releasing of drugs in therapeutic applications in biomedical field [62].

Alginate biopolymer has been recently used for the preparation of antimicrobial textiles due to its physicochemical characteristic of alginates such as gelling, high biocompatibility and easy modification [63]. In addition, it has good tissue compatibility. For this reason, it has been used in the biomedical field to coating, and stabilizes the nanoparticles with cellulose fibers [64]. However, alginate has emerged as an excellent material for antibacterial finishing of textiles [63].

Alginate is an unbranched anionic polysaccharide and can easily dissolve in aqueous solutions at room temperature without organic solutions, which can create a porous structure to biomaterials (3D) at mild conditions. The creation of porous structure is essential for a few medical applications. Because of its porous structures, scaffolds can hold cells, proteins and drugs and can deliver in a controlled manner [65, 66]. However, alginate plays a vital role in the preparation of 3D scaffolds in bone tissue engineering [65]. Recently, Taira et al. have reported on the electrochemical printing of calcium alginate/gelatin hydrogels [67]. Moreover, the importance of calcium alginate in 3D printing and its function with Ca^{2+}. Also, alginates have been used in the preparation of 3D tissue-like hydrogels to enhance their applicability in various sectors such as advanced tissue engineering, cancer and drug delivery applications [42, 68–71]. Alginate oligosaccharides are used to promote root and seeding growth of plants in agricultural applications [71, 72]. Still, in the future bioplastics could be achieved utilising low-cost renewable and accessible biomass by simplistic economical and sustainable methods (such as solvolytic liquefaction of biomass using polyhydric alcohols to obtain bio-polyols) in order to improve polymer processing for obtained effective biodegradable materials for real use applications [73–75].

3.5 Conclusions

Marine algae (brown biomass) are important sources to obtain alginate biopolymers. The impact of alginate polymer uses in several fields is significantly increased due to its biocompatibility, cell adhesion and biomaterial formation. It has been extracted from brown algae via acid, $CaCl_2$ and acid/$CaCl_2$ method. Hence, alginate polymer is a

potential one for the development of several biomaterials for advanced applications, for all intents and purposes, for the development of biodegradable films, gels and hydrogels for packaging, biomedical, energy and environmental technology applications.

Acknowledgments: The authors would like to thank the Chilean National Commission for Scientific and Technological Research [CONICYT/Fondecyt iniciación/cod. 11160073 and cod. 11160914; CONICYT/Programa de Cooperación Internacional/REDES180165; CONICYT; CIPA, CONICYT Regional, GORE BIO BIO, R17A10003] for financially supporting this research.

References

[1] Zia KM, Tabasum S, Nasif M, Sultan N, Aslam N, Noreen A, Zuber M. A review on synthesis, properties and applications of natural polymer based carrageenan blends and composites. Int J Biol Macromol, 2017, 96, 282–301. https://doi.org/10.1016/j.ijbiomac.2016.11.095

[2] Kumar S, Sahoo D. A comprehensive analysis of alginate content and biochemical composition of leftover pulp from brown seaweed Sargassum wightii. Algal Res, 2017, 23, 233–239. https://doi.org/10.1016/j.algal.2017.02.003.

[3] Rebours C, Marinho-Soriano E, Zertuche-González JA, Hayashi L, Vásquez JA, Kradolfer, P, Soriano G, Ugarte R, Abreu MH, Bay-Larsen I, Hovelsrud G, Rødven R, Robledo D. Seaweeds: An opportunity for wealth and sustainable livelihood for coastal communities. J Appl Phycol, 2014, 26(5), 1939–1951. https://doi.org/10.1007/s10811-014-0304-8

[4] Ardalan Y, Jazini M, Karimi K. Sargassum angustifolium brown macroalga as a high potential substrate for alginate and ethanol production with minimal nutrient requirement. Algal Res, 2018, 36(February), 29–36. https://doi.org/10.1016/j.algal.2018.10.010

[5] Khajouei RA, Keramat J, Hamdami N, Ursu AV, Delattre C, Laroche C, Gardarin C, Lecerf D, Desbrières J, Djelveh G, Michaud P. Extraction and characterization of an alginate from the Iranian brown seaweed Nizimuddinia zanardini. Int J Biol Macromol, 2018, 118, 1073–1081. https://doi.org/10.1016/j.ijbiomac.2018.06.154

[6] Prasad CV, Swamy BY, Narayana Reddy CL, Prasad KV, Sudhakara P, Subha MCS, . . . Rao KC. Formulation and characterization of sodium alginate g-hydroxy ethylacrylate biodegradable polymeric beads: In vitro release studies. J Polym Environ 2012, 20(2), 344–352. https://doi.org/10.1007/s10924-011-0401-6.

[7] Torres MR, Sousa APA, Silva Filho EAT, Melo DF, Feitosa, JPA, de Paula, RCM, Lima MGS. Extraction and physicochemical characterization of Sargassum vulgare alginate from Brazil. Carbohydr Res, 2007, 342(14), 2067–2074. https://doi.org/10.1016/j.carres.2007.05.022

[8] Varaprasad K, Nunez D, Yallapu MM, Jayaramudu T, Elgueta E, Oyarzun P. Nano-hydroxyapatite polymeric hydrogels for dye removal. RSC Adv 2018, 8(32). https://doi.org/10.1039/c8ra01887a

[9] Chee SY, Wong PK, Wong CL. Extraction and characterisation of alginate from brown seaweeds (Fucales, Phaeophyceae) collected from Port Dickson, Peninsular Malaysia. JAppl Phycol 2011, 23(2), 191–196. https://doi.org/10.1007/s10811-010-9533-7

[10] Alba, K., Kontogiorgos, V. Seaweed Polysaccharides (Agar, Alginate Carrageenan). Reference Module in Food Science. Elsevier. 2018, https://doi.org/10.1016/B978-0-08-100596-5.21587-4

[11] Abdul Khalil HPS, Saurabh CK, Tye YY, Lai TK, Easa AM, Rosamah E, . . . Banerjee A. Seaweed based sustainable films and composites for food and pharmaceutical applications: A review. Renew Sustain Energ Rev, 77 (September2016), 2017, 353–362. https://doi.org/10.1016/j.rser.2017.04.025
[12] Fertah M. Isolation and Characterization of Alginate from Seaweed. Seaweed Polysaccharides: Isolation, Biological and Biomedical Applications. Elsevier Inc. 2017, https://doi.org/10.1016/B978-0-12-809816-5.00002-5
[13] Fertah M, Belfkira A, Dahmane E montassir, Taourirte M, Brouillette F. Extraction and characterization of sodium alginate from Moroccan Laminaria digitata brown seaweed. Arab J Chem, 2017, 10, S3707–S3714. https://doi.org/10.1016/j.arabjc.2014.05.003
[14] Rhein-Knudsen N, Ale MT, Ajalloueian F, Meyer AS. Characterization of alginates from Ghanaian brown seaweeds: Sargassum spp. and Padina spp. Food Hydrocoll, 2017, 71, 236–244. https://doi.org/10.1016/j.foodhyd.2017.05.016
[15] Haug A, Smidsrod O, Skjak-Braek G. Uronic acid sequence in alginate from different sources. Carbohydr Res 1974, 32(2), 217–225. https://doi.org/10.1016/S0008-6215(00)82100-X
[16] Fenoradosoa TA, Ali G, Delattre C, Laroche C, Petit E, Wadouachi A, Michaud P. Extraction and characterization of an alginate from the brown seaweed Sargassum turbinarioides Grunow. J Appl Phycol 2010, 22(2), 131–137. https://doi.org/10.1007/s10811-009-9432-y
[17] Klöck G, Pfeffermann A, Ryser C, Gröhn P, Kuttler B, Hahn HJ, Zimmermann U. Biocompatibility of mannuronic acid-rich alginates. Biomaterials, 1997, 18(10), 707–713. https://doi.org/10.1016/S0142-9612(96)00204-9
[18] Manjula B, Varaprasad K, Sadiku R, Raju KM.Preparation and characterization of sodium alginate-based hydrogels and their in vitro release studies. Adv Polym Tech 2013, 32(2), 1–12. https://doi.org/10.1002/adv.21340
[19] Wang L, Campanella O, Patel B, Lu L.Preparation and sealing processing of sodium alginate based blending film. Math Probl Eng, 2015, https://doi.org/10.1155/2015/895637
[20] Kim S, Baek SK, Song KBin. Physical and antioxidant properties of alginate films prepared from Sargassum fulvellum with black chokeberry extract. Food Packaging and Shelf Life 2018, 18(July), 157–163. https://doi.org/10.1016/j.fpsl.2018.11.008
[21] Gao C, Pollet E, Avérous L. Properties of glycerol-plasticized alginate films obtained by thermo-mechanical mixing. Food Hydrocoll, 2017, 63, 414–420. https://doi.org/10.1016/j.foodhyd.2016.09.023
[22] Gomaa M, Fawzy MA, Hifney AF, Abdel-Gawad KM. Use of the brown seaweed Sargassum latifolium in the design of alginate-fucoidan based films with natural antioxidant properties and kinetic modeling of moisture sorption and polyphenolic release. Food Hydrocoll 2018, 82, 64–72. https://doi.org/10.1016/j.foodhyd.2018.03.053
[23] Kok JML, Wong CL. Physicochemical properties of edible alginate film from Malaysian Sargassum polycystum C. Agardh. Sustain Chem Pharm, 2018, 9(July), 87–94. https://doi.org/10.1016/j.scp.2018.07.001
[24] Li K, Zhu J, Guan G, Wu H. Preparation of chitosan-sodium alginate films through layer-by-layer assembly and ferulic acid crosslinking: Film properties, characterization, and formation mechanism. Int J Biol Macromol, 2019, 122, 485–492. https://doi.org/10.1016/j.ijbiomac.2018.10.188
[25] Yang M, Wang L, Xia Y. Ammonium persulphate induced synthesis of polymethyl methacrylate grafted sodium alginate composite films with high strength for food packaging. Int J Biol Macromol, 2018, 1238–1245. https://doi.org/10.1016/j.ijbiomac.2018.12.012
[26] Wang D, Lv R, Ma X, Zou M, Wang W, Yan L, Ding T, Ye X, Liu D. Lysozyme immobilization on the calcium alginate film under sonication: Development of an antimicrobial film. Food Hydrocoll, 2018, 83, 1–8. https://doi.org/10.1016/j.foodhyd.2018.04.021

[27] Abou-Okeil A, Fahmy HM, El-Bisi MK, Ahmed-Farid OA. Hyaluronic acid/Na-alginate films as topical bioactive wound dressings. Eur Polym J, 2018, 109(September), 101–109. https://doi.org/10.1016/j.eurpolymj.2018.09.003
[28] Shankar S, Kasapis S, Rhim JW. Alginate-based nanocomposite films reinforced with halloysite nanotubes functionalized by alkali treatment and zinc oxide nanoparticles. Int J Biol Macromol, 2018, 118, 1824–1832. https://doi.org/10.1016/j.ijbiomac.2018.07.026
[29] Moreira, D Gullón B, Gullón P, Gomes A, Tavaria F. Bioactive packaging using antioxidant extracts for the prevention of microbial food-spoilage. Food Funct, 2016, 7(7), 3273–3282. https://doi.org/10.1039/c6fo00553e
[30] Sirviö JA, Kolehmainen A, Liimatainen H, Niinimäki J, Hormi OEO. Biocomposite cellulose-alginate films: Promising packaging materials. Food Chem, 2014, 151, 343–351. https://doi.org/10.1016/j.foodchem.2013.11.037
[31] Gregurec D, Wang G, Pires RH, Kosutic M, Lüdtke T, Delcea M, Moya SE. Bioinspired titanium coatings: Self-assembly of collagen-alginate films for enhanced osseointegration. J Mater Chem B (2016), 4(11), 1978–1986. https://doi.org/10.1039/c6tb00204h
[32] Zhao F, Zhang W, Fu X, Xie W, Chen X. Fabrication and characterization of bioactive glass/alginate composite scaffolds by a self-crosslinking processing for bone regeneration. RSC Adv (2016), 6(94), 91201–91208. https://doi.org/10.1039/c6ra18309c
[33] Sharma S, Sanpui P, Chattopadhyay A, Ghosh SS. Fabrication of antibacterial silver nanoparticle – Sodium alginate-chitosan composite films. RSC Adv (2012), 2(13), 5837–5843. https://doi.org/10.1039/c2ra00006g
[34] Trevisol TC, Fritz ARM, de Souza SMAGU., Bierhalz ACK, Valle JAB. Alginate and carboxymethyl cellulose in monolayer and bilayer films as wound dressings: Effect of the polymer ratio. J Appl Polym Sci (2019), 136(3), 1–9. https://doi.org/10.1002/app.46941
[35] García-Torres, J., Gispert, C., Gómez, E., & Vallés, E. Alginate electrodeposition onto three-dimensional porous Co-Ni films as drug delivery platforms. Phys Chem Chem Phys (2015), 17(3), 1630–1636. https://doi.org/10.1039/c4cp04389h
[36] Pang Y, Xi F, Luo J, Liu G, Guo T, Zhang C. An alginate film-based degradable triboelectric nanogenerator. RSC Adv (2018), 8(12), 6719–6726. https://doi.org/10.1039/c7ra13294h
[37] Serrano-Aroca Á, Ruiz-Pividal JF, Llorens-Gámez M. Enhancement of water diffusion and compression performance of crosslinked alginate films with a minuscule amount of graphene oxide. Sci Rep (2017), 7(1), 1–8. https://doi.org/10.1038/s41598-017-10260-x
[38] Rhim JW. Physical and mechanical properties of water resistant sodium alginate films. LWT – Food Sci Technol(2004), 37(3), 323–330. https://doi.org/10.1016/j.lwt.2003.09.008
[39] Varaprasad K, Jayaramudu T, Rotimi E. Removal of dye by carboxymethyl cellulose, acrylamide and graphene oxide via a free radical polymerization process. Carbohydr Polym (2017), 164, 186–194. https://doi.org/10.1016/j.carbpol.2017.01.094
[40] Varaprasad K, Malegowd G, Jayaramudu T, Mohan M, Sadiku R. A mini review on hydrogels classification and recent developments in miscellaneous applications. Mater Sci Eng C (2017), 79, 958–971. https://doi.org/10.1016/j.msec.2017.05.096
[41] Hifney AF, Fawzy MA, Abdel-Gawad KM, Gomaa M. Upgrading the antioxidant properties of fucoidan and alginate from Cystoseira trinodis by fungal fermentation or enzymatic pretreatment of the seaweed biomass. Food Chem (2018), 269(April), 387–395. https://doi.org/10.1016/j.foodchem.2018.07.026
[42] Emami Z, Ehsani M, Zandi M, Foudazi R Controlling alginate oxidation conditions for making alginate-gelatin hydrogels. Carbohydr Polym (2018), 198(March), 509–517. https://doi.org/10.1016/j.carbpol.2018.06.080

[43] Park SH., Kim K, Lim JH, Seo CW, Oh JH, Lee SJ Selective lithium and magnesium adsorption by phosphonate metal-organic framework-incorporated alginate hydrogel inspired from lithium adsorption characteristics of brown algae. Sep Purif Technol (2019), 212 (July 2018), 611–618. https://doi.org/10.1016/j.seppur.2018.11.067

[44] Zhou M, Hu Q, Wang T, Xue J, Luo Y Alginate hydrogel beads as a carrier of low density lipoprotein/pectin nanogels for potential oral delivery applications. Int J Biol Macromol (2018), 120, 859–864. https://doi.org/10.1016/j.ijbiomac.2018.08.135

[45] Feng, D., Bai, B., Wang, H., & Suo, Y. Novel fabrication of biodegradable superabsorbent microspheres with diffusion barrier through thermo-chemical modification and their potential agriculture applications for water holding and sustained release of fertilizer. J Agric Food Chem (2017), 65(29), 5896–5907. https://doi.org/10.1021/acs.jafc.7b01849

[46] Leppiniemi J, Lahtinen P, Paajanen A., Mahlberg R, Metsä-Kortelainen S, Pinomaa T, . . . Hytönen VP. 3D-Printable Bioactivated Nanocellulose-Alginate Hydrogels. ACS Appl Mater Interfaces (2017), 9(26), 21959–21970. https://doi.org/10.1021/acsami.7b02756

[47] Zhang X, Wang Y, Luo X, Lu A, Li Y, Li B, Liu S. O / W pickering emulsion templated organo-hydrogels with enhanced mechanical strength and energy storage capacity. ACS Appl Bio Mater (2019), 2(1), 480–487. https://doi.org/10.1021/acsabm.8b00674

[48] Naseri N, Deepa B, Mathew AP, Oksman K, Girandon L. Nanocellulose-based interpenetrating polymer network (IPN) hydrogels for cartilage applications. Biomacromolecules (2016), 17(11), 3714–3723. https://doi.org/10.1021/acs.biomac.6b01243

[49] Wu D, Gao Y, Li W., Zheng X, Chen YG, Wang Q. Selective adsorption of La3+using a tough alginate-clay-poly(n-isopropylacrylamide) hydrogel with hierarchical pores and reversible re-deswelling/swelling cycles. ACS Sustain Chem Eng (2016), 4(12), 6732–6743. https://pubs.acs.org/doi/abs/10.1021/acssuschemeng.6b01691

[50] Liu M, Song X, Wen Y, Zhu JL, Li J. Injectable thermoresponsive hydrogel formed by alginate-g-poly(N-isopropylacrylamide) that releases doxorubicin-encapsulated micelles as a smart drug delivery system. ACS Appl Mater Interfaces (2017), 9(41), 35673–35682. https://doi.org/10.1021/acsami.7b12849

[51] Li M, Li H, Li X, Zhu H, Xu Z, Liu L, Zhang M. A bioinspired alginate-gum arabic hydrogel with micro-/nanoscale structures for controlled drug release in chronic wound healing. ACS Appl Mater Interfaces (2017), 9(27), 22160–22175. https://doi.org/10.1021/acsami.7b04428

[52] Fenn SL, Charron PN, Oldinski RA. Anticancer therapeutic alginate-based tissue sealants for lung repair. ACS Applied Materials and Interfaces (2017), 9(28), 23409–23419. https://doi.org/10.1021/acsami.7b04932

[53] Kondaveeti S, Bueno P V. de A., Carmona-Ribeiro AM, Esposito F, Lincopan N, Sierakowski MR, Petri DFS. Microbicidal gentamicin-alginate hydrogels. Carbohydr Polym (2018), 186 (January), 159–167. https://doi.org/10.1016/j.carbpol.2018.01.044

[54] Vueva Y, Connell LS, Chayanun S, Wang D, McPhail DS, Romer F, . . . Jones JR. Silica/alginate hybrid biomaterials and assessment of their covalent coupling. Appl Mater Today(2018), 11, 1–12. https://doi.org/10.1016/j.apmt.2017.12.011

[55] Bai YY, Lei YH, Shen XJ, Luo J, Yao, CL, Sun RC. A facile sodium alginate-based approach to improve the mechanical properties of recycled fibers. Carbohydr Polym (2017), 174, 610–616. https://doi.org/10.1016/j.carbpol.2017.06.091

[56] Ahmad F, Ulker Z, Erkey C. A novel composite of alginate aerogel with PET nonwoven with enhanced thermal resistance. J Non-Cryst Solids (2018), 491(January), 7–13. https://doi.org/10.1016/j.jnoncrysol.2018.03.023

[57] Nawaz M, Moztahida M, Kim J, Shahzad A, Jang J, Miran W, Lee DS. Photodegradation of microcystin-LR using graphene-TiO2/sodium alginate aerogels. Carbohydr Polym (2018), 199 (June), 109–118. https://doi.org/10.1016/j.carbpol.2018.07.007
[58] Szpankowski W. On a recurrence equation arising in the analysis of conflict resolution algorithms. Commun Stat. Stoch Models (1987), 3(1), 89–114. https://doi.org/10.1016/j.carbpol.2017.11.088
[59] Bilal M, Rasheed T, Iqbal HMN, Li C, Hu H, Zhang X. Development of silver nanoparticles loaded chitosan-alginate constructs with biomedical potentialities. Int J Biol Macromol (2017), 105, 393–400. https://doi.org/10.1016/j.ijbiomac.2017.07.047
[60] Golafshan N, Rezahasani R, Tarkesh Esfahani M, Kharaziha M, Khorasani SN. Nanohybrid hydrogels of laponite: PVA-Alginate as a potential wound healing material. Carbohydr Polym (2017), 176(August), 392–401. https://doi.org/10.1016/j.carbpol.2017.08.070
[61] Park JH, Shin EY, Shin ME, Choi MJ, Carlomagno C, Song JE, Khang G. Enhanced retinal pigment epithelium (RPE) regeneration using curcumin/alginate hydrogels: In vitro evaluation. Int J Biol Macromol (2018), 117, 546–552. https://doi.org/10.1016/j.ijbiomac.2018.05.127
[62] Yuan N. Ning, Li S. Ji, Li G. Qiang. Sodium alginate coated mesoporous silica for dual bio-responsive controlled drug delivery. J Drug Deliv Sci Technol (2018), 46 (May),348–353. https://doi.org/10.1016/j.jddst.2018.05.026
[63] Li J, He J, Huang Y. Role of alginate in antibacterial finishing of textiles. Int J Biol Macromol (2017), 94, 466–473. https://doi.org/10.1016/j.ijbiomac.2016.10.054
[64] Varaprasad K, Raghavendra GM, Jayaramudu T, Seo J. Nano zinc oxide–sodium alginate antibacterial cellulose fibres. Carbohydr Polym (2016), 135, 349–355. JOUR. https://doi.org/10.1016/j.carbpol.2015.08.078
[65] Teixidó M, Font D, Pallejà T, Tresanchez M, Nogués M, Palacín J. Definition of linear color models in the RGB vector color space to detect red peaches in orchard images taken under natural illumination. Sensors (Switzerland) (2012), 12(6), 7701–7718. https://doi.org/10.1039/c3tb20511h
[66] Pan X, Sun Q, Cai H, Gao Y, Tan W, Zhang W Encapsulated feeder cells within alginate beads for: Ex vivo expansion of cord blood-derived CD34+ cells. Biomater Sci (2016), 4(10), 1441–1453. https://doi.org/10.1039/c6bm00191b
[67] Taira N, Ino K, Robert J, Shiku H. Electrochemical printing of calcium alginate/gelatin hydrogel. Electrochim Acta (2018), 281, 429–436. https://doi.org/10.1016/j.electacta.2018.05.124
[68] Diaz-Rodriguez P, Garcia-Triñanes P, Echezarreta López MM, Santoveña A, Landin M. Mineralized alginate hydrogels using marine carbonates for bone tissue engineering applications. Carbohydr Polym (2018), 195(March), 235–242. https://doi.org/10.1016/j.carbpol.2018.04.101
[69] Read GH, Miura N, Carter JL, Kines KT, Yamamoto K, Devasahayam N, Kesarwala AH. Three-dimensional alginate hydrogels for radiobiological and metabolic studies of cancer cells. Coll Surf B: Biointerfaces(2018), 171(April), 197–204. https://doi.org/10.1016/j.colsurfb.2018.06.018
[70] Supramaniam J, Adnan R, Mohd Kaus NH, Bushra R. Magnetic nanocellulose alginate hydrogel beads as potential drug delivery system. Int J Biol Macromol (2018), 118, 640–648. https://doi.org/10.1016/j.ijbiomac.2018.06.043
[71] Wang M, Chen L, Liu Z, Zhang Z, Qin S, Yan P. Isolation of a novel alginate lyase-producing Bacillus litoralis strain and its potential to ferment Sargassum horneri for biofertilizer. MicrobiologyOpen (2016), 5(6), 1038–1049. https://doi.org/10.1002/mbo3.387
[72] Wang M, Chen L, Li Y, Chen L, Liu Z, Wang X, Qin S. Responses of soil microbial communities to a short-term application of seaweed fertilizer revealed by deep amplicon sequencing. Appl Soil Ecol (2018), 125 (October2017), 288–296. https://doi.org/10.1016/j.apsoil.2018.02.013
[73] Briones R, Torres L, Saravia Y, Serrano L, Labidi J. Liquefied agricultural residues for film elaboration. Ind Crops Prod (2015), 78 19–28. http://dx.doi.org/10.1016/j.indcrop.2015.10.021

[74] Kosmela P, Kazimierski P, Formela K, Haponiuk J, Piszczyk L. Liquefaction of macroalgae Enteromorpha biomass for the preparation of biopolyols by using crude glycerol. J Ind Eng Chem (2017) 56 399–406. http://dx.doi.org/10.1016/j.jiec.2017.07.037

[75] D'Souza J, Camargo R, Yan N. Biomass Liquefaction and Alkoxylation: A Review of Structural Characterization Methods for Biobased Polyols. Polym Rev (2017) 57, 668–694. http://dx.doi.org/10.1080/15583724.2017.

Simona M. Coman and Vasile I. Parvulescu

4 Supported metal catalysts for the sustainable upgrading of renewable biomass to value-added fine chemicals and fuels

4.1 The reactivity of supported metals

4.1.1 General characteristics of the metals

4.1.1.1 Individual metals

According to the Sabatier principle, a catalytic reaction requires a surface hosting the substrate at a specific site that allows the formation of unstable surface intermediates from the respective reactants. Such a process supposes a specific chemical bonding of these to the catalyst surface. For the particular case of the metals, this process is further controlled by additional factors such as (i) the dependence on the chemical identity and physical state of the metal and (ii) the effect of the chemical structure of the substrate and its reactivity, and the types of product it can give.

The development of high-surface-area metal catalysts in which all properties are well stabilized is a prerequisite to achieve a high catalytic efficiency. To do this, their morphology can be tuned from large crystalline particles to thin films, porous materials or finely divided materials such as (i) nanoparticles (NPs); (ii) clusters or even (iii) single atoms. It has also been shown that the same material can have different scaling relations depending on the surface considered. For example, the (111), (100) and stepped (211) metal surfaces obey different adsorbate and transition-state scaling relations [1, 2]. However, metal catalysis with isolate atoms is not possible and the deposition of the metals onto supports is leading to a partial transfer of electrons that changes their state in oxidized species.

The definition of the metal catalyst considers that the element should be dominantly in the zero oxidation state. The elements that fulfill this condition are Fe, Co, Ni, Cu, Ru, Rh, Pd, Ag, Ir, Pt and Au. In such a state, under normal conditions, differently to semimetals, they may exhibit larger coordination numbers as 12 [3]. The coordination number, the atomic ratio and the electronic properties of the surface atoms are influenced by the position in the periodic table. Thus while in the First Series iron, cobalt and nickel have almost the same bond lengths, in the later Series the minimum bond length is shown at ruthenium and iridium. Differences are also in the electronic properties of these elements. Gold is the most electronegative metal, and may form salt-like compounds with very electropositive elements (e.g., $Cs^{+}Au^{-}$) [4].

https://doi.org/10.1515/9783110538151-004

An active site can be defined as an atom or a collection of catalyst surface atoms that directly participate in a catalytic cycle, through chemical bond breaking and formation, and the neighboring atoms that could influence the energetics of these processes [5]. Nørskov et al. [6] reported consistent first-principles quantum mechanical calculation results confirming the specificity of the different metal elements in catalysis. As mentioned earlier, for the real metal catalysts the particle size can change from below 1 nm till microns. In the last case, it approaches a massive metal behavior. For these structures, the electronic states of transition metal surfaces are separated into the *sp*-bands and the *d*-bands, where the *sp*-bands originate from the metal valence *s* and *p* atomic orbitals that interact to form broad overlapping bands. The coupling to the metal *d* electrons can roughly be viewed as a two-level coupling [7] (Figure 4.1).

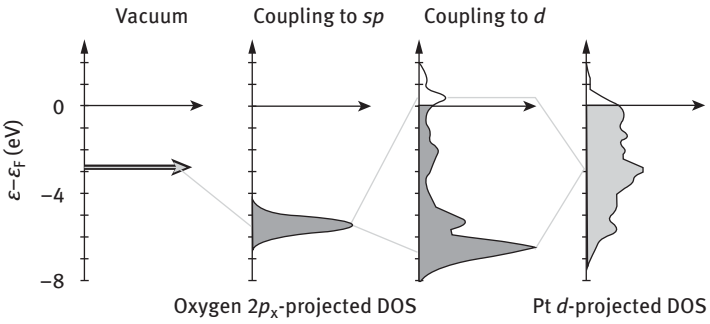

Figure 4.1: Schematic illustration of the change in local electronic structure at an oxygen atom upon adsorption on simple and transition/noble metal surfaces. First, the sharp atomic states of the gas phase are broadened into resonances and shifted down due to the interaction with the metal *sp* states. Next, these renormalized states interact with the narrow *d* bands at the transition and noble metal surfaces, forming covalent bonding and antibonding states below and above the initial adsorbate and surface states. The coupling to the metal *d* electrons can roughly be viewed as a two-level coupling. With accepted courtesy from [7].

Since all transition metals have similar half-filled broad *s*-bands, the energy associated with chemisorption of different molecules can be assumed to have a constant contribution for all metals. Hence, the adsorption energy difference from one metal to the next is determined by the interaction with the metal *d*-states [8]. According to the *d*-band model [9] since the coupling strength between the renormalized state and the *d*-states is weak, to a first approximation, variations in the binding energy only depend on the position of the *d*-states relative to the Fermi level.

For metal surfaces the electrons are available at the Fermi level, and the filling is given by the position of the antibonding states relative to this energy level. Accordingly, variations in bond and activation energies occur from one transition

metal to the next. The differences in the electronic properties of these metals become more important for small particle sizes as indicated by studies reported by the same group [7]. They show clear differences between a continuous band structure of highly delocalized electrons for large clusters (>2 nm) and the more discrete energy levels for smaller clusters (Figure 4.2) [6]. Depending on the nature of the metal, the variation of the adsorption energy on the NPs may follow even a linear dependence as a function of the number of the constituent atoms [10].

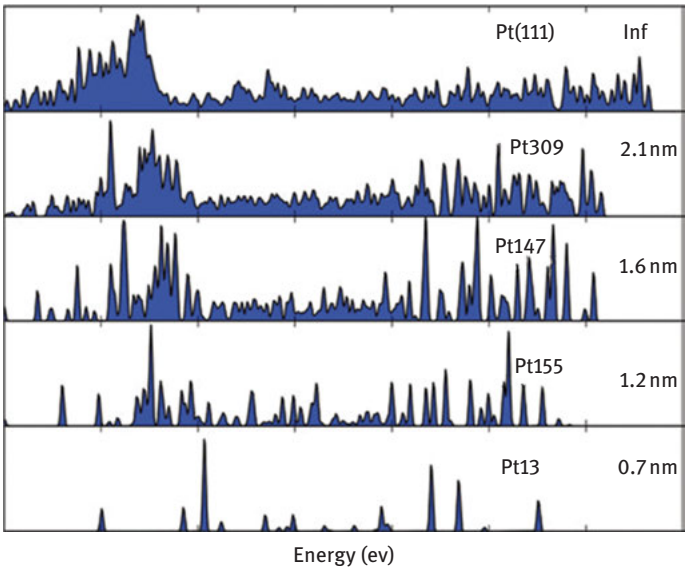

Figure 4.2: Calculated *s*-projected density of states (DOS) for a number of platinum clusters in the cuboctahedron structure in comparison with the calculated *s*-projected DOS for Pt(111). With accepted courtesy from [6].

Oxidation is an important reaction also for the biomass valorization. In this context, the simple *d*-band model also permeates understanding the trends in the variation of the adsorption energy. For example, adsorption energy profiles calculated as a function of the distance of an O atom above the surface shows that O binds most strongly on the metals to the left in the transition metal series and stronger to the 3*d* than to the 4*d* and 5*d* metals in a good concordance with experimental findings (Figure 4.3) [7]. Accordingly, Ru binds O much stronger than Pd and Ag, while Au shows a binding energy per O atom, which is less than that in the O_2 molecule. For Ag, its surface is just able to dissociate O_2 exothermically, whereas Cu forms quite strong bonds with O.

Figure 4.4 depicts the calculated metal *d*-projected densities of states (DOS) for the same metal surfaces together with the O 2*p*-projected DOS in the adsorbed state.

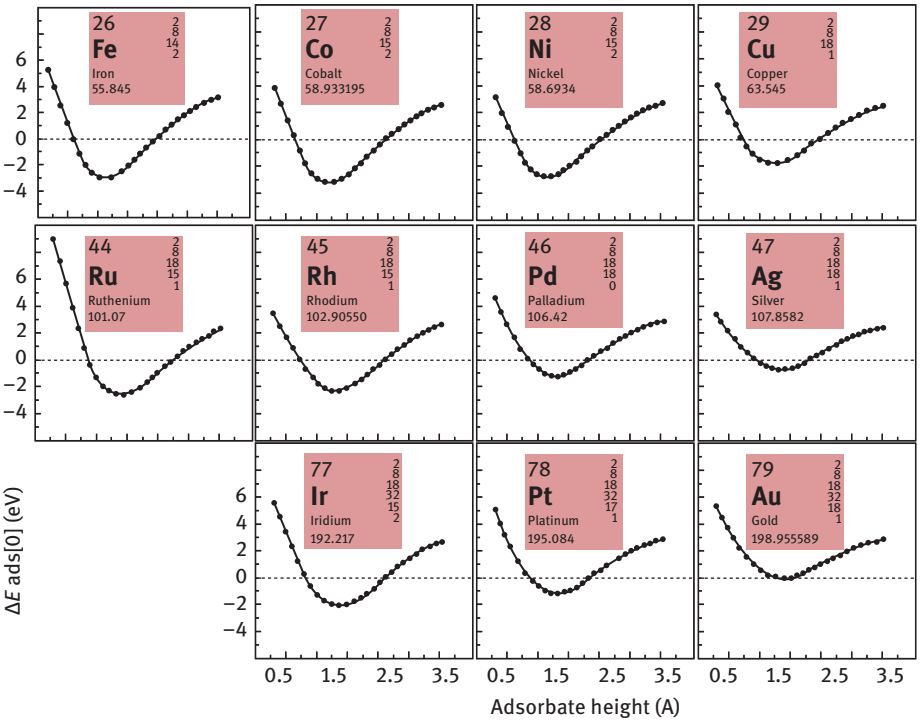

Figure 4.3: Calculated adsorption energies for atomic oxygen as a function of distance of the O atom above the surface for a range of close-packed transition metal surfaces (ordered according to their position in the periodic table). The highest coordination surface site was chosen for the adsorption in all cases. All energies are calculated relative to the energy of O_2 in the gas phase, shown as dotted lines in the plots. Adapted from [7].

The antibonding states for O on Ru are less filled than on Rh, Pd and Ag, confirming that the bonding becomes weaker when moving from left to right in the periodic table. The filling in turn depends on the energy of the antibonding state relative to the Fermi level, the distribution of metal *d*-states relative to the Fermi level, the energy of the O 2*p* state (after interaction with the metal *sp*-states, which is approximately the same for all transition metals) and the strength of the O2*p* and metal *d* coupling [6]. Au is inert with respect to oxygen. Filled *d*-bands generate the weakest oxygen binding since both bonding and antibonding adsorbate–metal states are filled and, accordingly, the interaction with the metal *d*-states is entirely repulsive. That is the reason Ag and Cu are more reactive.

The ability of noble metals to form bonds with H, C and O is governed by these electronic properties. Usually, noble metals, and especially gold, generate weak bonds. The formation of a new compound leads to the disruption of the metal–metal bonds and is controlled by the cohesive energy of the metal. Indeed, such a

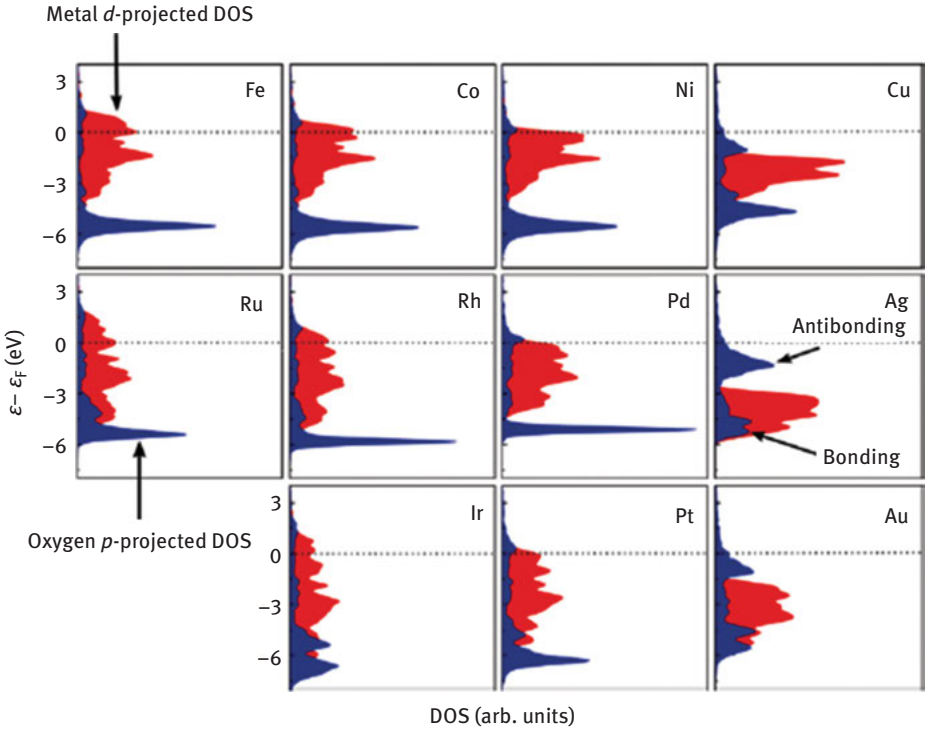

Figure 4.4: The DOS projected onto the *d*-states of the surface atoms (red) and (dark gray) and oxygen 2*p*-projected DOS for O adsorbed on the same surfaces (blue). The formation of bonding and antibonding states below and above the metal *d*-states is clearly seen. The O 2*p*-projected DOS shows the weight of a given state on the O2*p* state. The antibonding states that have more metal *d* character therefore appear weaker than the bonding states that are more O 2*p*-like for all metals except those cases (Ag, Au), where the *d*-states are as low in energy as the O 2*p*-like states. Dashed lines indicate the Fermi level. With courtesy from [6].

behavior makes Pt more "noble" than Cu although its surfaces are less reactive than those of platinum [11].

The variation of the surface structure corresponds to changes in the number of the metal neighbors or the coordination number of the surface metal atoms and, for a given type of transition metal, to changes in the bandwidth of the *d*-DOS and of the *d*-band center. Since the transition state energy defines the "chemisorption energy" of an activated molecule, the arguments behind the *d*-band are also applicable to the interactions in the transition state and in consequence the correlations between the *d*-band center and transition state energies exist as for chemisorption energies [6].

Low coordination numbers of a surface atom are associated with a loss in the electronic overlap between the atoms in the vicinity and create a narrower local *d*-DOS

distribution. The consequence is an upshift in the *d*-band center, which, according to the *d*-band model, results in a more reactive surface. Taking as an example Pt, for the (111) surface atoms have a coordination number of 9, while for the more open (100) and (110) surfaces, the coordination number decreases to 8 and 7, respectively [12]. Steps and kinks in surfaces and edges and corners on NPs have even lower coordination numbers, from 7 to as low as 5. As a result, the close-packed (111) surface binds CO weaker than the step and kink Pt atoms on the (211) and (532) surfaces by more than 0.5 eV.

4.1.1.2 Bi- and multimetallic particles (Au–Pd, Pd–Cu, Au–Ni and so on)

The formation of nanoparticle alloys can significantly enhance the catalytic activity and selectivity [13–16]. The reason for this action is that the formation of multimetallic particles by alloying or sandwiching changes furthers the electronic properties with a direct effect upon the catalytic behavior. For sandwiching, Kitchin et al. [17] considered the Pt(111) surface and a series of different 3*d* metals that have been sandwiched between the first and second layers. The aim was to search for the effect of the subsurface layer of atoms on the reactivity of a Pt(111) overlayer (Figure 4.5). Theoretical studies indicated that the interaction between Pt and a second different metal is similar to a ligand effect leading to a shift down of the *d*-band center that generates changes in the O and H adsorption energies that correspond to weaker bonds (Figure 4.5A). Exception makes Au and Ag. This process is accompanied by changes in the bandwidth due to the hybridization between the *d*-states of the Pt atoms in the surface and the electronic states in the second layer (Figure 4.5B). The same calculations indicate the additional contribution of strain effects caused by the condition to adapt to the lattice constant of the host metal. These are also related to a shift in the *d*-band center, the energetic position of which is crucial for determining the physical and chemical properties of the surface, and are reflected in the change in reactivity of the overlayer relative to the pure metal. A comprehensive picture of the sandwiching effect is shown in Figure 4.6 [18].

Alloying allows a more advanced interaction between the metals destroying the order existing in well-organized surfaces. It provides an another route for changing the electronic properties of metals as demonstrated for the Ni–Au system from density functional theory (DFT) calculations coupled with *in situ* STM investigations [19]. In a very good concordance with the catalytic behavior, they offered proofs of how the energetic barrier depends on the number of Au neighbors.

Figure 4.7 compares metals, alloys and metal-interfaced alloys tested in the electrochemical oxygen reduction reaction [5]. The volcano-like dependence on the OH adsorption energy differentiates between materials to the left where the adsorbates are strongly binded (poisoning adsorbates) and those to the right of which adsorb weakly (these materials are limited by their ability to activate O_2). This quantitative

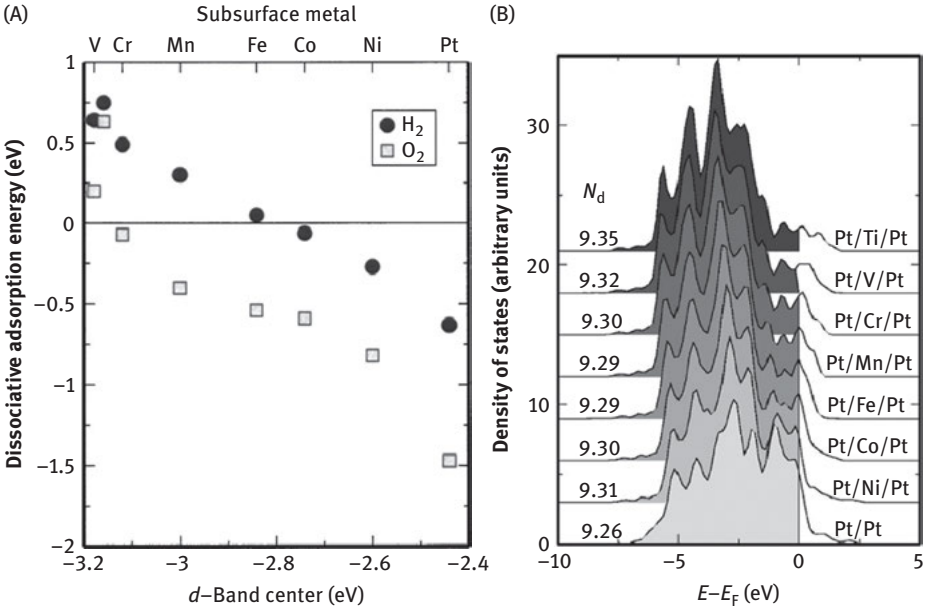

Figure 4.5: (A) Trends in dissociative adsorption energies for H_2 and O_2 on Pt(111) slabs containing subsurface 3*d* metals. (B) Calculated surface *d*-band DOS for subsurface-3*d*-metal-containing Pt slabs. The number of *d*-electrons/surface atom is shown for each band. With accepted courtesy from [17].

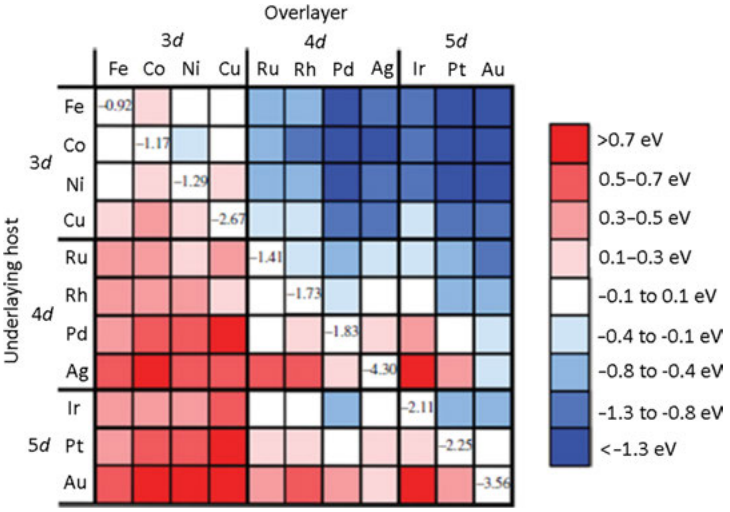

Figure 4.6: Calculated shifts in the *d*-band centers for a number of overlayer structures [18].

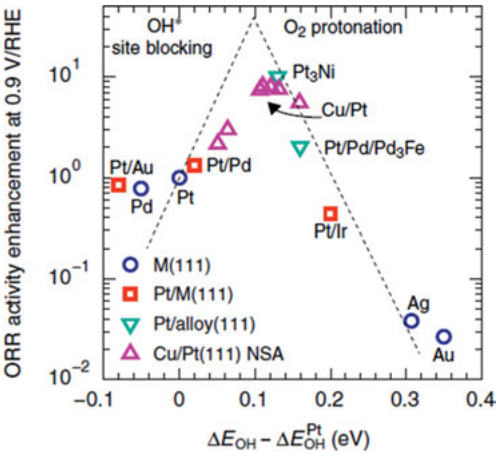

Figure 4.7: Experimentally measured rate enhancement of ORR (ratio to the rate on pure Pt(111)) as a function of DFT-calculated OH binding energies on various (111) surfaces: (○) different pure metal surfaces, (□) Pt monolayer on pure metal surfaces, (▽) Pt monolayer on alloy surfaces, (△) Cu/Pt near surface alloys, characterized by varying Cu content in the first subsurface layer of a Pt(111) crystal. With courtesy from [5].

relationship demonstrates a quite complex pattern in which alloy nanoparticles and interfaces between different metal facets or metal–alloy faces may contribute to a rate enhancement compared to single metal NPs.

4.1.2 Carrier characteristics

4.1.2.1 Nanometal particles supported on oxides

The real heterogeneous catalysts involving metals are more complex structures typically consisting of a catalytically active component that might be a metal, an alloy or a more complex metallic phase and an additional active component that might be an oxide or another compound, and a *support* (i.e., *carrier*) phase that is a high-surface-area material onto which the above NPs are anchored. The additional component may have the role to activate the metallic phase or to catalyze itself a sequence of the total reaction. Thus, it may act as an *electronic* or *structural promoter*. For the first case, an electronic interaction is typical induced for the systems generating the as-named strong metal-support interaction (SMSI), that is, by reducible oxides as TiO_2, Nb_2O_5, CeO_2, ZnO, SnO_2 and so on [20]. As vibrational spectroscopy demonstrated, this effect is caused by an initial flattening of the metal NPs on reduced oxide supports accompanied by an overgrowth of the metal surface by partially reduced oxide species. Finally, reduced moieties of the support migrate onto the metal leading with the formation of

an oxide over layer where it may persist in this form or undergo an additional reduction and alloy formation [21]. The structural promoter can also affect the surface structure by introducing bulk defects that anchor surface defects such as steps that have a high activity.

The interaction between the active metal and the support also determines the shape of the catalyst particle. A weak interaction means that the NP will have a form that is essentially unperturbed by the support. If the interaction is stronger, the interface area will tend to be larger to gain more of the interaction energy, and a truncated particle shape results. Besides the Ostwald ripening other processes associated with metal surface diffusion are also responsible for the NP size growth. For example, in addition to the deterioration in metal dispersion, carbon supports can show chemical instability leading to a partial degradation in the proximity of the NPs in both reducing and oxidizing environments [22].

Typical supports for metals with less electronic influence are metal oxides (Al_2O_3, SiO_2, etc.) and carbons, which can be prepared in a stable, porous form. However, in the absence of these influences, the stability of the supported metal NPs is limited. These cases require the presence of additional *textural promoters*. They are compounds able to preserve the nanoparticles in the form these are deposited on the support, thus avoiding further sintering. Obviously, the textural promoters are oxides like K_2O, MgO, CaO, SrO or BaO prone to generate salts with already existing oxides. As an effect, these basic oxides become stored on the metal surfaces [23]. In this way, the migration of the metal active species is limited under reductive conditions and the catalysts stability improved. Examples of these catalysts are Fe- and Ru-based catalysts.

The use of basic oxides (MgO, CaO, SrO and BaO) also ensures a higher stability of the metal NPs under temperature oxidative conditions. However, this process is controlled by the nature of the noble metal. Hence, Pt/MgO is more stable than Pt/γ-Al_2O_3 as a result of hindering the sintering by MgO compared to γ-Al_2O_3, where Pt particles as large as 30 nm were formed on the air-aged Pt/γ-Al_2O_3 catalyst. An explanation of this behavior considered the formation of Mg_2PtO_4 compounds during the air aging process [24]. On the contrary, magnesium is ineffective for the production of iridates. However, other group IIA-oxides as Ca, Sr or Ba can do this. Like for platinum, the oxidative stabilization is consistent with the formation of an immobile surface iridate via the reaction of a mobile, molecular iridium oxide species [25]. Noteworthy, the process is reversible, and the surface platinates and iridates are readily reduced to metal and the corresponding group IIA-oxide. However, under certain conditions, this process has its limitations. For instance, it has been reported that the oxidation and reduction can be useful for re-dispersion, provided (i) the metal can be oxidized under the conditions used; (ii) reduction can occur without sintering (i.e., sintering temperature is higher than the temperature for metal oxide decomposition) [26]. Oxidation/reduction cycles may also induce a re-dispersion, where the variation in metal–metal distances in the metal oxide surface layer and those in the unoxidized metal cause induced metal strain energy.

The acidic supports may act in a quite similar way with basic supports generating bifunctional catalysts. For example, supports like alumina may catalyze reactions in successive or separate sequences, and aromatization of alkanes represents a relevant example. For a long time it has been considered that this reaction is the result of a concerted participation of the acidic sites of the support and of the metallic sites. However, Pines and Nogueira [27] have shown that it may be catalyzed by "non-acidic" platinum–alumina. More recently, it has been demonstrated that the necessary condition for the realization of this aromatization requires the presence of highly dispersed platinum, and "hard" Lewis acid sites of that are not of the support but induced by its acidity. This Lewis acidity corresponds to ionic Pt forms generated during the synthesis of catalysts and result from strong interaction of the precursor of the active hydrogen hexachloroplatinate precursor with alumina surface defects (Al^{3+}, hard Lewis acid sites) during the course of reduction with hydrogen [28].

The support can also effectively participate only at the interface with the metal, where they generate new sites with different chemical properties than of the parent phases. Besides the effect of the control of the particle size, this is considered as another reason for which gold particles supported on TiO_2 exhibit catalytic properties different from those of unsupported gold [29].

4.1.3 Factors affecting the activity of metal/support catalysts

4.1.3.1 Metal dispersion and its particle size

Except very few examples most of the heterogeneous metal catalysts are used in a highly dispersed state on either inert (monofunctional catalysts) or active (bi- or multifunctional catalysts) supports [30]. The dispersion of the metal affords a large proportion of available metal atoms for the catalytic reaction, and therefore both dispersion and the mean size of the metal particles are important parameters for the characterization of the catalyst. For the practical applications, dispersion (D) is used to calculate the activity of the catalyst per surface metal atom (TOF), while the mean size (d) to evaluate geometric and electronic effects on activity and selectivity of the catalysts [31].

Obviously, these properties are quantified based on the chemisorption measurements. In one of the first attempts, for a given small crystallite shape (crystallite size $d < 100$ Å), Farin and Avnir [32] proposed the following formula (eq. (4.1)) that correlates with the two parameters:

$$D = \frac{k}{d^{(3-\mathrm{DC})}} \tag{4.1}$$

where d is the crystallite diameter, DC is a "chemisorption dimension" and k is a constant; DC > 2 (for $X_M = 1$, X_M is the mean chemisorption stoichiometry) reflects

the fractal surface roughness caused by the fact that the size of the metal atom is comparable with the size of small crystallites. DC and k are constants specific to a given crystallite shape. For large crystallites (d > 100 Å), DC is close to 2 (for X_M = 1).

However, there are factors that affect both the metal dispersion and its particle size and chemisorption measurements with direct implications on the catalytic behavior of the metal-supported catalysts [31]. They include (i) the crystallite-support binding effect, which may cause blocking of a number of surface metal atoms, rendering them inaccessible to the interaction with the reactants; (ii) the effect of imperfect crystallites (for the case of a large spectrum of particle sizes, the effect of imperfections is less important in catalytic practice due to the fact that it is considered in terms of average values); (iii) SMSI may cause changes in the shape of metal particles; (iv) partial metal poisoning as a result of covering of metal particles by products of chemical reactions occurring between a metal and a support; and (v) changes in the stoichiometry of chemisorption X_M with metal particle size, connected to the size-dependent geometric and electronic effects, occurring for small metal particles.

4.1.3.2 Surface area and pore size distribution

The increase in the surface area of a support may favor the increase in the dispersion of the metal catalyst with direct influence upon the increase in the catalytic productivity. It is now well accepted that nanostructures have higher surface areas than do conventional materials. High surface areas can be attained either by fabricating small particles or clusters, where the surface-to-volume ratio of each particle is high, or by creating materials where the void surface area (pores) is high compared to the amount of bulk support material. First category includes materials such as highly dispersed supported metal catalysts, while micro- and mesoporous (nanometer-pored) materials such as zeolites, high-surface-area inorganic oxides, porous carbons and amorphous silicas represent the second one [33].

The use of the micro- and mesoporous materials may offer a second very important advantage for catalysis, that is, the control of the selectivity. Such a control is also known as the shape-selective catalysis. Reaction selectivity is imparted by restricting the entry channel to the internal zeolite structure to molecular diameters that are smaller than the diameter of some potential reactants and products, requiring product formation to occur in a shape-selective manner [34, 35]. Following this strategy they developed synthetic methods that allow a precise control of the metal particle size (NPs in the 1.7–9.0 nm range) and tuning of the pore diameter for a quit large variety of supports. The concept is also including ligated molecular metal clusters, deposition of bare size-selected metal clusters from the gas phase and adsorption of metal complexes followed by treatment to form clusters [36, 37].

However, using conventional deposition methods (such as wet impregnation and ion exchange), the location of metal species cannot always be controlled and

the stability of metal clusters can be a limitation for their applications in heterogeneous catalysis at higher temperatures [38]. To avoid this, Corma et al. [38] proposed the generation of single Pt atoms and Pt clusters with exceptionally high thermal stability by stabilizing subnanometric Pt species during the growth of a two-dimensional MCM-22 zeolite into three dimensions. The procedure also preserved the size-selective catalysis (Figure 4.8). The strategy can be extended as well to other metals [39].

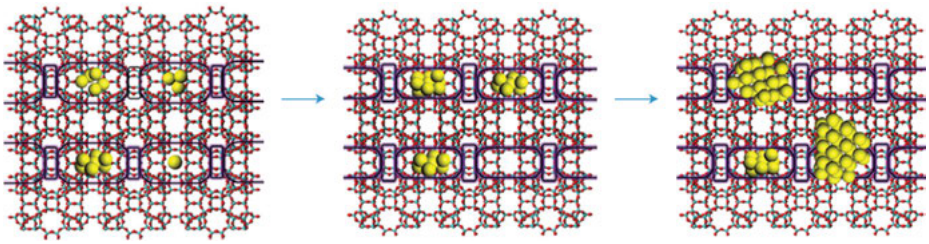

Figure 4.8: Schematic illustration of the evolution of individual Pt atoms and Pt clusters encapsulated in MCM-22 during the high-temperature oxidation–reduction treatments [38].

In addition to the confined molecules, the physicochemical properties of the metal NPs confined in a nanospace can also be modified by the confinement effect [40, 41]. The spatial restriction of metal NPs within a nanosized space can inhibit their sintering, aggregation, detachment and poisoning, thus prolonging activity. The modified electronic structures of the NPs induced by confinement can influence their catalytic performances, as redox reactions involve electron transfer between reactants and catalysts. Nanocatalysts confined in oxide nanotubes also exhibit electronic interactions between the NPs and oxide nanotubes [38, 41].

Procedures for the modification of mesopores affording the deposition of bi- and multimetallic catalytic systems have been largely investigated [42]. They include the use of nanobimetallic colloidal particles and organically modified aminosilicate and various solvents [43, 44]. It was also confirmed that the deposition of these NPs significantly improves to exhibit a protecting effect of the surface functionality [45, 46].

The properties of other oxides were also valorized by exploiting their surface area and pore size distribution. Due to its unique redox properties, ceria is an oxide with a range of applications. These were expanded by the combination of Pt or Rh with the 3D architecture of a ceria-based material resulting in NPs of 3–4 nm, most of them located inside the pores [47]. Atomic layer deposition is another technique that can provide a controllable method to fabricate confined catalysts [41]. Using this technique, confined Cu NPs were prepared by reducing CuO nanowires coated with Al_2O_3 or TiO_2, confined Cu and Au NPs were prepared starting from the corresponding

metal nanowires, and also multiple interfaces (Ni/Al_2O_3 and Pt/TiO_2) (Figure 4.9) in a confined nanospace and spatially separated Pt and CoO_x cocatalysts [48, 49].

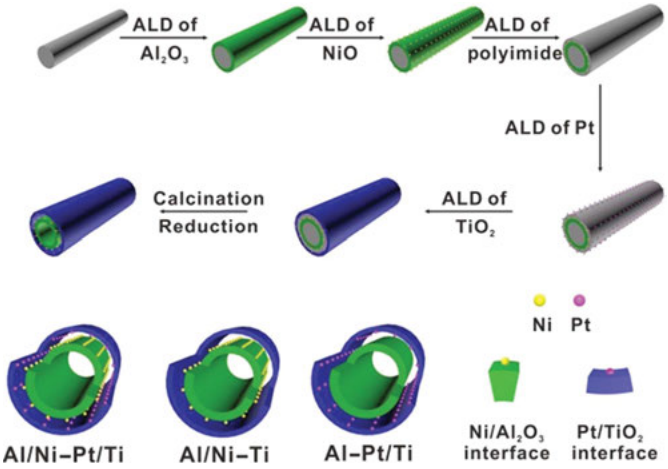

Figure 4.9: Schematic illustration of the synthesis procedure of the confined tandem catalyst with both Ni/Al_2O_3 and Pt/TiO_2 interfaces (Al/Ni–Pt/Ti) and semisectional views of the confined catalysts with single interfaces (Al/Ni–Ti and Al–Pt/Ti). Reproduced with permission from Ref. [41].

4.1.3.3 Redox properties of metals

The ability of transition metals to exist in more than one stable oxidation state makes them suitable catalysts for various reactions. This property becomes relevant in the moment they become coupled with an oxide system. For example, the redox properties of active Cu, Ni and Co in the case of promoted Mo catalysts are explained by the fact that the addition of these metals affects the reducibility of the Mo^{6+} species, which results in a shift of the H_2 consumption to a lower temperature [50]. This behavior has been related to the presence of active Cu^{+}/Cu^{0} and Mo^{5+}/Mo^{4+} redox species. For the glycerol dehydration the redox properties of the Mo species play an important role in the product distribution, which leads to allyl alcohol production with decreased hydroxyacetone yield.

Besides typical catalyzed metal reactions (hydrogenation and oxidation), the metals are also able to catalyze other reactions involving redox processes in which the presence of a promoter is not compulsory. Among these, coupling C–C and C–N reactions are currently very important [51]. However, even in this case metal/metal cooperation like Cu/Pd Sonogashira coupling could improve the catalytic performance [52].

4.1.3.4 Metal–metal interactions in the case of bimetallic catalysts

Besides the redox-type interaction, literature reported a long debate on the role of the supported alloy in catalysis, and the interest was mainly focused on noble metals in combination with Ag or Au. Among these, bimetallic heterogeneous Pd catalysts have elicited a large interest because of their superior selectivity and their resistance to deactivation, which has been observed in several processes of practical importance [53–55]. On the other hand, gold by itself, supported on SiO_2, Al_2O_3 or MgO, shows a rather low catalytic activity [56] but its addition to Pd was found to lead to an enhanced catalytic activity, which has been interpreted in terms of geometric or electronic effects [57].

However, these systems do not contain alloy particles. In addition, there was strong evidence that the addition of Au to Pd results in a marked decrease in the dispersion of the bimetallic catalyst systems [58, 59]. Real bimetallic alloys can only be prepared following the pre-prepared colloidal alloy particles strategy [60], followed by the so-called precursor concept [61]. Using this route, the colloids can be homogeneously dispersed on solid supports. However, the deposition of Pd–Au colloids onto SiO_2 did not produce an enhancement compared to Pd alone. The only positive effect of alloying was the increase in the stability [62].

The support also affects the interaction inside the metallic alloy. Thus, chemisorption and catalytic activity measurements show that the degree of metal–metal interaction in reduced Rh–Au bimetallic catalysts depends on the oxide used as a support ($SiO_2 > TiO_2 > A1_2O_3$). The differences in the degree of interaction are related to differences in the mobility of the metal precursor(s) on the oxide surfaces [63].

4.1.3.5 Morphology of support

The role of the support in modifying NP properties has been recognized from some time when Tauster introduced the concept of the SMSI [20]. Latter, this was treated in terms of charge transfer either to or from the NPs where the particle size itself may be governed by the interaction with the support [64, 65].

More recently, for Pd/Al_2O_3 and Pd/TiO_2 it has been demonstrated based on scanning tunneling microscopy measurements that any NP–support system is the influence of the support morphology as well [66, 67]. It was thus shown that supported metal NPs may exhibit properties differing from those of their single-crystal counterparts. Except the quantum size effects, SMSIs and some interplay between facets, these studies indicate that the support morphology can also have a decisive role in the NP properties. This effect was confirmed by CO chemisorption measurements.

4.2 Biomass upgrading reactions

4.2.1 Lignocellulose fragments upgrading reactions

Lignocellulose is a biomass polymer typically composed of cellulose, hemicellulose and lignin. Figure 4.10 gives a schematic representation of the catalytic reductive fractionation of lignocellulose producing these components [68]. Further valorization obviously considers these fragments and this is the reason for which the discussion will be separately focused on these three components.

4.2.1.1 Cellulose upgrading

Cellulose is a polymer of glucose linked by β-1,4-glycosidic bonds, and glucose is a potential precursor to useful chemicals such as bioethanol and plastics [69–72]. The cellulose valorization supposes a first reaction of hydrolysis to glucose monomers, which are subjected to upgrading via various selective reactions. In this respect, heterogeneous catalytic systems have already been demonstrated a series of advantages that overcome the drawbacks of the previous homogeneous-based technologies [73]. Hydrolytic hydrogenation of cellulose may provide a first shortcut in this process driving the fragmentation of cellulose directly to hexitols (Scheme 4.1) [74].

Hydrolytic hydrogenation of cellulose requires a bifunctional system in which metal-supported catalysts cooperate with an acidic species [75–80]. However, kinetic studies indicated that the metals can promote both hydrolysis and hydrogenation steps [81, 82]. The protons can be in situ generated via the dissociative adsorption of molecular hydrogen on the hydrogenating metal (i.e., Ru, Pt, Pd) and the reversible spillover of atomic H species to the support surface, as a source of acidity for the initial step of cellulose hydrolysis [76]. Also, at reaction temperatures (>200°C), the acidity needed for the initial cellulose hydrolysis may be provided by the hydronium ions generated under the subcritical water conditions applied [83]. This has been confirmed, for instance, for Ru/CMK-3 catalyst, which afforded the hydrolysis of cellulose to glucose via oligosaccharides in hot compressed water without adding any acid catalysts [84]. The use of acidic supports also catalyzes the hydrolysis step. Besides activated carbon materials in this quality may serve Al_2O_3 [85], heteropolyacids (HPA) [86] and various zeolites [87–89]. Sulfonated materials have also been mentioned but their stability has not been demonstrated.

The catalysts with larger mean sizes of Ru particles and abundant acidic sites exhibit better sorbitol yields, while those with smaller Ru particles and less acidic sites favor the formation of 3-β-D-glucopyranosyl-D-glucitol [90]. Cellobiose is first converted on these catalysts to 3-β-D-glucopyranosyl-D-glucitol via the hydrogenolysis, and then sorbitol was formed through the cleavage of β-1,4-glycosidic bond in 3-β-D-glucopyranosyl-D-glucitol (Scheme 4.2, route A). The catalyst with smaller Ru

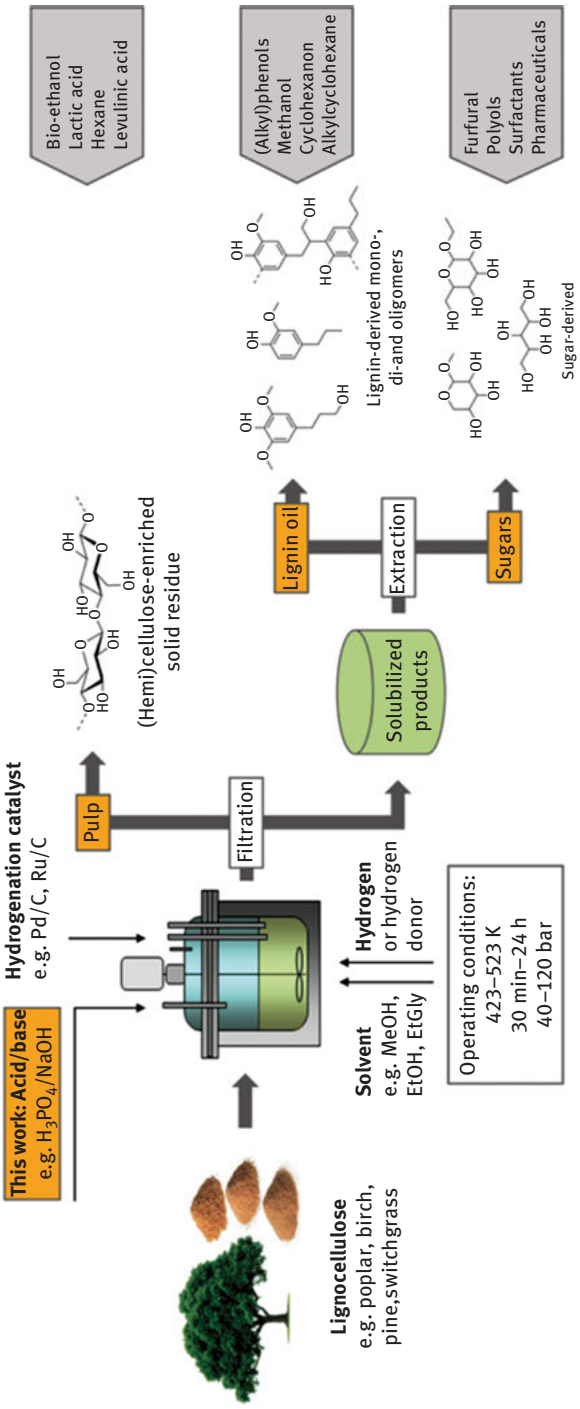

Figure 4.10: Schematic representation of the catalytic reductive fractionation of lignocellulose. Lignin is solvolytically extracted from the matrix and instantly depolymerized with a redox catalyst via hydrogenolysis [68].

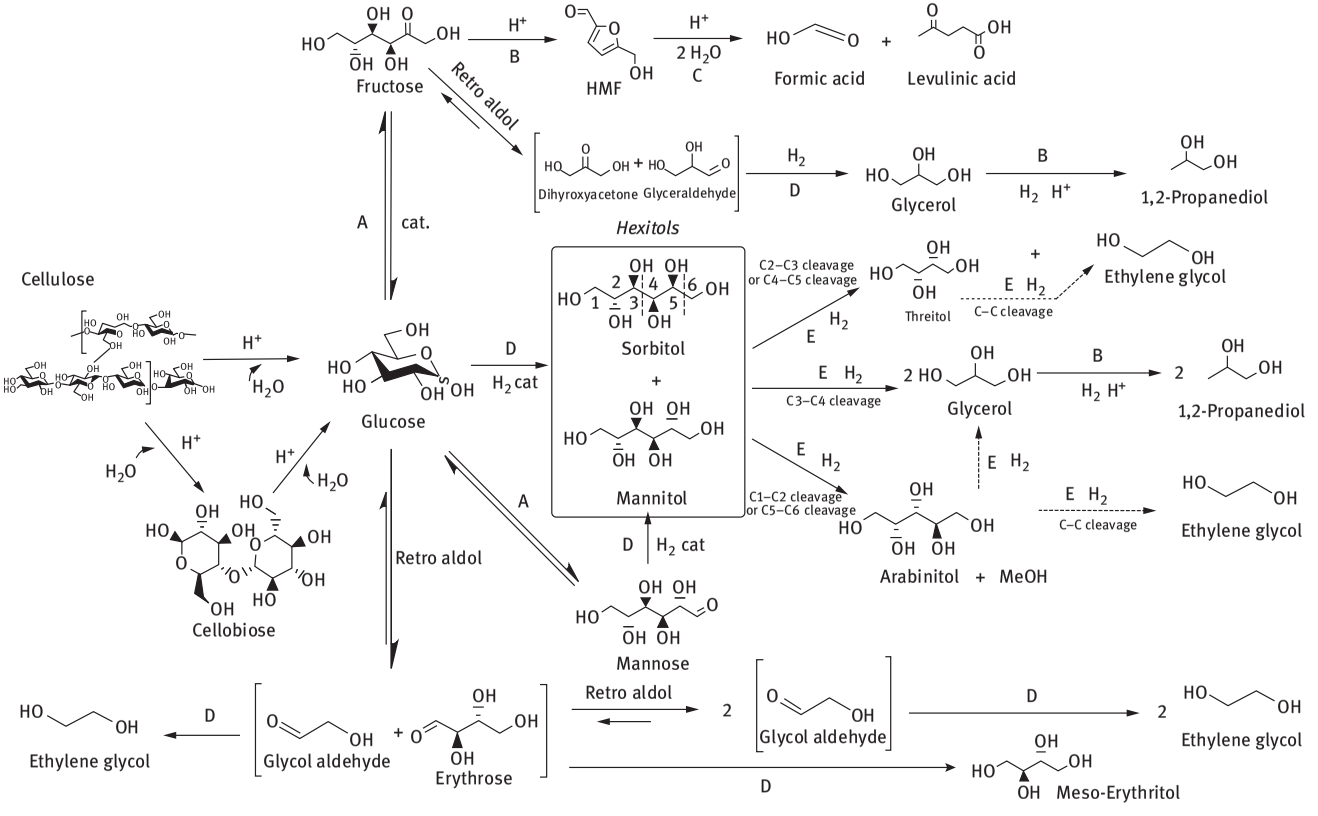

Scheme 4.1: Main reaction pathways in hydrolytic hydrogenation of cellulose with the various Ru and Pt catalysts supported on micro/mesoporous activated carbon (AC or AC-SO3H): (A) isomerization, (B) dehydration, (C) rehydration, (D) hydrogenation, (E) hydrogenolysis). With courtesy from [74].

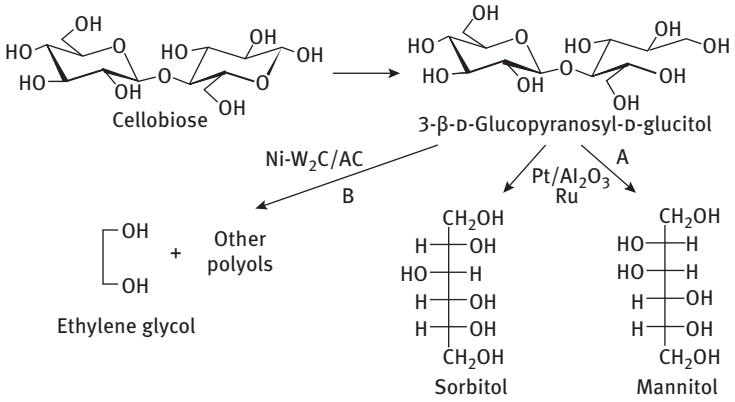

Scheme 4.2: Direct transformation of cellobiose to sorbitol and mannitol (route A) and ethylene glycol and polyols (route B). Adapted from Refs. [78, 90, 92].

particles favored the first step but was disadvantageous to the second step due to less acidity.

The combination of ruthenium with supports presenting various functionalities changes the selectivity of the process. Thus, the combination of HPA or AC-H_2WO_4 with metallic Ru NPs generates composite materials that are able to catalyze the hydrolysis of cellulose, in combination with C–C bond cleavage, and several hydrogenation steps, in cooperative association. While HPAs or AC-H_2WO_4 are efficient catalysts in the cellulose transformation into sugar intermediates and, subsequently, for the selective cleavage of the C–C bonds in these sugars, Ru/C catalyzes the hydrogenation reactions [86–91]. A similar behavior exerts a more simple catalyst, namely, nickel-promoted tungsten carbide (Ni-WC_x/C). It is more selective and in consequence affords the formation of ethylene glycol (EG) in a large extent (Scheme 4.2, route B) [92]. This catalyst is also effective for 1,2-PG production if the catalytic property of the tungsten species is modulated suitably to generate Lewis acid sites: for instance, by an interaction between tungsten and the support [92–94].

However, the one-pot catalytic conversion of cellulose is a complex reaction network, comprising hydrolysis, retro-aldol condensation, hydrogenation, isomerization, dehydrogenation, thermal side reactions and so on. Following this long trajectory, in addition to EG and 1,2-PG, a variety of byproducts such as sorbitol, mannitol, erythritol, 1,2-butanediol and glycerol may be coproduced [91].

The production of sorbitol from levoglucosan (1,6-anhydro-β-D-glucopyranose) and cellobiose, two sugars present in pyrolysis liquids, can be enhanced by using a mesoporous carbon-supported Ru catalyst [95]. Thus, Ru/CMK-3 shows superior catalytic performance compared to commercial Ru/C catalysts. In addition, CMK-3 contains considerable amounts of strong acid sites with beneficial effect upon the hydrogenolysis reactions.

The shortcut attempt to upgrade cellulose can also be achieved via the oxidation reactions onto the metal catalysts. As an example, gold NPs loaded on nitric acid-pretreated carbon nanotubes are efficient for the selective oxidation of cellobiose by molecular oxygen directly to gluconic acid in aqueous medium without a pH control yielding gluconic acid in 80% [96].

However, most of the researches follow the upgrading of the platform molecules, that is, intermediates resulted in the primary transformation of cellulose/glucose. Accordingly, several efficient and green routes of cellulose to different chemicals or intermediates, such as monomeric sugars [97], polyols [92, 98–100], 5-hydroxymethylfurfural (5-HMF) [101] and organic acids [102], have been explored in recent years. These platform molecules could be produced with high activities and selectivities.

4.2.1.1.1 Hydrogenation of glucose/xylose

Comparative hydrogenation of C6 (glucose) and C5 (xylose) sugars over Pt/Al_2O_3, Pt/HT and physical mixture of Pt/Al_2O_3 and HT indicated better performances in terms of both the yield and selectivity for the physical mixture. For glucose, besides the C6-alcohols, the formation of C5-sugar alcohol (xylitol), EG, 1,2-propanediol (1,2-PDO), glycerol, gluconic acid and levulinic acid (LA) has been observed (Scheme 4.3) [103]. For xylose, xylitol was the dominant hydrogenation product, while arabitol, glycerol and xylonic acid were produced only in small amounts (Scheme 4.3) [103].

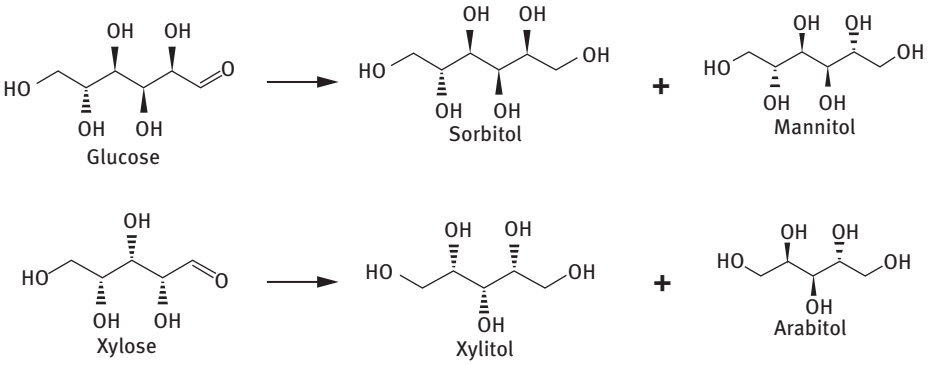

Scheme 4.3: Hydrogenation of glucose and xylose over Pt-based catalysts [103].

In the same process, Ni, Ru and Pt-SnO_x-based catalysts exhibit high activity for hydrogenation of the glucose intermediate to hexitols with improved selectivity, which would otherwise undergo degradation [85, 87, 100, 104–107]. By taking advantage of the basicity of SnO_x species, the direct conversion of cellulose to acetol on Pt-SnO_x/Al_2O_3 and Ni-SnO_x/Al_2O_3 catalysts was achieved [100]. A selective synthesis of sorbitol, EG and propylene glycol in the cellulose reaction was also

reported by tuning the structure of WO_3 domains and acid-basicity of the underlying supports, and particularly in the presence of basic carbon, the dominant formation of propylene glycol [98].

Metal alloys have also been evaluated for hydrogenation of D-glucose under aqueous phase condition. However, the reports are contradictory. For the specific case of Ni and Co, the results indicated that the Ni–Co nanoalloy is more active than the single metal nanocatalysts showing comparable activity and selectivity with that of Pd/C catalyst [108]. Metallic Ni in the nanoalloy is more negatively charged, which is favorable for improving the catalytic activity. However, recycling induces a slight aggregation, crystallization and surface oxidation. An enhancement was also reported for the Raney-type catalysts after promoting with Mo and Cr/Fe. However, both Fe and Ni in these catalysts gave leaching [109]. This behavior is very different from that of Ru which does not leach.

4.2.1.1.2 Multistep transformation of glucose

A one-pot conversion of monosaccharides (fructose and glucose) into 2,5-dimethylfuran (2,5-DMF) has been demonstrated over a multifunctional catalyst obtained by loading Pd on a Zr-based metal–organic framework (UiO-66) that is deposited on sulfonated graphene oxide (Pd/UiO-66@SGO). The Brønsted acidity associated with UiO-66@SGO activates the fructose dehydration to form 5-HMF, while the Pd NPs further convert 5-HMF to 2,5-DMF by hydrogenolysis and hydrogenation (Scheme 4.4) [110].

Biocatalysis and chemocatalysis conducted in multistep one-pot chemoenzymatic syntheses were recently considered revealing the importance of compatibility issues [111]. Owing to differences in optimal pH, temperature, atmosphere and substrate and catalyst interactions often do not allow both types of catalysis to work in tandem. Therefore, an important requirement to achieve an efficient and "real" one-pot hybrid system is to find suitable conditions and catalysts to enable reactions to proceed simultaneously. More robust enzymes and active and selective catalysts in the aqueous phase are prerequisite conditions. To achieve this goal, glucose was first fully hydrogenated to sorbitol by a conventional heterogeneous catalyst [112]. Then, sorbitol was subsequently selectively dehydrogenated to fructose by using a sorbitol dehydrogenase.

4.2.1.1.3 Hydrogenation and hydrogen transfer reduction of furfural and hydroxymethyl furfural

With an annual production close to 300 kTA, furfural is currently a commodity chemical, and the technology for its production is largely established [113]. Further, hydrogenation of furfural and hydroxymethyl furfural is obviously catalyzed using heterogeneous metal-based (i.e., Pd, Ru, Pt, Cu) catalysts supported on carbon, alumina or silica [114–118]. However, on these catalysts, under the reaction conditions,

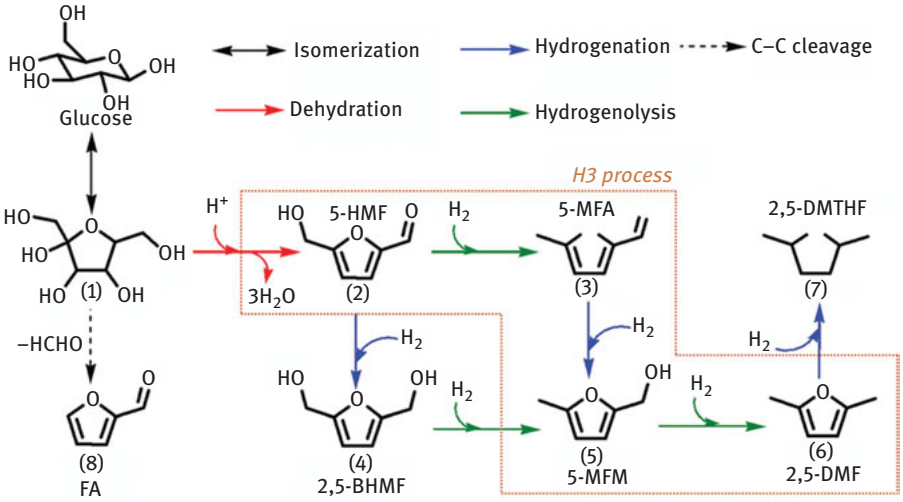

Scheme 4.4: Reaction pathways for glucose conversion to 2,5-dimethylfuran. (1) Fructose; (2) 5-hydroxymethylfurfural (5-HMF); (3) 5-methylfurfural (5-MFA); (4) 2,5-bis(hydroxymethyl)-furan (2,5-BHMF); (5) 5-methyl-furanmethanol (5-MFM); (6) 2,5-dimethylfuran (2,5-DMF); (7) 2,5-dimethyltetrahydrofuran (2,5-DMTHF); (8) furfural (FA). The H3 process indicates hydrogenolysis/hydrogenation/hydrogenolysis. With courtesy from Ref. [110].

besides the formation of condensation byproducts hydrogenation can be accompanied by secondary reactions such as hydrogenolysis of C–O bond, decarbonylation or hydrogenation of the furan ring [119]. This disadvantage can be diminished transferring the hydrogenation to a hydrogen transfer reaction using bimetallic Co–Ru/C catalysts [120]. The required Lewis acidity for this reaction is provided by the large number of surface defects associated with the oxygen vacancies generated by Co^{2+} species.

4.2.1.1.4 Hydrogenation of levulinic acid

LA has been recognized early in 1956 as a potential platform molecule [121], where several transformations require catalytic hydrogenation (Scheme 4.5). Basically, they involve two separate routes: (i) production of γ-valerolactone (GVL) either directly or via γ-angelica lactone or (ii) production of 5-methyl-2-pyrolidinone via an amination/hydrogenation reaction.

Hydrogenation of LA to GVL may occur on several supported metals, where the effect of both components is very important. The first candidate was nickel [121], which in a series of noble metal-free heterogeneous catalysts (Ni, Co, Cu and Fe) exhibits the best performances [122]. Its association with an oxophilic metal oxide (Ni–MoO_x) co-loaded carbon (C) improved the catalytic behavior due to a structure–activity relationship generated by the copresence of metallic Ni^0 species and partially reduced MoO_2.

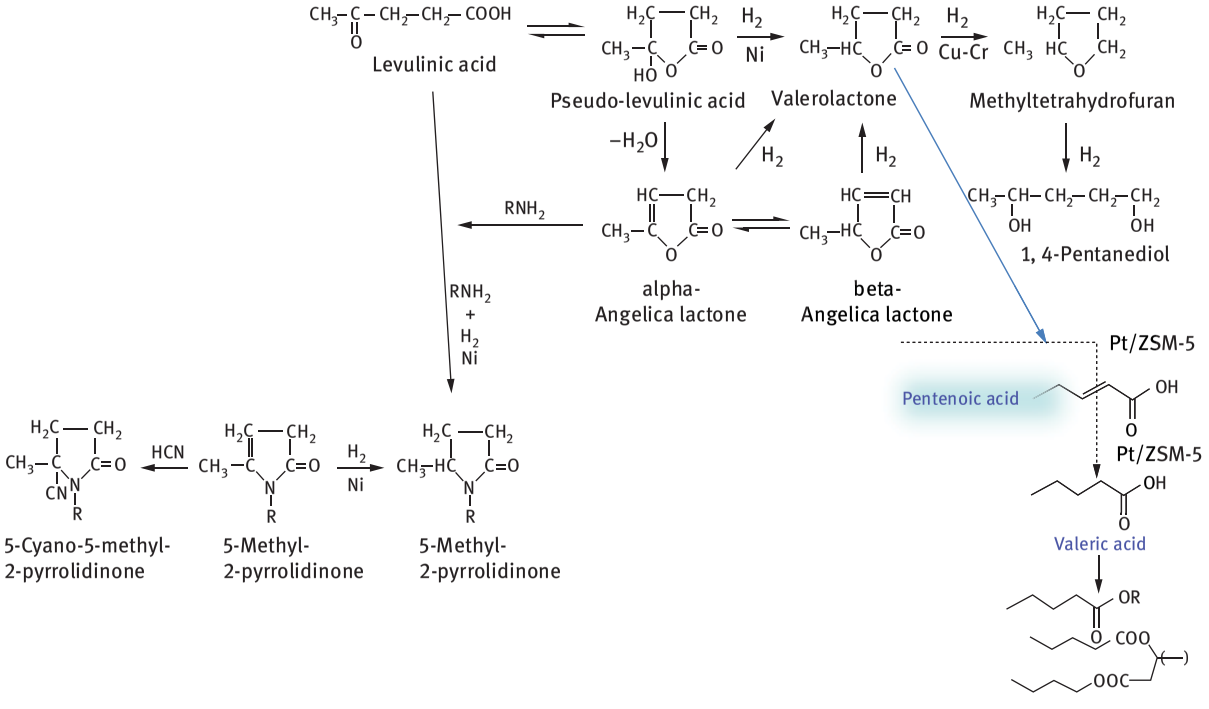

Scheme 4.5: Levulinic acid as a platform molecule for several hydrogenation reactions. Adapted from Ref. [121].

NiZrAl-LDH on the hierarchical three-dimensional Ni foam substrate prepared through a homogeneous nucleation mechanism also catalyzed this reaction [123].

Noble metals are more efficient in this reaction and, among various candidates, Pt/TiO_2 [124] and Ru/C [125] catalysts led to very good results. The addition of nickel [125] or tin [126] to Ru enhances its stability versus the time of stream. Other recent studies considering model mesoporous supported dendrimer-derived Ru and Pt catalysts evidenced the role of the particle size of these metals [127] Pd and Rh are also active; however, alloying Pt or Pd with other noble metals did not deliver measurable improvements. The nature of the precursor also affects the morphologic and structural properties of the noble metal catalysts as demonstrated for ruthenium using a series of precursors ($RuCl_3$, $RuNO(NO_3)_3$, $Ru(NH_3)_6Cl_3$) [128]. Other influencing factors include the ratio of various charged and noncharged Ru species, or the presence of minor amounts of residues from the catalyst precursors.

The effect of the morphology and size of the catalysts in the selective hydrogenation of LA to GVL has also been investigated for unsupported molybdenum carbide (β-Mo_2C) [129]. Depending on the synthesis route, the morphology of the resulting β-Mo_2C was different. The β-Mo_2 1D nanostructures presented a relatively higher activity than the others, which has been associated with the more exposed active sites.

Optically active GVL was also synthesized by the enantioselective hydrogenations of LA and its esters. A tartaric acid–NaBr-modified nickel catalyst produced the optically active GVL with a 60% enantiomeric excess (*ee*), and almost quantitative conversion and chemoselectivity (Scheme 4.6) [130].

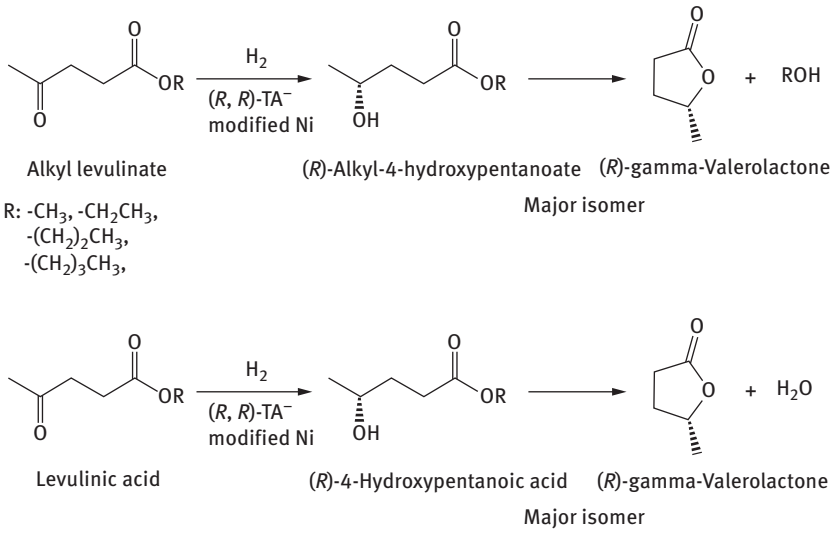

Scheme 4.6: The synthesis of the optically active GVL by the enantioselective hydrogenations of levulinic acid and its esters [130].

4.2.1.1.5 Hydrogenation of lactic acid

Hydrogenation of lactic acid shows potential synthetic routes to 1,2-PDO which already has multiple applications: (i) as a building block for unsaturated polyester resins, which are combined with for instance polystyrene and a filler into thermoset composite materials, or for polyethers used in urethane foams, and (ii) as antifreeze over solvent for food processing to a softening agent in skin care products [131]. However, this hydrogenation reaction has a very long history, dating back to 1926 and deals with the conversion of ethyl lactate with metallic sodium to 1,2-PDO. Then, the heterogeneous hydrogenation of the same substrate was achieved with nickel-Raney. The hydrogenation of LA to 1,2-PDO in the gas phase has also been reported using various Cu-based catalysts [132]. However, the reduction of the free acid in the liquid phase is much more challenging due to the low reactivity of the carboxylic acid group [133, 134]. It started with Re black and Ru [135, 136] in various organic solvents and continued with the hydrogenation of aqueous lactic acid using Ru/C catalyst [137]. The activity of Ru can be promoted by Re, Sn or Mo to enable the selective hydrogenation of carboxylic acids and their esters [138, 139]. However, this impaired the activity [140]. Differently, for the bimetallic catalysts the addition of Pd and Au slightly enhanced the performance of Ru/TiO_2. The influence of the support has also been evaluated using various materials (Al_2O_3, SiO_2, TiO_2 or CeO_2). For this series, catalytic tests revealed that TiO_2 yields the best Ru catalysts [140]. In the case of carbon, inelastic neutron scattering correlated with the properties of the ruthenium deposited onto the carbons by wet impregnation or sol-immobilization [141]. The provenience of the carbon supports corresponds to different surface hydrogen groups that finally influence the reduction degree of ruthenium. While for hydrogenation butanone to 2-butanol this had an important influence, the different Ru speciation did not significantly affect the rates of lactic acid hydrogenation.

4.2.1.1.6 Hydrogenolysis of 5-HMF, 2,5-dihydroxymethylfuran and derivatives

Compounds such as 2,5-DMF and also 2-methylfuran (2-MF) represent suitable potential liquid fuel for the transportation sector and may diminish the reliance on petroleum. With this scope, 5-HMF and 2,5-dihydroxymethylfuran (2,5-HMF) produced from fructose may serve as abundant renewable biomass resources [116]. Thus, to produce DMF and 2-MF, HMF and 2,5-HMF are exposed to a hydrogenolysis step that is carried out in an aqueous solution containing HCl and NaCl. By consequence, the catalyst should be resistant against chloride and the carbon-supported ruthenium catalyst fulfills this exigency. However, it performs hydrogenation leading to 2,5-dihydroxy-methyltetrahydrofuran. The addition of copper to this catalyst (CuRu/C) alleviates this disadvantage affording hydrogenolysis behavior combined with ruthenium-like chlorine resistance.

Hydrogenolysis of LA (Scheme 4.7) represents in fact the hydrogenolysis of 5-methyltetrahydrofuran-2-ol and 1,4-pentadiol produced from its hydrogenation and

Scheme 4.7: Reaction pathways for the hydrogenolysis of LA [142].

accompanied the hydrogenolysis of glycerol. The entire chain is catalyzed by Ru/C catalysts and facilitated by the acidity induced by LA [142].

4.2.1.1.7 Hydrogenolysis of polyols

Hydrogenolysis of sorbitol and other available polyols to EG and PDO is an important application because it can avoid intermediate steps in the valorization of biomass to these products. Several reports already confirmed the feasibility of this approach, all of these emphasize the importance of the presence of a strong basic component. Thus, in the presence of CaO, Ru/carbon nanofiber catalyzes this reaction to EG, PDO and glycerol [143], Ce-promoted Ni/Al_2O_3 catalysts to EG and PDO [144], $Cu–SiO_2$ affords the xylitol hydrogenolysis to PDO [145, 146] while Ni/C provided a combined selectivity to EG, PDO and glycerol [147]. With BaO Ni_2P/C led a good selectivity in the hydrogenolysis of xylitol to EG and PDO under relatively mild reaction conditions [148] and with MgO Ni catalyzed the sorbitol hydrogenolysis to the same products [149].

Insights in the reaction mechanism of hydrogenolysis of polyols were achieved from investigation of nine polyol stereoisomers ranging from three (glycerol), to four (erythritol), to five [adonitol (ribitol), D-xylitol, D-arabitol] and six [D-sorbitol, D-mannitol, dulcitol (galactitol), D-threitol] over a Ru–C catalyst [150]. They confirmed that the hydrogenolysis of polyols to form EG and PDO undergoes multiple steps [151–154] (Scheme 4.8), where the rate-limiting step is the catalytic dehydrogenation leading to an aldehyde or ketone [154]. However, the presence or role of 3-keto and 4-keto intermediates had a negligible effect on the hydrogenolysis of polyols when compared with aldehyde intermediates, which meant the primary hydroxyl groups were more readily dehydrogenated than the internal hydroxyl groups. Under basic conditions, the aldehyde or ketone suffers a C–C scission via the retro-aldol mechanism or a C–O scission by dehydration producing unsaturated bonds, which are subsequently hydrogenated by the metal catalyst [150]. Retro-aldol scission of internal C–C bonds was confirmed to occur by the tetritol product distribution from hexitols.

Further studies using a Ru catalyst with and without sulfur modification confirmed two parallel routes in this process, where the terminal C–C scission product distribution of higher polyols is an important step. The molecule sterics or adsorption phenomena involving the Ru surface or Ca^{2+} ions are affecting the rate-limiting dehydrogenation step involved with hydrogenolysis of higher polyols [150].

The support is not innocent in this reaction. Supported Ru clusters efficiently catalyzed the selective hydrogenolysis of sorbitol to EG and PDO in the presence of $Ca(OH)_2$. However, Ru/C was more selective to these two target glycols than Ru catalysts Al_2O_3, ZrO_2 and TiO_2 with similar Ru particle sizes (~2 nm). The reaction parameters, including the amount of $Ca(OH)_2$, H_2 pressure and temperature, strongly influenced the activity and selectivity of Ru/C, which reflects the bifunctional requirements of the sorbitol hydrogenolysis that involves the competitive Ru- and base-catalyzed reactions of ketose or aldose intermediates, derived primarily from

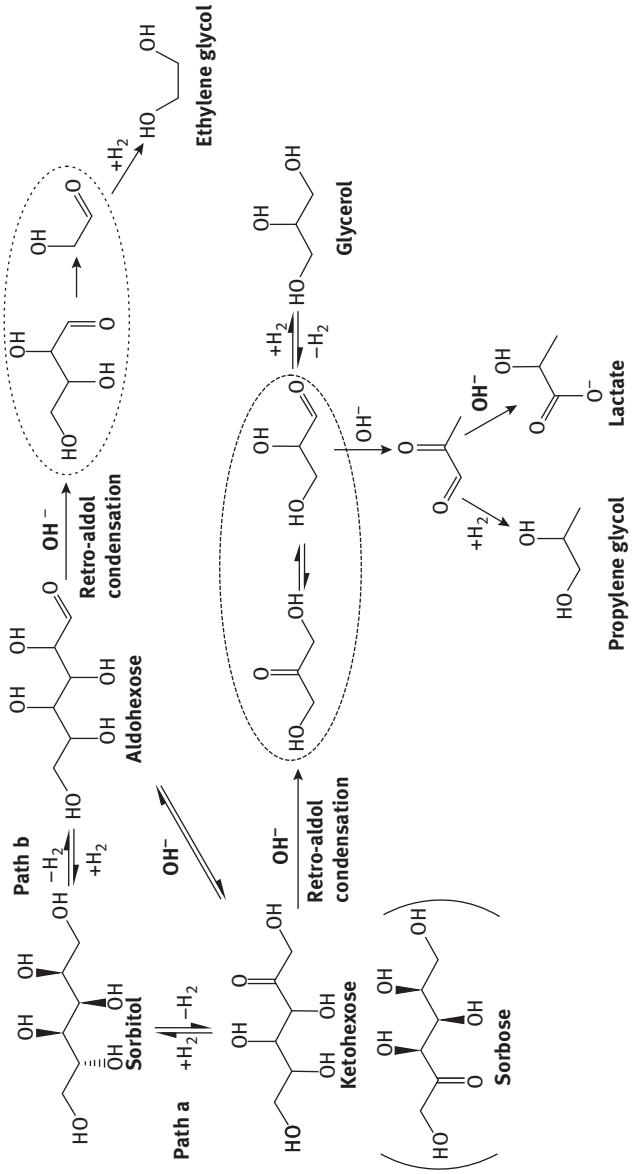

Scheme 4.8: Reaction pathways for sorbitol hydrogenolysis to C2 and C3 products in the presence of base and Ru/C catalysts [154].

sorbitol dehydrogenation. Kinetic isotopic studies with different deuterated sorbitols confirmed that such sorbitol dehydrogenation step preceded by preferential activation of its C(5)-H bond on the Ru surfaces. *Erythro* sequences of the vicinal hydroxyl groups adjacent to the primary carbons in the hexitol molecules, compared to *threo* sequences, tended to facilitate the hydrogenolysis reaction and the formation of C3 products over C2 products, most likely as a result of the effects of the different sequences of the hydroxyl groups on the adsorption and C–H bond activation of hexitols on Ru (Scheme 4.8) [155].

Cracking reactions can convert glycerol into light olefins using solid acid catalysts. However, the selectivity of this reaction is reduced since carbon oxides are also produced and the acid catalyst easily deactivates. Therefore, the hydrogenolysis reduces these drawbacks. Hence, single-step glycerol hydrogenolysis to 1,2-PDO and 1,3-propanediol (1,3-PDO) is considered one of the most promising routes for glycerol utilization because the current manufacture pathways (chlorohydrin process and hydroperoxide process) to 1,2-PDO are not environmental benign enough [156]. A recent technoeconomic and environmental assessment comparing the conventional industrial process for propylene glycol production, which uses petroleum-based propylene oxide as feedstock against different hydrogenolysis routes based on biodiesel glycerol, using process modeling and optimization tools reveals that there are process alternatives based on biodiesel glycerol that outperform the current propylene glycol production scheme simultaneously in profit and environmental impact [157].

The source of glycerol could be either hexitols produced from the valorization of cellulose or biodiesel. Consequently, in the last case, such a utilization of glycerol represents a route for reducing the cost of biodiesel production [158]. The reaction can even proceed further with the production of light olefins.

Carbon-supported noble metal catalysts in aqueous phase hydrogenolysis of hexitols afford only epimerization and cascade decarbonylation reactions with high selectivities to C5 and C4 alditols, and light alkanes at full conversion [159]. Therefore, the catalysts reported for the hydrogenolysis of polyols commonly utilized noble metals such as Pt, Pd, Rh and Au [160–162] or nonnoble (Cu, Ni, Co) metals and various supports as semiconductors (ZnO, TiO_2, Cr_2O_3), base (MgO, nonacidic (SiO_2) and weak (Al_2O_3) or strong (different zeolites, sulfated zirconia, polyoxometalates) acid materials [162–164]. However, the Pt-sulfated ZrO_2 catalyst is only selective in organic medium, which suffers from huge energy consumption to evaporate water from crude glycerol. Noble metals were also used in combination with nonnoble metals (using semiconductor or week acid materials) or promoted with oxophilic species (Re, Mo and W) when merely silica has been utilized as support [165]. The preparation of these catalysts included a wide type of methodologies such as impregnation, adsorption, ion-exchange, sol–gel, coprecipitation and solid fusion. Also, experiments have been carried out in the presence of homogeneous bases such as LiOH, NaOH, KOH, Li_2CO_3, Na_2CO_3 and K_2CO_3 [166].

The role of the oxophilic species like ReO_x in improving the selectivity to 1,3-PDO was associated with the acidity of the -OH groups present on its surface, which are capable of activating glycerol [167]. This has been confirmed for Ir–ReO_x/SiO_2 and Rh–ReO_x/SiO_2 catalysts that were tested for the hydrogenolysis of glycerol [168, 169]. However, the Re-modified noble metal catalysts necessitate sulfuric acid as the additive in most cases, which is plagued by corrosiveness to the reactor and unfriendliness to the environment [169, 170]. Therefore, the use of tungsten is much preferred.

Then, the role of the support in connection to this interaction was well demonstrated using three aluminum oxide materials (commercial γ-Al_2O_3, lab-synthesized γ-Al_2O_3 and pseudo-γ-AlO(OH) and a HZSM-5 zeolite) as supports of the bicomponent Pt–WO_x catalysts [171]. The tungsten surface density and the intimate contact between Pt and WO_x resulted to be key parameters. Tungsten surface density controls the formation of polytungstates, that is, the only species able to produce the weak Brønsted acidity that is required to selectively produce 1,3-PDO. The comparison between the HZSM-5 and the Al_2O_3 supports demonstrated that an increment on the medium Brønsted acidity is detrimental for the selective 1,3-PDO formation, as it promotes the reactions that yield 1-propanol and propane [171]. On the other side, the increase in the dispersion of Pt led to larger glycerol conversions and promoted the hydrogenolysis routes that lead to 1,2- and 1,3-PDO similarly. Finally, increasing the Pt metal content significantly favored the hydrogenolysis route leading to 1,3-PDO. It ensures a more intimate contact between Pt and WO_x prompting the hydrogenation to 1,3-PDO (Scheme 4.9).

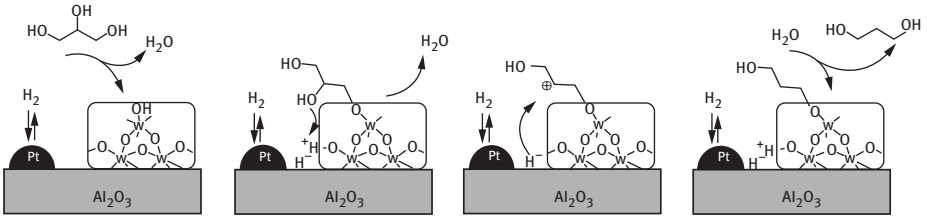

Scheme 4.9: Reaction mechanism proposed for the glycerol hydrogenolysis to 1,3-PDO. With courtesy from Ref. [171].

The advantage of the pseudo-AlO(OH) support results from a high concentration of hydroxy groups that allows the incorporation of larger W loadings leading to higher dispersions, which avoid the emergence of the undesired WO_3 NPs [171, 172]. The catalytic performances in the selective production of 1,3-PDO on the Pt/W–SBA-15 catalysts were attributed to a similar effect. The tungsten species was identified as the isolated WO_4 with Lewis acidity. During the reaction, the synergy between the Pt NPs and WO_4 in the H_2 atmosphere leads to the in situ generation of the hydrided WO_4 by spillover H atoms from Pt to WO_x, which functions as the highly selective

center for glycerol hydrogenolysis to 1,3-PDO [173]. In situ spectroscopic investigations suggested a triple role of tungsten oxide in this reaction, acting as (i) a strong anchoring site for the primary hydroxy group(s) of glycerol, (ii) a supplier of protons and (iii) a stabilizer of the secondary carbocation [171].

The influence of the type of acidity upon the selectivity of hydrogenolysis of polyols has also been confirmed by the investigation of acid-modified Co-Al_2O_3 catalysts prepared by the addition of B, Ce, Zr and HPA (HSiW, HPW, HPMo) [175]. Besides the increase in the acid strength, the acidity also increased the Co dispersion on the catalytic surface, which facilitated the hydrogenolysis of glycerol. Then, the modification of Co-Al with B, Ce or Zr species increased the Lewis acidity that enhanced the selectivity to 1,2-PDO. The introduction of HPAs increased the selectivity of 1,3-PDO, which is attributed to the existence of Brønsted acid sites on the modified Co–Al catalysts.

The selectivity to 1,2-PDO or 1,3-PDO can be tuned by a simple procedure. Thus, the addition of Au to a highly dispersed Pt/WO_x decreases the original surface Lewis-acid sites but greatly increases its in situ-generated Brønsted-acid sites with the assistance of H_2 through the formation of frustrated Lewis pairs [176]. These in situ formed and spatially separated pairs of H^+ and H^- function as the active sites in the glycerol conversion to 1,3-PDO.

The influence of the oxophilic species in the hydrogenolysis of glycerol has also been confirmed for nonnoble metals [177]. Ni and Cu mono- and bimetallic catalysts modified with various types of oxophilic oxides MO_x (M = Mo, V, W and Re) were tested for hydrogenolysis of glycidol, as an alternative route to hydrogenolysis of glycerol to obtain 1,3-PDO. As for the noble metals the presence of these species affected the dispersion and reducibility of the NiO particles, and the strength and amount of the acid sites. In this series, Re showed the highest activity, high PDOs selectivity and the highest 1,3-PrD/1,2-PrD ratio. The presence of vanadium and molybdenum modifiers made the reduction of NiO more difficult. Also, the reducibility of NiO got harder when the amount of metal loading was lower.

For Cu/ZnO catalysts the glycerol hydrogenolysis yield is associated with moderate or high Cu content that corresponds to a close contact between Cu and ZnO, while the deactivation corresponds to the changes in the Cu species during the reaction. Fouling of the Cu species by hydrocarbonaceous deposits and the oxidation of Cu metal produced during the first run are not the most relevant deactivation causes. But copper sintering, a process facilitated by the strong Zn leaching, is the cause of deactivation with the highest impact [178].

Pd alloy has very similar valence electron density as Cu, and it shows advanced catalytic performance in some catalysis reactions where Cu-based catalysts are required [179].

ZnPd alloy catalysts were suggested to have better stability than Cu, especially in the aqueous solution under harsh conditions [180] and these properties were associated with the performances of ZnPd/ZnO–Al_2O_3 catalysts for hydrogenolysis of glycerol to 1,2-PDO. The calcination temperature determined the distribution and

migration of different Al ($A^{(IV)}$, $Al^{(V)}$ and $Al^{(VI)}$) in ZnPd/ZnO–Al_2O_3, and hence affected the particle sizes of ZnPd, reduction of ZnO, oxygen vacancy density and the catalytic activity and stability [181]. The presence of the Zn^{2+} (from ZnO) donors may also avoid the leaching of Zn from the alloy and contributes to in situ formation/preservation of active PdZn alloy layers onto the support [182].

Very important from the practical point of view, some of these catalysts preserved the efficiency when they were evaluated for polyol hydrogenolysis in a continuous reactor [183, 184].

4.2.1.2 Lignin upgrading

Despite its heterogeneous complex structure, the use of lignin as feedstock for the production of chemicals become more important. However, it is critical for the viability of this approach to valorize lignin alongside polysaccharides. About 90% of lignin is obtained as a "lignin oil," comprising mainly of phenolic monomers like 4-*n*-propylguaiacol (PG) and 4-*n*-propylsyringol, next to dimers and small oligomers [185]. The composition of the cocktail is influenced by both the extraction and fragmentation procedures. Most lignin-transforming processes generate a variety of different products, in which propyl alkyls are degraded by the cleavage of C–C bonds (Figure 4.11). Hydrogenolysis or transfer hydrogenolysis conditions lead to a complicated mixture of saturated naphthenes and aromatics [186] than the oxidative reaction [187].

4.2.1.2.1 Hydrolysis reaction

The utilization of this cocktail for the production of commodities like polyurethanes and polyesters benefits from a high hydroxyl content [188]. Since hydrogenolysis of C–Obonds is a metal-dependent process, the control of the OH contents may likely be accomplished by an appropriate choice of the metal catalyst. For example, Pd, when compared to Ru, has a lower activity to alcohol hydrogenolysis that affords a higher selectivity toward hydroxyl-rich lignin monomers [189, 190]. The suggested pathway for the Pd-catalyzed reductive hydrolysis of aryl ethers proposes an initial partial hydrogenation of the arene ring to enol ether intermediates that are highly susceptible to water attack. This pathway contrasts the often postulated acid-catalyzed ether cleavage pathway, which does not require H_2 [191]. It is also distinct from metal-mediated direct ether cleavage (without direct H_2 participation) followed by recombination of the fragments with surface HC and COH radicals from water dissociation at the metal surface. The assumed reason for why Pd is better than Ni or Pt in this reaction is related to the activity of this metal to catalyze hydrogen addition to C=C bonds [191].

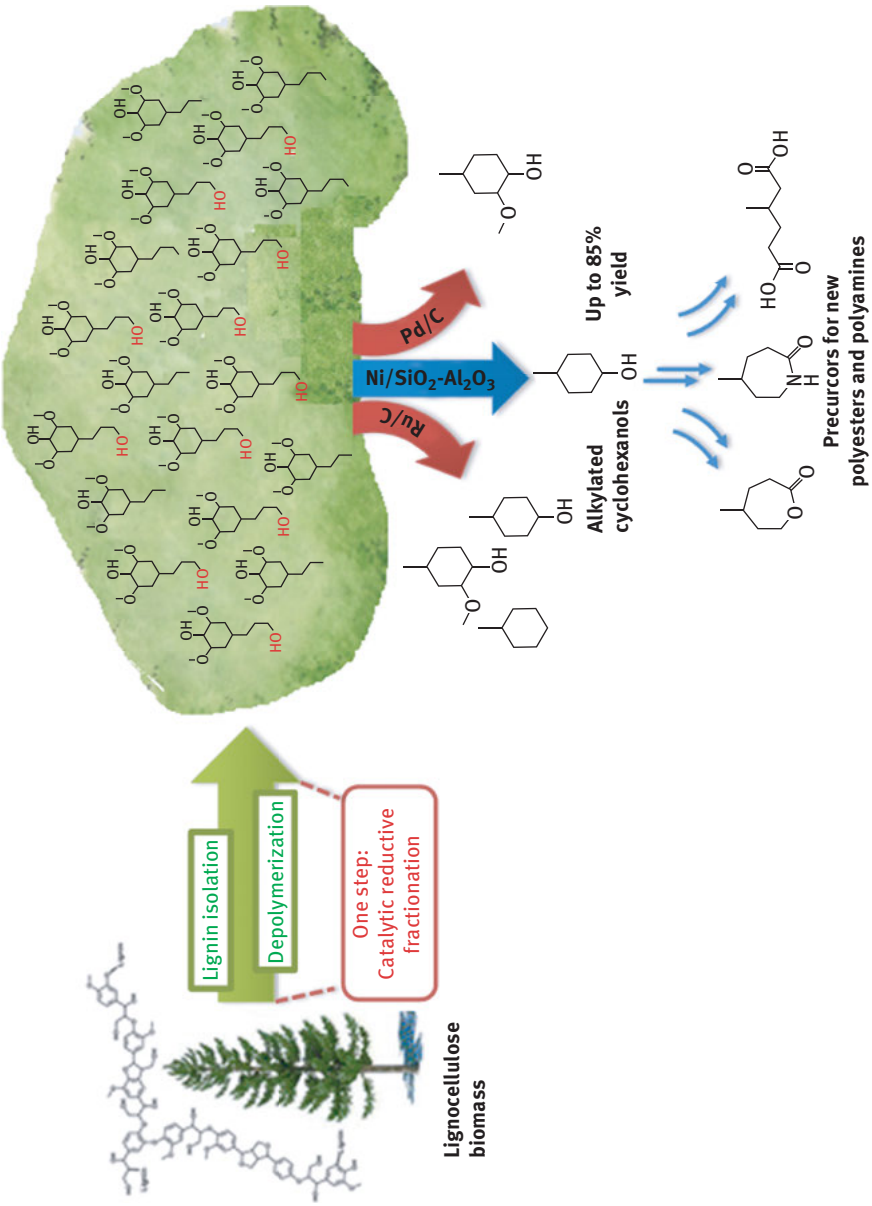

Figure 4.11: Monomeric products of the fragmentation of lignin. Adapted from Ref. [185].

4.2.1.2.2 Demethoxylation

Further, the processing of these hydroxyl-containing monomers may also require metal catalysts. 4-*n*-Propylcyclohexanol (PCol) is a precursor for novel polymer building blocks that can be produced via the reductive demethoxylation of PG. This reaction can be carried out in hexadecane liquid phase over commercial hydrogenation catalysts like 5 wt% Ru/C, 5 wt% Pd/C or 5 wt% $Ni/SiO_2–Al_2O_3$ at temperatures ranging from 200 to 300 °C under hydrogen atmosphere [192]. Mechanistic investigations suggested that the favored route is PG hydrodemethoxylation to 4-*n*-propylphenol, followed by its hydrogenation to PCol as this does not involve stable intermediates. However, the selectivity of the reaction might be affected by the formation of side products as 4-*n*-propyl-2-methoxycyclohexanol. Catalytic conversion of guaiacol, 4-methyl- and 4-ethylguaiacol in comparable circumstances occurred with similarly high yields of the corresponding cyclohexanols.

4.2.1.2.3 Hydroformilation

The hydroformylation of naturally occurring olefins such as eugenol, safrole, estragole or anethole, all readily available from lignin-biomass, is another important and useful synthetic tool to obtain oxygenated products relevant in the flavor, food and pharmacy industries. Usually, such reactions are performed in homogeneous conditions using water-soluble Rh-based organometallic catalysts [193]. However, promising results in this reaction were also achieved under biphasic media using heterogeneous complexated rhodium catalysts over 3-(mercapto)propyl- and 3-(1-thioureido)propyl-functionalized silica gel [194].

4.2.1.2.4 Hydrogenation

Muconic acid can be converted into numerous downstream products, including adipic acid, which is the most commercially important dicarboxylic acid [195]. Functional conjugated muconate fragments are versatile building blocks in organic synthesis [196, 197]. Adipic acid has a market volume of 2.6 million tons per year with an annual demand growth forecast of 3–3.5% globally [198]. It has uses as a polymer precursor for nylon, plasticizers, lubricants and polyester polyols. However, the conventional adipic acid production involving nitric acid oxidation of benzene is highly damaging to the environment. As an alternative, the metabolic engineering may provide intermediates that can be further upgraded in a heterogeneous catalytic process. It is also the case of the *cis, cis*-muconic acid, which after a subsequent hydrogenation can afford adipic acid (Scheme 4.10). Pd/C was identified as a highly active catalyst for this reaction hydrogenation, where both the conversion and the selectivity are higher than 97% (TOFs of 23–30 s^{-1}) [199].

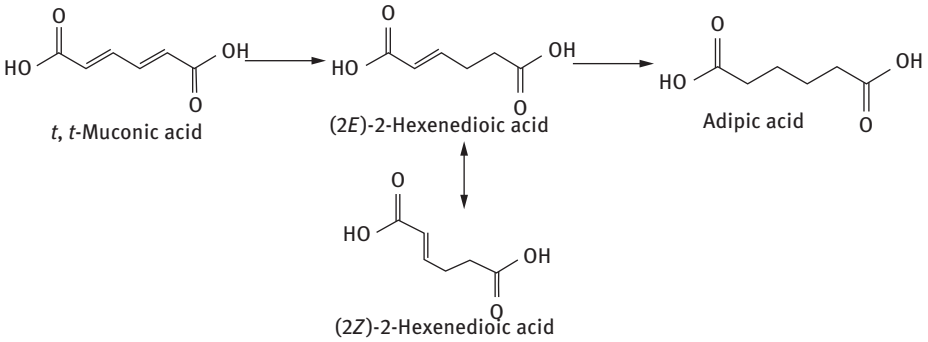

Scheme 4.10: Hydrogenation/esterification of muconic acid [199].

In the presence of various alcohols, both Pd/C and Pt/C catalysts can also catalyze the esterification/*trans*-esterification of muconic acid/muconic acid esters [200, 201]. For small reaction times onto the commercial 5% Pd/C, the hydrogenation can also be stopped at the 2-hexenedioic acid, where the dominant isomer is the *trans* (2*E*)-2-hexenedioic acid (Scheme 4.11) [202].

Aqueous phase catalytic upgrading of eugenol to hydrocarbons has been achieved on a combination of Pd/C with zeolite catalysts (H-ZSM-5) in the presence of H_2 [203]. Hydrogenation of the C=C, C=O and aromatic ring, and isomerization are catalyzed by Pd, while the presence of the zeolite affords the dealkylation, hydrolysis and dehydration steps (Scheme 4.12). However, the role of the solvent is important and it accommodates with the catalyst. Working with nickel catalysts, it was found that Ni/C is more efficient in these reactions in water than in *n*-hexane, while on Ni/HZSM-5 oxygen-containing functional groups could be removed from the aromatic ring completely in *n*-hexane [205]. These results also revealed that Brønsted acid sites show superior advantages over Lewis acid in the dehydration of 4-propylcyclohexanol.

Nitrogen-enriched highly mesoporous carbons were adapted as a proper support for the fabrication of well-dispersed Pd catalysts for the transfer hydrogenation of vanillin in the water phase with formic acid as the hydrogen donor. They afford a total vanillin conversion with 2-methoxy-4-methylphenol as the sole product [208]. Its behavior has been associated with the electron-deficient Pd ($Pd^{\delta+}$) percentage that is affected by the N species, and the strong Pd–N interaction that generates the coexistence of $Pd^{\delta+}$ and metallic Pd (Pd^{0}). These result in a Pd/NMC as a novel bifunctional nanocatalyst for both formic acid dehydrogenation and vanillin hydrogenation. The Pd/NMC catalyst also demonstrates enhanced acid resistance in acid media and adsorption of substrates.

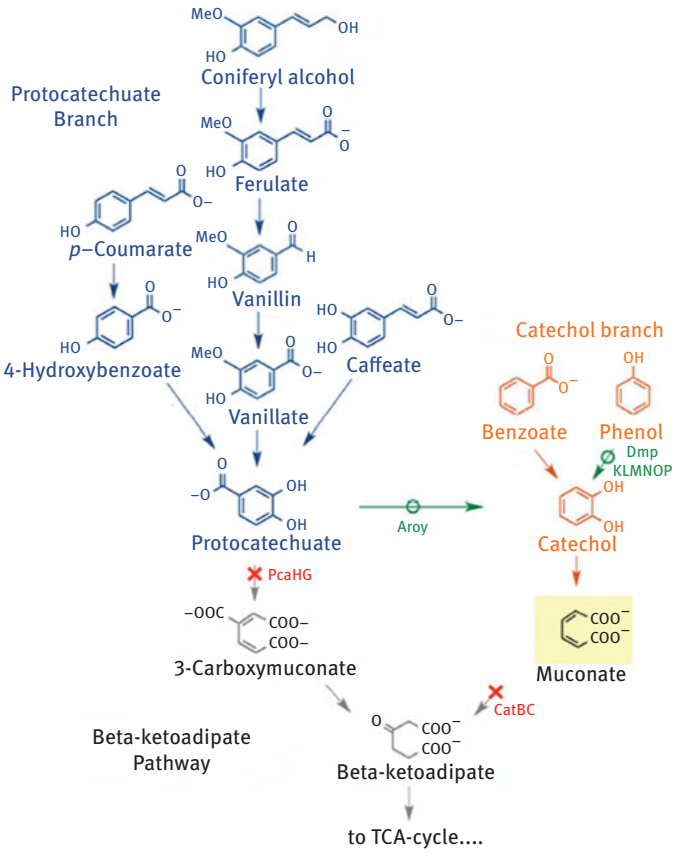

Scheme 4.11: Routes of valorization of coniferyl alcohol. With courtesy from Ref. [202].

4.3 Concluding remarks

The ability of noble metals to form bonds with H, C and O is governed by their electronic properties. Also, the formation of multimetallic particles further changes the electronic properties, with a direct effect upon the catalytic behavior.

The real metal-based heterogeneous catalysts are more complex structures consisting of an anchored catalytically active component (e.g., metal, alloy or metallic phase – oxide mixture) onto a support phase that is a high surface area material.

Literature reports have largely evidenced the strong capabilities of the metal-based solid catalysts for the biomass transformation to chemicals. The high versatility of these materials, which can combine different metals with different dispersions and redox properties with supports with different surface areas, pore distribution and morphologies, makes them ideal for chemical valorization of the lignocellulosic biomass. Adjusting the chemical and physical structure it is possible to orientate

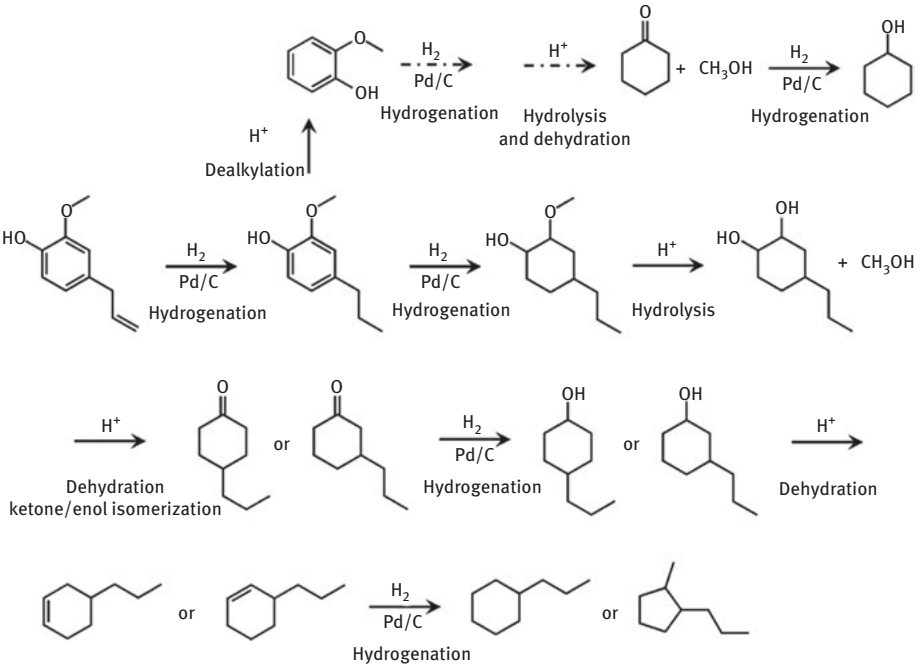

Scheme 4.12: Catalytic upgrading of eugenol to cyclohexanol and hydrocarbons. With courtesy from Ref. [203].

the catalytic reaction to the desired one (depolymerization, hydrolysis, hydrogenation, dehydration, isomerization, etc.).

Apart from these considerations, the evolution of the metal/support catalysts for the biomass upgrading must be in agreement with the principles of green chemistry. One of these principles is the efficient utilization of raw materials; thus, the catalysts should be designed for the deconstruction of residual lignocellulosic biomass in order to avoid any competition with the food supply. This is a very challenging task since the use of the residual biomass in more realistic conditions should make face to strong deactivating species such as sulfur- and nitrogen-containing compounds. Despite this, the success on using metal/support catalysts for this purpose would also contribute in the decrease of the CO_2 footprint.

References

[1] Abild-Pedersen F, Greeley JP, Studt F, Rossmeisl J, Munter TR, Moses PG, Skúlason E, Bligaard T, Nørskov JK. Phys Rev Lett 2007, 99, 016105.

[2] Nørskov JK, Abild-Pedersen F, Studt F, Bligaard T. Proc Natl Acad Sci USA 2011, 108, 937.

[3] Edwards PP, Johnston RL, Rao CNR. In: Metal Clusters in Chemistry, 3, Braunstein P, Oro LA, Raithby PR. (Eds.), Wiley-VCH, Weinheim, 1998, 1454.
[4] Bond GC, Metal-Catalysed Reactions of Hydrocarbon, Springer, Science, 2005, 8.
[5] Holewinski A, Xin H, Nikolla E, Linic S. Curr Opin Chem Eng 2013, 2, 312.
[6] Nørskov JK, Studt F, Abild-Pedersen F, Bligaard T. Fundamental Concepts in Heterogeneous Catalysis, John Wiley & Sons, Inc, Hoboken, New Jersey, 2014.
[7] Hammer B, Nørskov JK. Adv Catal 2000, 45, 72.
[8] Vojvodic A, Nørskov JK. Abild-Pedersen F, Top Catal 2014, 57, 25.
[9] Hammer B, Nørskov JK. Surf Sci 1995, 343, 211.
[10] Ma X, Xin H, Phys Rev Lett 2017, 118, 036101.
[11] Hammer B, Nørskov JK. Nature 1995, 376, 238.
[12] Yates JT. Jr, J Vac Sci Technol 1995, A13, 1359.
[13] Edwards JK, Freakley SJ, Carley AF, Kiely CJ, Hutchings GJ. Acc Chem Res 2014, 47, 845.
[14] Edwards JK, Solsona B, Ntainjua NE, Carley AF, Herzing AA, Kiely CJ, Hutchings GJ. Science 2009, 323, 1037.
[15] Chen M, Kumar D, Yi CW, Goodman DW. Science 2005, 310, 291.
[16] Freakley SJ, He Q, Harrhy JH, Lu L, Crole DA, Morgan DJ, Ntainjua EN, Edwards JK, Carley AF, Borisevich AY, Kiely CJ, Hutchings GJ. Science 2016, 351, 965.
[17] Kitchin JR, Nørskov JK, Barteau MA, Chen JG. J Chem Phys 2004, 120, 10240.
[18] Ruban A, Hammer B, Stoltze P, Skriver HL, Nørskov JK. J Mol Catal A Chem 1997, 115, 421.
[19] Besenbacher F, Chorkendorff I, Clausen BS, Hammer B, Molenbroek AM, Nørskov JK, Stensgaard I. Science 1998, 279, 1913.
[20] Tauster SJ. Acc Chem Res 1987, 20, 389.
[21] Strunk J, Bañares MA, Wachs IE. Top Catal 2017, 60, 1577.
[22] Kordas K, Rautio A-R, Lorite GS, Mohl M, Mäki-Arvela P, Mikkola J-P, Murzin D, Ge L, Ajayan PM, Vajtai R. Top Catal 2015, 58, 1127.
[23] Kowalczyk Z. , Sentek J, Jodzis S, Muhler M, Hinrichsen O. J Catal 1997, 169, 407.
[24] Nagai Y, Hirabayashi T, Dohmae K, Takagi N, Minami T, Shinjoh H, Matsumoto S. J Catal 2006, 242, 103.
[25] McVicker GB, Garten RL, Baker RTK. J Catal 1978, 54, 129.
[26] Morgan K, Goguet A, Hardacre C. C ACS Catal 2015, 5, 3430.
[27] Pines H, Nogueira L. J Catal. 1981, 70, 391.
[28] Pashkov V.V, Golinsky D.V, Udras IE, Paukshtis EA, Belyi AS. Petrol Chem 2011, 51, 286.
[29] Akita T, Lu P, Ichikawa S, Tanaka K, Haruta M. Surf Interface Anal 2001, 31, 73.
[30] Che M, Bennett CO, Adv Catal 1989, 36, 55.
[31] Borodziński A, Bonarowska M. Langmuir 1997, 13, 5613.
[32] Farin D, Avnir D. J Catal. 1989, 120, 55.
[33] Cox DM. High surface area materials, Chapter 4, In: Nanostructure Science and Technology, Siegel RW, Hu E, Roco MC. (Eds.) Springer, Springer Science, Dordrecht, 1999, 49–66.
[34] Rioux RM, Song H, Hoefelmeyer JD, Yang P, Somorjai GA, J Phys Chem B 2005, 109, 2192.
[35] Song H, Rioux RM, Hoefelmeyer JD, Komor R, Nies K, Grass M, Yang P, Somorjai GA. J Am Chem Soc 2006, 128, 3027.
[36] Guzman J, Gates BC, Dalton Trans 2003, 1, 3303.
[37] Kulkarni A, Lobo-Lapidus RJ, Gates BC. Chem Commun 2010, 46, 5997.
[38] Liu L, Diaz U, Arenal R, Agostini G, Concepcion P, Corma A. Nat Mater 2017, 16, 132.
[39] Otto T, Zones SI, Iglesia E, J Catal. 2016, 339, 195.
[40] Yang X, Yu X, Long LZ, Wang TJ, Ma LL, Wu LP, Bai Y, Li XJ, Liao SJ. Chem Commun 2014, 50, 2794.
[41] Gao Z, Qin Y. Acc Chem Res 2017, 50, 2309.

[42] Zienkiewicz-Strzałka M, Deryło-Marczewska A, Pikus S. Micropor Mesopor Mat 2016, 227, 228.
[43] D'Souza L, Bera P, Sampath S. J. Colloid Interface Sci 2002, 246, 92.
[44] Chen CH, Sarma LS, Wang GR, Chen JM, Shih SC, Tang MT, Hwang BJ. J Phys Chem B 2006, 110, 10287.
[45] LohA, Medlin JW, J Am Chem Soc 2008, 130, 5507.
[46] Abbasi N, Shahbazi P, Kiani A. J Mater Chem A 2013, 1, 9966.
[47] Roiban L, Koneti S, Morfin F, Nguyen T-S, Mascunan P, Aouine M, Epicier T, Piccolo L. Chem Cat Chem 2017, 9, 4607.
[48] Ge H, Zhang B, Gu X, Liang H, Yang H, Gao Z, Wang J, Qin Y. Angew Chem Int Ed 2016, 55, 7081.
[49] Zhang J, Yu Z, Gao Z, Ge H, Zhao S, Chen C, Chen S, Tong X, Wang M, Zheng Z, Qin Y. Angew Chem, Int Ed 2017, 56, 816.
[50] Santos RCR, Braga DMV, Pinheiro AN, Leite ER, Freire VN, Longhinotti E, Valentini A. Catal Sci Technol 2016, 6, 4986.
[51] Pintauer T, Matyjaszewski K. Chem Soc Rev 2008, 37, 1087.
[52] Pye DR, Mankad NP. Chem Sci 2017, 8, 1705.
[53] Sinfelt JH, Via GH, Lytle FW. Catal Rev Sci Eng 1984, 26, 81.
[54] Bond GC. Chem Soc Rev 1991, 20, 441.
[55] Tanke RS, Celanese Hoechst. US Pat 1, 616 015, 1996.
[56] Galvagno S, Parravano G. J. Catal 1978, 55, 178.
[57] Sachtler JW, Somorjai GA. J Catal 1983, 81, 77.
[58] Juszczyk W, Karpinski Z, Lomot D, Pielaszek J, Sobtzek JW. J Catal 1995, 151, 67.
[59] Schmid G, Lehnert A, Malm J-O, Bovin J-O. Angew Chem 1991, 103, 852.
[60] Bönnemann H, Brinkmann R, Brijoux W, Dinjus E, Joussen Th, Korall B. Angew Chem 1991, 103, 1344.
[61] Bönnemann H, Brijoux W. In; Advanced Catalysts and Nanostructured Materials, Moser W.R. (Ed.), Academic Press, San Diego, 1996, 165–196.
[62] Bönnemann H, Endruschat U, Tesche B, Rufínska A, Lehmann CW, Wagner FE, Filoti G, Pârvulescu V, Pârvulescu VI. Eur J Inorg Chem 2000, 12, 819.
[63] Nunez GM, Rouco AJ. J Catal 1988, 111, 41.
[64] Yoon B, Häkkinen H, Landman U, Wörz AS, Antonietti JM, Abbet S, Judai K, Heiz U. Science, 2005, 307, 403.
[65] Farmer JA, Campbell CT. Science, 2010, 329, 933.
[66] Højrup Hansen K, Worren T, Stempel S, Lægsgaard E, Bäumer M, Freund H-J, Besenbacher F, Stensgaard I. Phys Rev Lett 1999, 83, 4120.
[67] Yim CM, Pang CL, Hermoso DR, Dovera CM, Muryn CA, Maccherozzi F, Dhesi SS, Pérez R, Thornton G. PNAS, 2015, 112, 7903.
[68] Renders T, Schutyser W, Van den Bosch S, Koelewijn S-F, Vangeel T, Courtin CM, Sels B.F. ACS Catal 2016, 6, 2055.
[69] Chheda JN, Huber GW, Dumesic JA. Angew Chem Int Ed 2007, 46, 7164.
[70] Guha SK, Kobayashi H, Fukuoka A. In: Thermochemical Conversion of Biomass to Liquid Fuels and Chemicals, Crocker M. (Ed.), RSC Publishing, Cambridge, 2010, 344.
[71] Bozell JJ, Petersen GR. Green Chem 2010, 12, 539.
[72] Komanoya T, Kobayashi H, Hara K, Chun W-J, Fukuoka A. Appl Catal A General 2011, 407, 188.
[73] Rinaldi R, Schüth F. Chem Sus Chem 2009, 2, 1096.
[74] Lazaridis PA, Karakouli SA, Teodorescu C, Apostol N, Macovei D, Panteli A, Delimitis A, Coman SM, Parvulescu VI, Triantafyllidis KS. Appl Catal B Environ 2017, 214, 1.
[75] Fukuoka A, Dhepe PL. Angew Chem Int Ed 2006, 45, 5161.

[76] Dhepe PL, Fukuoka A. Chem Sus Chem 2008, 1, 969.
[77] Van de Vyver S, Geboers J, Dusselier M, Schepers H, Vosch T, Zhang L, Tendeloo GVan, Jacobs PA, Sels BF. Chem Sus Chem 2010, 3, 698.
[78] Geboers J, Van de Vyver S, Carpentier K, de Blochouse K, Jacobs P, Sels B. Chem Commun 2010, 46, 3577.
[79] Van de Vyver S, Geboers J, Schutyser W, Dusselier M, Eloy P, Dornez E, Seo JW, Courtin CM, Gaigneaux EM, Jacobs PA, Sels BF. Chem Sus Chem 2012, 5, 1549.
[80] Besson M, Gallezot P, Pinel C. Chem Rev 2014, 114, 1827.
[81] Jollet V, Chambon F, Rataboul F, Cabiac A, Pinel C, Guillon E, Essayem N. Green Chem 2009, 11, 2052.
[82] Kobayashi H, Ito Y, Komanoya T, Hosaka Y, Dhepe PL, Kasai K, Hara K, Fukuoka A. Green Chem 2011, 13, 326.
[83] Luo C, Wang S, Liu H. Angew Chem Int Ed 2007, 46, 7636.
[84] Kobayashi H, Komanoya T, Hara K, Fukuoka A. Chem Sus Chem, 2010, 3, 440.
[85] Deng W, Tan X, Fang W, Zhang Q, Wang Y. Catal Lett 2009, 133, 167.
[86] Almohalla M, Rodríguez-Ramos I, Ribeiro LS, Órfão JJM, Pereira MFR, Guerrero-Ruiz A. Catal Today 2018, 301, 65.
[87] Liang G, Cheng H, Li W, He L, Yu Y, Zhao F. Green Chem 2012, 14, 2146.
[88] Liang G, He L, Cheng H, Li W, Li X, Zhang C, Yu Y, Zhao F. J Catal 2014, 309, 468.
[89] Negoi A, Triantafyllidis K, Parvulescu VI, Coman SM Catal Today 2014, 223, 122.
[90] Deng W, Liu M, Tan X, Zhang Q, Wang Y. J Catal 2010, 271, 22.
[91] Zheng M, Pang J, Sun R, Wang A, Zhang T. ACS Catal 2017, 7, 1939.
[92] Ji N, Zhang T, Zheng M, Wang A, Wang H, Wang X, Chen JG. Angew Chem Int Ed 2008, 47, 8510.
[93] Wang A, Zhang T. Acc Chem Res 2013, 46, 1377.
[94] Zheng M, Pang J, Wang A, Zhang T. Chin J Catal 2014, 35, 602.
[95] Yin W, Tang Z, Venderbosch RH, Zhang Z, Cannilla C, Bonura G, Frusteri F, Heeres HJ. ACS Catal 2016, 6, 4411.
[96] Tan X, Deng W, Liu M, Zhang Q, Wang Y. Chem Commun 2009, 7179.
[97] Suganuma S, Nakajima K, Kitano M, Yamaguchi D, Kato H, Hayashi S, Hara MJ. Am Chem Soc, 2008, 130, 12787.
[98] Liu Y, Luo C, Liu H. Angew Chem Int Ed 2012, 51, 3249.
[99] Tai Z, Zhang J, Wang A, Zheng M, Zhang T. Chem Commun 2012, 48, 7052.
[100] Deng T, Liu H. Green Chem 2013, 15, 116.
[101] Binder JB, Raines RT. J Am Chem Soc 2009, 131, 1979.
[102] Zhang J, Liu X, Sun M, Ma X, Han Y. ACS Catal 2012, 2, 1698.
[103] Tathod A, Kane T, Sanil ES, Dhepe PL. J Mol Catal A Chemical 2014, 388–389, 90.
[104] Van de Vyver S, Geboers J, Jacobs PA, Sels BF. Chem Cat Chem 2011, 3, 82.
[105] Kobayashi H, Fukuoka A. Green Chem 2013, 15, 1740.
[106] Geboers J, Van de Vyver S, Carpentier K, Jacobs PA, Sels BF. Chem. Commun 2011, 47, 5590.
[107] Liu M, Deng W, Zhang Q, Wang Y.L, Wang Y. Chem Commun 2011, 47, 9717.
[108] Dong Q, Huang Y, Yang H, Pei J, Li K, Yuan M, Xiao W, Ni W, Hou Z. Top Catal 2017, 60, 666.
[109] Hoffer BW, Crezee E, Mooijman PRM, Dvan Langeveld A, Kapteijn F, Moulijn JA. Catal Lett 2003, 79–80, 35.
[110] Insyani R, Verma D, Kim SM, Kim J. Green Chem 2017, 19, 2482.
[111] Groger H, Hummel W. Curr Opin Chem Biol 2014, 19, 171.
[112] Gimbernat A, Guehl M, Capron M, Lopes Ferreira N, Froidevaux R, Girardon J-S, Dhulster P, Delcroix D, Dumeignil F. Chem Cat Chem 2017, 9, 2080.

[113] Mariscal R, Maireles-Torres P, Ojeda M, Sadaba I, Lopez-Granados M. Energ Environ Sci 2016, 9, 1144.
[114] Li H, Luo H, Zhuang L, Dao W, Qiao M. J Mol Catal A Chem 2003, 203, 267.
[115] Zheng HY, Zhu YL, Teng BT, Bai ZQ, Zhang CH, Xiang HW, Li YW. J Mol Catal A Chem 2006, 246, 18.
[116] Roman-Leshkov Y, Barrett CJ, Liu ZY, Dumesic JA. Nature 2007, 47, 982.
[117] Hronec M, Fulajtarova K. Catal Commun 2012, 24, 100.
[118] Sitthisa S, Pham T, Prasomsri T, Sooknoi T, Mallinson RG, Resasco DE. J Catal 2011, 280, 17.
[119] Scholz D, Aellig C, Hermans I. Chem Sus Chem 2014, 7, 268.
[120] Gao Z, Yang L, Fan G, Feng Li. Chem Cat Chem 2016, 8, 3769.
[121] Leonard RH, Ind Eng Chem 1956, 48, 1330.
[122] Shimizu K, Kanno S, Kon K. Green Chem, 2014, 16, 3899.
[123] Li W, Fan G, Yang L, Li F. Chem Cat Chem, 2016, 8, 2724.
[124] Lange J-P, Price R, Ayoub PM, Louis J, Petrus L, Clarke L, Gosselink H. Angew Chem Int Ed, 2010, 49, 4479.
[125] Yang Y, Gao G, Zhang X, Liu F. ACS Catal 2014, 4, 1419.
[126] Wettstein SG, Bond JQ, Alonso DM, Pharn HN, Datye AK, Dumesic JA. Appl Catal B 2012, 117–118, 321.
[127] Nemanashi M, Noh , Meijboom R. J-HAppl Catal A General 2018, 550, 77.
[128] Piskun AS, Ftouni J, Tang Z, Weckhuysen BM, Bruijnincx PCA, Heeres HJ. Appl Catal A General 2018, 549, 197.
[129] Quiroz J, Mai EF, Teixeira da Silva V. Top Catal 2016, 59, 148.
[130] Osawa T, Tanabe Y. Catal Lett 2017, 147, 686.
[131] Dusselier M, Van Wouwe P, Dewaele A, Makshina E, Sels BF. Energy Env Sci 2013, 6, 1415.
[132] Simonov MN, Simakova IL, Parmon VN. React Kinet Catal Lett 2009, 97, 157.
[133] Adkins HI, Pavlic AA. J Am Chem Soc 1947, 69, 3039.
[134] Adkins HI, Billica HR. J Am Chem Soc 1948, 70, 3121.
[135] Broadbent HS. Ann NY Acad Sci, 1967, 145, 58.
[136] Carnahan JE, Ford TA, Gresham WF, Grigsby WE, Hager GF. J Am Chem Soc, 1955, 77, 3766.
[137] Zhang Z, Jackson , Miller DJ. JEAppl Catal A General 2001, 219, 89.
[138] Manyar , Paun C, Pilus R, Rooney DW, Thompson JM, Hardacre C. HGChem Commun 2010, 46, 6279.
[139] Primo A, Concepcion P, Corma A. Chem Commun 2011, 47, 3613.
[140] Liu K, Huang X, Pidko EA, Hensen EJM. Chem Cat Chem 2018, DOI: 10.1002/cctc.201701329.
[141] Jones DR, Iqbal S, Kondrat SA, Lari GM, Miedziak PJ, Morgan DJ, Parkerbc SF, Hutchings GJ. PhysChemChemPhys 2016, 18, 17259.
[142] Wu Z, Zhang M, Yao Y, Wang J, Wang D, Zhang M, Li Y. Catal Today 2018, 302, 217.
[143] Zhou JH, Zhang MG, Zhao L, Li P, Zhou XG, Yuan WK. Catal Today 2009, 147, S225.
[144] Ye LM, Duan XP, Lin HQ, Yuan YZ. Catal Today 2012, 183, 65.
[145] Liu H, Huang Z, Xia C, Jia Y, Chen J, Liu H. Chem Cat Chem 2014, 6, 2918.
[146] Huang Z, Chen J, Jia Y, Liu H, Xia C, Liu H. Appl Catal B 2014, 147, 377.
[147] Sun J, Liu H. Catal Today 2014, 234, 75.
[148] Sotak T, Schmidt T, Hronec M. Appl Catal A 2013, 459, 26.
[149] Chen XG, Wang XC, Yao SX, Mu XD. Catal Commun 2013, 39, 86.
[150] Deutsch KL, Lahr DG, Shanks BH. Green Chem 2012, 14, 1635.
[151] Sohounloue DK, Montassier C, Barbier J. React Kinet Catal Lett 1983, 22, 391.
[152] Montassier C, Menezo JC, Hoang LC, Renaud C, Barbier J. J Mol Catal 1991, 70, 99.
[153] Peereboom L, Jackson JE, Miller DJ. Green Chem 2009, 11, 1979.
[154] Lahr DG, Shanks BH. J Catal 2005, 232, 386.

[155] Jia Y, Liu H. Catal Sci Technol 2016, 6, 7042.
[156] Zhou CH, Beltramini JN, Fan YX, Lu GQ. Chem Soc Rev 2008, 37, 527.
[157] Gonzalez-Garay A, Gonzalez-Miquel M, Guillen-Gosalbez G. ACS Sustain Chem Eng 2017, 5, 5723.
[158] Pagliaro M, Ciriminna R, Kimura H, Rossi M, Pina CD. Angew Chem Int Ed 2007, 46, 4434.
[159] Rivière M, Perret N, Cabiac A, Delcroix D, Pinel C, Besson M. Chem Cat Chem 2017, 9, 2145.
[160] Arundhathi R, Mizugaki T, Mitsudome T, Jitsukawa K, Kaneda K. Chem Sus Chem, 2013, 6, 1345.
[161] Wang J, Zhao XC, Lei N, Li L, Zhang LL, Xu ST, Miao S, Pan XL, Wang AQ, Zhang T. Chem Sus Chem 2016, 9, 784.
[162] Nanda MR, Yuan Z, Qin W, Xua C. Catal Rev Sci Eng 2016, 58, 309.
[163] Oh J, Dash S, Lee H. Green Chem 2011, 13, 2004.
[164] Wu Z, Zhao K, Ge S, Qiao Z, Gao J, Dou T, Yip ACK, Zhang M. ACS Sustain Chem Eng 2016, 4, 4192.
[165] Shinmi Y, Koso S, Kubota T, Nakagawa Y, Tomishige K. Appl Catal B Environ 2010, 94, 318.
[166] Feng J, Wang J, Zhou Y, Fu H, Chen H, Li X. Chem Lett 2007, 36, 1274.
[167] Chia M, Pagán-Torres YJ, Hibbitts D, Tan Q, Pham HN, Datye AK, Neurock M, Davis RJ, Dumesic JA. J Am Chem Soc, 2011, 133, 12675.
[168] Nakagawa Y, Shinmi Y, Koso S, Tomishige K. J Catal 2010, 272, 191.
[169] Chen K, Koso S, Kubota T, Nakagawa Y, Tomishige K. Chem Cat Chem 2010, 2, 547.
[170] Amada Y, Watanabe H, Tamura M, Nakagawa Y, Okumura K, Tomishige K. J Phys Chem C 2012, 116, 23503.
[171] García-Fernández S, Gandarias I, Tejido-Núñez Y, Requies J, Arias PL. Chem Cat Chem 2017, 9, 4448.
[172] Gu M, Shen Z, Yang L, Peng B, Dong W, Zhang W, Zhang Y. Ind Eng Chem Res 2017, 56, 13572.
[173] Fan Y, Cheng S, Wang H, Ye D, Xie S, Pei Y, Hu H, Hua W, Li Z.H, Qiao M, Zong B. Green Chem 2017, 19, 2174.
[174] Mane R, Patil S, Shirai M, Rayalu S, Rode C. Appl Catal B Environ 2017, 204, 134.
[175] Cai F, Song X, Wu Y, Zhang J, Xiao G. ACS Sustain Chem 2018, 6, 110.
[176] Wang J, Yang M, Lei N, Li L, Hou B, Miao S, Pan X, Wang A, Zhang T. Chem Sus Chem 2017, 10, 819.
[177] Gebrestadik FB, Llorca J, Salagre P, Cesteros Y. Chem Cat Chem 2017, 9, 3670.
[178] Duran-Martin D, López Granados M, Fierro JLG, Pinel C, Mariscal R. Top Catal 2017, 60, 1062.
[179] Penner S, Jenewein B, Gabasch H, Klötzer B, Wang D, Knop-Gericke A, Schlögl R, Hayek K. J Catal 2006, 241, 14.
[180] Li X, Zhang B, Wu Q, Zhang C, Yu Y, Li Y, Lin W, Cheng H, Zhao F. J Catal 2016, 337, 284.
[181] Li X, Wu Q, Zhang B, Zhang C, Lin W, Cheng H, Zhao F. Catal Today 2018, 302, 210.
[182] Sun Q, Wang S, Liu H. ACS Catal 2017, 7, 4265.
[183] Zheng L, Li X, Du W, Shi D, Ning W, Lu X, Hou Z. Appl Catal B Environ 2017, 203, 146.
[184] Freitas IC, Manfro RL, Souza MMVM. Appl Catal B Environ 2018, 220, 31.
[185] Van den Bosch S, Schutyser W, Koelewijn S-F, Renders T, Courtin CM, Sels BF. Chem Commun 2015, 51, 13158.
[186] Zhang W, Chen J, Liu R, Wang S, Chen L, Li K. ACS SustainChem Eng, 2014, 2, 683.
[187] Fargues C, Mathias A, Rodrigues A. Ind Eng Chem Res 1996, 35, 28.
[188] Gandini A. Green Chem 2011, 13, 1061.
[189] Dasari MA, Kiatsimkul P-P, Sutterlin WR, Suppes GJ. Appl Catal A 2005, 281, 225.
[190] Furikado I, Miyazawa T, Koso S, Shimao A, Kunimori K, Tomishige K. Green Chem 2007, 9, 582.

[191] Wang M, Shi H, Camaioni DM, Lercher JA. Angew Chem Int Ed 2017, 56, 1.
[192] Schutyser W, Van den Bossche G, Raaffels A, Van den Bosch S, Koelewijn S-F, Renders T, Sels BF. ACS Sustainable Chem Eng 2016, 4, 5336.
[193] Gandilhon P. US Patent 4,138,411, (1979) for Rhone-Poulenc S. A.
[194] Melean LG, Rodriguez M, Romero M, Alvarado ML, Rosales M, Baricelli PJ. Appl Catal A General 2011, 394, 117.
[195] de Vyver SV, Roman-Leshkov Y. Catal Sci Technol 2013, 3, 1465.
[196] Matsumoto A, Odani T, Sada K, Miyata M, Tashiro K. Nature 2000, 405, 328.
[197] Yet L. Chem Rev 2003, 103, 4283.
[198] Polen T, Spelberg M. and Bott M. J Biotechnol 2013, 167, 75.
[199] Vardona DR, Frandena MA, Johnsona CW, Karpa EM, Guarnieria MT, Lingera JG, Salma MJ, Strathmannb TJ, Beckham GT. Energ Environ Sci 2015, 8, 617.
[200] Jastrzebski R, Weckhuysen BM, Bruijnincx PCA. Chem Commun 2013, 49, 6912.
[201] Li X, Wu D, Lu T, Yi G, Su H, Zhang Y. Angew Chem Int Ed, 2014, 53, 1.
[202] Capellia S, Rosengart A, Villa A, Citterio A, Di Michele A, Bianchi CL, Prati L, Pirola C. Appl Catal B Environ 2017, 218, 220.
[203] Zhang C, Xing J, Song L, Xin H, Lin S, Xing L, Li X. Catal Today 2014, 234, 145.
[204] Qia J, Sun X, Tang S-F, Sun Y, Xu C, Li X, Li X. Appl Catal A General 2017, 535, 24.
[205] Nie R, Peng X, Zhang H, Yu X, Lu X, Zhou D, Xia Q. Catal Sci Technol 2017, 7, 627.

K.S. Triantafyllidis, S.D. Stefanidis, S.A. Karakoulia, A. Pineda,
A. Margellou, K.G. Kalogiannis, E.F. Iliopoulou, A.A. Lappas

5 State-of-the-art in biomass fast pyrolysis using acidic catalysts: direct comparison between microporous zeolites, mesoporous aluminosilicates and hierarchical zeolites

Abstract: In this chapter, a direct comparison of the performance of the most representative conventional microporous zeolites, amorphous mesoporous aluminosilicates and hierarchical (meso/macroporous) zeolites in catalytic fast pyrolysis (CFP) of biomass is presented, based on experiments performed under the same conditions in a bench scale fixed bed (down flow) reactor. Furthermore, a comprehensive overview of the state-of-the-art on biomass CFP with these types of catalysts is also included, aiming to highlight the most representative previously reported results. On the basis of both the experimental and literature data, it was shown/verified that biomass CFP with acidic micro/meso/macroporous materials can be effectively utilized for tuning the composition and properties of the bio-oil, depending on its targeted final use as source of chemicals (phenolics, aromatics), as fuel additive (aromatics) or as biocrude for downstream hydrodeoxygenation toward hydrocarbon fuels.

5.1 Overview of state-of-the-art

The ever-growing world energy demand, in combination with the dependency on finite energy resources and concerns over energy security and environmental issues, has spurred research into alternative energy resources. Recently, the extreme weather phenomena observed around the globe have led nations to sign an agreement known as the *Paris Agreement*, whose central aim is to limit the global temperature *rise* below 2 °C above preindustrial levels in this century, and to promote actions for further reduction of the global temperature increase to 1.5 °C [1]. Renewable energy sources have a key role to play in meeting long-term climate and sustainability goals, and excellent progress has already been made in the electricity sector. However, electricity is only a small portion of the world energy demand and progress in the heat and transport sectors is needed as well. Biomass derived solid, liquid and gaseous fuels will have significant contributions in these two sectors in the near future (2018–2023) [2]. The use of electric vehicles has grown in the recent years, but there is still a need for renewable fuels in the aviation, maritime and heavy freight sectors where biofuels are

https://doi.org/10.1515/9783110538151-005

the only practical alternative [3]. First-generation biofuels already contribute to the energy mix of the transport sector; however, there are several limitations and concerns associated with their production, most importantly their competition with the food supply chain. Advanced biofuels mitigate those concerns as they are derived from residues, wastes or dedicated high-yield nonfood energy crops. Recently, the European Commission proposed a cap of 3.8% on the energy share of first-generation biofuels in the transportation sector by 2030 and a target of 6.8% by the same year for the energy share of advanced biofuels and renewable electricity [4].

Lignocellulose is a nonedible form of biomass that is abundant, low-cost and can be used for the production of advanced biofuels. One of the most promising technologies to convert biomass into liquid, solid and gas fuels or fuel precursors is fast pyrolysis (FP). During FP, biomass is heated at very high heating rates under inert atmosphere and atmospheric pressure. Under these conditions, biomass is thermally decomposed to smaller fragments and the produced pyrolysis vapors are rapidly quenched to form mainly a liquid product known as bio-oil (or biomass pyrolysis oil). Bio-oil is a mixture of oxygenated compounds derived from the thermal decomposition of the three structural components of biomass, i.e. cellulose, hemicellulose and lignin. The oxygenates in bio-oil are responsible for a series of adverse properties that render bio-oil a low-quality product which is unstable under storage and transportation conditions and it is difficult to upgrade via downstream processes. In order to produce a higher-quality product, catalytic fast pyrolysis (CFP) has been developed. This process is very similar to FP, with the difference that the pyrolysis vapors come in contact with a solid catalyst before they are quenched. The catalytic reactions that take place remove oxygen from the pyrolysis vapors in the form of CO, CO_2 and H_2O and as such, a less oxygenated and more stable liquid product (catalytic bio-oil) is produced. This can be achieved either “in situ,” that is, the biomass and the catalysts are mixed together forming a single bed in the reactor, or “ex situ or in two stage” when the produced thermal-FP vapors are driven through a separate catalytic bed (preferably in a separate reactor for better control of the upgrading temperature, which could be lower than the temperature in the pyrolysis reactor) [5]. In this latter case, deactivation of the acidic catalysts by deposition of the alkali or alkaline earth metals present in biomass can be avoided [6]. Catalytic bio-oil is an intermediate product that can be used as a source of renewable high value-added chemicals and/or be upgraded to drop-in biofuels via downstream processes such as hydrodeoxygenation or coprocessing with petroleum feeds in fluid catalytic cracking processes, using existing refinery infrastructure [7]. Depending on the catalyst used and its properties, the yield of catalytic bio-oil and the deoxygenation degree can be optimized, while specific high value-added products, such as benzene, toluene and xylene hydrocarbons (BTX) can be produced.

So far, a wide range of catalysts have been evaluated for their performance in the CFP of biomass, mostly in the microscale (i.e., Py/GC-MS systems), but also in bench- and pilot-scale reactors. These include acidic, basic and bifunctional catalysts, microporous zeolites, mesoporous aluminosilicates, hierarchical mesoporous zeolites,

mixed metal oxides and others. A recent extensive literature review on this subject has been published by Iliopoulou et al. [8]. Zeolites are microporous acidic catalysts that are widely used in oil refineries for the cracking of hydrocarbon molecules in heavy oil fractions to produce lighter products. Since similar reaction mechanisms apply in the pyrolysis/cracking of lignocellulose oligomers, zeolites have been also used for biomass CFP. The most commonly utilized catalyst for biomass CFP is the ZSM-5 zeolite, which has been found in many studies to be very effective for the reduction of heavy compounds in the bio-oil and for the deoxygenation of intermediates in the pyrolysis vapors, leading to the production of a catalytic bio-oil with reduced oxygen content [9–14]. ZSM-5 is also known to be very effective for the conversion of oxygenates in the pyrolysis vapors into desirable aromatic hydrocarbons [12–14, 15–25]. This has been attributed to the combined effect of ZSM-5's relatively strong Brønsted acidity and the unique medium-size channel-like microporous structure, which favor the formation of monoaromatic hydrocarbons (MAH) (Figure 5.1) via Diels Alder reactions of furan intermediates or classical cyclization-aromatization of small alkanes (i.e., ethylene, propylene) [5, 8, 22, 24, 26–29], while at the same time restricting, in some cases, the undesirable coke formation [21, 26, 29]. A schematic overview of the generally accepted reaction pathways for the production of aromatics in biomass CFP by ZSM-5 zeolites is shown in Figure 5.2 [30].

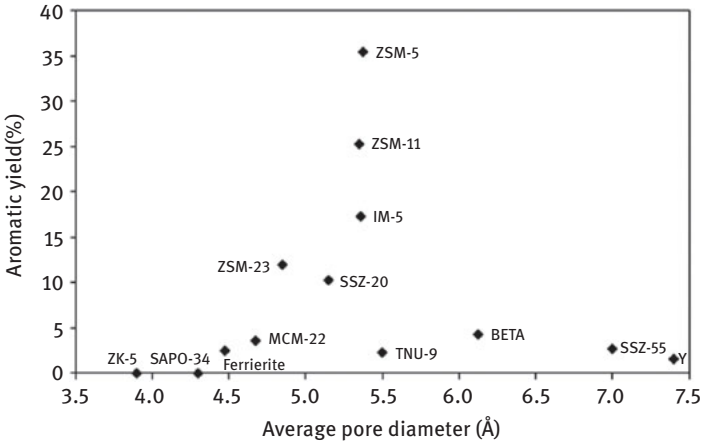

Figure 5.1: Yield of aromatic hydrocarbons from the catalytic pyrolysis of glucose with different zeolite catalysts as a function of their average pore diameter. (Reproduced from Ref. [26] with permission from Elsevier).

While ZSM-5's acidity and unique microporous structure offer these beneficial effects to its performance in biomass CFP, these same properties are also responsible for some limitations of this catalyst. High acidity has been observed to result in faster catalyst deactivation due to a more pronounced formation of coke [31, 32] and in selectivity

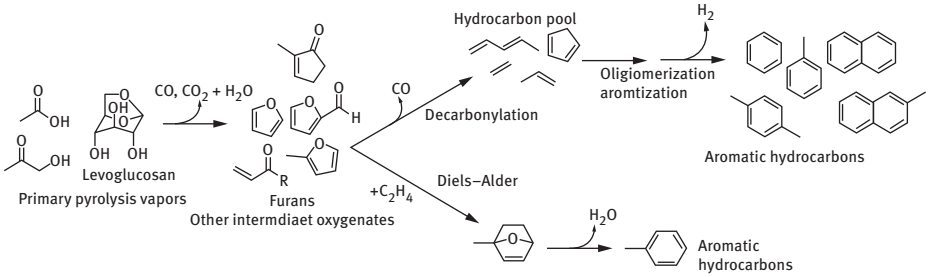

Figure 5.2: Simplified pathway showing conversion and deoxygenation of primary pyrolysis vapors to aromatic hydrocarbons. (Reproduced from Ref. [30] with permission from American Chemical Society.).

shift from MAH to polycyclic aromatic hydrocarbons (PAH) [25, 28]. Moreover, a part of the pyrolysis vapors is composed of large intermediate fragments which cannot enter the zeolite micropore network, where most of the active sites are located. As a result, these intermediates can only be cracked on the external surface of the zeolite and, therefore, a significant portion of the internal surface of the zeolite crystals remains underutilized. Moreover, the diffusion of the initially formed MAHs or other monomers, such as alkyl-phenols, from the interior of the ZSM-5 crystal toward its external surface and eventually to the product stream is also hindered, thus favoring secondary cracking, (de)alkylation and condensation reactions that lead to the formation of larger products (PAHs, phenolic oligomers) and coke, which block the pores and active acid sites of the zeolites.

In general, the deactivation of zeolitic catalysts, mainly of ZSM-5, in the so-called in situ CFP, that is, when the biomass and the catalyst particles are mixed and fed together in the pyrolysis reactor, is attributed: (a) to pore blocking and masking of acid sites by formed coke (reversible deactivation), (b) to partial framework dealumination of the zeolite (due to the hydrothermal conditions in the pyrolysis reactor or during regeneration/burning of the coke) which leads to Brønsted acidity loss and (c) to accumulative ash deposition that also blocks the pores and acid sites [33, 34]. A recent study on the effect of alkali metals (i.e., potassium) deposition on ZSM-5 zeolite has shown that it can effectively change the selectivity of the pyrolysis products towards alkyl phenols and methyl furan instead of aromatics that are favored by the highly acidic parent ZSM-5 zeolite [35]. In the more recently studied ex situ CFP, that is, where the biomass was initially thermally pyrolyzed and the produced vapors passed/reacted over a separate catalytic bed, ash accumulation on the catalyst was avoided and the only means of deactivation was coking [6].

Considering the above, mesoporous aluminosilicates, such as MCM-41 (Mobil Composition of Matter), SBA-15 (Santa Barbara Amorphous) and MSU (Michigan State University) materials, have also attracted attention for biomass CFP due to their milder acidity and larger pores, which can facilitate the accessibility of pyrolysis

intermediates towards the active sites and the faster diffusion of catalytic products. These types of materials have been shown to be very active catalysts in biomass CFP and to promote the formation of acids and furans from biomass biopolymers [19, 36, 37], as well as the overall reduction of oxygenates in the catalytic bio-oil [19, 38–40]. They have been also found to promote the formation of light phenolic compounds [36, 38, 40, 41]. However, due to the lack of strong acidity and of a shape-selective micropore structure, their efficiency toward MAH formation is moderate [18, 36, 40], especially when compared to zeolites [18, 24, 42] (see Figure 5.3).

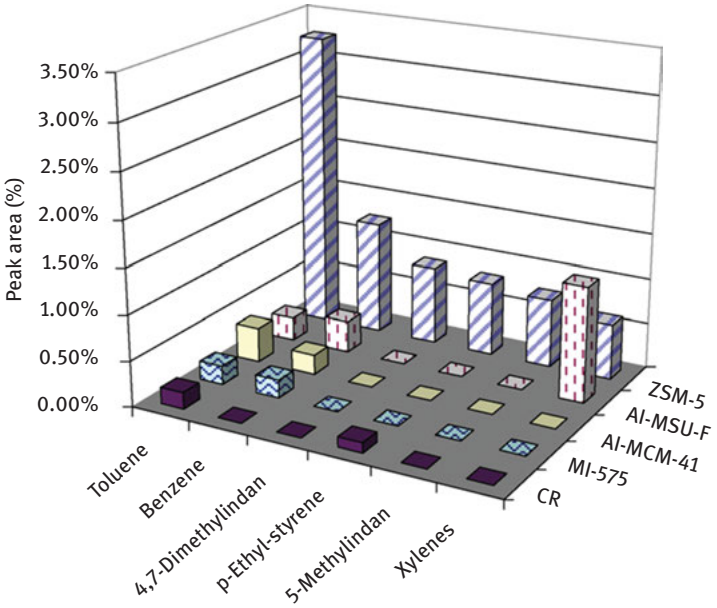

Figure 5.3: The effect of ZSM-5 on the production of aromatic hydrocarbons from the catalytic pyrolysis cassava rhizome in comparison with an Al-MSU-F, an Al-MCM-41 catalyst, an alumina-stabilized ceria catalyst and noncatalytic pyrolysis. (Reproduced from Ref. [18] with permission from Elsevier.).

More recently, zeolites with high external surface area (nanosized zeolites) or with a secondary meso/macropore network (hierarchical zeolites) have also attracted attention in biomass CFP [43]. These types of materials combine the benefits of enhanced accessibility to the active acid sites and easier diffusion of the catalytic products with the benefits of shape-selective micropore structure and strong acidity of the zeolite crystals. As such, they are expected to be more active than conventional zeolites, while maintaining or enhancing the yields of deoxygenated liquid products such as MAH. However, inconsistent results have been reported so far in the literature. Hierarchical zeolites synthesized with mesoporogen surfactants were reported to be

more active than conventional zeolites [44–46] and to promote the formation of aromatic hydrocarbons [44, 46, 47], but were also found to be more prone towards coking [29, 47]. Other groups have reported reduced acidity and aromatic hydrocarbon formation with this type of materials [29, 48] and only comparable activity to that of conventional microporous zeolites [47]. Hierarchical zeolites by postsynthesis treatment methods (i.e., desilication/dealumination) have also been tested in biomass CFP. Depending on the severity of the treatment, increased activity [49, 50] and aromatic hydrocarbon formation [51–54] have been reported, despite the reduced acidity in most cases [50–52]. Reduced catalytic coke formation was also reported [49, 51, 53], while, on the other hand, other groups have reported increased acidity [53] and coke formation [52].

Many efforts to mitigate the coking tendency, still maintaining the benefits of enhanced accessibility and acidity of mesoporous zeolites, have been based on the incorporation of metals/metal oxides, such as Zr, Ga, Mg, Zn, Sn, Cu, Ni and so on. It has been reported that highly dispersed ZrO_2 (in nano- or meso-ZSM-5 zeolites) effectively decreased the extent of secondary reactions, such as severe cracking and coke formation, and promoted the conversion of the oligomers formed initially by lignocellulose pyrolysis providing a high-quality partially deoxygenated bio-oil (high mass and energy yields); however, the yields of nonoxygenated aromatics were lower compared to those obtained by the parent nano/meso-zeolites [55]. Slightly increased aromatics and decreased coke were obtained by Ga-modified MSU-MFI mesoporous zeolites [56]. Hierarchical cerium-incorporated (in the zeolitic framework) MFI zeolite catalysts were also investigated, exhibiting less coke and increased CO production in glucose FP, while shifting the selectivity in bio-oil components from classical BTX aromatics (with parent meso-MFI) to valuable oxygenated chemicals (furans, ketones, aldehydes) [48].

MgO-modified hierarchical zeolites exhibited relatively high deoxygenation activity via different reaction pathways, such as ketonization and condensation, compared to those catalyzed by zeolitic strong Brønsted acid sites, that is, dehydration, cracking and aromatization [57–59]. The reactivity of MgO via its basic surface properties in biomass CFP and the ability to enhance deoxygenation of bio-oil via ketonization and condensation reactions has been clearly demonstrated previously [60, 61]. It was also suggested that the Lewis acid sites, formed by insertion of Mg at ion-exchange sites of the hierarchical ZSM-5 zeolites could favor ketonization reactions of acids with aldehydes to produce ketones [58]. A slightly lower deoxygenation rate was obtained with Cu-loaded zeolites, attributing the enhanced production of CO to the increased decarbonylation of acids to aldehydes over the Cu exchanged cations. A similar deoxygenation mechanism via decarbonylation and decarboxylation reactions on the Lewis acid sites was suggested for the Ni and Sn-ZSM-5 hierarchical zeolite catalysts. However, with all metal-exchanged hierarchical ZSM-5 zeolites, the production of aromatics was decreased due to the lower amount of Brønsted acid sites (Figure 5.4). In all the above studies of metal-modified hierarchical zeolites, the major

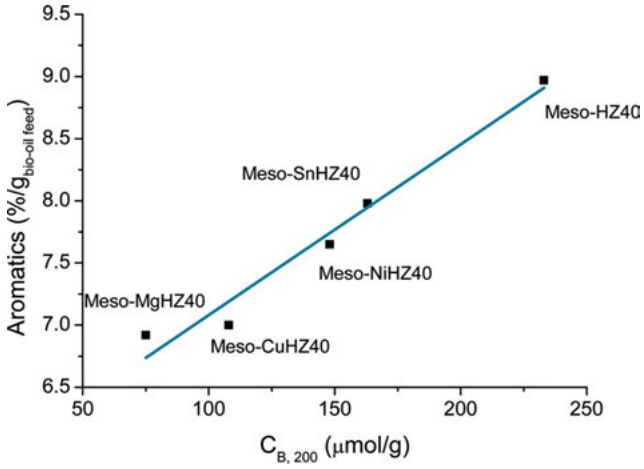

Figure 5.4: Variation of the formation of aromatics in the upgrading of woody biomass pyrolysis vapors with various metal-exchanged meso-ZSM-5 catalysts. (Reproduced from Ref. [58] with permission from American Chemical Society.).

effects identified were attributed to the tuning/suppression of zeolitic Brønsted acidity, the incorporation and related reactivity of Lewis acid sites due to the metal oxides, as well as of basic sites (especially with MgO). Similar effects were observed by the incorporation of transition or noble metals in conventional microporous zeolites or amorphous mesoporous aluminosilicates (see recent reviews [5, 8] and papers within).

In the following sections, a direct comparison of the performance of the most representative conventional microporous zeolites, amorphous mesoporous aluminosilicates and hierarchical (meso/macroporous) zeolites in CFP of biomass is presented, based on experiments performed under the same conditions in a bench scale fixed bed (down flow) reactor.

5.2 Direct comparison of the most representative conventional microporous zeolites, amorphous mesoporous aluminosilicates and hierarchical zeolites in catalytic fast pyrolysis of biomass

5.2.1 Characterization of biomass feedstock

The biomass used for the FP experiments was beech wood sawdust (Lignocel, HBS 150–500) with an average particle size of 150–500 μm. The main characteristics

(elemental analysis, ash, inorganics and humidity content, extractives and main structural components, higher heating value) of the biomass feedstock are listed in Table 5.1.

Table 5.1: Physicochemical characteristics of Lignocel (beech wood sawdust).

Lignocel, HBS 150–500	
Carbon (wt.%)	45.30
Hydrogen (wt.%)	6.4
Oxygen (wt.%)	47.70
Ash (wt.%)	0.66
Humidity (wt.%)	8.60
Extractives (wt.%)	6.90
Lignin (wt.%) (acid insoluble)	20.30
Lignin (wt.%) (acid soluble)	3.30
Cellulose (wt.%)	40.10
Hemicellulose (wt.%)	19.10
Higher heating value (MJ/kg)	19.09
K (ppm)	1014
Na (ppm)	50
Mg (ppm)	376
Fe (ppm)	87
Al (ppm)	24
Ca (ppm)	1519

5.2.2 Catalysts and their main characteristics

The catalysts that were compared in biomass FP can be classified as conventional microporous zeolites, amorphous mesoporous aluminosilicates and hierarchical micro/meso/macroporous zeolites. A comprehensive description of their physicochemical characteristics and representative properties is provided in Table 5.2, while more detailed characterization data can be found in previous relevant publications [5, 8, 13, 27, 28, 34, 38, 41, 50, 62–68].

Table 5.2: The catalysts used in catalytic biomass FP.

Catalyst code/name	Material type	Characteristics
Microporous zeolites		
ZSM-5 (11.5, 25.0, 40.0)	ZSM-5 zeolite (MFI structure)	Si/Al = 11.5, 25.0, 40.0/strong acid sites and high Brønsted/Lewis (B/L) acid sites ratio (especially for Si/Al = 40.0)
Silicalite	Silicalite-type zeolite (MFI structure)	Si/Al > 1000/few acid sites due to aluminum "impurities" in the zeolite synthesis procedure
ZSM-5 (dil.)	ZSM-5 zeolite, diluted with silica-alumina (30% zeolite), formulated in microsphere morphology	Similar characteristics with the "pure" crystalline ZSM-5 zeolites, "diluted" with silica-alumina at about 30 wt.% zeolite, plus the characteristics of typical mesoporous, mildly acidic silica-alumina. It has also been subjected to pyrolysis – regeneration cycles in a fluidized bed FP reactor with catalyst recirculation
H-Y (2.5)	Zeolite Y (faujasite)	Si/Al = 2.5/weak/medium and less strong acid sites, high B/L ratio
USY (6)	Ultra-stable zeolite Y (faujasite)	Si/Al = 6/medium-strong acid sites, low B/L ratio (> 1)
Beta (12.5, 37.5)	Beta-type zeolite	Si/Al = 12.5, 37.5 /medium-strong acid sites, low B/L ratio (> 1)
Mordenite (10)	Mordenite-type zeolite	Si/Al = 10 / medium-strong acid sites, high B/L ratio
Ferrierite (10)	Ferrierite-type zeolite	Si/Al = 10 / medium-strong acid sites, high B/L ratio
Amorphous mesoporous (alumino)silicates		
MCM-41	Mesoporous silica material	High surface area, ordered network of tubular mesopores (3 nm) in hexagonal array, negligible acidity
Al-MCM-41 (20)	Mesoporous aluminosilicate material	Si/Al = 20, high surface area, ordered network of tubular mesopores (3 nm) in hexagonal array, relatively low number of weak-medium acid sites, low B/L ratio (< 1)
Al-MCM-41 (50)	Mesoporous aluminosilicate material	Si/Al = 50, high surface area, ordered network of tubular mesopores (3 nm) in hexagonal array, relatively low number of weak-medium acid sites, low B/L ratio (< 1)

Table 5.2 (continued)

Catalyst code/name	Material type	Characteristics
Al-MCM-41 (50)-nano	Mesoporous aluminosilicate material with very small particles which add additional high external surface area	Si/Al = 50, high surface area, ordered network of tubular mesopores (3 nm) in hexagonal array, high external surface area, relatively low number of weak-medium acid sites, low B/L ratio (< 1)
SBA-15	Mesoporous silica material	High surface area, ordered network of tubular mesopores (10 nm) in hexagonal array, negligible acidity
Al-SBA-15 (20)	Mesoporous aluminosilicate material	Si/Al = 20, high surface area, ordered network of tubular mesopores (11 nm) in hexagonal array, relatively low number of weak-medium acid sites, low B/L ratio (< 1)
MSU-J	Mesoporous silica material	High surface area, 3D network of wormhole-like mesopores with narrow pore size distribution (8.5 nm)
Al-MSU-J (50)	Mesoporous aluminosilicate material	Si/Al = 50, high surface area, 3D network of wormhole-like mesopores with narrow pore size distribution (7.5 nm), relatively low number of weak-medium acid sites, low B/L ratio (< 1)
γ-Al_2O_3	Aluminum oxide	Mesoporous alumina with moderate/ lower surface area compared to those of the ordered aluminosilicate materials, relatively wide pore size distribution (13–15 nm), only Lewis acid sites
ASA (35)	Amorphous silica-alumina	Mesoporous silica-alumina with moderate/low surface area compared to those of the ordered aluminosilicate materials, relatively wide pore size distribution (6 nm), low number of weak-medium acid sites and low B/L ratio (< 1)
Hierarchical micro/meso/macroporous zeolite materials		
MesoZSM-5(2.2)	ZSM-5 Zeolite with intracrystal mesoporous 2.2 nm, prepared with classical hydrothermal synthesis of ZSM-5 using in addition the appropriate mesoporogen templates	Zeolite ZSM-5 with strong Brønsted acid sites, higher surface area with small intreacrystal mesopores (2.2. nm), lower micropore and higher mesopore volume compared to those of conventional microporous ZSM-5, high B/L ratio

Table 5.2 (continued)

Catalyst code/name	Material type	Characteristics
MesoZSM-5(5.2)	ZSM-5 Zeolite with intracrystal mesoporous 5.2 nm, prepared with classical hydrothermal synthesis of ZSM-5 using in addition the appropriate mesoporogen templates	Similar with MesoZSM-5(5.2), with larger mesopores (5.2 nm), enhanced mesoporosity and decreased microporosity
ZSM-5 (nano)	ZSM-5 zeolite with small crystal/particles and very high external surface area	ZSM-5 zeolite with small crystallites/particles that provide high external surface area, similar acid properties with those of the conventional ZSM-5 zeolite, but with more exposed/accessible acid sites (due to the high external surface area)
ZSM-5 (3%cr.)	ZSM-5 zeolite with very low crystallinity (3%) and high external surface area	Aluminosilicate material with low crystallinity of ZSM-5 type, relatively small particles which add high external surface area, low amount of weak acid sites, almost similar to silica-alumina

5.2.3 Bench-scale fixed bed downflow reactor for the biomass pyrolysis experiments

The biomass pyrolysis experiments were carried out in a lab-scale fixed bed downflow reactor, made of stainless steel 316 and equipped with a three zone furnace. A schematic representation of the pyrolysis unit is shown in Figure 5.5. In a typical run, 1.5 g of biomass and 0.3–0.7 g catalyst were inserted in the hot reactor zone with the aid of a piston and heated at 500 °C coming in contact with a hot glass wool layer. Afterward, the produced pyrolysis vapors were driven through the catalytic bed (placed below the hot glass wool layer) with the aid of a constant nitrogen gas flow. Then, the produced vapors were removed from the reactor and condensed in a glass trap, immersed in a bath at –17 °C for the recovery of bio-oil. The noncondensable vapors were removed from the trap and collected in a gas collection system.

During condensation of the biomass pyrolysis vapors, three phases were formed: a liquid organic phase, a liquid aqueous phase and solid deposits on the trap walls. For the efficient collection of whole bio-oil, ethyl acetate was used as homogenizing agent. The amount of the produced bio-oil was determined by weighting the trap before and after the experiment, while the amount of the solid products (biomass residues and coke deposits on catalyst) was determined by direct weighing. The volume of gaseous products was measured by the liquid displacement method.

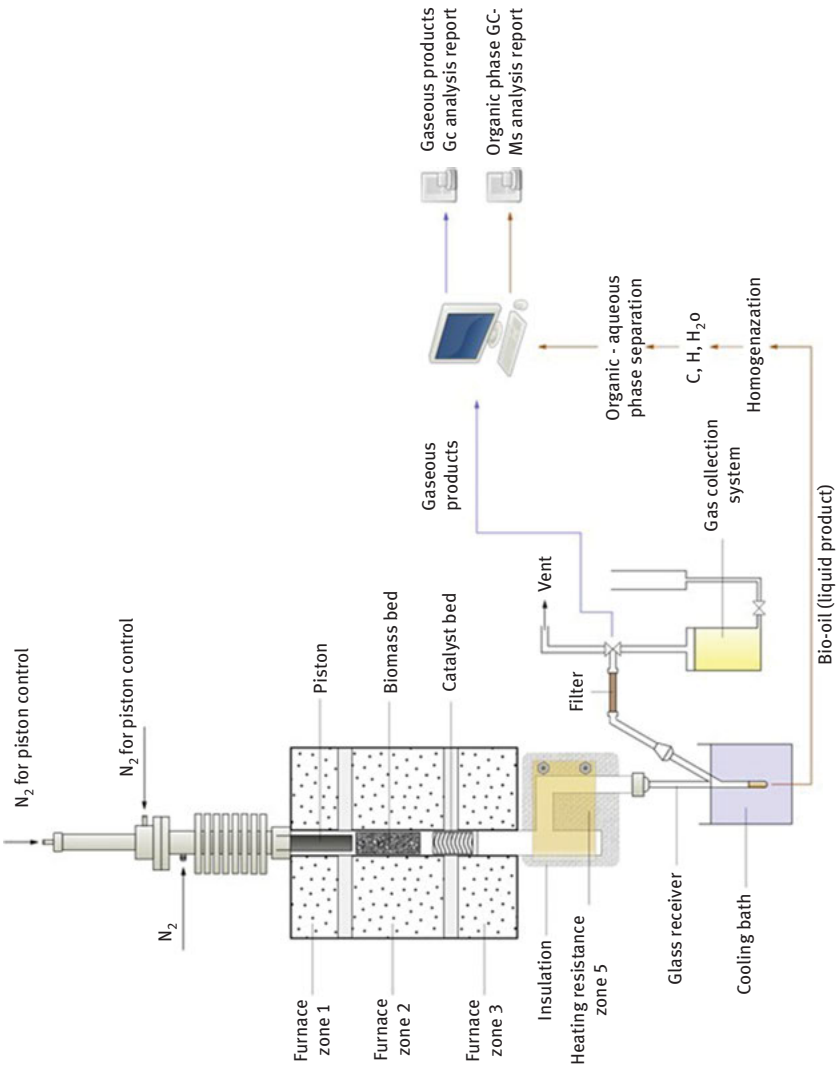

Figure 5.5: Schematic representation of biomass pyrolysis reactor.

The elemental composition (carbon, hydrogen, oxygen) of the bio-oil was determined with a LECO-800 LECO Corporation elemental analyzer and the water content via Karl–Fischer analysis. The organic phase was separated from the aqueous phase with dichloromethane and analyzed by gas chromatography-mass spectrometry (GC-MS) in an Agilent 7890A/5975C (electron energy 70 eV, emission 300 V, helium flow rate 0.7 cm^3/min, column HP-5MS 30 m × 0.25 mm ID × 0.25 m) system. The NIST 05 library was used for the identification of the compounds.

The gaseous products were analyzed by gas chromatography in an HP 5890 Series II chromatograph, equipped with four columns (precolumn: OV-101, columns: Porapak N, Molecular Sieve 5A and Rt-Qplot 30 m × 0.53 mm ID) and two detectors (TCD and FID).

The amount of the produced solids was determined by weighting the reactor before and after the reaction.

5.2.4 Product yields and bio-oil composition

The following representative results from the biomass FP tests are provided below, in order to present a direct comparison of the performance of the various catalyst types:

- Products yields (wt.% on biomass): total gases, total liquids (bio-oil), aqueous phase of bio-oil, organic phase of bio-oil, solids (unconverted biomass and char, plus reaction coke for the catalytic experiments)
- Gas yields (wt.% on biomass): CO, CO_2, H_2 and hydrocarbons C_1–C_6.
- Oxygen amount (wt.% on organic phase of bio-oil) based on the amount of organic phase of bio-oil.
- Composition of bio-oil organic phase (% relative intensity of GC-MS peaks). The compounds were categorized in the following groups: aromatics with one aromatic ring (AR), aliphatic hydrocarbons (AL), phenolics (PH), furans (FUR), acids (AC), esters (EST), alcohols (ALC), ethers (ETH), aldehydes (ALD), ketones (KET), polycyclic aromatic hydrocarbons (PAH), sugars (SUG), nitrogen compounds (NIT) and unidentified (UN).

Depending on their effect on bio-oil properties, as well as on the aimed use of bio-oil (i.e., as deoxygenated fuel or bio-crude for the production of hydrocarbon fuels, or as source of nonoxygenated aromatics, or as source of various oxygenated chemicals such phenolics, ketones, furans, etc.), the identified compounds can also be classified as “desirable” or “undesirable.” Ketones, aldehydes and higher molecular weight oligomers are considered responsible for the bio-oil aging and polymerization during its storage and transport. High content of organic acids makes the bio-oil corrosive to common metals and hinders its potential use as fuel. Furthermore, acids can catalyze polymerization reactions, decreasing further the stability of the bio-oil. PAHs are carcinogenic and, consequently, environmentally undesirable. Esters, ethers and oxygen

containing compounds in general decrease the heating value of bio-oil. As a consequence, all the above compounds are considered to be undesirable, especially when the bio-oil will be used in energy/fuel production applications. On the other hand, phenolics and furans are considered as high value-added chemicals and higher yields could increase the sustainability of the process. The presence of aromatic and aliphatic hydrocarbons and alcohols is preferred toward the production of biofuels.

The catalytic results described in the following sections are categorized per catalyst group in order to identify any trends and effects by systematic variation of their properties.

5.2.4.1 Catalytic fast pyrolysis (CFP) of biomass over conventional microporous zeolites

The results of noncatalytic (silica sand) and CFP of biomass over conventional microporous zeolites (first group of Table 5.2) are listed in Table 5.3 and in Figures 5.6 and 5.7. The noncatalytic pyrolysis resulted in 59 wt.% bio-oil (37.5 wt.% organic phase and 21.5 wt.% water), 17.8 wt.% non-condensable gases and 23.2 wt.% solids (char and

Table 5.3: Product yields for the catalytic pyrolysis of beech wood (wt.% on dry biomass) over conventional microporous zeolites.

	Bio-oil	Water	Organic fraction	Solids	Gases	CO_2	CO	CH_4	$C_{2=}$	$C_{3=}$	Total C_4–C_6
Silica sand	59.0	21.5	37.5	23.2	17.8	9.5	6.5	0.9	0.2	0.1	0.3
ZSM-5 (11.5)	47.8	29.6	18.2	26.2	25.9	11.0	11.2	0.9	1.1	0.7	0.6
ZSM-5 (25)	43.6	29.5	14.1	29.4	27.0	10.1	12.3	1.0	1.4	1.1	0.8
ZSM-5 (40)	41.9	36.4	5.5	26.5	31.6	11.9	14.5	1.1	1.6	1.2	0.8
Silicalite	51.5	28.4	23.1	24.7	23.8	10.8	9.7	1.1	0.5	0.5	0.9
ZSM-5 (dil.)	48.7	27.0	21.7	27.4	23.9	10.9	9.8	0.9	0.5	0.5	1.1
H-Y	45.6	31.9	13.7	31.4	23.0	9.2	10.1	1.7	0.6	0.5	0.5
USY	42.0	32.5	9.5	29.5	28.5	10.4	13.1	2.1	0.9	0.7	0.8
Beta (12.5)	35.6	30.2	5.4	34.3	30.1	11.7	13.1	1.7	1.1	0.9	0.8
Beta (37.5)	41.0	29.3	11.6	31.2	27.9	10.8	12.7	1.4	0.7	0.8	1.0
Mordenite (10)	49.5	26.6	22.9	26.9	23.6	10.2	10.2	1.3	0.8	0.3	0.4
Ferrierite (10)	58.8	30.2	28.7	20.0	21.2	10.1	8.2	0.7	0.7	0.6	0.6

H_2 yield was below <0.1 wt.%; ethane and propane yields were ≤ 0.3 wt.%; solids: unconverted biomass and char, plus reaction coke for the catalytic experiments.

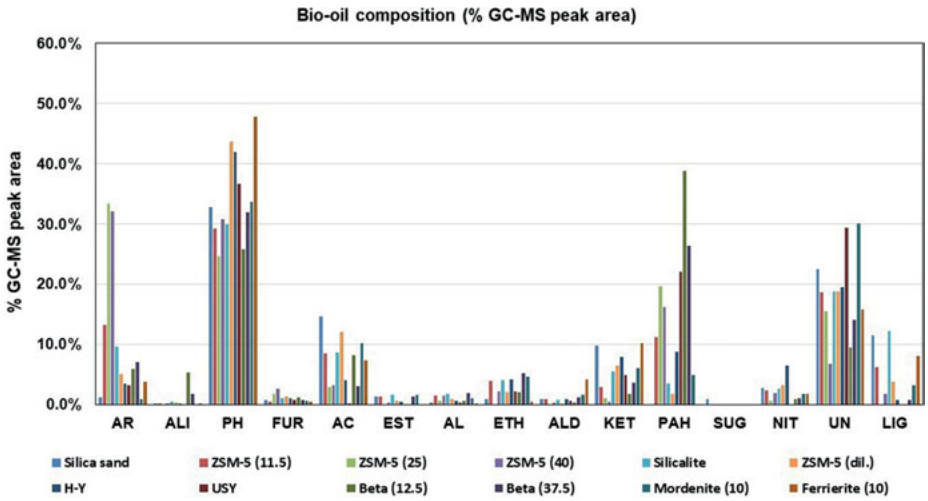

Figure 5.6: Composition analysis (% GC-MS peak area) of the bio-oil organic phase produced from the catalytic pyrolysis of beech wood over conventional microporous zeolites.

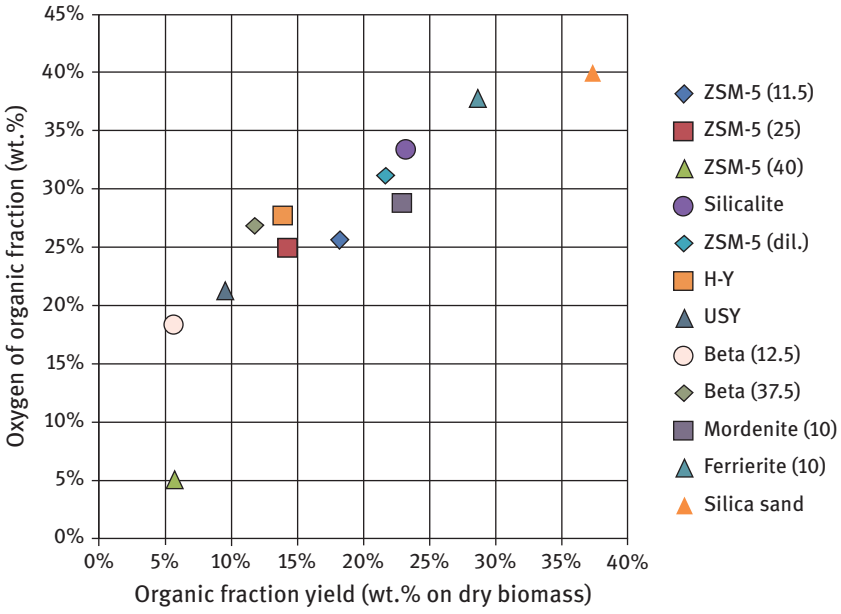

Figure 5.7: Oxygen content of the organic phase as a function of organic fraction yield over conventional microporous zeolites.

coke). Beta zeolite with relatively high aluminum content (i.e., Si/Al = 12.5) was the most active in the conversion of bio-oil, that is, biomass pyrolysis vapors initially formed and converted in situ (in the same reactor, over the catalyst bed), toward gaseous and solid (coke) products. The organic phase of bio-oil was reduced from 37.5 wt.% in the noncatalytic experiment to 5.4 wt.% with Beta(12.5), exhibiting also the highest increase of solids (due to coke formation) among all zeolite catalysts tested as well as very high yield of gases. Similar activity was obtained by ZSM-5(40) zeolite (e.g., organic phase of bio-oil at 5.5 wt.%), which exhibited lower coking tendency but higher gases production compared to Beta(12.5). The water content of bio-oil with ZSM-5(40) was also the highest one obtained. Comparing the two zeolitic microporous structures, at similar low Si/Al ratios, that is, Beta(12.5) versus ZSM-5 (11.5), it can be seen that the former zeolite is much more reactive, possibly due to the slightly larger micropore size of the Beta structure. However, at higher Si/Al ratio, that is, Beta(37.5) versus ZSM-5(40), ZSM-5 is more reactive than Beta, driving the products toward gases instead of coke. This can be attributed to the previously identified relatively high strength of the Brønsted acid sites of ZSM-5 zeolites with Si/Al ratio higher than ca. 25, especially those with Si/Al of ~40 [62, 65]. Silicalite zeolite exhibited some reactivity, due to the traces of aluminum that usually exist in this zeolite and offer few but relatively strong Brønsted acid sites [28, 69, 70]. Similar moderate activity was also observed for the diluted/equilibrium ZSM-5 zeolite, ZSM-5 (dil.), since its activity is significantly reduced compared to fresh, purely crystalline zeolite [27, 33, 34, 66]. The activity of Mordenite(10) and Ferrierite(10) in converting bio-oil was also moderate (Ferrierite was the less active among all zeolites tested), despite having relatively high aluminum content and number of Brønsted acid sites. Zeolite Y, and especially USY that possesses fewer but stronger Brønsted acid sites than H-Y zeolite, showed increased reactivity, but still not as high as that of Beta and ZSM-5 zeolites. Both the parent Y and USY zeolites also exhibit increased tendency toward coke formation. With regard to gas composition, all zeolites led to significant increase of CO, compared to the noncatalytic experiment, with minor increase of CO_2; this being indicative of enhanced deoxygenation via decarbonylation (and dehydration due to the increased water fraction) instead of decarboxylation, in accordance with previous studies [5, 8, 60]. Zeolite ZSM-5 was also more selective toward the production of light alkenes (ethylene and propylene), while the rest of zeolites favored the formation of methane [5, 8, 28].

With regard to the composition of the organic phase of bio-oil (Figure 5.6), noncatalytic pyrolysis produced mainly phenolics (alkoxy- and alkyl-phenols from the thermal decomposition of lignin [62]), acids (mainly acetic acid from the acetyl groups in biomass) and ketones. ZSM-5 zeolites, especially those with Si/Al = 25 and 40, were very selective toward monoaromatic compounds, accompanied by the decrease of acids and ketones, minor decrease of phenolics and moderate formation of PAHs, mainly naphthalenes. This is a typical behavior of “fresh” pure ZSM-5 zeolite owing to its strong Brønsted acidity and unique tubular micropores with medium size (i.e.,

~5.5 Å) [5, 8, 27, 28, 34, 60, 62, 64]. Obviously, only the dimers/monomers present in the biomass pyrolysis vapors with appropriate size can enter the micropores of ZSM-5 and benefit from its strong acidity and space confinement for the formation of monoaromatics, as well as naphthalenes to some extent. Silicalite and ZSM-5(dil.) showed similar trends with the fresh pure ZSM-5 zeolites, but to a smaller extent due to their reduced acidity. However, ZSM-5(dil.) was very selective toward phenolics, as it possesses enough acidity strength (also resulting from the amorphous silica-alumina matrix) to crack oxygenated dimers/oligomers, but not capable to induce further deep deoxygenation of phenolics and/or aromatization of light alkanes and furans towards aromatics. None of the rest of the conventional microporous zeolites, some of them having larger micropores compared to those of ZSM-5 and high number of Brønsted acid sites, favored the formation of monoaromatics. Monoaromatics are most probably formed with USY, Beta(12.5) and Beta(37.5) but are further converted to PAHs, due to their slightly larger micropores compared to those of ZSM-5. Acids and ketones are also reduced with these zeolites, while phenolics are kept at relatively high concentration. On the other hand, H-Y leads to low concentration of both monoaromatics and PAHs, lower acids and ketones and substantial increase of phenolics compared to noncatalytic pyrolysis. This relative distribution of products could be attributed to the high number of Brønsted acid sites of moderate strength and the relatively bigger micropores compared to the other zeolites. Mordenite had a minor effect on the composition of bio-oil, inducing all the above changes but to a small extent while Ferrierite exhibited a clear preference for the formation of phenolics (the highest concentration amongst all zeolites tested) with very low monoaromatics and PAHs.

The correlation of oxygen content of the organic phase of bio-oil with the yield of the organic phase is graphically depicted in Figure 5.7 for all zeolites tested and for the noncatalytic experiments. Interestingly, an almost linear correlation is revealed, which does not encounters for the various zeolites having different porous, acidic and catalytic properties in biomass pyrolysis, as shown above. Only one zeolite clearly deviated from this correlation: the zeolite ZSM-5 (40) that was one of the two (the other one being Beta(12.5)) most active zeolites in converting thermal bio-oil, and was also one of the two (the other one being ZSM-5(25)) most selective toward the formation of monoaromatics. Zeolite ZSM-5 (40) exhibited significant reduction of oxygen (to about 5 wt.%) but for organic phase yield of just 5–6 wt.%.

5.2.4.2 Catalytic fast pyrolysis (CFP) of biomass over amorphous mesoporous aluminosilicates

The results for this group of catalysts (2nd group of Table 5.2) are shown in Table 5.4 and in Figures 5.8 and 5.9. The mesoporous (alumino)silicate materials,

Table 5.4: Product yields for the catalytic pyrolysis of beech wood (wt.% on dry biomass) over amorphous mesoporous aluminosilicates.

	Bio-oil	Water	Organic fraction	Solids	Gases	CO_2	CO	CH_4	$C_{2=}$	$C_{3=}$	Total C_4–C_6
Silica sand	59.0	21.6	37.5	23.2	17.8	9.5	6.5	0.9	0.2	0.1	0.3
MCM-41	51.1	24.5	26.6	28.7	20.2	9.6	8.1	1.1	0.3	0.2	0.6
Al-MCM-41(20)	39.9	31.2	8.6	32.2	28.0	11.6	11.6	1.7	0.6	0.8	1.2
Al-MCM-41(50)	40.2	27.8	12.3	32.7	27.1	11.6	11.3	1.6	0.5	0.6	1.2
Al-MCM-41(50)-nano	38.5	32.1	6.4	32.6	28.8	12.1	12.0	1.8	0.6	0.7	1.2
SBA-15	53.0	25.3	27.7	27.8	19.2	9.0	7.9	1.1	0.3	0.2	0.5
Al-SBA-15(20)	40.6	29.6	11.0	33.3	26.1	10.9	11.0	1.6	0.5	0.6	1.1
MSU-J	50.5	23.7	26.8	26.8	22.9	10.6	9.4	1.3	0.3	0.3	0.6
Al-MSU-J(50)	39.8	29.0	10.8	34.4	25.8	11.1	11.0	1.4	0.5	0.6	0.9
γ-Al_2O_3	38.4	19.0	19.4	31.7	29.8	13.2	11.6	2.0	0.6	0.8	1.1
ASA	45.7	32.6	13.1	28.5	25.9	11.1	10.9	1.5	0.4	0.6	1.0

H_2 yields were <0.1 wt.%; ethane yields were ≤ 0.4 wt.% and propane yields were <0.1 wt.%; solids: unconverted biomass and char, plus reaction coke for the catalytic experiments.

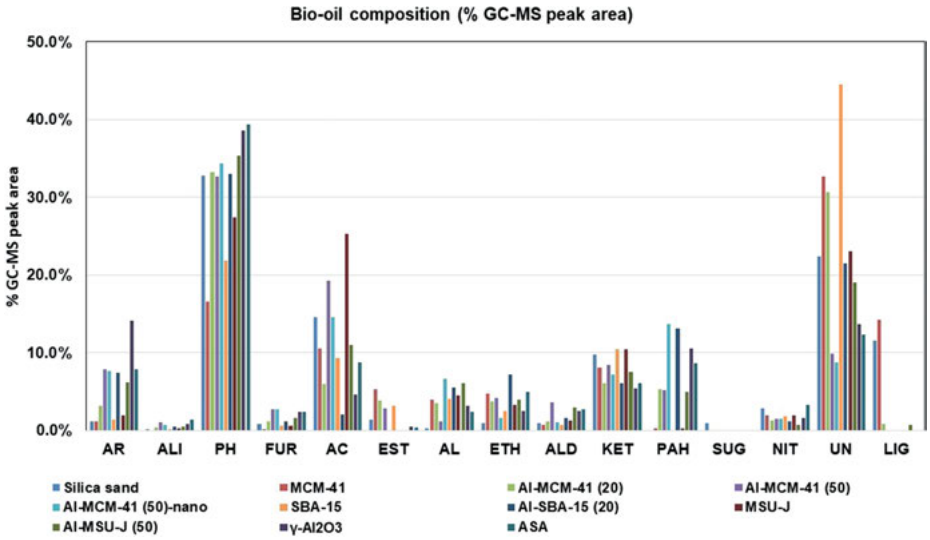

Figure 5.8: Composition analysis (% GC-MS peak area) of the bio-oil organic phase produced from the catalytic pyrolysis of beech wood over amorphous mesoporous aluminosilicates.

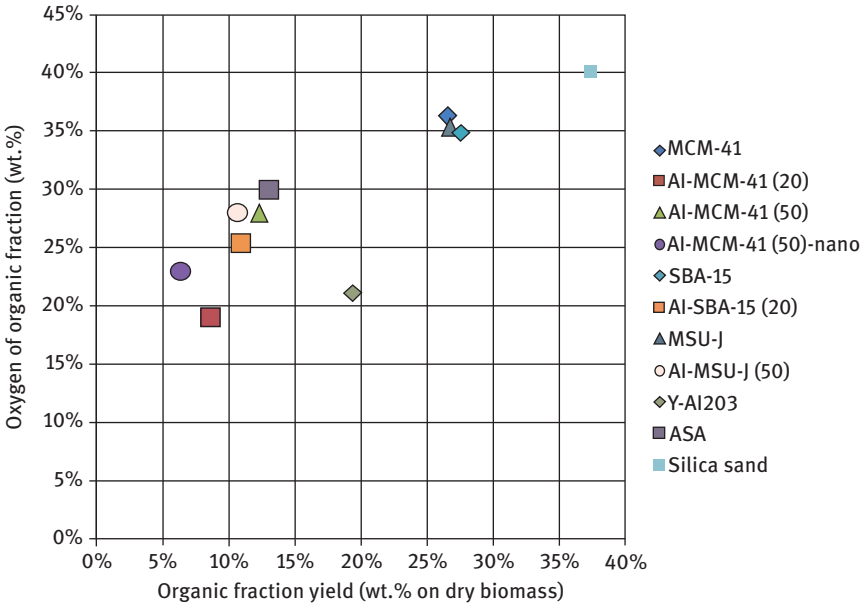

Figure 5.9: Oxygen content of the organic phase as a function of organic fraction yield over amorphous mesoporous aluminosilicates.

despite having fewer and weaker acid sites compared to zeolites, as well as of higher Lewis to Brønsted ratio, were capable of converting the organic phase of bio-oil with simultaneous increase of water, solids and gases (Table 5.4). Even the pure mesoporous silica (MCM-41, SBA-15, MSU-J) materials showed some activity, that is, organic phase yield was reduced by up to 30% compared to the noncatalytic experiment, due to the high surface area that enhanced thermal pyrolysis reactions and/or dehydration of intermediate pyrolysis products [68]; the possible reactivity of the surface hydroxyl groups of these silicas could also play a role. By introducing acidity to the mesoporous materials they became more active, with those containing more aluminum (i.e., having more acid sites) converting the organic phase to higher extent. The organic phase with Al-MCM-41(20) was as low as 8.6 wt.% (e.g., this value was 5.5 wt.% for the highly reactive ZSM-5(40) zeolite), while that for Al-MCM-41(50) being 12.3 wt.%. An additional increase of reactivity was provided by the small particles of Al-MCM-41(50)-nano, having both intraparticle mesoporosity and very high external area, leading to the lowest organic phase yield for the mesoporous materials tested of 6.4 wt.%. Comparing the different mesoporous structures of MCM-41 (small tubular mesopores in hexagonal arrangement), SBA-15 (larger tubular mesopores in hexagonal arrangement) and MSU-J (3D wormhole-like mesopores with sizes similar to SBA-15), no significant variation and effect could be identified on their reactivity for converting the

organic bio-oil to gases and coke. With regard to the solids (char and reaction coke) and gases, it can be seen that all mesoporous aluminosilicates favor the formation of coke instead of gases, similar to the highly reactive Beta(12.5) zeolite, and in contrast to the also highly reactive H-ZSM-5(40) zeolite. As far as the gas composition is concerned, the increase of CO is not as pronounced as with the zeolitic catalysts and CO_2 is in general slightly higher with the mesoporous materials, thus indicating a relative enhancement of the decarboxylation mechanism, still decarbonylation being the prominent one. Methane was produced to similar values as those for zeolites, but mesoporous materials were not selective toward light alkenes (i.e., ethylene and propylene), as these are typical intermediates/products of cracking reactions over zeolites with relatively strong acidity.

With regard to the composition of the organic phase of bio-oil (Figure 5.8), all the pure silica mesoporous materials were inactive toward monoaromatics and PAHs formation, as it was expected being nonacidic. On the other hand, all the mesoporous aluminosilicates produced some monoaromatics and PAHs, with the more selective toward monoaromatics being γ-Al_2O_3 (~14% of GC-MS chromatogram area). It is interesting to note that only the ZSM-5 zeolites (with Si/Al ratio of 25 and 40) were more selective toward monoaromatics (~33% of GC-MS chromatogram area), whereas all the rest of the zeolites exhibited similar or even lower selectivity toward these compounds compared to the mesoporous aluminosilicates. Acids and ketones were in general reduced by the mesoporous aluminosilicates (except some cases), while phenolics were at similar levels or increased with respect to the noncatalytic experiment, in accordance with previous works [68].

The oxygen content of the organic phase of the bio-oil is well correlated with the organic fraction yield for all the mesoporous materials tested (Figure 5.9), in accordance with the behavior of zeolitic catalysts, with the exception of γ-Al_2O_3 which deviated from the mean curve (almost linear) and resulted in more pronounced deoxygenation of bio-oil. This result can be also related with the unexpected (since it contains only Lewis acid sites) high selectivity of γ-Al_2O_3 toward monoaromatics.

5.2.4.3 Catalytic fast pyrolysis (CFP) of biomass over hierarchical zeolites

The results for the hierarchical micro/meso/macroporous zeolites (third group of Table 5.2) are shown in Table 5.5 and in Figures 5.10–5.13. The catalysts tested comprised of two mesoporous ZSM-5 zeolites with intracrystal mesopores with an average size of 2.2 nm and 5.2 nm, respectively, one nanosized crystalline ZSM-5 zeolite with high external area, and one partially crystalline (only 3% crystallinity) ZSM-5-based material also exhibiting relatively small particles and high external area. For comparison reasons, the highly active ZSM-5(40) zeolite was also included, but being evaluated at lower catalyst/biomass mass ratio (1/5) compared to the experiments presented in Section 5.2.4.1 (1/3). The catalyst/biomass ratio was kept relatively lower for all

Table 5.5: Product yields for the catalytic pyrolysis of beech wood (wt.% on dry biomass) over hybrid micro/mesoporous zeolite materials.

	Bio-oil	Water	Organic fraction	Solids	Gases	CO_2	CO	CH_4	$C_{2=}$	$C_{3=}$	Total C_4–C_6
Silica Sand	59.0	21.6	37.5	23.2	17.8	9.5	6.5	0.9	0.2	0.1	0.3
ZSM-5 (dil.)[(1)]	48.7	27.0	21.7	27.4	23.9	10.9	9.8	0.9	0.5	0.5	1.1
ZSM-5 (40)	50.3	27.1	23.2	25.0	24.7	10.9	10.4	0.9	0.9	0.6	0.5
MesoZSM-5(2.2)	45.3	31.4	13.9	26.6	28.1	11.3	12.4	1.1	0.9	0.9	1.2
MesoZSM-5(5.2)	42.8	30.8	12.0	28.6	28.6	11.6	12.9	1.2	0.8	0.8	1.0
ZSM-5 (nano)	42.9	29.4	13.5	28.9	28.2	11.2	12.7	1.1	0.9	0.9	1.1
ZSM-5 (3% cr.)	51.9	23.3	28.6	27.7	20.4	9.4	8.3	1.1	0.3	0.3	0.7

[(1)]The amount of catalysts tested was 0.3 g, except of ZSM-5(dil.) that was 0.5 g.H_2 yields were <0.1 wt.%; ethane yields were ~0.2 wt.% and propane yields were <0.1 wt.%; solids: unconverted biomass and char, plus reaction coke for the catalytic experiments.

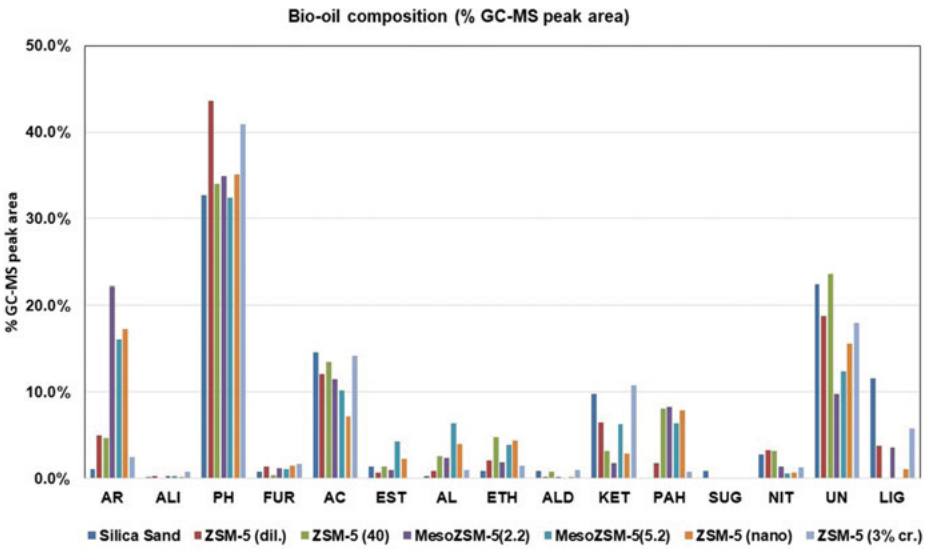

Figure 5.10: Composition analysis (% GC-MS peak area) of the bio-oil organic phase produced from the catalytic pyrolysis of beech wood over hybrid micro/mesoporous zeolite materials.

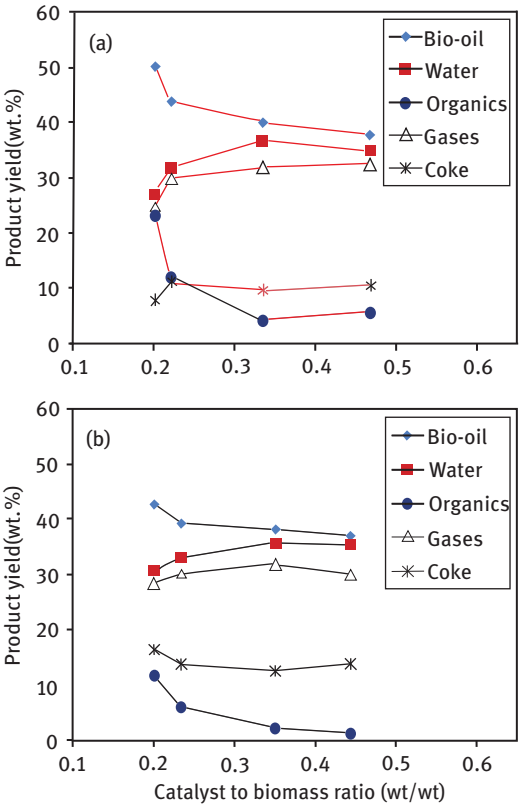

Figure 5.11: Effect of catalyst to biomass ratio on product yields for (a) conventional microporous ZSM-5(40) zeolite, and (b) MesoZSM-5(4.4) mesoporous zeolite with intracrystal mesopores of 4.4 nm average size.

catalysts in this set of experiments, in order to mediate the conversion of bio-oil and detect any possible effects of meso/macroporosity of the hierarchical ZSM-5 zeolites, taking into account the three hierarchical ZSM-5 zeolites and the conventional ZSM-5 (40) zeolite have similar acidic properties. Indeed, all three crystalline hierarchical ZSM-5 zeolites, the two mesoporous with intracrystal mesopores and the nanosized sample, exhibited significantly higher conversion of the organic phase of the bio-oil, compared to the conventional ZSM-5 zeolite (Table 5.5), that is, from 37.5 wt.% in the noncatalytic experiment to 23.2 wt.% with ZSM-5(40), 13.9 wt.% for MesoZSM-5(2.2), 12.0 wt.% for MesoZSM-5(5.2) and 13.5 wt.% for ZSM-5(nano). It appears that both the higher accessibility of the internal acid sites provided by the intracrystal mesopores as well as the higher abundance of external sites due to high external area can facilitate the conversion of dimer/oligomer intermediates in the biomass pyrolysis vapors, compared to the conventional microporous ZSM-5 zeolite. Water (in bio-oil), gases and solids (due to coke on catalyst) with the hierarchical zeolites follow the classical

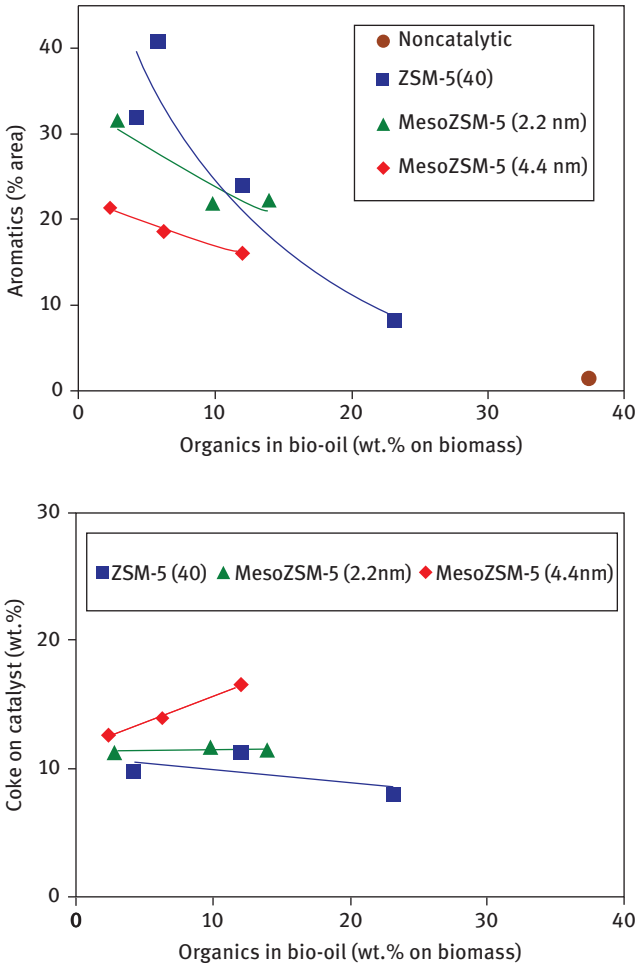

Figure 5.12: Correlation between monoaromatics and phenols relative concentration (% GC-MS peak area) and coke-on-catalyst (wt.%) with the yield of organic bio-oil.

increasing trend as for microporous ZSM-5 zeolites. However, a closer look at the data of Tables 5.3 and 5.5 reveals that the three hierarchical zeolites have a higher tendency to form coke compared to the conventional ZMS-5(40) zeolite. For example, even at pronounced conversion level of bio-oil (i.e., 5.5 wt.% organic phase) with ZSM-5(40), the solid products were only 26.5 wt.% (Table 5.3), while at moderate conversion of bio-oil (~ 12–14 wt.% organic phase) with the hierarchical zeolites, the solid products were much higher, that is, 26.6 – 28.9 wt.% (Table 5.5). The partially/low crystallinity ZSM-5-based sample exhibited limited reactivity in converting bio-oil, even lower than that of the diluted/equilibrium ZSM-5(dil.) catalyst, due to its very low acidity, despite its high external area.

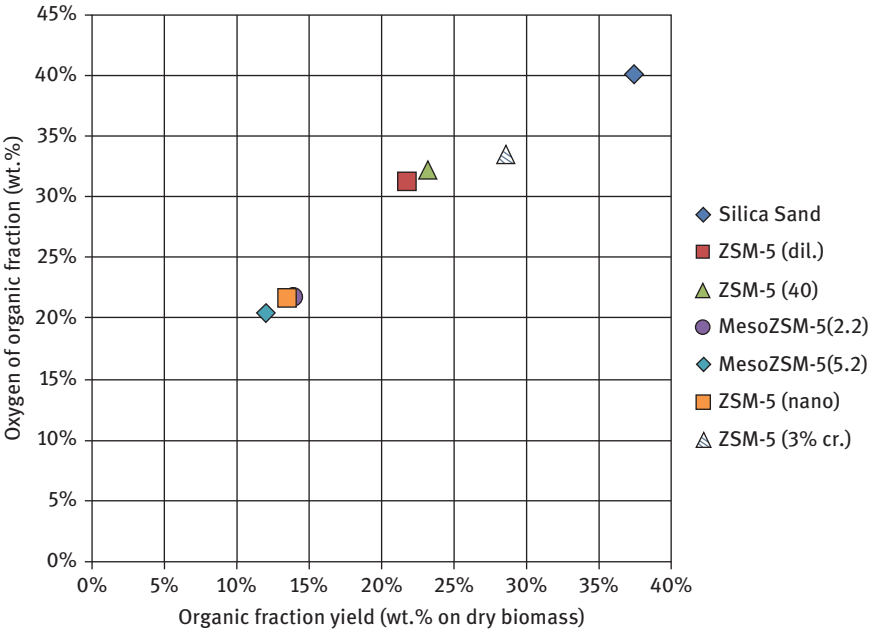

Figure 5.13: Oxygen content of the organic phase as a function of organic fraction yield over hierarchical and conventional microporous ZSM-5 zeolites.

With regard to gas composition, the hierarchical ZSM-5 zeolites led to a significant increase of CO, compared to the noncatalytic experiment, with minor increase of CO_2, similar to the behavior of the conventional ZSM-5(40) zeolite. On the other hand, they were not so selective toward light alkenes (ethylene and propylene) but favored C4–C6 production (compare data of Tables 5.3 and 5.5 for ZSM-5 zeolites, at similar yield of organic phase of bio-oil). The analysis of the organic phase of bio-oils showed that the three hierarchical zeolites induced higher formation of monoaromatics compared to ZSM-5(40). However, it should be noted that the degree of bio-oil deoxygenation/conversion is almost double with the former zeolites. At similar yields of organic bio-oil, that is, ~14 wt.% with ZSM-5(25), the concentration of monoaromatics for the conventional ZSM-5 zeolite was about 30%, compared to that of the hierarchical zeolites, for example, ~ 20% (compare data between Tables 5.3 and 5.5, and between Figures 5.6 and 5.10). Interestingly, PAHs were almost half (~10%) with the hierarchical zeolites, at similar bio-oil yield, possibly due to the enhanced condensation and polymerization reactions on these zeolites toward the formation of coke. The concentration of phenolics was not affected by hierarchical zeolites, while the highest selectivity to phenolics was provided by the two low acidity samples, that is, ZSM-5(dil.) and ZSM-5(3% cr.).

A better overview of the effect of catalyst/biomass ratio and degree of organic phase conversion on products yields and selectivity by the conventional microporous

ZSM-5(40) zeolite and two mesoporous ZSM-5 zeolites, with 2.2 nm and 4.4 nm intracrystal mesopores (similar sample to the one with 5.2 nm mesopores), can be seen in Figures 5.11 and 5.12. The trends in product yield changes with increasing cat/biomass ratio are similar for both ZSM-5(40) and the mesoporous ZSM-5(4.4), with a clear difference in the yield of coke-on-catalyst, which is by ca. 5 wt.% higher with the mesoporous zeolite (Figure 5.11). Furthermore, it can be seen (Figure 5.12) that the coke formation tendency for the mesoporous ZSM-5(2.2) zeolite, with the smaller mesopores, is similar (slightly higher) with that of the microporous ZSM-5(40) zeolite. An interesting observation is that the coke formation of MesoZSM-5(4.4) decreases as catalyst loading increases (i.e., at lower yields of organic bio-oil), indicating that a part of coke-on-catalyst at low conversion degrees could be attributed to sorbed/trapped biomass pyrolysis oligomers within the mesopores and not to reaction coke formed via aromarization and condensation reactions. As far as the selectivity toward monoaromatics is concerned, it can be seen that at moderate organic bio-oil yields it is similar for ZSM-5 (40) and MesoZSM-5(2.2) but increases in favor of the former zeolite at lower yields (Figure 5.12), that is, increased degrees of bio-oil conversion, due probably to their further condensation toward coke over the mesoporous zeolite. For this reason, MesoZSM-5(4.4) with the larger mesopores is less selective toward monoaromatics over the whole range of organic bio-oil yield.

Similar to all the conventional zeolites and most of the amorphous mesoporous aluminosilicates, the correlation of oxygen content of the organic phase of bio-oil with the yield of the organic phase for all the hierarchical zeolites, including the low acidity ones, is depicted by an almost linear curve (Figure 5.13).

5.3 Conclusions and outlook

The catalytic biomass FP results presented in this chapter, having derived from a systematic study of a wide range of conventional microporous zeolites, amorphous mesoporous aluminosilicates and hierarchical micro/meso/macroporous zeolites, under the same experimental conditions and reactor set up, verified the scattered data available in the literature and further provided new insight and understanding of the catalyst properties–performance relationships.

The microporous zeolites ZSM-5 and Beta were the most active in the in situ (i.e., single reactor, dual bed configuration) conversion of the organic fraction of bio-oil toward water (in the bio-oil), gases and coke, with a significant effect of their Si/Al ratio. However, due to the unique strong Brønsted acidity and tubular micropore structure of ZSM-5, this zeolite was very selective toward monoaromatics (i.e., benzene, toluene, xylene) in contrast to Beta zeolite that favored the formation of PAHs and coke on catalyst, possibly due to its slightly bigger micropores and/or the presence of higher relative amount of Lewis acid sites (their effect on condensation–polymerization reactions

of pyrolysis intermediates needs to be further investigated). A diluted/partially deactivated ZSM-5 zeolite catalyst with reduced acidity, which may representative of the equilibrium state of a continuous CFP process with alternating steps of pyrolysis and regeneration, exhibited very low aromatization capability but provided high selectivity to phenolics. The rest of the typical microporous zeolites, that is, H-Y, USY, Mordenite and Ferrierite, showed very low selectivity to monoaromatics and increased concentration of phenolics. All microporous zeolites induced a significant increase in the yields of CO compared to CO_2, thus verifying that their enhanced deoxygenation activity occurs mainly via decarbonylation (and dehydration due to the increased water fraction) instead of decarboxylation, which is the most preferred pathway. Zeolite ZSM-5 was also more selective toward the production of light alkenes (ethylene and propylene) compared to the rest of the zeolites, thus supporting the mechanism of cyclization, dehydrogenation and aromatization of small alkenes on ZMS-5 toward monoaromatics, in addition to other proposed pathways, that is, via Diels–Alder reactions between furans and alkenes.

Despite their weak acidity, being of Brønsted and Lewis type, all the amorphous-ordered mesoporous aluminosilicates studied (e.g., Al-MCM-41, Al-SBA-15, Al-MSU-J) exhibited remarkable activity for the conversion of organic bio-oil toward water, gases and coke, at similar catalyst-to-biomass ratio as with the strongly acidic zeolites. The highest reactivity was achieved by an Al-MCM-41 material, with very small particles (nanoparticles), which, in addition to the typical intraparticle mesoporosity, possesses high external area. Although they produced some monoaromatics, the mesoporous aluminosilicates were highly selective toward phenolics. With regard to gas composition, CO increase was not as pronounced as with zeolites, and light alkenes (i.e., ethylene and propylene) were also reduced, thus verifying that these two effects are associated with reaction pathways that are catalyzed only by strong zeolitic acidity.

It was clearly shown that hierarchical ZSM-5 zeolites, with relatively small intracrystal mesopores (2.2 – 5.2 nm) prepared by direct templated hydrothermal synthesis, as well as nanocrystalline ZSM-5 zeolite with high external area, were more reactive than the most active conventional microporous zeolite ZSM-5(40), when compared at relatively low catalyst-to-biomass ratio and moderate degrees of organic oil conversion. At these conditions, they were also much more selective toward monoaromatics, thus verifying the beneficial role of meso/macropores in ZSM-5. However, at increased degrees of organic bio-oil conversion, associated with higher catalyst to biomass ratios, the microporous ZSM-5(40) was more selective toward monoaromatics, as the hierarchical zeolites exhibited increased coke formation; this was especially true for the mesoporous ZSM-5 zeolite with the bigger mesopores and the nano-sized zeolite.

Based on the literature review and the systematic comparative data provided in this chapter, it is clear that biomass CFP with acidic micro/meso/macroporous materials can be effectively utilized for tuning the composition and properties of the bio-oil, depending on its targeted final use. It can range from a bio-oil enriched

with phenolics for use in relevant applications of polymers and resin production to a highly deoxygenated and aromatic bio-oil for further use as BTX chemicals source or as additive in aviation fuels. Alternatively, a mildly deoxygenated bio-oil by using the appropriate acidic catalyst can serve as a bio-crude for the downstream hydrodeoxygenation toward hydrocarbon fuels. However, in the case of high, almost complete deoxygenation, the yield of organic bio-oil is very low, not exceeding ca. 5–10 wt.% of the initial dry biomass. This is inevitable if one considers that a typical content of oxygen in lignocellulosic biomass is about 40–50 wt.% and that deoxygenation pathways only via dehydration (and not via decarbonylation and decarboxylation) seem difficult to occur. It was shown that an almost linear correlation exists between the oxygen content in the organic phase of bio-oil with the yield of organic bio-oil, for all different acidic catalysts tested, with the exception of the conventional microporous ZSM-5 zeolite with Si/Al of 40, which exhibited an enhanced deoxygenation activity compared to all the rest of the catalysts. With regard to the latest developments on using hierarchical zeolites, careful control of the intracrystal meso/macroporosity and the related acidity, that is, the acid sites located on the meso/macropores surface, is of paramount importance for increasing conversion of intermediate pyrolysis oligomers and production of monoaromatics and for suppressing polymerization reactions and coke formation.

References

[1] United Nations Framework Convention on Climate Change (UNFCCC), The Paris Agreement. UNFCCC, New York, 2015.
[2] IEA. Market Report Series: Renewables 2018. In: IEA Publications, 2018.
[3] IRENA. Innovation Outlook: Advanced Liquid Biofuels: International Renewable Energy Agency, 2016. Report No.: 978-92-95111-51-6.
[4] European Commission. Proposal for a DIRECTIVE OF THE EUROPEAN PARLIAMENT AND OF THE COUNCIL on the promotion of the use of energy from renewable sources (recast)., 2016.
[5] Iliopoulou EF, Triantafyllidis KS, Lappas AA. Overview of catalytic upgrading of biomass pyrolysis vapors toward the production of fuels and high-value chemicals. WIRES: Energ Environ 2019,8, e322.
[6] Kalogiannis KG, Stefanidis SD, Lappas AA. Catalyst deactivation, ash accumulation and bio-oil deoxygenation during ex situ catalytic fast pyrolysis of biomass in a cascade thermal-catalytic reactor system. Fuel Process Technol 2019, 186, 99–109.
[7] Stefanidis SD, Kalogiannis KG, Lappas AA. Co-processing bio-oil in the refinery for drop-in biofuels via fluid catalytic cracking. WIRES: Energ Environ 2018, 7, e281.
[8] Iliopoulou EF, Lazaridis PA, Triantafyllidis KS. Nanocatalysis in the Fast Pyrolysis of Lignocellulosic Biomass. In: Van de Voorde M, Sels B, eds. Nanotechnology in Catalysis – Applications in the Chemical Industry, Energy Development, and Environment Protection. Weinheim, Germany: Wiley-Blackwell, 2017, 655–713.
[9] Horne PA, Williams PT. Premium quality fuels and chemicals from the fluidised bed pyrolysis of biomass with zeolite catalyst upgrading. Renew Energ 1994,5, 810–812.

[10] Lappas AA, Samolada MC, Iatridis DK, Voutetakis SS. Biomass pyrolysis in a circulating fluid bed reactor for the production of fuels and chemicals. Fuel 2002, 81, 2087–2095.
[11] Atutxa A, Aguado R, Gayubo AG, Olazar M, Bilbao J. Kinetic description of the catalytic pyrolysis of biomass in a conical spouted bed reactor. Energ Fuel 2005, 19, 765–774.
[12] Zhang H, Xiao R, Huang H, Xiao G. Comparison of non-catalytic and catalytic fast pyrolysis of corncob in a fluidized bed reactor. Bioresour Technol 2009, 100, 1428–1434.
[13] Stefanidis SD, Kalogiannis KG, Iliopoulou EF, Lappas AA, Pilavachi PA. In-situ upgrading of biomass pyrolysis vapors: catalyst screening on a fixed bed reactor. Bioresour Technol 2011, 102, 8261–8267.
[14] Hernando H, Jiménez-Sánchez S, Fermoso J, Pizarro P, Coronado JM, Serrano DP. Assessing biomass catalytic pyrolysis in terms of deoxygenation pathways and energy yields for the efficient production of advanced biofuels. Catal Sci Technol 2016, 6, 2829–2843.
[15] Williams PT, Horne PA. Analysis of aromatic hydrocarbons in pyrolytic oil derived from biomass. J Anal Appl Pyrol 1995, 31, 15–37.
[16] Adjaye JD, Bakhshi NN. Production of hydrocarbons by catalytic upgrading of a fast pyrolysis bio-oil. Part I: Conversion over various catalysts. Fuel Process Technol 1995, 45, 161–183.
[17] Adjaye JD, Katikaneni SPR, Bakhshi NN. Catalytic conversion of a biofuel to hydrocarbons: Effect of mixtures of HZSM-5 and silica-alumina catalysts on product distribution. Fuel Process Technol 1996,48, 115–143.
[18] Pattiya A, Titiloye JO, Bridgwater AV. Fast pyrolysis of cassava rhizome in the presence of catalysts. J Anal Appl Pyrol 2008, 81, 72–79.
[19] Qiang L, XiFeng Z, WenZhi L, Ying Z, DengYu C. On-line catalytic upgrading of biomass fast pyrolysis products. Chinese Sci Bull 2009, 54, 1941–1948.
[20] Carlson TR, Tompsett GA, Conner WC, Huber GW. Aromatic production from catalytic fast pyrolysis of biomass-derived feedstocks. Top Catal 2009, 52, 241–252.
[21] Carlson TR, Vispute TP, Huber GW. Green Gasoline by Catalytic Fast Pyrolysis of Solid Biomass Derived Compounds. ChemSusChem 2008, 1, 397–400.
[22] Mihalcik DJ, Mullen CA, Boateng AA. Screening acidic zeolites for catalytic fast pyrolysis of biomass and its components. J Anal Appl Pyrol 2011, 92, 224–232.
[23] Zhang B, Zhong Z, Ding K, Cao Y, Liu Z. Catalytic Upgrading of Corn Stalk Fast Pyrolysis Vapors with Fresh and Hydrothermally Treated HZSM-5 Catalysts Using Py-GC/MS. Ind Eng Chem Res 2014, 53, 9979–9984.
[24] Kelkar S, Saffron CM, Andreassi K et al. A survey of catalysts for aromatics from fast pyrolysis of biomass. Appl Catal B-Environ 2015, 174–175, 85–95.
[25] Engtrakul C, Mukarakate C, Starace AK, Magrini KA, Rogers AK, Yung MM. Effect of ZSM-5 acidity on aromatic product selectivity during upgrading of pine pyrolysis vapors. Catal Today 2016, 269, 175–181.
[26] Jae J, Tompsett GA, Foster AJ et al. Investigation into the shape selectivity of zeolite catalysts for biomass conversion. J Catal 2011, 279, 257–268.
[27] Psarras AC, Michailof CM, Iliopoulou EF et al. Acetic acid conversion reactions on basic and acidic catalysts under biomass fast pyrolysis conditions. Mol Catal 2019, 465, 33–42.
[28] Stephanidis S, Nitsos C, Kalogiannis K, Iliopoulou EF, Lappas AA, Triantafyllidis KS. Catalytic upgrading of lignocellulosic biomass pyrolysis vapours: Effect of hydrothermal pre-treatment of biomass. Catal Today 2011, 167, 37–45.
[29] Foster AJ, Jae J, Cheng Y-t, Huber GW, Lobo RF. Optimizing the aromatic yield and distribution from catalytic fast pyrolysis of biomass over ZSM-5. Appl Catal A-Gen 2012, 423–424, 154–161.

[30] Mullen CA, Tarves PC, Raymundo LM, Schultz EL, Boateng AA, Trierweiler JO. Fluidized Bed Catalytic Pyrolysis of Eucalyptus over HZSM-5: Effect of Acid Density and Gallium Modification on Catalyst Deactivation. Energ Fuel 2018, 32, 1771–1778.
[31] Paasikallio V, Lindfors C, Lehto J, Oasmaa A, Reinikainen M. Short Vapour Residence Time Catalytic Pyrolysis of Spruce Sawdust in a Bubbling Fluidized-Bed Reactor with HZSM-5 Catalysts. Top Catal 2013, 56, 800–812.
[32] Du S, Gamliel DP, Giotto MV, Valla JA, Bollas GM. Coke formation of model compounds relevant to pyrolysis bio-oil over ZSM-5. Appl Catal A: Gen 2016, 513, 67–81.
[33] Stefanidis SD, Kalogiannis KG, Pilavachi PA, Fougret CM, Jordan E, Lappas AA. Catalyst hydrothermal deactivation and metal contamination during the in situ catalytic pyrolysis of biomass. Catal Sci Technol 2016, 6, 2807–2819.
[34] Iliopoulou EF, Stefanidis S, Kalogiannis K et al. Pilot-scale validation of Co-ZSM-5 catalyst performance in the catalytic upgrading of biomass pyrolysis vapours. Green Chem 2014, 16, 662–674.
[35] Mullen CA, Tarves PC, Boateng AA. Role of potassium exchange in catalytic pyrolysis of biomass over ZSM-5: Formation of alkyl phenols and furans. ACS Sustain Chem Eng 2017, 5, 2154–2162.
[36] Adam J, Blazsó M, Mészáros E et al. Pyrolysis of biomass in the presence of Al-MCM-41 type catalysts. Fuel 2005, 84, 1494–1502.
[37] Aho A, Kumar N, Lashkul AV et al. Catalytic upgrading of woody biomass derived pyrolysis vapours over iron modified zeolites in a dual-fluidized bed reactor. Fuel 2010, 89, 1992–2000.
[38] Antonakou E, Lappas A, Nilsen MH, Bouzga A, Stocker M. Evaluation of various types of Al-MCM-41 materials as catalysts in biomass pyrolysis for the production of bio-fuels and chemicals. Fuel 2006, 85, 2202–2212.
[39] Qiang L, Wen-zhi L, Dong Z, Xi-feng Z. Analytical pyrolysis–gas chromatography/mass spectrometry (Py–GC/MS) of sawdust with Al/SBA-15 catalysts. J Anal Appl Pyrol 2009, 84, 131–138.
[40] Wang D, Xiao R, Zhang H, He G. Comparison of catalytic pyrolysis of biomass with MCM-41 and CaO catalysts by using TGA-FTIR analysis. J Anal Appl Pyrol 2010, 89, 171–177.
[41] Nilsen MH, Antonakou E, Bouzga A, Lappas A, Mathisen K, Stocker M. Investigation of the effect of metal sites in Me-Al-MCM-41 (Me = Fe, Cu or Zn) on the catalytic behavior during the pyrolysis of wooden based biomass. Micropor Mesopor Mat 2007, 105, 189–203.
[42] Jackson MA, Compton DL, Boateng AA. Screening heterogeneous catalysts for the pyrolysis of lignin. J Anal Appl Pyrol 2009, 85, 226–230.
[43] Khan W, Jia X, Wu Z, Choi J, Yip ACK. Incorporating Hierarchy into Conventional Zeolites for Catalytic Biomass Conversions: A Review. Catalysts 2019, 9, 127.
[44] Park HJ, Heo HS, Jeon J-K et al. Highly valuable chemicals production from catalytic upgrading of radiata pine sawdust-derived pyrolytic vapors over mesoporous MFI zeolites. Appl Catal B-Environ 2010, 95, 365–373.
[45] Shetti VN, Kim J, Srivastava R, Choi M, Ryoo R. Assessment of the mesopore wall catalytic activities of MFI zeolite with mesoporous/microporous hierarchical structures. J Catal 2008, 254, 296–303.
[46] Park K-H, Park HJ, Kim J et al. Application of hierarchical MFI zeolite for the catalytic pyrolysis of Japanese Larch. J Nanosci Nanotechno 2010, 10, 355–359.
[47] Park HJ, Park K-H, Jeon J-K et al. Production of phenolics and aromatics by pyrolysis of miscanthus. Fuel 2012, 97, 379–384.
[48] Neumann GT, Hicks JC. Novel Hierarchical Cerium-Incorporated MFI Zeolite Catalysts for the Catalytic Fast Pyrolysis of Lignocellulosic Biomass. ACS Catal 2012, 2, 642–646.

[49] Zhu X, Lobban LL, Mallinson RG, Resasco DE. Tailoring the mesopore structure of HZSM-5 to control product distribution in the conversion of propanal. J Catal 2010, 271, 88–98.
[50] Stefanidis S, Kalogiannis K, Iliopoulou EF et al. Mesopore-modified mordenites as catalysts for catalytic pyrolysis of biomass and cracking of vacuum gasoil processes. Green Chem 2013, 15, 1647–1658.
[51] Li J, Li X, Zhou G et al. Catalytic fast pyrolysis of biomass with mesoporous ZSM-5 zeolites prepared by desilication with NaOH solutions. Appl Catal A-Gen 2014, 470, 115–122.
[52] Puértolas B, Veses A, Callén MS, Mitchell S, García T, Pérez-Ramírez J. Porosity-Acidity Interplay in Hierarchical ZSM-5 Zeolites for Pyrolysis Oil Valorization to Aromatics. ChemSusChem 2015, 8, 3283–3293.
[53] Gamliel DP, Cho HJ, Fan W, Valla JA. On the effectiveness of tailored mesoporous MFI zeolites for biomass catalytic fast pyrolysis. Appl Catal A-Gen 2016, 522, 109–119.
[54] Jia LY, Raad M, Hamieh S et al. Catalytic fast pyrolysis of biomass: superior selectivity of hierarchical zeolites to aromatics. Green Chem 2017, 19, 5442–5459.
[55] Hernando H, Hernández-Giménez AM, Ochoa-Hernández C et al. Engineering the acidity and accessibility of the zeolite ZSM-5 for efficient bio-oil upgrading in catalytic pyrolysis of lignocellulose. Green Chem 2018, 20, 3499–3511.
[56] Kelkar S, Saffron CM, Li Z et al. Aromatics from biomass pyrolysis vapour using a bifunctional mesoporous catalyst. Green Chem 2014, 16, 803–812.
[57] Hernando H, Moreno I, Fermoso J et al. Biomass catalytic fast pyrolysis over hierarchical ZSM-5 and Beta zeolites modified with Mg and Zn oxides. Biomass Convers Bior 2017, 7, 289–304.
[58] Veses A, Puértolas B, López JM, Callén MS, Solsona B, García T. Promoting Deoxygenation of Bio-Oil by Metal-Loaded Hierarchical ZSM-5 Zeolites. ACS Sustain Chem Eng 2016, 4, 1653–1660.
[59] Fermoso J, Hernando H, Jana P et al. Lamellar and pillared ZSM-5 zeolites modified with MgO and ZnO for catalytic fast-pyrolysis of eucalyptus woodchips. Catal Today 2016, 277, 171–181.
[60] Kalogiannis KG, Stefanidis SD, Karakoulia SA et al. First pilot scale study of basic vs acidic catalysts in biomass pyrolysis: Deoxygenation mechanisms and catalyst deactivation. Appl Catal B: Environ 2018, 238, 346–357.
[61] Stefanidis SD, Karakoulia SA, Kalogiannis KG et al. Natural magnesium oxide (MgO) catalysts: A cost-effective sustainable alternative to acid zeolites for the in situ upgrading of biomass fast pyrolysis oil. Appl Catal B: Environ 2016, 196, 155–173.
[62] Lazaridis PA, Fotopoulos AP, Karakoulia SA, Triantafyllidis KS. Catalytic fast pyrolysis of Kraft lignin with conventional, mesoporous and nanosized ZSM-5 zeolite for the production of alkyl-phenols and aromatics. Front Chem 2018;6.
[63] Custodis VBF, Karakoulia SA, Triantafyllidis KS, van Bokhoven JA. Catalytic fast pyrolysis of lignin over high-surface-area mesoporous aluminosilicates: Effect of porosity and acidity. ChemSusChem 2016, 9, 1134–1145.
[64] Lappas AA, Kalogiannis KG, Iliopoulou EF, Triantafyllidis KS, Stefanidis SD. Catalytic pyrolysis of biomass for transportation fuels. WIRES: Energ Environ 2012, 1, 285–297.
[65] Komvokis VG, Karakoulia S, Iliopoulou EF et al. Upgrading of Fischer–Tropsch synthesis bio-waxes via catalytic cracking: Effect of acidity, porosity and metal modification of zeolitic and mesoporous aluminosilicate catalysts. Catal Today 2012, 196, 42–55.
[66] Iliopoulou EF, Stefanidis SD, Kalogiannis KG, Delimitis A, Lappas AA, Triantafyllidis KS. Catalytic upgrading of biomass pyrolysis vapors using transition metal-modified ZSM-5 zeolite. Appl Catal B: Environ 2012, 127, 281–290.
[67] Park DH, Kim SS, Wang H et al. Selective petroleum refining over a zeolite catalyst with small intracrystal mesopores. Angew Chem Int Ed 2009, 48, 7645–7648.

[68] Iliopoulou EF, Antonakou EV, Karakoulia SA, Vasalos IA, Lappas AA, Triantafyllidis KS. Catalytic conversion of biomass pyrolysis products by mesoporous materials: Effect of steam stability and acidity of Al-MCM-41 catalysts. Chem Eng J 2007, 134, 51–57.
[69] Karakoulia SA, Triantafyllidis KS, Tsilomelekis G, Boghosian S, Lemonidou AA. Propane oxidative dehydrogenation over vanadia catalysts supported on mesoporous silicas with varying pore structure and size. Cataly Today 2009, 141, 245–253.
[70] Triantafillidis CS, Vlessidis AG, Nalbandian L, Evmiridis NP. Effect of the degree and type of the dealumination method on the structural, compositional and acidic characteristics of H-ZSM-5 zeolites. Micropor Mesopor Mat 2001, 47, 369–388.

Francisco Ivars-Barceló, Esther Asedegbega-Nieto,
Elena Rodríguez Aguado, Juan Antonio Cecilia,
Antonia Infantes Molina, Enrique Rodríguez-Castellón*

6 Advances in the application of transition metal phosphide catalysts for hydrodeoxygenation reactions of bio-oil from biomass pyrolysis

6.1 Introduction

Transition metal phosphides (TMPs) have a broad range of technological applications [1, 2], partly due to the wide variety of structures and physicochemical properties accessible by combining phosphorus and a transition metal with different stoichiometries. They are represented by the general formula M_xP_y and their compositions extend from phosphorus-rich ($x < y$) to metal-rich ($x > y$) phosphides [1–11].

The ability of phosphorus to form homonuclear bonds as polyphosphide networks (only exceeded by carbon) offers infinite synthetical and structural possibilities for phosphorus-rich TMPs [5, 6, 12], specially characterized by their properties as semiconductors with small band gap [2]. However, the high reactivity of polyphosphides gives rise to low thermal and chemical stabilities, limiting the scope of their applications, the most common of which is anode materials for Li-ion batteries [1]. On the contrary, TMPs with high metal/phosphorus ratios (≥1) possess a pronounced metal–metal bonding, which provides them with intermediate properties between oxides and metals [8]. Thus, they offer high chemical, thermal and mechanical stabilities, as well as good heat and electrical conductivity [1, 2]. These properties make them potentially suitable as solid catalysts [7–9], among other applications such as coatings for corrosion or oxidation resistance and waterproof materials [13, 14]. With respect to catalysis applications, transition metal-rich phosphides have been found especially active in reactions involving the transference of hydrogen [3, 8, 9], which along with their relatively high tolerance to sulfur and nitrogen convert these materials to unique hydrotreating catalysts [8, 9].

As part of hydroprocessing technology for oil refining, catalytic hydrotreating processes, such as hydrogenation and hydrogenolysis reactions, use hydrogen to remove unsaturated species and heteroatoms from oil components, respectively.

Hydrodesulfurization (HDS) and hydrodenitrogenation (HDN) are the main hydrogenolysis reactions to remove sulfur and nitrogen, respectively. These are employed for crude-derived oils that are additionally upgraded with hydrogenation reactions to reduce the content in aromatic compounds, the latter ones responsible for CO_2 emissions.

https://doi.org/10.1515/9783110538151-006

Increasingly demanding restrictions in SO_x, NO_x and CO_2 emissions from fuel combustion, along with the progressively decreasing quality of fossil fuels as a consequence of their depletion, are the most encouraging reasons behind seeking enhanced catalytic behaviors for these hydroprocessing reactions. One of the main drawbacks is the deactivation of conventional catalysts induced by sulfur species contained in the crude oils. Furthermore, for the specific case of HDS, the presence of nitrogen compounds, as well as the main reaction product H_2S itself, induces reaction inhibition [7, 15]. In this sense, TMPs are found to be especially convenient as they are active and stable under HDS conditions [7, 16].

On the other hand, hydrodeoxygenation (HDO) to remove oxygen content is the most required hydroprocessing treatment to upgrade biomass-derived oils (bio-oils), where the sulfur and nitrogen contents are negligible but the presence of oxygen-containing compounds is considerably high (20–50 wt%) [17]. Bio-oil, also named as biocrude or pyrolysis oil, is obtained by thermal biomass decomposition in the absence of oxygen [18]. This process is called pyrolysis and is considered the most promising thermochemical method for direct liquefaction of biomass to produce liquid biofuels [19, 20]. Production of biofuels from biomass has attracted a special attention from both industrial and research sectors over the last decades, among the number of alternative energy sources approached as a response to the prospective threat of fossil fuels shortage. The origin of fossil fuels, derived from organic material transformed by both biological and geological processes, is responsible for their exhaustible finite nature which makes them unable to fulfill in perpetuity the increasing world energy demand. Moreover, combustion processes of fossil fuels bring about pollution and unsustainable development, producing nowadays the majority of CO_2 emissions in the Earth's atmosphere, which is responsible for global warming. On the contrary, biofuels are energy-enriched chemicals derived from organic materials exclusively obtained from biological processes. Hence, energy production by combustion of biofuels from plant-derived biomass is considered to be carbon neutral, since the CO_2 released is equivalent to that captured by photosynthesis during the lifetime of the plant at issue. Indeed, most of biomass energy actually originates from solar energy which is absorbed by plants to capture and transform CO_2 into organic matter, being the only renewable energy source that is naturally and effectively stored. Accordingly, the biofuel nature is inherent to their unique characteristics such as renewable energy source, biodegradable, low toxicity, diversity and with a location availability easy to control (unlike the fossil fuels linkage to geopolitical instability), which can be potentially time bound unlimited with the appropriate management [21–23]. Nevertheless, removing the high oxygen content in bio-oils is essential to produce high-quality hydrocarbon fuels, since the presence of oxygen-containing compounds provides nonvolatility, corrosiveness, chemical and thermal instabilities, and a strong tendency to repolymerize under air exposure [24].

In view of the exposed background, the aim of this chapter is to offer a comprehensive vision of the HDO reaction and representative catalytic systems addressed

to upgrade bio-oils toward the biofuel status, with an emphasis on the most relevant advances and insights obtained by employing ultimate transition metal-rich phosphide catalysts.

6.2 Hydrodeoxygenation of bio-oils

In general, HDO is a hydrotreating process to remove oxygen, as a heteroatom contained in organic compounds, by hydrogenolysis [25]. The reaction consists in the cleavage of the bonds between the oxygen and the rest of the molecule by means of molecular hydrogen, giving rise to the elimination of the oxygen heteroatom in the form of water and the organic leftover reduced with hydrogen. Deoxygenation and hydrogenation reactions might take place in separated steps, although the process might be simplified in one-step reaction, as follows:

$$R_2O + 2H_2 \rightarrow H_2O + 2RH \tag{6.1}$$

Considering the nature of this process, HDO appears to be very convenient for the production of biofuels. This is not only in terms of obtaining low oxygen content mixtures of hydrocarbons, but also to reduce the amount of aromatic compounds.

Biofuels compatible with existing transportation fuels and thereby with current combustion engines are the final aim of using biomass as a renewable energy resource. However, biomass consists of oxygen-rich compounds such as sugars or lipids, among others. Consequently, the thermal decomposition of those precursors in the absence of oxygen (pyrolysis) results in a mixture of oxygenated aromatic and aliphatic compounds forming the corresponding derived bio-oil [26–28]. Although removal of oxygen and aromaticity is essential to obtain suitable biofuels, the complex composition of bio-oils makes their upgrading a challenge not only restricted to HDO reactions. Indeed, HDO is just one from a set of catalytic methods employed as a part of the upgrading process, including physical and other chemical methods [26]. Those methods will not be discussed here. Notwithstanding, the concept gives a clearer idea of bio-oil complexity which helps to explain that most of the HDO studies use model compounds contained in bio-oils, rather than actual pyrolysis of oil samples at lab scale [29, 30]. Phenol, guaiacol, anisole, 2-methyltetrahydrofuran (2-MTHF) and dibenzofuran (DBF) are the bio-oil model molecules mostly employed in HDO studies of TMPs (Figure 6.1).

The purpose consists in simplifying the system to allow better understanding of HDO reaction networks and mechanisms, needed for the rational design of HDO catalysts with predefined and enhanced catalytic behavior [31].

Model molecules for HDO studies are mostly selected as a representative for the main active compounds responsible for the bio-oil instability. Aromatic compounds have high energy density and represent almost about the 30% of bio-oil composition.

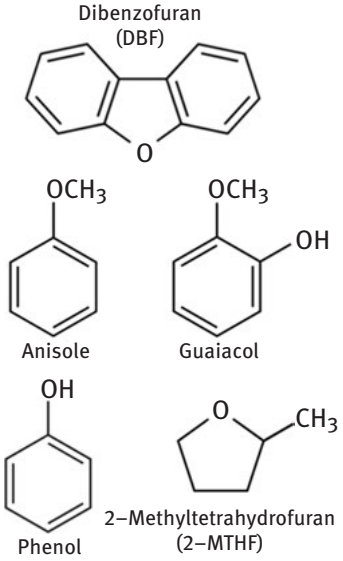

Figure 6.1: Chemical structure of the most studied bio-oil model molecules.

From these, phenolic compounds are considered as the primary cause for the catalyst deactivation by coke formation. Thus, phenol, anisole and guaiacol are the most studied model molecules as a representative of aromatic monomers with simple structure, methoxyl group or two kinds of C–O groups (hydroxyl and methoxyl), respectively. On the other hand, phenolic dimers are especially selected as model aromatic dimers to investigate the cleavage of typical linkages in pyrolytic lignin, which accounts 25–30 wt% of bio-oil as a water-insoluble fraction responsible for viscosity in addition to instability [26, 32]. Finally, furans, carboxylic acids, alcohols and carbohydrates are also among the classes of model compounds selected as common products in biomass pyrolysis [26].

6.3 Conventional catalysts for HDO

The nature of HDO is shared by HDS and HDN, all three hydrogenolysis reactions to remove oxygen, sulfur and nitrogen heteroatoms, respectively, from organic compounds. These reactions are part of the catalytic hydrotreating process conventionally used for crude oil refining. However, due to the meaningless oxygen content in fossil-derived oils compared with that of sulfur and nitrogen, HDS and HDN have been by far much more studied than HDO during the fossil fuels pioneer age. Later, when the interest in bio-oils started up, accompanied by the need for reducing their oxygen content, HDO began to get relevance.

It is coherent that conventional hydrotreating catalysts for crude oil refining, mostly studied in HDS and HDN reactions, were the first ones to be investigated for HDO upgrading of bio-oils derived from biomass pyrolysis. Among these catalysts, transition metal sulfide systems have been the most effective in petroleum refining and the first ones employed in upgrading pyrolysis of bio-oil [15, 29, 33]. Actually, phenol, guaiacol, 2,3-dihydrobenzofuran or anisole are among the main model molecules that have been used for HDO studies on sulfide systems [26] (Figure 6.1). Especially relevant are supported sulfide nickel–molybdenum or cobalt–molybdenum catalysts, using Mo as an active component, and Co or Ni as a promoter [33–36]. In the case of Ni, the maximum synergy was observed at a Ni/(Mo + Ni) molar ratio of 0.3 [33].

With respect to the support, γ-Al_2O_3 was initially investigated, although studies using CoMo sulfides supported on mesoporous silicates showed comparatively a much higher catalytic activity [36]. Indeed, the catalytic performance of transition metal sulfides was found to be strongly influenced by the support morphology, among other properties. For CoMo sulfides, the most effective catalytic behavior was displayed on the cubic mesoporous silica support SBA-16 [36]. Beyond CoMo and NiMo systems, a number of sulfide catalysts suitable for the HDO of biomass-derived oils have been investigated so far, most of which are discussed in a recent review by Pawelec and Garcia Fierro [37]. In general, it is important to point out that transition metal sulfide catalysts experience sulfur leaching during the HDO reaction, causing severe carbon deposition on the catalyst surface. This fact, together with the negligible content of sulfur in bio-oil, demands the addition of a sulfur source like H_2S to the feed stream in order to keep the sulfide form and so the catalytic activity. Nevertheless, prevention of coke deposition is still a challenge limiting the use of these catalysts for HDO of bio-oils.

Nanostructured noble metals, such as Pt, Pd, Rh and Ru, represent another catalytic system exhibiting, in general, high activity for hydrotreating pyrolysis oil by HDO reactions [26, 38–43]. In particular Pt, Pd and Rh supported on zirconia have been reported to present catalytic activities higher than conventional CoMo sulfides supported on alumina [38], with the least carbon deposition observed for Rh, and the highest activity achieved with Pd.

In general, regardless of the support, it is also important to highlight the capacity of Pt on oxygen removal from pyrolysis oil, which is found to be more effective than NiMo and CoMo sulfide catalysts under the same HDO conditions [26].

Beyond the pure metal, synergy effects have been reported in HDO reactions by modifying the noble metal with phases of different nature. As a case in point, TiO_2 was found to suppress the sintering of Pd nanoparticles supported on SiO_2, as well as to improve the deoxygenation activity for HDO of guaiacol as a model bio-oil molecule [42]. Moreover, enhancement of H-spillover processes during HDO reactions on the surface of Pd-based catalysts has been described by using solid acid supports consisting of a mixture of alumina and the acid form of zeolite Y (HY) [43]. At this

point, it must be reminded that HY is the classic example of a solid acid extensively used as a catalyst in the crude oil industry since 1970 [44, 45]. In the same vein, enhanced HDO performance has been obtained using bifunctional catalysts combining Pt and the acid form of Zeolite Beta (H-Beta) as an active support [39, 40].

On the other hand, nanostructured metallic systems based on a nonnoble transition metal also present appropriate catalytic properties for upgrading bio-oil by HDO hydrotreating reaction [18, 46–49]. Among the nonnoble transition metals investigated, Ni has proved by far to provide the best catalytic performance, which has been demonstrated to be radically affected by the nature and properties of the support, as similarly observed for noble metals. In that sense, oxides appear as the most adequate supports for metal Ni catalysts used in HDO of bio-oil model molecules [18, 46, 47]. Especially good performance for HDO of phenol has been reported on Ni using ZrO_2 as a support. Comparatively, meaningless activity was obtained with Ni supported on amorphous carbon (AC) at similar conditions [46]. However, a negative effect of carbonaceous supports on the HDO catalytic performance of Ni cannot be generalized, since up to 100% conversion of a different model molecule (guaiacol) has been reported using Ni supported on carbon nanotubes [49].

The oxide form of Ni has also been studied for HDO purposes [50]. In fact, oxides, carbides and nitrides of transition metals, in general, have been investigated as HDO catalysts, as well as phosphides that represent the main purpose of this chapter and will be discussed next in a separated section.

Despite Ni oxides, Mo oxides have also been significantly assessed for HDO purposes, alone or combined with other oxides [50, 51].

It is important to highlight the capability of transition metal carbides to exceed the catalytic activity of Pt-group metals (PGMs) for hydrogenation and dehydrogenation reactions [52]. Especially relevant are Mo and W carbides, which have been the most studied for HDO reactions [17, 53]. Carbon from the carbide seems to induce an enhancement in the surface reactivity of the transition metal, which at least in the case of W and Mo has been reported to approach that displayed by PGMs [54]. Indeed, high conversion values have been reported for HDO of model bio-oil molecules using W and Mo carbides [55–57]. However, formation of oxygenate species on the catalyst surface has been claimed to substantially prevent hydrogenation, leading to high selectivity toward aromatic compounds instead of forming the most convenient saturated hydrocarbons. In that sense, W shows stronger oxygen affinity and thus forms a stronger W–O bond when compared with Mo [57].

Regarding the interest in the nitrides of transition metals, it arises from their bifunctionality created by the coexistence of acid and basic sites as a result of the significant difference in the electronegativity between the nitrogen and the metal. Although nitrides are scarcely studied, some interesting results, especially on Mo nitride catalysts, can be found [58, 59].

6.4 Transition metal phosphides for HDO

The product selectivity obtained with transition metal-rich phosphides in HDO reactions resembles that of conventional sulfidic catalysts. In fact, transition metal-rich phosphides have structural aspects and properties in common with sulfide forms, as well as with carbides and nitrides [15, 26, 60]. However, the phosphide catalysts generally exhibit a catalytic activity higher than that found for equivalent HDO reactions using transition metal sulfides, carbides or nitrides as catalysts. Beyond the similarities shared by those transition metal-based compounds, the phosphide systems have structural singularities, which bestow them unique catalytic reactivity among other properties. On the one hand, unlike what happens in carbide and nitride structures, the comparatively larger size of the phosphorus atom does not allow an octahedral structure for the coordination of six metal atoms around itself, but rather a trigonal prismatic coordination instead (Figure 6.2). The latter structure favors more isolation for the nonmetallic atom, which results in poor P–P interactions into a lattice where metal–metal lengths are found within metallic and covalent bond ranges. Thus, metal-rich TMPs are majorly governed by the arrangement of metal atoms, which can reach up to nine metal ligands around the phosphorus in a tricapped trigonal prismatic coordination (Figure 6.2).

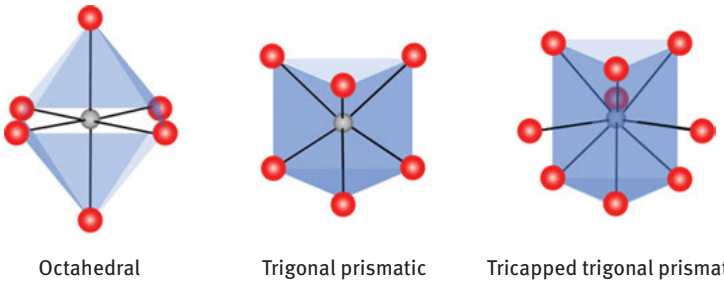

Figure 6.2: Three-dimensional representation of octahedral and trigonal prismatic geometries of sixfold coordination, and tricapped trigonal prismatic of ninefold coordination.

Metal–metal interactions gain increasingly relevance as the metal/phosphorus ratio increases in the global lattice, leading to higher electron delocalization in the metal sublattice of the phosphide. On the other hand, similar trigonal prismatic coordination is displayed as well by transition metal sulfides. Nevertheless, the triangular prism units are arranged forming layers in sulfides, while in phosphides those building blocks can grow in all directions forming three-dimensional structures (Figure 6.3).

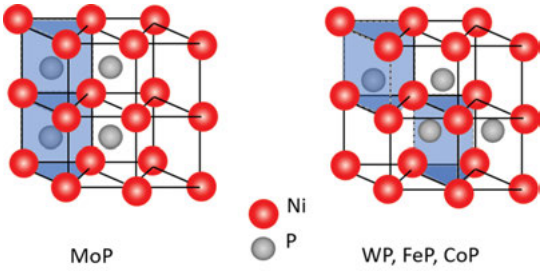

Figure 6.3: Three-dimensional representations of general structures for TMP phases with a phosphorus:metal stoichiometry of 1:1, displaying different trigonal prism arrangements.

The versatile arrangement of triangular prism building blocks results in different structures of TMPs with a large variety of metal–metal bonds. The surface exposure of metal atoms is especially favored on TMP structures, as active corner and edge sites, which allows greater access for the fluid phase reactants of the catalytic reaction compared to other catalyst structures.

6.4.1 Nickel phosphide catalysts for HDO

In general, nickel phosphide catalysts, especially those based on Ni_2P, have been reported to be the monometallic TMP system presenting the best catalytic activities and stability for HDO reactions in the valorization of lignocellulosic biomass [61, 62] and the synthesis of green diesel [63–65]. The Ni_2P system appears as the least affected by changes in H_2/feed ratio for HDO reactions compared to other TMPs under equivalent reaction conditions [61]. These aspects have encouraged the major number of investigations on the application of TMPs in HDO reactions to focus in Ni_2P phase.

As already justifiably discussed, most of the HDO studies use model samples consisting of only one type of bio-oil representative O-containing molecule. Nevertheless, the effectivity for oxygen content reduction of actual bio-oil samples over Ni_2P-based catalysts has also been assessed [66–68]. In this respect, reductions of oxygen content to about half compared to the original levels in pyrolysis bio-oil samples have been reported using Ni_2P catalysts, with catalytic activities, at moderate temperatures (300–350 °C) under atmospheric H_2 pressure, exceeding those of nanostructured metal-based catalysts such as Ni/SiO_2 or Pd/C, and other commercial catalysts for fluid catalytic cracking [68]. In that sense, the presence of phosphorus in Ni–P catalysts has been confirmed to enhance the deoxygenation activity over the cracking activity, the latter leading to lighter hydrocarbons. Cracking activity is practically suppressed on Ni_2P, while comparatively favored

in nanostructured Ni metal catalysts [68, 69]. Beyond HDO and hydrogenation reactions, decarbonylation and hydrolysis have also been experimentally confirmed to occur during bio-oil upgrading employing Ni_2P-based catalysts [68].

Furthermore, the superior catalytic behavior of Ni_2P phase has been related to the intrinsic greater presence of P–OH species that is suggested to prevent metal phase oxidation, in turn acting as Brønsted acid sites that can easily react with O-containing species. Moreover, P–OH surface species can also act as H-donors to carry out hydrogenation reactions [3, 8, 9], while spillover species would be responsible for cleaning the surface of carbon deposits avoiding deactivation. Anyway, slight deactivation gradually increasing with reaction time has been observed by coke formation on the surface of SiO_2-supported Ni_2P catalysts for HDO of real bio-oil streams [68].

In the same vein, greater amount of surface H-active species was found to be responsible for the enhanced stability of bimetallic $Ni_{1.8}M_{0.2}P$-based catalysts promoted with noble metals (M = Rh, Ru or Ir) and their catalytic activity in HDO reactions [70]. HDO conversions of DBF obtained at 300 °C and 30 bar of H_2 pressure are comparatively displayed in Figure 6.4 for SiO_2-supported catalysts based on pure Ni_2P, doped with noble metal and pure noble metals.

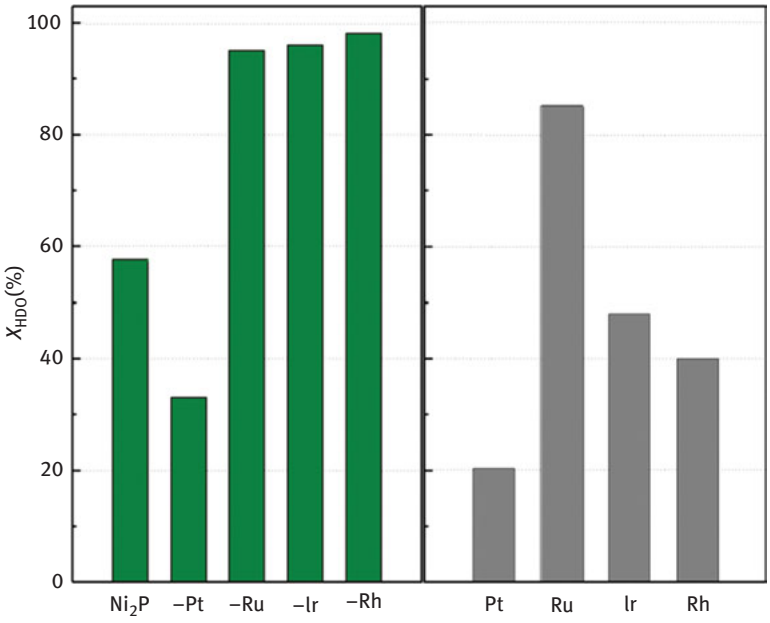

Figure 6.4: Comparative HDO conversion of dibenzofuran on pure noble metal catalysts (right), and pure Ni_2P or doped with noble metals (left): $Ni_{1.8}M_{0.2}P$ (M = Pt, Ru, Ir, Rh). All catalysts supported on SiO_2 with 5 wt% metal loading. Reaction temperature at 300 °C and 3 bar H_2 pressure.

The promoter effect of these noble metals seemed to favor a higher presence of surface Ni sites, which is associated with an increase in Ni sites with square pyramidal coordination on the catalyst surface [70]. At this point it should be mentioned that there are two different Ni sites present in the structure of a Ni_2P phase (Figure 6.5), named as Ni(1) and Ni(2), with coordination number 4 in tetrahedral geometry and coordination number 5 in square pyramidal geometry, respectively [71].

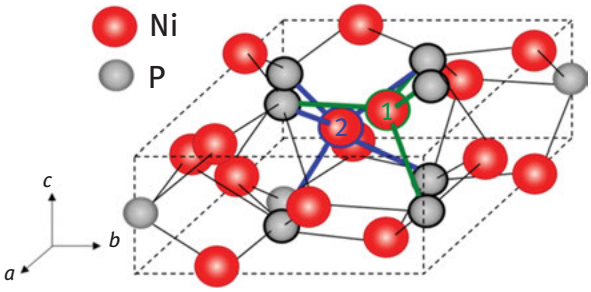

Figure 6.5: Unit cell of Ni_2P structure with a couple of tetrahedral Ni(1) and square pyramidal Ni(2) coordination, highlighted in green and blue, respectively.

The catalytic activity for hydrogenation processes in Ni_2P systems has been reported to be strongly correlated with the surface density of Ni(2) sites [7, 72]. Surface Ni(2) sites are favored on decreasing the Ni_2P crystallite size and are intrinsically linked to a greater presence of phosphorus on the surface due to the higher coordination number of those sites compared with the tetrahedral geometry of Ni(1) ones [7]. The outermost phosphorus is capable of forming P–OH surface groups, which provide Brønsted acid sites able to activate O-containing compounds as well as surface hydrogen species that help to minimize deactivation by coke formation [73]. Further, the presence of hydrogen on the surface of TMPs is also associated with a higher resistance against catalyst deactivation by oxidation of the active Ni_2P phase [70].

Unlike the synergy found between the above-mentioned noble metals and the Ni_2P phase [70, 74], the doping with Pt under comparable conditions gave rise to a drop in the Ni-surface exposure and consequently a poor HDO catalytic activity was obtained [70]. The highest activity appeared for the $Ni_{1.8}Rh_{0.2}P$ catalyst with 88% HDO conversion at 225 °C could be increased to 99% at 300 °C, while pure Ni_2P or Rh catalysts showed 80% and 59%, respectively, for the latter temperature [70].

As a case in point, smaller Ni_2P clusters are reported to be formed on SiO_2 compared with using ZrO_2 and Al_2O_3 supports due to the stronger interaction between the phosphorus precursor and an acid support, requiring higher reduction

temperature [75]. The smaller Ni_2P cluster leads to a higher activity in H-transfer processes for the SiO_2-supported catalysts [76]. Accordingly, although the initial trend of intrinsic activity dependent on the support, measured for atmospheric HDO of guaiacol as a model molecule, was $Ni_2P/SiO_2 < Ni_2P/Al_2O_3 < Ni_2P/ZrO_2$, after the first hour of onstream reaction, the situation turned over. Henceforth, the higher activity was obtained on the Ni_2P/SiO_2 catalyst which was suggested to be due to a low coke accumulation on the SiO_2-supported catalysts, as well as to a better maintenance of a fully phosphide state favored by a phosphorus excess most likely acting as a reservoir for replenishment of the Ni_2P active phase. Despite the value of absolute catalytic activity, the influence of the support on the catalyst performance of the active phase has proved to exhibit an important role in the HDO pathway, significantly influencing the selectivity. Thus, depending on the properties of the support, different reaction pathways are favored, consequently providing distinct distribution of products [76, 77]. As a representative example, it is worth to mention the formation of benzene as a major product in HDO of the model molecule anisole using Ce_2O as Ni_2P support. The high selectivity to the aromatic product was related to the support-induced electron enrichment of $Ni^{\delta+}$ surface sites that favored the easy desorption of the deoxygenated product (benzene) once formed over the active phase surface. Unlikely, the addition of Ti_2O to obtain a mixed $Ti_2O–Ce_2O$ substrate used to support Ni_2P, triggered the shrink for the electron density of Ni surface sites, which together with the especially acidic functionality of the support, promoted benzene hydrogenation to give rise to the corresponding saturated alkane cyclohexane as a major product. Regardless of these differences, both substrates were demonstrated to provide the adsorption sites for anisole molecules, thus improving the catalytic performance compared with unsupported Ni_2P catalysts [77]. Different reaction routes were also reported to be favored in HDO of guaiacol using Ni_2P supported on ZrO_2, Al_2O_3 or SiO_2 [76]. Among them, SiO_2 was found to promote the most desired direct deoxygenation. Considering the additional advantages discussed earlier, it is not a coincidence that Si_2O is used as a support by default in most of the studies on the parameters influencing the HDO catalytic performance of Ni_2P. Nevertheless, substrates other than Si_2O have been reported to present additional benefits for the HDO catalytic behavior of Ni_2P, for example, using ZSM-5 as support was proved to provide removal of oxygen with higher oil yield compared with SiO_2 under equivalent reaction conditions [68]. Additionally, the nature of the model bio-oil molecule must be also taken into account to consider the eventual effect of the support. As a case in point, deoxygenation of *m*-cresol was described to be enhanced on Ni_2P using zirconia as a support compared with silica, due to a more favored adsorption undergone by *m*-cresol over the oxophilic Zr^{3+}/Zr^{4+} sites [78].

The dispersion of the Ni_2P catalyst on the SiO_2 has also been reported by Hsu and Lin [79]. They pointed out that the use of mesoporous silica as SBA-15 increases the dispersion of the Ni_2P particles in comparison with a fumed silica, which is

directly related to the catalytic activity in the HDO of 4-methylguaiacol [79]. In this way, the incorporation of citric acid in the synthetic step generates an internal complex with the Ni^{2+} species, which favors the dispersion of the metallic species after their calcination and subsequent reduction [80].

The effect of employing phosphate, phosphite or even hypophosphite species as phosphorus precursors on the catalytic activity of resulting SiO_2-supported Ni_2P catalysts has been studied in detail [81, 82]. The standard phosphate method used Ni(II) nitrate and $(NH_4)_2HPO_4$, while $Ni(OH)_2$ and H_3PO_3 were employed for the phosphite method. Selectivity and turnover frequency did not change regardless of the method. However, the total conversion was higher for the catalyst derived from the phosphate, while the opposite was found for the conversion to HDO products, with an 81% versus the 85% reached on the phosphite-derived catalyst, at 275 °C and 1 atm. Moreover, the catalysts obtained from the phosphite showed around 23% higher surface area (ca. 220 $m^2\ g^{-1}$) and required a reduction temperature of 30 °C below that of the corresponding phosphate-derived ones.

Employing the improved method based on phosphite precursor, the effect of Ni loading (from 2.5 to 10 wt%) in SiO_2-supported Ni_2P catalysts as well as the influence of the nominal P/Ni ratio in the synthesis for a constant intermediate load of Ni (5 wt%), were studied for HDO of DBF [83]. Increasingly Ni loadings brought about an enhanced HDO conversion until the sample with 7.5 wt% from which higher Ni content led to lower catalytic activity. However, the HDO of the furfural requires higher active phase content, obtaining the highest conversion values when the Ni_2P-based catalyst displays a 15 wt% of Ni. This is attributed to the fact that furfural molecule is highly reactive and tends to form higher proportion of carbonaceous deposits, which causes a severe deactivation of the catalyst along the time onstream [84].

The presence of phosphorus species in the nickel phosphide catalysts causes a drastic decrease in the specific surface area and in the pore volume [83–85]. However, the surface density of acid sites (Brønsted and Lewis), considered as the active sites for hydrogenolysis and hydrogenation processes in HDO reaction [86], increased either with greater Ni loadings or higher P/Ni synthesis ratios. These results were consistent with previous works (Table 6.1), assigning the presence of acid sites in the final catalysts to either phosphate or phosphite species incompletely reduced [87, 88] or Ni species undergoing high electron transfer to phosphorus [86].

On the other hand, better dispersion of the active Ni_2P phase, with smaller particle size, was induced by lower Ni loading on the SiO_2 support, as well as by excess of phosphorus in synthesis, that is, high P/Ni ratios. Indeed, a phosphorus excess has been reported to favor the formation of the $Ni(HPO_3H)_2$ precursor for the Ni_2P active phase formation. Furthermore, while the SiO_2-supported Ni_2P catalyst prepared with P/Ni molar ratio of 1 undergoes a gradual deactivation from the second hour during the HDO test, those prepared with phosphorus excess (P/Ni ratios of 2–3) displayed

Table 6.1: Representative studies on parameters affecting HDO performance of SiO_2-supported Ni phosphide catalysts.

Catalyst	Parameter	Model molecule	Conditions		X_{HDO} (%)	M.P.S (%)	Ref.
			T (°C)	P_{H2} (bar)			
Ni_2P[a]	Phosphate	2-MTHF	275	1	81%	Pentane (61%)	[81]
Ni_2P	Phosphite	2-MTHF	275	1	85%	Pentane (67%)	
Ni_2P[b]	Ni load (2.5%)	DBF	300	30	37%	Bicyclohexane (42%)	[83]
Ni_2P	Ni load (7.5%)	DBF	300	30	94%	Bicyclohexane (42%)	
Ni_2P[c]	PGM promoter	DBF	225	30	23%	HHDBF (16%)	[70]
$(Ni_{1.8}Rh_{0.2})P$		DBF	225	30	78%	BCH (88%)	
$^{i}Ni_2P$[d]	H_2 Pressure	Guaiacol	300	1	57%	Benzene (62%)	[96]
$^{i}Ni_2P$		Guaiacol	300	8	98%	Cyclohexane (91%)	

[a]GHSV = 8,000 h^{-1}; [b]WHSV = 32 h^{-1}, [c]Ni load 5%, LHSV = 6 h^{-1}, [d]Ni load 5.6%, LHSV = 2 h^{-1}.

high stability with no deactivation for the time tested (12 h) at 300 °C below $4{\cdot}10^4$ ppm of reactant feed concentration.

It is important to consider that deactivation of the active Ni_2P phase, by means of surface oxidation, has also been reported to be induced by water, inherently present in bio-oils and also a by-product in their HDO reactions [29, 30, 86]. In that sense, a very recent research has shown that Ni_2P phase becomes unstable during HDO of phenolic compounds in aqueous phase under reaction conditions where the water is mainly present in gaseous state [89]. Thus, on increasing the temperature under reaction conditions, unsupported Ni_2P underwent gradual decomposition into a mixture of Ni_5P_2 and $Ni_{12}P_5$ structures through the intermediate formation of an amorphous phase. Prompt access to increasing reaction temperatures favored further surface oxidation and consequent partial formation of $Ni(PO_3)_2$ phase. An absolute structural collapse into a mixture of Ni_5P_2, $Ni_{12}P_5$ and $Ni(PO_3)_2$ phases was reached after 270 min of HDO at 350 °C, which resulted in a complete loss of HDO activity. On the contrary, proper gradual access to increasing reaction temperatures was proved to mitigate surface oxidation of nickel phosphides, inducing a major formation of Ni_3P structure at expenses of Ni_5P_2 and $Ni_{12}P_5$ phases. In addition to be stable under such reaction conditions, the Ni_3P bulk catalyst displayed high catalytic activity for aqueous HDO of phenol providing approximately 97% conversion with 80% selectivity to HDO product (mainly cyclohexane) at 350 °C. Ni_3P was also successfully tested for aqueous HDO of catechol and *o*-cresol, with approximately 100% and 86% conversion, and approximately 90% and 70% selectivity to HDO products, respectively, at 350 °C. Furthermore, the effectivity of Ni_3P for HDO reaction in organic phase (instead of aqueous) was also proven reaching approximately 100% selectivity to HDO products for HDO of *o*-cresol in decalin at near 100% conversion versus the 20% conversion obtained for Ni_2P under analogous conditions [89].

6.4.2 Co, Fe, Mo and W phosphide catalysts for HDO

Cobalt, iron, molybdenum and tungsten are the main transition metals other than Ni that form phosphides worth to mention as investigated catalysts for HDO of bio-oils. In general, these catalysts show lower catalytic activity in HDO reactions compared with Ni-based catalysts. Nevertheless, it must be pointed out that quantitative comparison of the catalytic activity between HDO catalysts is not straightforward, due to the strong influence, as a result of many factors that are not kept constant between the different studies. Among these factors is the large number of model molecules, with even different nature, that can be used, or the different and complex composition when comparing actual bio-oil samples. Other important parameters are the active phase support, already discussed above, or the H_2 pressure employed in the catalytic studies, which can be found varying within a large range, from atmospheric pressure up to 90 bar. Moreover, the contact time has been proven to strongly influence either the catalytic conversion or the distribution of products, with even a different trend depending on the TMP employed as catalysts [61, 81, 90]. These are just some of the most representative factors affecting the catalytic behavior, which might present, in turn, interdependencies between them. Most of the times it is not possible to find the impact of a certain parameter studied for all of the main TMP catalysts. That is not the case for the effect of the phosphorus source employed to synthesize the corresponding TMP, which has been reported for at least all the transition metals discussed in this work [81]. Thus, with exception of Co and W, the synthesis method employing phosphite precursor (phosphorus acid reactant) enhances HDO conversion of a model bio-oil molecule (2-MTHF) over the final TMP catalysts (for Ni, Mo and Fe), compared with the method from phosphate precursor (ammonium phosphate reactant). Regardless of the phosphorus precursor, all these TMP catalysts displayed higher HDO conversion than a commercial Al_2O_3-supported Pd catalyst [81].

The P/metal molar ratio introduced in synthesis of TMPs is another parameter commonly studied, which despite of Ni (already discussed earlier) can also be found for Fe and Co [91, 92]. For the case of Fe, different stoichiometries of the final silica-supported iron phosphide, Fe_2P, FeP and FeP_2, were obtained as setting the initial P/Fe molar ratio to 0.5–1, 2 and 3, respectively. The particle size and dispersion, as well as the metallic surface exposure and acidity increased when decreasing the P/Fe ratio, accordingly correlated with the trend displayed for the HDO conversion of phenol used as model molecule: Fe_2P > FeP > FeP_2 [91]. On the contrary, the silica-supported Co_2P phase was reported as the less active in HDO of phenol (ca. 20% at 300 °C) compared with CoP_2 and CoP phases, both achieving close to 100% conversion [92]. In this case, the common trend for Ni and Fe was inverted, and HDO was improved by increasing the amount of P into the phosphide structure, that is, by decreasing the metallic character of the phosphide (Figure 6.6).

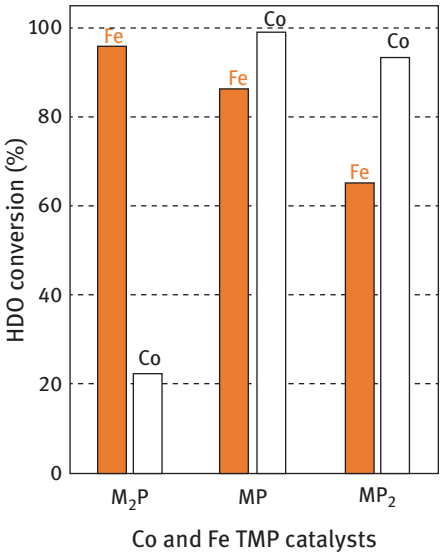

Figure 6.6: Comparative HDO conversion of phenol on Fe and Co TMP series of catalysts consisting of phases with different P/M stoichiometric ratio. All catalysts supported on SiO_2 with 5 wt% metal loading (Co) or 15 wt% (Fe). Reaction temperature at 300 °C and H_2 pressure of 30 and 15 bar, for Co and Ni catalysts, respectively.

On the other hand, several authors have synthesized bimetallic phosphide-based catalysts. Among them, the isomorphic substitution of small proportions of $Ni^{\delta+}$ species by $Fe^{\delta+}$ species has caused an improvement of the turnover frequency in the HDO of methyltetrahydrofuran [93] and phenol [73], which is in agreement with those reported by other authors for HDS reaction [72, 94]. In the same way, NiMoP-based catalysts [86, 95] have been tested in HDO reaction considering the excellent catalytic behavior of the nickel phosphide and the high dispersion of the MoP catalysts [62, 81].

6.5 Conclusions

In the last decade, TMPs have emerged as an active phase in hydrotreating reactions, and specially in HDO reaction, as an alternative to the traditional catalysts such as metal sulfides or nanostructured noble metals, which are highly susceptible to be oxidized along the catalytic process or display low availability and high cost, respectively.

The highly hydrogenating character of the TMPs together with its resistance to the deactivation by modification of the active phase or the coke deposition are among the main qualities supporting the large potential of TMP catalysts for HDO of bio-oils.

In spite of the high activity and stability that TMPs have shown in the HDO reaction, several goals are required to obtain more sustainable catalysts. In this sense, the most available and so inexpensive transition metal, that is, iron, has hardly been studied in their phosphide phases for the HDO reaction. Thus, the scientific community must develop effective iron phosphide phases to reduce the cost on an industrial scale. On the other hand, nowadays, most of the research is carried out for the HDO reaction of target molecules, which is far from reality. Thus, the main efforts should be focused on the use of bio-oils as feed or the use of bifunctional catalysts that allow to integrate several catalytic processes in only one step.

Acknowledgments: This work was partially supported by the project 2017-T1/IND-6025 (Programa Atracción y Retención de Talento Investigador de la Comunidad de Madrid) and the project RTI2018-099668-BC22 of Ministerio de Ciencia, Innovación y Universidades, Spain and FEDER funds. Antonia Infantes Molina thanks Ramon y Cajal Program RyC2015-17870 (Spanish Ministry of Economy and Competitiveness, Spain).

References

[1] Carenco S, Portehault D, Boissière C, Mézailles N, Sanchez C. Nanoscaled Metal Borides and phosphides: Recent developments and perspectives. Chem Rev 2013, 113, 7981–8065.
[2] Aronsson B, Lundström T, Rundqvist S. Borides, Silicides, and Phosphides: A Critical Review of Their Preparation, Properties and Crystal Chemistry, Methuen, 1965.
[3] Stinner C, Prins R, Weber T. Binary and ternary transition-metal phosphides as HDN catalysts. J Catal 2001, 202, 187–194.
[4] Barry BM. Synthesis of transition metal polyphosphides. PhD (Doctor of Philosophy) thesis. Iowa (U.S.), University of Iowa, 2010.
[5] Barry BM, Gillan EG. Low-temperature solvothermal synthesis of phosphorus-rich transition-metal phosphides. Chem Mater 2008, 20, 2618–2620.
[6] Von Schnering HG, Hoenle W. Chemistry and structural chemistry of phosphides and polyphosphides. 48. Bridging chasms with polyphosphides. Chem. Rev 1988, 88, 243–273.
[7] Oyama ST, Gott T, Zhao H, Lee Y-K. Transition metal phosphide hydroprocessing catalysts: A review. Catal Today 2009, 143, 94–107.
[8] Oyama ST. Transition Metal Carbides, Nitrides, and Phosphides. Handbook of Heterogeneous Catalysis, Wiley-VCH Verlag GmbH & Co. KGaA. Weinheim, Germany. 2008.
[9] Oyama ST. Novel catalysts for advanced hydroprocessing: Transition metal phosphides. J Catal 2003, 216, 343–352.
[10] Brock Stephanie L, Perera Susanthri C, Stamm Kimber L. Chemical routes for production of transition-metal phosphides on the nanoscale: Implications for advanced magnetic and catalytic materials. Chem – A Eur J 2004, 10, 3364–3371.
[11] R. Pöttgen WH, von Schnering, HG. Phosphides: Solid-State Chemistry. Encyclopedia of Inorganic Chemistry R. B. King, R. H. Crabtree, C. M. Lukehart, D. A. Atwood and R. A. Scott, John Wiley & Sons Inc. 2016.

[12] Marianne B. Chain and Ring phosphorus compounds – Analogies between phosphorus and carbon chemistry. Angew Chem Int Ed Engl 1982, 21, 492–512.
[13] Motojima S, Haguri K, Takahashi Y, Sugiyama K. Chemical vapor deposition of nickel phosphide Ni2P. J Less Common Met 1979, 64, 101–106.
[14] Motojima S, Wakamatsu T, Sugiyama K. Corrosion stability of vapour-deposited transition metal phosphides at high temperature. J Less Common Met 1981, 82, 379–383.
[15] Furimsky E. Metal carbides and nitrides as potential catalysts for hydroprocessing. Appl Catal A: Gen 2003, 240, 1–28.
[16] Layan Savithra GH, Muthuswamy E, Bowker RH, Carrillo BA, Bussell ME, Brock SL. Rational design of nickel phosphide hydrodesulfurization catalysts: Controlling particle size and preventing sintering. Chem Mater 2013, 25, 825–833.
[17] Wang H, Male J, Wang Y. Recent advances in hydrotreating of pyrolysis bio-oil and its Oxygen-containing model compounds. ACS Catal 2013, 3, 1047–1070.
[18] Alessio Z, Francisco I, Rafael L. Advances in nanocatalyst design for biofuel production. ChemCatChem 2018, 10, 1968–1981.
[19] Hansen AC, Kyritsis, DC. and Lee, C. f. Characteristics of Biofuels and Renewable Fuel Standards. In: A. A. Vertès NQ, H. P., Blaschek and H. Yukawa, eds. Biomass to Biofuels, Blackwell Publishing Ltd., 2010, p. 1–26.
[20] Akia M, Yazdani F, Motaee E, Han D, Arandiyan H. A review on conversion of biomass to biofuel by nanocatalysts. Biofuel Res J 2014, 1, 16–25.
[21] Ragauskas AJ, Williams CK, Davison BH, et al. The path forward for biofuels and biomaterials. Science 2006, 311, 484–489.
[22] Marchetti JM, Miguel VU, Errazu AF. Possible methods for biodiesel production. Renew Sust Energ Rev 2007, 11, 1300–1311.
[23] Rodionova MV, Poudyal RS, Tiwari I, et al. Biofuel production: challenges and opportunities. Int J Hydrogen Energ 2017, 42, 8450–8461.
[24] Crocker M. Thermochemical Conversion of Biomass to Liquid Fuels and Chemicals, RSC Publishing, 2010.
[25] Furimsky E. Chemistry of catalytic hydrodeoxygenation. Catal Rev 1983, 25, 421–458.
[26] Si Z, Zhang X, Wang C, Ma L, Dong R. An overview on catalytic hydrodeoxygenation of pyrolysis oil and its model compounds. Catalysts 2017, 7, 1–22.
[27] Zhao C, He J, Lemonidou AA, Li X, Lercher JA. Aqueous-phase hydrodeoxygenation of bio-derived phenols to cycloalkanes. Journal of Catalysis 2011, 280, 8–16.
[28] Resasco DE, Crossley SP. Implementation of concepts derived from model compound studies in the separation and conversion of bio-oil to fuel. Catal Today 2015, 257, 185–199.
[29] Maggi R, Delmon B. A review of catalytic hydrotreating processes for the upgrading of liquids produced by flash pyrolysis. In: Froment GF, Delmon B, Grange P, eds. Studies in Surface Science and Catalysis, Elsevier, 1997, 99–113.
[30] Furimsky E. Catalytic hydrodeoxygenation. Appl Catal A: Gen 2000, 199, 147–190.
[31] Shafaghat H, Rezaei PS, Ashri Wan Daud WM. Effective parameters on selective catalytic hydrodeoxygenation of phenolic compounds of pyrolysis bio-oil to high-value hydrocarbons. RSC Adv 2015, 5, 103999–104042.
[32] Mullen CA, Boateng AA. Characterization of water insoluble solids isolated from various biomass fast pyrolysis oils. J Anal Appl Pyrol 2011, 90, 197–203.
[33] Yoosuk B, Tumnantong D, Prasassarakich P. Amorphous unsupported Ni–Mo sulfide prepared by one step hydrothermal method for phenol hydrodeoxygenation. Fuel 2012, 91, 246–252.
[34] Laurent E, Delmon B. Study of the hydrodeoxygenation of carbonyl, carboxylic and guaiacyl groups over sulfided CoMo/γ-Al_2O_3 and NiMo/γ-Al_2O_3 catalysts: I Catalytic reaction schemes.. Appl Catal A: Gen 1994, 109, 77–96.

[35] Bui VN, Laurenti D, Afanasiev P, Geantet C. Hydrodeoxygenation of guaiacol with CoMo catalysts. Part I: Promoting effect of cobalt on HDO selectivity and activity. Appl Catal B: Environ 2011, 101, 239–245.
[36] Nava R, Pawelec B, Castaño P, Álvarez-Galván MC, Loricera CV, Fierro JLG. Upgrading of bio-liquids on different mesoporous silica-supported CoMo catalysts. Appl Catal B: Environ 2009, 92, 154–167.
[37] Pawelec B, Garcia Fierro JL. CHAPTER 8 Hydrodeoxygenation of Biomass-Derived Liquids over Transition-Metal-Sulfide Catalysts. Catalytic Hydrogenation for Biomass Valorization, The Royal Society of Chemistry, 2015, 174–203.
[38] Ardiyanti AR, Gutierrez A, Honkela ML, Krause AOI, Heeres HJ. Hydrotreatment of wood-based pyrolysis oil using zirconia-supported mono- and bimetallic (Pt, Pd, Rh) catalysts. Appl Catal A: Gen 2011, 407, 56–66.
[39] Zhu X, Lobban LL, Mallinson RG, Resasco DE. Bifunctional transalkylation and hydrodeoxygenation of anisole over a Pt/HBeta catalyst. J Catal 2011, 281, 21–29.
[40] Zhu X, Nie L, Lobban LL, Mallinson RG, Resasco DE. Efficient conversion of m-Cresol to aromatics on a bifunctional Pt/HBeta catalyst. Energ Fuel 2014, 28, 4104–4111.
[41] Dwiatmoko AA, Zhou L, Kim I, Choi J-W, Suh DJ, Ha J-M. Hydrodeoxygenation of lignin-derived monomers and lignocellulose pyrolysis oil on the carbon-supported Ru catalysts. Catal Today 2016, 265, 192–198.
[42] Lu M, Zhu J, Li M, Shan Y, He M, Song C. TiO2-modified Pd/SiO2 for catalytic hydrodeoxygenation of Guaiacol. Energ Fuel 2016, 30, 6671–6676.
[43] Echeandia S, Pawelec B, Barrio VL, et al. Enhancement of phenol hydrodeoxygenation over Pd catalysts supported on mixed HY zeolite and Al2O3. An approach to O-removal from bio-oils. Fuel 2014, 117, 1061–1073.
[44] Warner TE, Galsgaard Klokker M, Nielsen UG. Synthesis and Characterization of Zeolite Na–Y and Its Conversion to the Solid Acid Zeolite H–Y. J Chem Educ 2017, 94, 781–785.
[45] Lutz W. Zeolite Y. Synthesis, modification, and properties – A case revisited. Adv Mater Sci Eng 2014, 2014, 20.
[46] Mortensen PM, Grunwaldt J-D, Jensen PA, Jensen AD. Screening of catalysts for hydrodeoxygenation of phenol as a model compound for bio-oil. ACS Catal 2013, 3, 1774–1785.
[47] Shafaghat H, Rezaei PS, Daud WMAW. Catalytic hydrodeoxygenation of simulated phenolic bio-oil to cycloalkanes and aromatic hydrocarbons over bifunctional metal/acid catalysts of Ni/HBeta, Fe/HBeta and NiFe/HBeta. J Ind Eng Chem 2016, 35, 268–276.
[48] Qi S-C, Zhang L, Einaga H, Kudo S, Norinaga K, Hayashi J-i. Nano-sized nickel catalyst for deep hydrogenation of lignin monomers and first-principles insight into the catalyst preparation. J Mater Chem A 2017, 5, 3948–3965.
[49] Dongil AB, Ghampson IT, Garcia R, Fierro JLG, Escalona N. Hydrodeoxygenation of guaiacol over Ni/carbon catalysts: Effect of the support and Ni loading. RSC Adv 2016, 6, 2611–2623.
[50] Selvaraj M, Shanthi K, Maheswari R, Ramanathan A. Hydrodeoxygenation of guaiacol over MoO3-NiO/mesoporous silicates: Effect of incorporated heteroatom. Energ Fuel 2014, 28, 2598–2607.
[51] Ranga C, Lødeng R, Alexiadis VI, et al. Effect of composition and preparation of supported MoO3 catalysts for anisole hydrodeoxygenation. Chem Eng J 2018, 335, 120–132.
[52] Hwu HH, Chen JG. Surface chemistry of transition metal carbides. Chem Rev 2005, 105, 185–212.
[53] Levy RB, Boudart M. Platinum-like behavior of tungsten carbide in surface catalysis. Sci 1973, 181, 547–549.

[54] Frühberger B, Chen JG. Reaction of ethylene with clean and carbide-modified Mo(110): Converting surface reactivities of molybdenum to Pt-Group metals. J Am Chem Soc 1996, 118, 11599–11609.
[55] Lee W-S, Wang Z, Wu RJ, Bhan A. Selective vapor-phase hydrodeoxygenation of anisole to benzene on molybdenum carbide catalysts. J Catal 2014, 319, 44–53.
[56] Chen C-J, Lee W-S, Bhan A. Mo2C catalyzed vapor phase hydrodeoxygenation of lignin-derived phenolic compound mixtures to aromatics under ambient pressure. Appl Catal A: Gen 2016, 510, 42–48.
[57] Lu Q, Chen C-J, Luc W, Chen JG, Bhan A, Jiao F. Ordered mesoporous metal carbides with enhanced anisole hydrodeoxygenation selectivity. ACS Catal 2016, 6, 3506–3514.
[58] Ghampson IT, Sepúlveda C, Garcia R, et al. Guaiacol transformation over unsupported molybdenum-based nitride catalysts. Appl Catal A: Gen 2012, 413–414, 78–84.
[59] Sepúlveda C, Leiva K, García R, et al. Hydrodeoxygenation of 2-methoxyphenol over Mo2N catalysts supported on activated carbons. Catal Today 2011, 172, 232–239.
[60] Bu Q, Lei H, Zacher AH, et al. A review of catalytic hydrodeoxygenation of lignin-derived phenols from biomass pyrolysis. Bioresour Technol 2012, 124, 470–477.
[61] Infantes-Molina A, Gralberg E, Cecilia JA, Finocchio E, Rodriguez-Castellon E. Nickel and cobalt phosphides as effective catalysts for oxygen removal of dibenzofuran: Role of contact time, hydrogen pressure and hydrogen/feed molar ratio. Catal Sci Technol 2015, 5, 3403–3415.
[62] Zhao H, Li D, Bui P, Oyama S. Hydrodeoxygenation of guaiacol as model compound for pyrolysis oil on transition metal phosphide hydroprocessing catalysts. Appl Catal A Gen 2011, 391(1–2), 305–310.
[63] Yang Y, Ochoa-Hernández C, de la Peña O'Shea V, Pizarro P. Transition metal phosphide nanoparticles supported on SBA-15 as highly selective hydrodeoxygenation catalysts for the production of advanced biofuels. J Nanosci Nanotechnol 2015, 15(9), 6642–6650.
[64] Chen J, Shi H, Li L, Li K. Deoxygenation of methyl laurate as a model compound to hydrocarbons on transition metal phosphide catalysts. Appl Catal B Environ 2014, 144, 870–884.
[65] Alvarez-Galvan M, Brieva G, Maricarmen S, Morales-delaRosa S, Campos-Martin J, L.G. Fierro J. Metal phosphide catalysts for the hydrotreatment of non-edible vegetable oils. Catal Today 2018, 302, 242–249.
[66] Guo C, Rao KTV, Yuan Z, He S, Rohani S, Xu C. Hydrodeoxygenation of fast pyrolysis oil with novel activated carbon-supported NiP and CoP catalysts. Chem Eng Sci 2018, 178, 248–259.
[67] Zarchin R, Rabaev M, Vidruk-Nehemya R, Landau MV, Herskowitz M. Hydroprocessing of soybean oil on nickel-phosphide supported catalysts. Fuel 2015, 139, 684–691.
[68] Koike N, Hosokai S, Takagaki A, et al. Upgrading of pyrolysis bio-oil using nickel phosphide catalysts. J Catal 2016, 333, 115–126.
[69] Lan X. Transition metal phosphides: Synthesis and catalytic properties in hydrodesulfurization and hydrodeoxygenation. PhD (Doctor of Philosophy) thesis. Eindhoven, Technische Universiteit Eindhoven, 2018.
[70] Cecilia JA, Infantes-Molina A, Sanmartin-Donoso J, Rodriguez-Aguado E, Ballesteros-Plata D, Rodriguez-Castellon E. Enhanced HDO activity of Ni2P promoted with noble metals. Catal Sci Technol 2016, 6, 7323–7333.
[71] Rundqvist S. X-Ray Investigations of Mn3P, Mn2P, and Ni2P. Acta Chem Scand 1962, 16, 992.
[72] Ted Oyama S, Zhao H, Freund H-J, Asakura K, Włodarczyk R, Sierka M. Unprecedented selectivity to the direct desulfurization (DDS) pathway in a highly active FeNi bimetallic phosphide catalyst. J Catal 2012, 285, 1–5.

[73] Rodríguez-Aguado E, Infantes-Molina A, Ballesteros-Plata D, Cecilia JA, Barroso-Martín I, Rodríguez-Castellón E. Ni and Fe mixed phosphides catalysts for O-removal of a bio-oil model molecule from lignocellulosic biomass. Mol Catal 2017, 437, 130–139.
[74] Li Y, Yang X, Zhu L, Zhang H, Chen B. Hydrodeoxygenation of phenol as a bio-oil model compound over intimate contact noble metal-Ni2P/SiO2 catalysts. RSC Adv 2015, 5, 80388–80396.
[75] Cecilia JA, Infantes-Molina A, Rodríguez-Castellón E, Jiménez-López A. The influence of the support on the formation of Ni2P based catalysts by a new synthetic approach. Study of the catalytic activity in the hydrodesulfurization of dibenzothiophene. J Phys Chem C 2009, 113, 17032–17044.
[76] Wu S-K, Lai P-C, Lin Y-C, Wan H-P, Lee H-T, Chang Y-H. Atmospheric Hydrodeoxygenation of Guaiacol over Alumina-, Zirconia-, and Silica-Supported Nickel Phosphide Catalysts. ACS Sustain Chem Eng 2013, 1, 349–358.
[77] Pitakjakpipop P. Effects of support for Ni2P catalysts on hydrogenation of bio-oil using anisole as guaiacol as model compounds. PhD (Doctor of Philosophy) thesis. Pennsylvania (U.S.), The Pennsylvania State University, 2016.
[78] Gonçalves VOO, de Souza PM, Cabioc'h T, da Silva VT, Noronha FB, Richard F. Hydrodeoxygenation of m-cresol over nickel and nickel phosphide based catalysts. Influence of the nature of the active phase and the support. Appl Catal B: Environ 2017, 219, 619–628.
[79] Hsu P-J, Lin Y-C. Hydrodeoxygenation of 4-methylguaiacol over silica-supported nickel phosphide catalysts: The particle size effect. J Taiwan Inst Chem Eng 2017, 79, 80–87.
[80] Jiang N, Xu X-W, Song H-L, Song H, Zhang F-Y. Effect of citric acid on the hydrodesulfurization performance of unsupported nickel phosphide. Ind Eng Chem Res 2016, 55, 555–559.
[81] Bui P, Cecilia JA, Oyama S, et al. Studies of the synthesis of transition metal phosphides and their activity in the hydrodeoxygenation of a biofuel model compound. J Catal 2012, 294, 184–198.
[82] Guan Q, Li W, Zhang M, Tao K. Alternative synthesis of bulk and supported nickel phosphide from the thermal decomposition of hypophosphites. J Catal 2009, 263(1), 1–3.
[83] Cecilia JA, Infantes-Molina A, Rodríguez-Castellón E, Jiménez-López A, Oyama ST. Oxygen-removal of dibenzofuran as a model compound in biomass derived bio-oil on nickel phosphide catalysts: Role of phosphorus. Appl Catal B: Environ 2013, 136–137, 140–149.
[84] Jiménez-Gómez CP, Cecilia JA, Moreno-Tost R, Maireles-Torres P. Nickel phosphide/Silica catalysts for the gas-phase hydrogenation of furfural to high–added–value chemicals. ChemCatChem 2017, 9, 2881–2889.
[85] Cecilia JA, Dr A, Rodriguez-Castellon E, Jiménez-López A. A novel method for preparing an active nickel phosphide catalyst for HDS of dibenzothiophene. J Catal 2009, 263(1), 4–15.
[86] Li K, Wang R, Chen J. Hydrodeoxygenation of anisole over silica-supported Ni2P, MoP, and NiMoP catalysts. Energ Fuel 2011, 25, 854–863.
[87] Abu II, Smith KJ. HDN and HDS of model compounds and light gas oil derived from Athabasca bitumen using supported metal phosphide catalysts. Appl Catal A: Gen 2007, 328, 58–67.
[88] Lee Y-K, Oyama ST. Bifunctional nature of a SiO2-supported Ni2P catalyst for hydrotreating: EXAFS and FTIR studies. J Catal 2006, 239, 376–389.
[89] Yu Z, Wang Y, Sun Z, et al. Ni3P as a high-performance catalytic phase for the hydrodeoxygenation of phenolic compounds. Green Chem 2018, 20, 609–619.
[90] Zhao HY, Li D, Bui P, Oyama ST. Hydrodeoxygenation of guaiacol as model compound for pyrolysis oil on transition metal phosphide hydroprocessing catalysts. Appl Catal A: Gen 2011, 391, 305–310.

[91] Rodríguez-Aguado E, Infantes-Molina A, Ballesteros-Plata D, et al. Iron phosphides presenting different stoichiometry as nanocatalysts in the HDO of phenol. Catal Today. 2018. doi.org/10.1016/j.cattod.2018.05.023
[92] Rodríguez-Aguado E, Infantes-Molina A, Cecilia JA, Ballesteros-Plata D, López-Olmo R, Rodríguez-Castellón E. CoxPy Catalysts in HDO of Phenol and Dibenzofuran: Effect of P content. Top Catal 2017, 60, 1094–1107.
[93] Cho A, Shin J, Takagaki A, Kikuchi R, Oyama ST. Ligand and ensemble effects in bimetallic NiFe phosphide catalysts for the hydrodeoxygenation of 2-methyltetrahydrofuran. Top Catal 2012, 55, 969–980.
[94] Danforth S, Liyanage D, Hitihami Mudiyanselage A, Ilic B, Brock S, E. Bussell M. Probing hydrodesulfurization over bimetallic phosphides using monodisperse Ni2–xMxP nanoparticles encapsulated in mesoporous silica. Surf Sci 2015, 648.
[95] Yun G-N, Ahn S-J, Takagaki A, Kikuchi R, Oyama ST. Hydrodeoxygenation of γ-valerolactone on bimetallic NiMo phosphide catalysts. J Catal 2017, 353, 141–151.
[96] Moon J-S, Kim E-G, Lee Y-K. Active sites of Ni2P/SiO2 catalyst for hydrodeoxygenation of guaiacol: A joint XAFS and DFT study. J Catal 2014, 311, 144–152.

José Miguel Hidalgo, Hector de Paz Carmona, Jakub Fratczak

7 Bio-waste and petroleum fractions coprocessing to fuels

7.1 Introduction

The coprocessing of renewable bio-wastes or solid biomass and fossil resources is a highly promising way to protect the environment by decreasing the net CO_2 emissions. Concretely, petroleum is a fossil resource, which is found in many unstable territories; the increasing demand and the production of contaminants and greenhouse gases forced its coprocessing with other renewable resources [1]. Thus, the coprocessing will not only help to protect the environment but also to improve the energy strategy in countries with less petroleum, thus lending a hand for supplying enough feedstock to meet the worldwide crude oil demands [2–5]. In addition, coprocessing can be considered as a moderate and an effective way to step-by-step transform a society based on petroleum fuels (and chemicals) to a society based on renewable fuels, thereby avoiding radical changes such as stopping the production of petroleum and to use only renewable fuels which are not, by the moment, in enough amounts for a world which, now a days, is completely dependent of petroleum. Moreover, coprocessing the second-generation biofuels instead of the first-generation biofuels is an advantage. First-generation biofuels cannot be considered as feedstock for the coprocessing because it implies the processing in refinery of petroleum fraction and a second feedstock together. Furthermore, some disadvantages of the using of first-generation biofuels, such as the freezing point or the low energy density due to its oxygen content, favored the catalytic hydroprocessing of bio-based feedstocks in refineries (Figure 7.1) and so the industrial coprocessing [6].

Bio-waste sources can be easily found and can be used directly (lipids [1, 7], biomass) or indirectly (bio-oils from the pyrolysis of biomass [1], Fisher Tropsch paraffins from biomass [8], hydrogen and biogas from biomass or refinery waste sludge [9]) for the coprocessing in refineries. The most common bio-waste source is the triglycerides-based materials such as used cooking oils, which have been widely studied and industrially used for the green diesel production – these processes being the characteristic technology of oil refineries for by-products utilization [7]. Petroleum fractions used are mostly gas oil fractions [1], which are mainly used for obtaining diesel or gasoline fractions after the hydrotreatment/hydrocracking of the feedstock. Moreover, heavy oils such as vacuum residue mixed with biomass or nonedible triglycerides were also studied [10, 11]. Furthermore, light cycle oil (which is not a petroleum fraction but a commonly used secondary product from the fluid catalytic cracking) or kerosene fraction has been coprocessed with triglycerides [12], with the aim of obtaining diesel fuels.

https://doi.org/10.1515/9783110538151-007

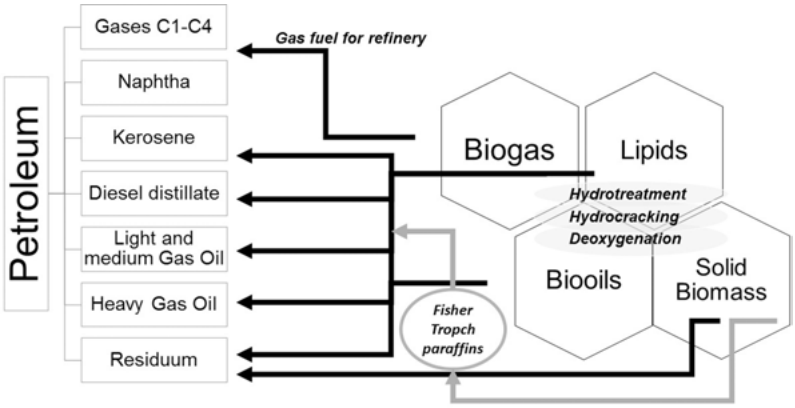

Figure 7.1: Feedstocks scheme for adding to different petroleum fractions.

Some important reviews were written about this topic [1, 13–17], about biofuels in general [13], coprocessing of renewable feeds in general [6], hydroprocessing of biomass-derived oils [14], biomass direct uses [15] and hydrocracking of biomass-derived oils and bio-oils [16] by fluid catalytic cracking [17]. Therefore, this chapter is centered at the use of wastes from biological origin.

7.2 Types of bio-waste and petroleum fractions for coprocessing

Nonedible lipids and low-value biomass can be considered as wastes, which are used as feedstocks for the coprocessing in refineries. Bio-oils are obtained from the biomass and so they can be selected indirectly as bio-waste feed for the coprocessing. Fisher Tropsch paraffins can be obtained from biomass and then they can be used directly as an indirect waste-feedstock. The different types of bio-waste and petroleum fractions used are discussed in the next sections.

7.2.1 Bio-wastes

7.2.1.1 Lipids

Waste bio-feedstock such as cooking or frying oils, animal fat and other residual oils are being used for the production of transport fuels by coprocessing with petroleum fractions. Triglycerides are considered easy-to-convert feedstocks for second-generation biofuels. Residual oils have to be purified to avoid food residues and

mechanical impurities, which could present a problem in flow systems, thereby damaging pumps or blocking pipelines. Other inorganic impurities (including alkali and alkaline earth metals) could also change the activity or to form inorganic solid deposits in the systems [5]. Animal fat can be used from the waste feedstock produced in slaughterhouses and carcasses of livestock. Furthermore, a high amount of this feedstock is considered as nonusable for animal feeding (brown lard), so these materials are being considered as cheap material for the production of green diesel [18–21]. However, the animal fat can entail some problems such as the metal and phosphorous contents, which could affect the catalytic activity during the processing with the petroleum fraction [20]. Animal fats contain not only triglycerides but also a large amount of free fatty acids, phosphorus, nitrogen and sulfur and, as for the residual oils, alkali and alkaline earth metals that can affect the coprocessing activity [20].

7.2.1.2 Solid biomass, (to) bio-oils and (to) Fisher Tropsch paraffins

Normally a solid biomass cannot be used for refinery and due to that it cannot be used in flow systems. However, it can be processed in batch reactor with the heavier part (vacuum residue) of the petroleum [10]. Thus, the solid biomass is treated for the production of bio-oils, which are liquids with a high amount of aromatic compounds. Lignocellulosic biomass is an abundant and a low-cost resource. With fast pyrolysis, a thermochemical process that is carried out at atmospheric pressure and intermediate temperature (450–550 °C), the biomass can be converted to liquids (bio-oils) with yields up to 80 wt.% [17] and then after purification (water, solid residues) it can be coprocessed in refinery. Fisher Tropsch paraffins (syncrude) feedstock is not a bio-waste, but it was obtained by two processes: (i) bio-waste gasification and (ii) Fisher Tropsch process obtaining stable and nontoxic product (see equations below) where 50 wt.% of this product can be distilled up to 360 °C.
(i) Bio-waste or low-value biomass gasification:

$$(\mathrm{A})\mathrm{C} + \mathrm{H_2O} \leftrightarrow \mathrm{CO} + \mathrm{H_2}$$

$$(\mathrm{B})\mathrm{C} + \mathrm{CO_2} \leftrightarrow 2\mathrm{CO}$$

$$(\mathrm{C})\mathrm{CO} + \mathrm{H_2O} \leftrightarrow \mathrm{H_2} + \mathrm{CO_2}$$

$$(\mathrm{D})\mathrm{CH_4} + \mathrm{H_2O} \leftrightarrow \mathrm{CO} + 3\mathrm{H_2}$$

(ii) Fisher Tropsch process:

$$(\mathrm{E})\mathrm{CO} + (2n+1)\ \mathrm{H_2} \rightarrow \mathrm{C}n\mathrm{H_{2n+2}} + n\mathrm{H_2O}(\text{alkanes})$$

$$(\mathrm{F})\ n\mathrm{CO} + 2n\mathrm{H_2} \rightarrow \mathrm{C_}n\mathrm{H_{2n}} + n\mathrm{H_2O}(\text{alkenes})$$

Then, the light fractions of gasoline and diesel can be directly converted into clean fuels. However, they will need to remove water-derived compounds previously,

which are present in emulsion together with paraffins and other upgrading processes such as the isomerization. They can be also coprocessed in refinery (they present in their composition mainly waxes C_{24+}, hot condensate (C_{12}–C_{24}) and cold condensate (C_5–C_{12}) and aqueous products (water, carboxylic acids, alcohols and dissolved paraffins)) [8, 22]. The distillation residues can be cracked to improve the light fractions quantity. So, they can be used for coprocessing with heavy refinery fractions, decreasing the sulfur content of the final product.

7.2.1.3 Biogas

Biogas is produced from anaerobic digestion through industrial waste such as sludge for producing biogas rich in methane, which is usually used as fuel in refinery [9]. Another possibility for the gas rich in methane can be the methane reforming for obtaining hydrogen. However, this process can be considered as no-cost-efficient.

7.2.2 Petroleum fractions

Petroleum is a fossil fuel that was formed from the remains of plants and animals that died millions of years ago. It is a complex mixture formed mainly by hydrocarbons, and when it is distilled under atmospheric or vacuum conditions in the refinery, different distillation fractions are produced as known and published in many articles, books and so on. In theory, all petroleum fractions could be used for coprocessing with bio-wastes. However, the most commonly used petroleum fractions are vacuum gasoil, atmospheric gasoil (AGO) and also vacuum residue or the indirectly produced light cycle oil [5, 23–26]. Vacuum gasoil is produced from the distillation of the atmospheric residue from petroleum under vacuum conditions obtaining light vacuum gasoil (C_{25}–C_{35}) and heavy vacuum gasoil (C_{30}–C_{45}), which contains long paraffins, aromatics and other many compounds in lower amounts containing sulfur, nitrogen and metals depending on the origin of petroleum. The AGO or straight run gasoil is directly obtained by the distillation of petroleum under atmospheric conditions with a boiling point of 250–350 °C containing mainly paraffins, aromatics and other sulfur and nitrogen compounds in much lower amounts. The final residue after atmospheric and vacuum distillation is the vacuum residue, which is normally used for road construction or for consecutive hydrocracking processes for obtaining lighter fractions that can be used for fuels and other compounds. Light cycle oil is widely produced worldwide, resulting from the cracking of vacuum distillates, atmospheric residues and other high boiling fractions from the fluid catalytic cracking. It usually contains a high amount of polyaromatics and sulfur and has high density, and so it has to be hydrotreated normally in coprocessing with other oil fractions.

7.3 The coprocessing

The coprocessing of bio-waste and petroleum fractions can be performed by many different routes. The bio-wastes and petroleum fraction can be treated by cohydroprocessing and cohydrocracking. However, because the bio-oils were also treated in literature [1, 14, 15] and they are not directly bio-waste but their products after the pyrolysis of biomass, the topic development in this chapter was only dedicated for direct bio-wastes, concretely for lipids, which were extensively studied as ideal biofeedstocks because of their chemical properties, fluid properties and boiling points. Vacuum residue and solid biomass coprocessing was also studied using *Calotropis procera* as petro-crop [10] by thermal cracking, showing an improvement on the yield to lighter products.

7.3.1 Catalytic cohydroprocessing of bio-wastes with middle distillates

The catalytic cohydroprocessing of bio-wastes (used cooking oil, animal fat, etc.) with middle distillates in a hydrotreating unit is a promising route to obtain fuels at industrial scale because environmental contaminant residues are eliminated, turning them into high-quality paraffinic biofuels compatible with the present-days fuels [27]. In addition, the existing refinery infrastructures for hydrotreating could be used for these purposes by assuming a significant reduction in the operative cost or investment required to incorporate this technology into refineries. Several studies have been carried out about the coprocessing of bio-wastes at pilot plant scale, both with heavy as light gasoils [5]. These results have demonstrated the technical feasibility of this coprocessing, with the important conclusion that the coprocessing of triglycerides (5–10 wt.%) does not produce a significant interaction in the normal activity of the hydrotreating units. The conditions used in that cases were similar to that used for obtaining pure hydrotreated vegetable oil, which is a biofuel formed mainly by linear paraffins. It is obtained from the catalytic hydrotreatment of triglycerides at high temperatures and pressures (300–400 °C, 70–80 bar) [18].

Different chemical reactions occur during the catalytic coprocessing of bio-wastes: (i) the sulfur (HDS – hydrodesulfurization) and nitrogen (HDN – hydrodenitrogenation) removal from the petroleum feedstock, which means the formation of hydrogen sulfide or ammonia, respectively, and (ii) the oxygen removal from the triglycerides feedstock. The deoxygenation reaction of triglycerides occurs following three parallel reactions: hydrodeoxygenation (HDO), hydrodecarboxylation (HDC) and hydrodecarbonylation (HDCn), in accordance with the mechanism proposed in Figure 7.2, widely described and discussed in [28].

During the first part of the mechanism, the triglyceride molecule is completely saturated by hydrogen, followed by hydrogenolysis of the structure, resulting in

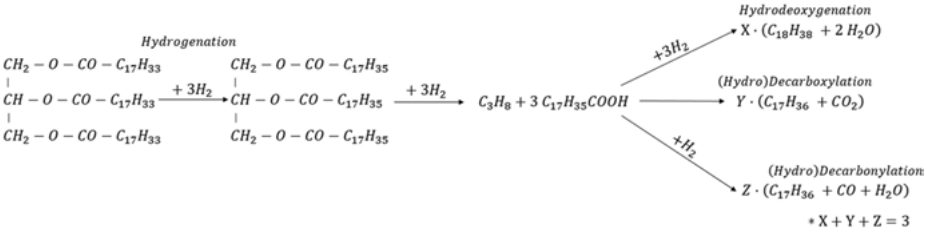

Figure 7.2: Reaction pathways proposed during triglycerides deoxygenation [28].

three molecules of free fatty acids and one molecule of propane. Then, the mechanism continues according the following reactions pathways: HDO reaction, producing linear paraffins with even number of carbons (in general nC$_{16}$ or nC$_{18}$) and two molecules of water; HDC reaction, resulting in linear paraffins with odd number of carbons (nC$_{15}$ or nC$_{17}$) and one molecule of carbon dioxide and the HDCn reaction, producing linear paraffins with odd number of carbons (analogous to HDC pathway), as well as carbon monoxide and water molecules.

The catalyst selectivity during the triglycerides deoxygenation depends on the operating conditions or catalysts used. In this way, high reaction temperatures (> 350 °C) or high amount of triglycerides in the feedstock (> 10 wt.%) promote the HDC and HDCn reactions instead the HDO pathway [5]. This fact implies less hydrogen consumption (6–9 molecules of H_2 instead 12 per triglyceride molecule deoxygenated), but higher production of light gases such as CO, CO_2 and propane. On the other hand, the catalysts with nickel or palladium promote the HDC/HDCn reaction by the rupture of the C–C bonds [29], while the NiMo/Al_2O_3 and CoMo/Al_2O_3 catalysts promote the rupture of C–O bonds, promoting the HDO reactions [30].

As previously commented, the main product of the triglycerides coprocessing is the linear paraffins in the range of nC$_{15}$ and nC$_{18}$ (80–85 wt.%), which could be easily analyzed and determined in the desulfurized gasoil by a gas chromatography (GC) analysis or mass spectrometry. These linear paraffins, with a similar boiling point of diesel range, are incorporated to the desulfurized gasoil, increasing their content in diesel range compounds. Figure 7.3 shows the derivative boiling point distribution of different desulfurized gasoil produced during 0 and 20 wt.% of coprocessing of AGO with used frying oil (UFO).

When 20 wt.% of UFO was used for the coprocessing, a significant increment of linear paraffins occurred, particularly the paraffins with 17 and 18 carbon atoms, having a boiling point of 302 and 317 °C, respectively. This increment of the paraffin content gave rise to a significant improve in some physical properties of the produced desulfurized gasoil, such as density at 15 °C or kinematic viscosity, which experimented a decrease due the lower density of these paraffins compared to the other corresponding compounds of the standard desulfurized gasoil [31, 32]. In the

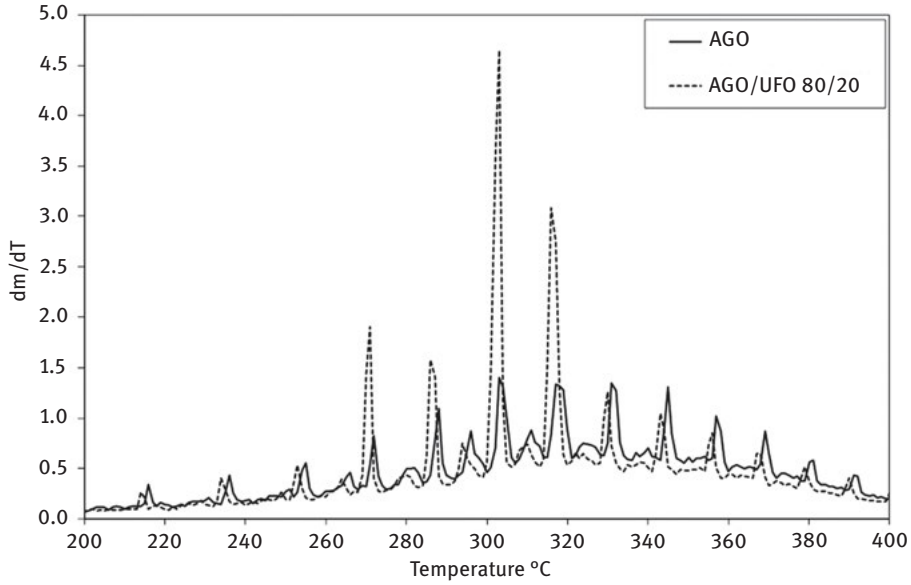

Figure 7.3: Derivative boiling point distribution of desulfurized gasoil produced during AGO and AGO/UFO hydrotreatment [5].

same way, these alkanes have high cetane numbers, in the order of 95–105, which lead to a significant increment of the inflammability or the cetane number of the gasoil, producing a diesel with better ignition quality [14]. However, an increment of paraffins content in desulfurized product could negatively affect their low-temperature properties such as cold filter plugging point, cloud point or pour point, due the high melting point of the linear paraffins. This effect has been widely described in bibliography, which became significant in the case of bio-waste coprocessing of more than 10 wt.% [5, 18, 32]. Nevertheless, this effect could be fixed by additives addition or blending application.

The commercial catalysts used for these processes are generally composed by a support of alumina (Al_2O_3), with an active phase formed by a mixture of cobalt and molybdenum oxides ($CoMo/Al_2O_3$) or nickel instead cobalt ($NiMo/Al_2O_3$) [33]. The composition of this active phase depends on the reaction interested to catalyze. In this sense, CoMo catalyst could be used when HDS high rate is required, and nickel with molybdenum when HDN high rate is needed. Tungsten is chosen to promote the hydrocracking reactions, with low activity in CoMo and NiMo catalysts. These catalysts require a previous sulfidation of their metal oxides supported for obtaining active metal sulfide sites.

The determination of the HDS/HDN rates during this stage is necessary to study the effect of the triglycerides coprocessing over the activity of the catalysts. In this sense, it has been demonstrated that during the coprocessing of bio-wastes with

heavy gasoil [34, 35] or AGO [5], there is not a significant decrease of catalysts activity (HDS/HDN) in a range up to 20 wt.% over NiMo catalyst. This could be explained by taking into account the fact that the catalyst presents enough actives centers to allow both reactions (HDS/HDN and deoxygenation), without a mutual inhibition by competing the actives centers of the catalyst [36].

However, when $CoMo/Al_2O_3$ is used, a decrease of its activity has been reported, which could be due the negative effect of the by-products produced during the coprocessing. An inhibition of CoMo catalyst was observed by the effect of monoxide of carbon, gas produced during the HDCn reaction [37]. In the same way, a decrease of the activity HDS/HDN was reported by the effect of the dioxide of carbon, produced in the HDC reaction [38]. No negative effects have been described for water during coprocessing [39]. This fact could be due the partial blocking of active centers or the partial reduction of the sulfide phase in the catalyst surface [40]. Thus, $NiMo/Al_2O_3$ conventional catalyst could be more attractive for bio-wastes coprocessing to reduce the possible effects derived from the addition of triglycerides in the feedstock.

7.3.2 Analysis and evaluation results

To analyze the effects of bio-wastes addition in a hydrotreating process, it is necessary to perform a blank run in the unit. This stage consists of a gasoil processing using the same conditions as those used during the coprocessing. After reaching the steady state, it is possible to start the coprocessing, which helps to determine its effects over the catalyst activity (defined as HDS/HDN), as well as the physical properties of desulfurized gasoil.

The complete conversion of the triglycerides in paraffins could be verified by IR-ATR analysis [5]. The absence of specific peaks in the spectra of the liquid products (1,745–1,710 cm^{-1} for carbonyl functional group, 1,350–1,500 cm^{-1} for angular deformation of CH_2 and CH_3 and 1,159 cm^{-1} for saturated acyl groups) can confirm the total deoxygenation of the triglycerides.

7.3.2.1 Yields of products

The yield of the main reaction products, that is, HVO or paraffins, water and light gases (CO, CO_2 and C_3H_8) can be determined by the mass balances results during the corresponding coprocessing stage, according to the following equation:

$$\text{Product yield}(\%) = \frac{\text{Product formed}(g)}{\text{triglycerides in feedstock}(g)} \cdot 100$$

where the "product formed" is refers to the amount of that reaction product formed as a consequence of the triglycerides feedstock coprocessed. On the other hand, the "triglycerides in the feedstock" correspond just to the amount of the bio-waste (UCO, animal fat, etc.) used during the coprocessing.

7.3.2.2 Catalysts selectivity

Based on the results of GC analysis, the linear paraffins produced in the desulfurized product could be quantitatively determined. According to this data, the catalysts selectivity could be determined during the triglycerides deoxygenation using the following equations:

$$\mathrm{HDO}[\%] = \frac{n\mathrm{C}_{16} + n\mathrm{C}_{18}}{n\mathrm{C}_{15} + n\mathrm{C}_{16} + n\mathrm{C}_{17} + n\mathrm{C}_{18}} \cdot 100$$

$$\mathrm{HDC/HDCn}[\%] = \frac{n\mathrm{C}_{15} + n\mathrm{C}_{17}}{n\mathrm{C}_{15} + n\mathrm{C}_{16} + n\mathrm{C}_{17} + n\mathrm{C}_{18}} \cdot 100$$

where $n\mathrm{C}_{16} + n\mathrm{C}_{18}$ and $n\mathrm{C}_{15} + n\mathrm{C}_{17}$ are referred as the linear paraffins formed (wt.%) following the HDO pathway and HDC/HDCn reactions, respectively. $n\mathrm{C}_{15} + n\mathrm{C}_{16} + n\mathrm{C}_{17} + n\mathrm{C}_{18}$ is the total paraffins formed during the coprocessing. If HDO ratio is higher than HDC/HDCn, it means that the catalyst, at the operating conditions used, promote the HDO pathway, with a higher hydrogen consumption and water product as the main by-product.

7.3.2.3 Heteroatom removal

The catalyst activity can be analyzed by taking into account the HDS and HDN rates of the catalyst. This is determined by considering the sulfur or nitrogen content in the feedstock, the products, as well as the yield of the process, which is defined as the relationship between the mass of desulfurized gasoil obtained and the corresponding feedstock processed. Thus, the HDS activity of the catalyst can be calculated according to the following equation:

$$\mathrm{HDS}\,[\%] = \frac{(S_0 - (S_\mathrm{p}.\eta))}{S_0} \cdot\ 100$$

where S_0, S_p and η represent the sulfur content of the feedstock, the sulfur content of the liquid product (wt-ppm) and the process yield (%), respectively. Analogously, the HDN activity can be determined according to the following equation:

$$\mathrm{HDN}\,[\%] = \frac{\left(N_0 - \left(N_\mathrm{p}.\eta\right)\right)}{N_0} \cdot 100$$

where N_0 and N_p represent the nitrogen content of the feedstock and the liquid product (wt-ppm), respectively. A value close to 100% corresponds to the almost removal rate of sulfur or nitrogen compounds of the petroleum feedstock used during the coprocessing.

7.4 Conclusions and perspectives

Coprocessing is a necessary option for obtaining fuels for decreasing the net final CO_2 production and obtaining more environmental friendly final fuels. Bio-waste is a good option because of its properties and compatibility of being directly used in actual refineries, giving time for a progressive transformation from fossil to renewable fuels. Although many publications discuss about the great possibilities of using these materials for the coprocessing, which is a ready-to-use technology, the refineries are not yet massively using these feedstocks. Nevertheless, according to European legislation [41] and new expected worldwide legislation about having more renewable fuels, the industry will be obligated to use this available methodology in the near future, and so the best way can be the direct use of the existent refineries. Bio-waste is a very abundant resource that can be found directly at home (UFO) or in industry-agriculture (lignocellulosic biomass), and that can be used directly or indirectly, i.e. to previously process it for obtaining mainly organic compounds to be coprocessed in refinery. Thus, a balanced environment/economy/legislation has to be taken into account for applying this procedure in the industry. The most promising procedures are the coprocessing of waste-derived triglycerides and bio-oils with middle distillates and the less studied procedures are the direct use of solid bio-waste as petrocrops or other lignocellulosic materials, which unfortunately result in a high amount of nonparaffinic compounds that can be a problem in the processing for the industry. However, in those cases, the fast pyrolysis for producing bio-oils, gasification, and so on are the available procedures for preparing such feeds for refinery.

Acknowledgments: This publication is a result of the project Development of the UniCRE Centre (project code LO1606), which was financially supported by the Ministry of Education, Youth and Sports of the Czech Republic under the National Programme for Sustainability I.

References

[1] Bezergianni S, Dimitriadis A, Kikhtyanin O, Kubička D. Refinery co-processing of renewable feeds. Prog Energy Combust Sci 2018, 68, 29–64.

[2] Menoufy MF, Ahmed HS, Betiha MA, Sayed MA. A Comparative study on hydrocracking and hydrovisbreaking combination for heavy vacuum residue conversion. Fuel 2014, 119, 106–110. DOI: 10.1016/j.fuel.2013.11.017

[3] Viet TT, Lee JH, Ma F, Kim GR, Ahn IS, Lee CH. Hydrocracking of petroleum vacuum residue with activated carbon and metal additives in a supercritical m-xylene solvent. Fuel 2013, 103, 553–561.

[4] Joshi JB, Pandit AB, Kataria KL, Kulkarni RP, Sawarkar AN, Tandon D, Ram Y, Kumar MM. Petroleum residue upgradation via visbreaking: A review. Ind Eng Chem Res 2008, 47, 8960–8988.

[5] De Paz Carmona H, Horáček J, Brito Alayón A, Macías Hernández JJ. Suitability of used frying oil for co-processing with atmospheric gas oil. Fuel 2018, 214, 165–173.

[6] Kovács S, Boda L, Leveles L, Thernes A, Hancsók J. Catalytic Hydrotreating of Triglycerides for the Production of Bioparaffin Mixture. Chem Eng Trans 2010, 21, 1321–1326.

[7] Kalnes T, Marker T, Shonnard DR. Green diesel: A second generation biofuel. Int J Chem React Eng 2007, 5, 1542–6580. DOI: 10.2202/1542-6580.1554

[8] Snehesh AS, Mukunda HS, Mahapatra S, Dasappa S. Fischer-Tropsch route for the conversion of biomass to liquid fuels – Technical and economic analysis. Energ 2017, 130, 182–191.

[9] Haak L, Roy R, Pagilla K. Toxicity and biogas production potential of refinery waste sludge for anaerobic digestion. Chemosphere 2016, 144, 1170–1176.

[10] Ahmaruzzaman M, Sharma DK. Coprocessing of petroleum vacuum residue with plastics, coal, and biomass and its synergistic effects. Energ Fuels 2007, 21, 891–897.

[11] Hidalgo JM, Horaček J, Matoušek L, Vráblík A, Tišler Z, Černý R. Catalytic hydrocracking of vacuum residue and waste cooking oil mixtures. Monatsh Chem 2018, 149, 1167–1177.

[12] Wang H, Farooqi H, Chen J. Co-hydrotreating light cycle oil-canola oil blends. Front Chem Sci Eng 2015, 9, 64–76.

[13] Luque R, Herrero-Davila L, Campelo JM, Clark JH, Hidalgo JM, Luna D, Marinas JM, Romero AA. Biofuels: A technological perspective. Energ Environ Sci 2008, 1, 542–564.

[14] Al-Sabawi M, Chen JW. Hydroprocessing of biomass-derived oils and their blends with petroleum feedstocks: A review. Energ Fuels 2012, 26, 5373–99.

[15] Melero JA, Iglesias J, Garcia A. Biomass as renewable feedstock in standard refinery units. Feasibility, opportunities and challenges. Energy Environ Sci 2012, 5, 7393–420.

[16] Al-Sabawi M, Chen JW, Ng S. Fluid catalytic cracking of biomass-derived oils and their blends with petroleum feedstocks: A review. Energ Fuels 2012, 26, 5355–5372.

[17] Stefanidis SD, Kalogiannis KG, Lappas AA. Co-processing bio-oil in the refinery for drop-in biofuels via fluid catalytic cracking. Wiley Interdiscip Rev Energ Environ 2017, e281.

[18] Bezergianni S, Dimitriadis A. Comparison between different types of renewable diesel. Renew Sustain Energy Rev 2013, 21, 110–6.

[19] Eller Z, Varga Z, Hancsok J. Advanced production process of jet fuel components from technical grade coconut oil with special hydrocracking. Fuel 2016, 182, 713–720.

[20] Baladincz P, Hancsók J. Fuel from waste animal fats. Chem Eng J 2015, 282, 152–160.

[21] Nebel BA, Mittelbach M. Biodiesel from extracted fat out of meat and bone meal. Eur J Lipid Sci Technol 2006, 108, 1438–7697.

[22] Snehesh AS, Mukunda HS, Mahapatra S, Dasappa S. Fischer-Tropsch route for the conversion of biomass to liquid fuels – Technical and economic analysis. Energ 2017, 130, 182–191.

[23] Sági D, Baladincz P, Varga Z, Hancsók J. Co-processing of FCC light cycle oil and waste animal fats with straight run gas oil fraction. J Clean Prod 2016, 111, 34–41.
[24] Wang YX, He T, Liu KT, Wu JH, Fang YM. From biomass to advanced bio-fuel by catalytic pyrolysis/hydro-processing: hydrodeoxygenation of bio-oil derived from biomass catalytic pyrolysis. Bioresour Technol 2012, 108, 280–284.
[25] Hidalgo JM, Horaček J, Matoušek L, Vráblík A, Tišler Z, Černý R. Catalytic hydrocracking of vacuum residue and waste cooking oil mixtures. Monatsh Chem 2018, 149, 1167–1177.
[26] Dukanovic Z, Glisic SB, Cobanin VJ, Niciforovic M, Georgiou CA, Orlovic AM. Hydrotreating of straight-run gas oil blended with FCC naphtha and light cycle oil. Fuel Process Technol 2013, 106, 160–5.
[27] Mikkonen S. Second-generation renewable diesel offers advantages. Hydrocarb Proc. 2008, 87(2), 63–66.
[28] Kubička D. Future refining catalysis-introduction of biomass feedstocks. Czech Chem Commun 2008, 73, 1015–1044.
[29] Horaček J, Tišler Z, Rubáš V, Kubička, D. HDO catalyst for triglycerides conversion into pyrolysis and isomerization feedstock. Fuel 2014, 121, 57–64.
[30] Kim SK, Han JY, Lee H, Yum T, Kim Y, Kim J. Production of renewable diesel via catalytic deoxygenation of natural triglycerides: Comprehensive understanding of reaction intermediates and hydrocarbons. Appl Energ 2014, 116, 199–205.
[31] De Paz Carmona H, Romero Vázquez MA, Frontela Delgado J, Macías Hernández JJ, Brito Alayón A. Catalytic co-processing of used cooking oil with straight run gas oil in a hydrotreatment pilot plant. Hydrocarb Proc 2016, 95, 59–66.
[32] Walendziewski J, Stolarski M, Łużny R, Klimek B. Hydroprocessing of light gas oil – rape oil mixtures. Fuel Process Technol. 2009, 90, 686–691.
[33] Ho TC. Deep HDS of diesel fuel: Chemistry and catalysis. Catal Today 2004, 98, 3–18.
[34] Bezergianni S, Dimitriadis A, Karonis D. Diesel decarbonization via effective catalytic Co-hydroprocessing of residual lipids with gas-oil. Fuel 2014, 136, 366–373.
[35] Bezergianni S, Dimitriadis A, Meletidis G. Effectiveness of CoMo and NiMo catalysts on co-hydroprocessing of heavy atmospheric gas oil-waste cooking oil mixtures. Fuel 2014, 125, 129–136.
[36] Furimsky E, Massoth FE Deactivation of hydroprocessing catalysts. Catal Today 1999, 52, 381–495.
[37] Egeberg E, Michaelsen N, Skyum L, Zeuthen P. Hydrotreating in the production of green diesel. PTQ 2010, 15(3), 101–113.
[38] Bezergianni S, Dagoniku V. Effect of CO2 on catalytic hydrotreatment of gas-oil. Can J Chem Eng 2015, 93, 1017–1023.
[39] Kubička D, Horáček J Deactivation of HDS catalysts in deoxygenation of vegetable oils. Appl Catal A 2011, 394, 9–17.
[40] Bezergianni S, Dagonikou V, Sklari S. The suspending role of H2O and CO on catalytic hydrotreatment of gas-oil; myth or reality? Fuel Process Technol 2016, 144, 20–26.
[41] Directive 2009/28/EC of the European Parliament and of the Council of 23 April 2009 on the promotion of the use of energy from renewable sources and amending and subsequently repealing Directives 2001/77/EC and 2003/30/EC In force (20 October 2019).Online accessed on 21.October.2019. https://eur-lex.europa.eu/legal-content/EN/TXT/?qid=1571570724621&uri=CELEX:32009L0028

Backmatter

Since the beginning of time, societies have been using the resources that nature has offered for their development. After decades of fast but unsustainable progress based on the use of fossil resources, and also in order to face current environmental problems, a scientific effort emerges toward an exhaustive use of biomass and biowastes produced worldwide from human activities, for the development of necessary renewable products (energy, chemicals and materials). This book addresses this issue, from the use of new biomass resources to its transformation into products through new, more sustainable and efficient processes.

https://doi.org/10.1515/9783110538151-008

Index

https://doi.org/10.1515/9783110538151-009